**UNIVERSITAT POLITÈCNICA DE VALÈNCIA**

**Departamento de Ingeniería Mecánica y de Materiales**

**TESIS DOCTORAL**

---

# Multibody Approach For Railway Dynamic Analysis

---

*Presentada por*: D. Ramy Elsayed Shaltout
*Dirigida por*: Dr. D. Luis Baeza González

Valencia, Marzo de 2013

Thesis

---

# Multibody Approach For Railway Dynamic Analysis

---

For obtaining

the title of

Doctor of Philosophy in Mechanical Engineering

by

**Ramy Elsayed Shaltout**

In

Department of Mechanical and Material Engineering

UNIVERSITAT POLITÈCNICA DE VALÈNCIA

Under supervision of

**Dr. Luis Baeza González**

Valencia, March 2013

TESIS DOCTORAL

---

# Multibody Approach For Railway Dynamic Analysis

---

que para la obtención

del título de

Doctor en Ingeniería Industrial

presenta

**D. Ramy Elsayed Shaltout**

en el

Departamento de Ingeniería Mecánica y de Materiales
de la Universitat Politècnica de València

Dirigida por

**Dr. D. Luis Baeza González**

Valencia, Marzo de 2013

TESIS DOCTORAL

# Multibody Approach For Railway Dynamic Analysis

*Presentada por*: D. Ramy Elsayed Shaltout
*Dirigida por*: Dr. D. Luis Baeza González

TRIBUNAL CALIFICADOR

PRESIDENTE: Dr. D. Vicente Mata Amela
VOCALES: Dr. D. Francisco David Denia Guzmán
Dr. D. Javier Cuadrado Aranda
Dr. D. João Carlos Elói de Jesus Pombo
Dr. D. Astrid Pieringer

En Valencia, Marzo de 2013.

# Abstract

In the work presented, a computational tool used for the dynamic simulation of railway vehicle systems is developed using multibody systems formulation based on the multibody techniques proposed by Shabana. With respect to other existing methodologies, the developed model uses a combined frame of references that permit the use of independent coordinates, without the possibility to have singularity configurations depending on the rotation sequence. The combined frames of reference used as a base for the formulation and modelling of wheel-rail contact problem with high precision. The program is designed in a flexible form that permits the study of different configurations of the railway vehicles as well as various track combinations. The main structure of the program has the ability of making changes for enhancement of the wheel-rail contact model or the implementation of dynamic structure of the track. An efficient contact model is implemented in the current work to precisely detect the coordinates of the contact points located at the wheel-rail interface. The developed simulation tool is applied for different case tests in order to validate the suitability of the proposed methodology for the analysis of railway systems. A comparison is made between the obtained results by the simulation tool presented in this work and the results offered by various simulation packages for the analysis of the Manchester Benchmark Vehicle. The tool is used to carry out the dynamical analysis for TGV 001 locomotive vehicle and the results obtained are compared with these offered by SIMPACK package for the same vehicle model, at the same operating conditions. From the quality of the obtained results, it can be concluded that the presented simulation tool is reliable and efficient to be used in the dynamic analysis of different railway systems.

# Resumen

En este trabajo se ha llevado a cabo el desarrollo de una herramienta computacional para la simulación dinámica de vehículos ferroviarios. El modelo está basado en técnicas multicuerpo debidas a Shabana. Con respecto a otras metodologías existentes, la propuesta hace uso de un conjunto de sistemas de referencia que permite el empleo de coordenadas independientes sin la posibilidad de configuraciones singulares debidas a grandes giros. El conjunto de sistemas de referencia sirve de base para formular de manera precisa el problema de contacto rueda-carril. El programa está diseñado para considerar de forma flexible distintas configuraciones de vehículo, así como diversas geometrías de trazado. La estructura del programa está abierta a cambios orientados a la mejora del modelo de contacto rueda-carril o a la implementación de la dinámica estructural de la vía. Se ha implementado un modelo eficiente que permite detectar con precisión las coordenadas de los puntos en contacto localizados en la interfase entre la rueda y el carril. La herramienta de simulación desarrollada en esta tesis se ha aplicado para diferentes casos-estudio con el objetivo de validar la idoneidad de la metodología propuesta en el análisis del sistema ferroviario. Se ha realizado una comparación entre los resultados obtenidos por la herramienta de simulación presentada y los resultados ofrecidos por varios programas comerciales de simulación dinámica en el análisis del vehículo del Manchester Benchmark. Además, la herramienta se ha empleado para desarrollar un análisis dinámico de la locomotora de un TGV 001, y los resultados obtenidos se han comparado con los ofrecidos por el programa comercial SIMPACK para el mismo modelo de vehículo, bajo las mismas condiciones de operación. Finalmente, sobre la base de la calidad de los resultados, se puede concluir que la herramienta de simulación es fiable y eficiente para emplearse en el análisis dinámico de los diferentes sistemas ferroviarios.

# Resum

En este treball s'ha portat a terme el desenrotllament d'una ferramenta computacional per a la simulació dinàmica de vehicles ferroviaris. El model està basat en tècniques multi-cos degudes a Shabana. Respecte a altres metodologies existents, la proposta fa ús d'un conjunt de sistemes de referència que permet l'ocupació de coordenades independents sense la possibilitat de configuracions singulars degudes a grans girs. El conjunt de sistemes de referència servix de base per a formular de manera precisa el problema de contacte roda-carril. El programa està dissenyat per a considerar de forma flexible distintes configuracions de vehicle així com a diverses geometries de traçat. L'estructura del programa està oberta a canvis orientats a la millora del model de contacte roda-carril o a la implementació de la dinàmica estructural de la via. S'ha implementat un model eficient que permet detectar amb precisió les coordenades dels punts en contacte localitzats en la interfase entre la roda i el carril. La ferramenta de simulació desenrotllada en esta tesi s'ha aplicat per a diferents casos-estudi amb l'objectiu de validar la idoneïtat de la metodologia proposada en l'anàlisi del sistema ferroviari. S'ha realitzat una comparació entre els resultats obtinguts per la ferramenta de simulació presentada i els resultats oferits per diversos programes comercials de simulació dinàmica en l'anàlisi del vehicle del Manchester Benchmark. A més, la ferramenta s'ha emprat per a desenrotllar una anàlisi dinàmica de la locomotora de un TGV 001 i els resultats obtinguts s'han comparat amb els oferits pel programa comercial SIMPACK per als mateixos models de vehicle i baix les mateixes condicions d'operació. Finalment, sobre la base de la qualitat dels resultats, es pot concloure que la ferramenta de simulació és fiable i eficient per a emprar-se en l'anàlisi dinàmica dels diferents sistemes ferroviaris.

# Keywords

Multibody system Dynamics, Track parametrization, Railway Dynamics, Wheel-Rail Contact, Creep Forces.

# Palabras Clave

Dinámica de sistemas de multicuerpos, Parametrización de la vía, Dinámica de vehículos ferroviarios, Contacto rueda-carril, Fuerzas tangenciales al contacto.

*To my Family*

# Agradecimientos/ Acknowledgments

Agradecimientos/ Acknowledgments

En primer lugar quiero expresar mi agradecimiento a mi director Luis Baeza por su orientación, ayuda y apoyo durante la realización de esta Tesis, así como por dirigirme mediante sus amplios conocimientos y experiencia profesional. De él he aprendido que para llegar lejos en la investigación hay que trabajar de manera incansable. He sido un privilegiado al haberlo tenido como director de Tesis, habiéndome beneficiado de sus cualidades como profesor e investigador. Me ha proporcionado la inmensa motivación que ha de ser siempre el estado anímico de un investigador. Gracias por todo.

Unas cuantas líneas son poco para mostrar mi aprecio hacia Mohamad y Antoine; doy gracias por haber tenido la suerte de contar con dos amigos como estos. Sus palabras eran como una guía para mí, mostrándome el camino. Siempre motivando, escuchando y esforzándose. A ellos les agradezco su preocupación, sus consejos y su constante disposición a ayudar en el complejo camino que supone para un estudiante el inicio de una carrera investigadora. Nunca olvidaré lo que habéis hecho por mí. Muchas gracias.

Profundo agradecimiento también para Andrés Rovira, por su apoyo y consejos durante todo el tiempo que he pasado en Valencia, y por la experiencia que me ha aportado tanto en el trabajo como en la vida social. Gracias Andrés por todo el tiempo que hemos pasado conversando, por las rutas de bici que hemos hecho y por lo que vamos a hacer en el futuro.

Quiero agradecer a mis amigos y compañeros del CITV y en especial a José, Fede, Rafa, Octavio, Vicente, Enrique, Virginia, Héctor, Guillem, Juan Giner y Justo por los momentos muy agradables que hemos tenido y las conversaciones tomando el café cada mañana. También doy las gracias a mis amigos del ITM, Lissette e Irma. Me habéis hecho sentir como si estuviera en casa, me habéis dado fuerza cuando la necesitaba. Los almuerzos, comidas y cenas que hemos compartido han sido momentos inolvidables.

First of all, praise to Allah the greatest, the most merciful, the all beneficent, the omniscient, who guided the man to know which he did not know.

I would like to say that my words would not be enough to transfer what I'm feeling inside me. My mother, without you and your praying for me, I would not reach this level. My brothers (Mohamed, Hany, Moataz), thanks for all your encouragements and animation during all this time.

My sincerest thanks go to Dr. Stefano Bruni for his useful scientific discussions through the period i passed with his group in Politecnico di Milano. I especially appreciate his honest insights into the wider research community, giving me a right perspective from which to grow as a researcher.

I would like to thank all my dear friends in Valencia specially Maher, Abeer, Tarek, Abdelhedi and Nidhal. For all the moments that we have passed together and for the animation that they have given to me. Many thanks for being beside me during the period that i have spent in Valencia, many thanks for all of you.

Many thanks To my friends Ahmed and Abdelrahman, and all who have crossed my path during my lifetime, given me spiritual or intellectual guidance, appealed to my senses or my energy or my desire for adventures, or have otherwise challenged me to think in new ways, I thank you.

Esta Tesis se enmarca dentro del desarrollo de los proyectos de investigación TRA2007-67167/AUT y TRA2010-1566, financiados por FEDER y los ministerios de Educación y Ciencia, Ciencia e Inovación y Economia y Competitividad de España.

I wish to express my thanks for financial support provided by the Ministry of Science and Technology of Spain. The financing of this work by means of the programme of FPI grant with a reference BES-2008-006817.

# Contents

**Abstract** i

**Resumen** iii

**Resum** v

**Agradecimientos** xi

**List of Symbols** xxix

**Abbreviations** xxxiii

**1 Introduction** 1
- 1.1 Introduction 1
- 1.2 Work motivation 2
- 1.3 Literature review 2
- 1.4 Scope and work organization 9

**2 Multibody system analysis** 11
- 2.1 Multibody systems and joints 12
- 2.2 Dependent and independent coordinates 12
- 2.3 Kinematic analysis of multibody systems 13
  - 2.3.1 Frames of reference for a multibody system 13
  - 2.3.2 Transformation matrix 15
- 2.4 Rigid body kinematics 17
  - 2.4.1 General displacement 17
  - 2.4.2 Velocity analysis 18
  - 2.4.3 Acceleration analysis 19
- 2.5 Dynamic analysis of multibody systems 20
  - 2.5.1 Generalized coordinates 20
  - 2.5.2 Virtual work 20
  - 2.5.3 Equations of motion of multibody system 22

**3 Dynamics of railway systems** 25

3.1 Introduction . . . . . 25
3.2 Track geometric description . . . . . 26
3.2.1 Terminology of railway tracks . . . . . 27
3.2.1.1 Track gauge . . . . . 27
3.2.1.2 Horizontal curves . . . . . 28
3.2.1.3 Track width . . . . . 28
3.2.1.4 Super-elevation . . . . . 28
3.2.1.5 Track grad . . . . . 28
3.2.2 Cant angle definition in the track model . . . . . 28
3.2.3 Spatial track centreline . . . . . 30
3.2.4 Transition curves and super-elevation ramps . . . . . 31
3.2.4.1 Transition curves . . . . . 32
3.2.4.2 Transition curves in the space . . . . . 32
3.2.4.3 Mathematical definition of the transition curves . . . 33
3.3 Wheel-rail interaction phenomenon . . . . . 36
3.3.1 Classification of the wheel-rail contact theories . . . . . 37
3.4 Geometrical contact problem . . . . . 38
3.4.1 Proposed solutions for the geometric contact problem . . . . . 39
3.4.2 The visible profile method . . . . . 39
3.4.3 Contact points detection using geometric relational properties . 41
3.4.4 The wheel-rail differential contact method . . . . . 43
3.5 Normal contact problem . . . . . 45
3.5.1 Hertz normal contact force . . . . . 46
3.5.2 Size and shape of the contact patch . . . . . 47
3.6 Tangential contact problem . . . . . 48
3.6.1 Creepage phenomenon . . . . . 49
3.6.1.1 Longitudinal Creepage . . . . . 50
3.6.1.2 Lateral Creepage . . . . . 50
3.6.1.3 Spin Creepage . . . . . 51
3.6.2 The Linear Theory of rolling contact . . . . . 52
3.6.3 FASTSIM algorithm . . . . . 55
3.6.3.1 Mathematical development of FASTSIM algorithm . . 55
3.6.3.2 Calculation of the flexibility parameter . . . . . 57
3.6.4 Polach nonlinear creep force model . . . . . 58
3.6.4.1 Mathematical development of Polach algoritm . . . . 58

**4 Multibody methodology for railway analysis 63**
4.1 Introduction . . . . . 63
4.2 Reference frames description . . . . . 65
4.2.1 Reference frames . . . . . 66
4.2.2 Fixed reference frame . . . . . 67
4.2.3 Track reference frame . . . . . 67
4.2.4 Body reference frame . . . . . 68
4.3 Reference frame transformations . . . . . 69

4.3.1 Transformation from track to fixed reference frame . . . . . . . 69
4.3.2 Transformation from body to fixed reference frame . . . . . . 70
4.4 Track model . . . . . . . . . . . . . . . . . . . . . . . . . . . . 72
4.4.1 Track modelling using analytical segments . . . . . . . . . . . . 73
4.4.2 Straight line stage . . . . . . . . . . . . . . . . . . . . . . . . 73
4.4.3 Transition curve stage . . . . . . . . . . . . . . . . . . . . . . 75
4.4.4 Circular curve stage . . . . . . . . . . . . . . . . . . . . . . . 77
4.5 Theoretical development of the proposed methodology . . . . . . . . . 78
4.5.1 Kinematic analysis of rigid body system . . . . . . . . . . . . . 78
4.5.2 Total kinetic energy of the system . . . . . . . . . . . . . . . . 79
4.5.3 Translational kinetic energy of the system . . . . . . . . . . . . 80
4.5.4 Rotational kinetic energy of the system . . . . . . . . . . . . . 80
4.5.5 Dynamic analysis of rigid body system . . . . . . . . . . . . . . 81
4.5.5.1 Lagrangian approach for calculating the equations of motion . . . . . . . . . . . . . . . . . . . . . . . . . 81
4.5.5.2 Quadratic velocity vector . . . . . . . . . . . . . . . . 82
4.5.5.3 Derivatives of the K.E with respect to generalized coordinates . . . . . . . . . . . . . . . . . . . . . . . . 83
4.5.6 Generalized forces associated to the generalized coordinates . . 83
4.5.6.1 Virtual displacement . . . . . . . . . . . . . . . . . . 84
4.5.6.2 Generalized force corresponding to generic force vector applied on the body . . . . . . . . . . . . . . . . . . 84
4.5.6.3 Virtual work . . . . . . . . . . . . . . . . . . . . . . 84
4.5.6.4 Generalized force . . . . . . . . . . . . . . . . . . . . 84
4.6 Equations of motion development . . . . . . . . . . . . . . . . . . . 85
4.6.1 Translational equation of motion . . . . . . . . . . . . . . . . . 85
4.6.2 Rotational equation of motion . . . . . . . . . . . . . . . . . . 85
4.6.3 Equations of motion of wheelset . . . . . . . . . . . . . . . . . 86
4.6.3.1 Wheelset . . . . . . . . . . . . . . . . . . . . . . . . 86
4.6.3.2 Wheelset frame of reference . . . . . . . . . . . . . . 87
4.6.3.3 Kinematic analysis of wheelset system . . . . . . . . . 88
4.7 Wheel-rail contact model . . . . . . . . . . . . . . . . . . . . . . . 89
4.7.1 Contact geometric problem . . . . . . . . . . . . . . . . . . . . 89
4.7.1.1 Procedure used in the solution of the geometrical contact problem . . . . . . . . . . . . . . . . . . . . . . . 90
4.7.1.2 Assumptions . . . . . . . . . . . . . . . . . . . . . . 90
4.7.1.3 Contact surfaces definitions . . . . . . . . . . . . . . . 91
4.7.1.4 Procedure used to obtain the intersection between contact surfaces . . . . . . . . . . . . . . . . . . . . . . . 92
4.7.1.5 Intersection between straight line and conical segment 94
4.7.1.6 Strip definition . . . . . . . . . . . . . . . . . . . . . 97
4.7.2 Position vector of the contact point . . . . . . . . . . . . . . . 99
4.7.3 Velocity vector of the contact point . . . . . . . . . . . . . . . 101
4.8 Wheelset dynamic analysis . . . . . . . . . . . . . . . . . . . . . . 102

4.8.1 Generalized forces corresponding to contact forces . . . . . . . 102
4.8.2 Generalized forces corresponding to the spin contact moment . 103
4.8.3 Generalized forces corresponding to internal forces . . . . . . . 104

**5 Simulation results 109**
5.1 Introduction . . . . . . . . . . . . . . . . . . . . . . . . . . . . . . 109
5.2 General description of the simulation tool . . . . . . . . . . . . . . . . 110
5.2.1 Data entry to the simulation tool . . . . . . . . . . . . . . . . 110
5.2.2 Program flow chart . . . . . . . . . . . . . . . . . . . . . . . . 115
5.2.3 Program run and extracted data . . . . . . . . . . . . . . . . . 122
5.3 Testing the simulation tool using simplified contact model . . . . . . . 123
5.3.1 Transversal geometry of the designed track . . . . . . . . . . . 123
5.3.2 Multibody model for TGV 001 vehicle . . . . . . . . . . . . . . 124
5.3.3 Simplified contact model . . . . . . . . . . . . . . . . . . . . . 130
5.3.4 Simulation scenarios and obtained results . . . . . . . . . . . . 132
5.3.4.1 Single bogie negotiating a straight track . . . . . . . . 133
5.3.4.2 Single bogie negotiating a curved track . . . . . . . . 136
5.3.4.3 Complete vehicle negotiating straight track . . . . . . 137
5.3.4.4 Complete vehicle negotiating curved track . . . . . . . 138
5.4 Comparison with the Manchester Benchmark . . . . . . . . . . . . . . 141
5.4.1 Track case definition . . . . . . . . . . . . . . . . . . . . . . . 141
5.4.2 Benchmark Vehicle 1 . . . . . . . . . . . . . . . . . . . . . . . 142
5.5 Application and comparison with SIMPACK program . . . . . . . . . 155
5.6 Application of Polach contact model . . . . . . . . . . . . . . . . . . 166

**6 Conclusions and Future works 171**
6.1 Conclusions . . . . . . . . . . . . . . . . . . . . . . . . . . . . . . . 171
6.2 Future developments . . . . . . . . . . . . . . . . . . . . . . . . . . 174

**A Kinematic and Dynamic Background 175**
A.1 Introduction . . . . . . . . . . . . . . . . . . . . . . . . . . . . . . . 175
A.2 Rotation matrix . . . . . . . . . . . . . . . . . . . . . . . . . . . . . 175
A.2.1 Rotation matrix definition . . . . . . . . . . . . . . . . . . . . 175
A.2.2 Derivation of the rotation matrix . . . . . . . . . . . . . . . . 176
A.2.3 Euler angles . . . . . . . . . . . . . . . . . . . . . . . . . . . . 176
A.2.4 Basic rotations . . . . . . . . . . . . . . . . . . . . . . . . . . 177
A.2.4.1 Rotation about X-axis . . . . . . . . . . . . . . . . . . 177
A.2.4.2 Rotation about Y-axis . . . . . . . . . . . . . . . . . . 177
A.2.4.3 Rotation about Z-axis . . . . . . . . . . . . . . . . . . 178
A.3 Successive rotations . . . . . . . . . . . . . . . . . . . . . . . . . . . 179
A.3.1 Single-frame method . . . . . . . . . . . . . . . . . . . . . . . 179
A.3.2 Multiframe method . . . . . . . . . . . . . . . . . . . . . . . . 179
A.4 Transformation matrices . . . . . . . . . . . . . . . . . . . . . . . . . 180
A.4.1 Track transformation matrix . . . . . . . . . . . . . . . . . . . 180
A.4.2 Solid transformation matrix . . . . . . . . . . . . . . . . . . . 181

A.4.3 Intermediate transformation matrix . . . . . . . . . . . . . . . . 181
A.5 Angular velocity matrices . . . . . . . . . . . . . . . . . . . . . . . . . . 181
A.5.1 Absolute angular velocity matrix . . . . . . . . . . . . . . . . . . 181
A.5.2 Skew symmetric matrix of the track angular velocity vector . . 182
A.5.3 Track angular velocity vector represented in track frame . . . . 182
A.5.4 Absolute relative angular velocity of the solid . . . . . . . . . . 182
A.6 Inertia properties of the solid body . . . . . . . . . . . . . . . . . . . . 184
A.6.1 Mass matrix of solid . . . . . . . . . . . . . . . . . . . . . . . . . 184
A.6.2 Inertia matrix of solid . . . . . . . . . . . . . . . . . . . . . . . . 184
A.7 Time derivative of transformation matrices . . . . . . . . . . . . . . . 184
A.7.1 Time derivative of the track transformation matrix . . . . . . . 184
A.7.2 Time derivative of body transformation matrix . . . . . . . . . 185
A.7.3 Time derivative of intermediate transformation matrix . . . . . 185

**B Tables Used** **187**

**Bibliography** **191**

# List of Figures

2.1 Body corrdinate systems . . . . . . . . . . . . . . . . . . . . . . . . 14
2.2 Fixed and local frame of references . . . . . . . . . . . . . . . . . . . . 15
2.3 Successive rotations about the inertial axes of the body . . . . . . . . 16

3.1 Track gauge description . . . . . . . . . . . . . . . . . . . . . . . . . 27
3.2 Horizontal circular curve . . . . . . . . . . . . . . . . . . . . . . . . . 28
3.3 Centrifugal force affecting a circulating railway vehicle . . . . . . . . . 29
3.4 Cant and Cant angle . . . . . . . . . . . . . . . . . . . . . . . . . . . 30
3.5 Frenet Principle vectors and spatial definition of the cant angle . . . . 30
3.6 Railway track cant angle . . . . . . . . . . . . . . . . . . . . . . . . . 31
3.7 Transition Curves and Super-elevation Ramps . . . . . . . . . . . . . . 31
3.8 Spatial presentation of the transition curve . . . . . . . . . . . . . . . 33
3.9 Planar definition of the Clothoid curve . . . . . . . . . . . . . . . . . . 34
3.10 Planar definition of Oval curve . . . . . . . . . . . . . . . . . . . . . . 34
3.11 Planar definition of Lemniscate curve . . . . . . . . . . . . . . . . . . . 35
3.12 Wheel profile projection: (a) $\psi$=0 (b) $\psi \neq 0$ . . . . . . . . . . . . . . . 40
3.13 Contact point forward movement; extracted from [11] . . . . . . . . . 41
3.14 Candidate points for contact between two parametric surfaces, extracted frome [52] . . . . . . . . . . . . . . . . . . . . . . . . . . . . . . 42
3.15 Candidate points for contact between two parametric surfaces, *extracted from* [52] . . . . . . . . . . . . . . . . . . . . . . . . . . . . . . 42
3.16 Domains, boundaries and contact areas, extracted from [39] . . . . . . 44
3.17 Wheel and rail radii of curvatures . . . . . . . . . . . . . . . . . . . . . 46
3.18 Longitudinal and transversal semi axes of the contact ellipse . . . . . . 48
3.19 Wheel rolling over rail:a) Longitudinal creepage; b) Lateral creepage . 50
3.20 The principle tangent, normal, and longitudinal vector at the left wheel represented by number(1) and at the right wheel represented by number(2) . . . . . . . . . . . . . . . . . . . . . . . . . . . . . . . . . . 51
3.21 Spin creepage . . . . . . . . . . . . . . . . . . . . . . . . . . . . . . . . 52
3.22 Creepages velocities and tangential forces on the contact patch . . . . 54
3.23 Normal and tangential stress destribution in the contact area according to Polach model [47] . . . . . . . . . . . . . . . . . . . . . . . . . 59

4.1 Reference frames combination . . . . . . . . . . . . . . . . . . . . . . . . 66
4.2 Fixed Reference Frame . . . . . . . . . . . . . . . . . . . . . . . . . . . . 67
4.3 Track Reference Frame . . . . . . . . . . . . . . . . . . . . . . . . . . . . 68
4.4 Local position of point $p$ in Track reference frame . . . . . . . . . . . . 68
4.5 Local position of point $p$ in the body reference frame . . . . . . . . . . 69
4.6 Transformation from Solid to Track reference frame . . . . . . . . . . . 70
4.7 Transformation from Body reference frame to Fixed reference frame . 71
4.8 Successive transformations between frame of references . . . . . . . . . 72
4.9 Track model used in the dynamic simulation . . . . . . . . . . . . . . . 74
4.10 Track segments definitions . . . . . . . . . . . . . . . . . . . . . . . . . 74
4.11 Track segment lengths . . . . . . . . . . . . . . . . . . . . . . . . . . . . 75
4.12 Transition curve presented by Clothoid curve . . . . . . . . . . . . . . 76
4.13 Conventional wheelset . . . . . . . . . . . . . . . . . . . . . . . . . . . . 86
4.14 Intermediate reference system associated to wheelset system . . . . . . 87
4.15 Representation of the Wheelset, Track and Fixed reference frame combination . . . . . . . . . . . . . . . . . . . . . . . . . . . . . . . . . . 88
4.16 Measured Wheel and Rail profiles . . . . . . . . . . . . . . . . . . . . . 91
4.17 System of references of the wheel and rail surfaces used in the definition of the contact geometry problem . . . . . . . . . . . . . . . . . . . . . 93
4.18 Wheel and rail segments used to find the intersection between the wheel-rail surfaces . . . . . . . . . . . . . . . . . . . . . . . . . . . . . . 93
4.19 Determination of a generic point on a segment on the wheel profile . . 94
4.20 3D view for the intersection between a straight line $i$ with a conical segment $j$ . . . . . . . . . . . . . . . . . . . . . . . . . . . . . . . . . 95
4.21 Definition of a strip forming the interpenetration area . . . . . . . . . 98
4.22 Determination of the rolling raduis of each strip . . . . . . . . . . . . . 99
4.23 Determination maximum penetration between wheel and rail profiles . 99
4.24 Transformation schem between the different reference frames . . . . . 100
4.25 Concentrated contact moment $\boldsymbol{M}_c$ acting on contact area . . . . . . . 104
4.26 Position vector of two connection points of a spring element between two bodies $i$ and $j$. . . . . . . . . . . . . . . . . . . . . . . . . . . . . . 105

5.1 S1002 wheel profile in contact with UIC60 rail profile . . . . . . . . . . 113
5.2 Curvature values for the left and right wheel profile . . . . . . . . . . . 113
5.3 Curvature values for the UIC60 rail profile . . . . . . . . . . . . . . . . 114
5.4 Smoothed curvature values for the UIC60 rail profile . . . . . . . . . . 115
5.5 Multibody program flow chart- a . . . . . . . . . . . . . . . . . . . . . . 116
5.6 Track segments data for the designed track . . . . . . . . . . . . . . . 123
5.7 Track Super-elevation Ramps . . . . . . . . . . . . . . . . . . . . . . . . 124
5.8 Three dimensional model of railway vehicle . . . . . . . . . . . . . . . 124
5.9 Schematic diagram of the rigid bodies used in the dynamic analysis . . 125
5.10 Identification of the solids numbers . . . . . . . . . . . . . . . . . . . . 126
5.11 Identification of the spring numbers connecting the rigid bodies forming the TGV 001 vehicle . . . . . . . . . . . . . . . . . . . . . . . . . . 128

5.12 Knife edge model of the wheel-rail interaction . . . . . . . . . . . . . . 130
5.13 Contact penetration produced from the movement of the wheelset . . 131
5.14 Contact penetration calculation for the left and right wheel . . . . . . 132
5.15 Single bogie frame used in the simulation . . . . . . . . . . . . . . . . 133
5.16 Lateral displacement and yaw angle of front wheelset . . . . . . . . . . 134
5.17 Lateral displacement of the front and rear wheelset of the bogie . . . . 134
5.18 Lateral displacement of front wheelset and rear wheelset . . . . . . . 135
5.19 Lateral displacement and yaw angle of the bogie frame . . . . . . . . . 135
5.20 Lateral displacement of front and rear wheelset negotiating transition curve stage . . . . . . . . . . . . . . . . . . . . . . . . . . . . . . . 136
5.21 Yaw angle of the front and rear wheelset of the bogie frame . . . . . . 137
5.22 Roll angle of the front and rear wheelset of the bogie frame . . . . . . 137
5.23 Lateral displacement and yaw angle of the front wheelset of the front bogie frame of the complete vehicle model . . . . . . . . . . . . . . . 138
5.24 Lateral displacement of the wheelsets attached to the front and rear bogie frames . . . . . . . . . . . . . . . . . . . . . . . . . . . . . . . 139
5.25 Yaw angle variation of the wheelsets attached to the front and rear bogie frames . . . . . . . . . . . . . . . . . . . . . . . . . . . . . . . 139
5.26 Roll angle change of front and rear bogie frames . . . . . . . . . . . . 140
5.27 Roll angle change of car body . . . . . . . . . . . . . . . . . . . . . . 140
5.28 Track case 1 for the Manchester Benchmark . . . . . . . . . . . . . . . 142
5.29 Manchester Benchmark Vehicle 1, Case1 -Lateral displacement of Wheelset 1 . . . . . . . . . . . . . . . . . . . . . . . . . . . . . . . . . . 143
5.30 Manchester Benchmark Vehicle 1, Case1 -Lateral displacement of the Wheelsets . . . . . . . . . . . . . . . . . . . . . . . . . . . . . . . . . 144
5.31 Manchester Benchmark Vehicle 1, Case1 - Yaw angle Wheelset 1 . . . 145
5.32 Manchester Benchmark Vehicle 1, Case1 - Yaw angle for each wheelset 146
5.33 Manchester Benchmark Vehicle 1, Case1 - Roll angle for each wheelset 146
5.34 Manchester Benchmark Vehicle 1, Case1 -Total Lateral Guiding Forces: Wheelset 1- Left wheel . . . . . . . . . . . . . . . . . . . . . . . . . 147
5.35 Manchester Benchmark Vehicle 1, Case1 - Total Lateral Guiding Forces: Wheelset 1- Right wheel . . . . . . . . . . . . . . . . . . . . . . . . 147
5.36 Manchester Benchmark Vehicle 1, Case1 - Ratio of Lateral to Vertical Forces: Wheelset 1, Left Wheel . . . . . . . . . . . . . . . . . . . . . 148
5.37 Manchester Benchmark Vehicle 1, Case1 - Ratio of Lateral to Vertical Forces: Wheelset 1, Left and Right Wheel . . . . . . . . . . . . . . . 148
5.38 Manchester Benchmark Vehicle 1, Case1 - Longitudinal force: Wheelset 1, Left and Right Wheel . . . . . . . . . . . . . . . . . . . . . . . . . 150
5.39 Manchester Benchmark Vehicle 1, Case1 - Longitudinal force: Wheelset 2, Left and Right Wheel . . . . . . . . . . . . . . . . . . . . . . . . . 150
5.40 Manchester Benchmark Vehicle 1, Case1 - Longitudinal force: Wheelset 3, Left and Right Wheel . . . . . . . . . . . . . . . . . . . . . . . . . 151
5.41 Manchester Benchmark Vehicle 1, Case1 - Longitudinal force: Wheelset 4, Left and Right Wheel . . . . . . . . . . . . . . . . . . . . . . . . . 151

5.42 Manchester Benchmark Vehicle 1, Case1 - Lateral force: Wheelset 1, Left and Right Wheel . . . . . . . . . . . . . . . . . . . . . . . . . . 152
5.43 Manchester Benchmark Vehicle 1, Case1 - Lateral force: Wheelset 3, Left and Right Wheel . . . . . . . . . . . . . . . . . . . . . . . . . . 152
5.44 Manchester Benchmark Vehicle 1, Case1 - Lateral force: Wheelset 4, Left and Right Wheel . . . . . . . . . . . . . . . . . . . . . . . . . . 153
5.45 Manchester Benchmark Vehicle 1, Case1 - Normal force: Wheelset 1, Left and Right Wheel . . . . . . . . . . . . . . . . . . . . . . . . . . 153
5.46 Manchester Benchmark Vehicle 1, Case1 - Normal force: Wheelset 2, Left and Right Wheel . . . . . . . . . . . . . . . . . . . . . . . . . . 154
5.47 Manchester Benchmark Vehicle 1, Case1 - Normal force: Wheelset 3, Left and Right Wheel . . . . . . . . . . . . . . . . . . . . . . . . . . 154
5.48 Manchester Benchmark Vehicle 1, Case1 - Normal force: Wheelset 4, Left and Right Wheel . . . . . . . . . . . . . . . . . . . . . . . . . . 155
5.49 TGV0 01 car model in SIMPACK environment . . . . . . . . . . . . 156
5.50 Contact Models in SIMPACK . . . . . . . . . . . . . . . . . . . . . . 157
5.51 Divisions of the wheel profile . . . . . . . . . . . . . . . . . . . . . . 157
5.52 Lateral shift of the leading and trailing wheelsets of the front bogie for a forward velocity of 25.6m/s, using VIA and SIMPACK simulation tools 159
5.53 Lateral shift of the leading and trailing wheelsets of the rear bogie for a forward velocity of 25.6m/s, using VIA and SIMPACK simulation tools 160
5.54 Lateral velocity of the leading and trailing wheelsets of the front bogie, using VIA and SIMPACK simulation tools . . . . . . . . . . . . . . . 160
5.55 Lateral velocity of the leading and trailing wheelsets of the rear bogie, using VIA and SIMPACK simulation tools . . . . . . . . . . . . . . . 161
5.56 Yaw angle variation for the leading and trailing wheelsets of the front bogie, using VIA and SIMPACK simulation tools . . . . . . . . . . . 161
5.57 Yaw angle variation for the leading and trailing wheelsets of the rear bogie, using VIA and SIMPACK simulation tools . . . . . . . . . . . 162
5.58 Yaw velocity variation for the leading and trailing wheelsets of the front bogie, using VIA and SIMPACK simulation tools . . . . . . . . . . . 163
5.59 Yaw velocity for both wheelsets attached to the rear bogie frame, using VIA and SIMPACK simulation tools . . . . . . . . . . . . . . . . . . 163
5.60 Roll velocity for the first and second wheelsets . . . . . . . . . . . . 164
5.61 Lateral velocity of the front and rear bogie frames . . . . . . . . . . 164
5.62 Yaw velocity of the front and rear bogie frames . . . . . . . . . . . . 165
5.63 Longitudinal creep forces on the left and right wheels of the leading wheelset attached to the front bogie, using VIA and SIMPACK simulation tools . . . . . . . . . . . . . . . . . . . . . . . . . . . . . . . 165
5.64 Lateral guiding foces on the left wheel(L.W) and right wheel(R.W) of the leading wheelset for a forward velocity of 25.6m/s, using VIA and SIMPACK simualtion tools . . . . . . . . . . . . . . . . . . . . . . . 166
5.65 Lateral shift of the leading and trailing wheelset of the fornt bogie for a forward velocity of 25.6m/s, using FASTSIM and Polach models . . 167

5.66 Lateral shift of the leading and trailing wheelset of the rear bogie for a forward velocity of 25.6m/s, using FASTSIM and Polach models . . 167
5.67 Yaw angle variation for the leading and trailing wheelset of the fornt bogie for a forward velocity of 25.6m/s, using FASTSIM and Polach models . . . . . . . . . . . . . . . . . . . . . . . . . . . . . . . . . . . 168
5.68 Yaw angle variation for the leading and trailing wheelset of the rear bogie for a forward velocity of 25.6m/s, using FASTSIM and Polach models . . . . . . . . . . . . . . . . . . . . . . . . . . . . . . . . . . . 168
5.69 Longitudinal creep forces on the left and right wheels of the leading wheelset attached to the front bogie, using FASTSIM and Polach models 169
5.70 Lateral creep forces on the left and right wheels of the leading wheelset attached to the front bogie, using FASTSIM and Polach models . . . . 169

A.1 Two different coordinate systems X Y Z and $\mathrm{X_i}$ $\mathrm{Y_i}$ $\mathrm{Z_i}$ . . . . . . . . . 176
A.2 Rotation about X-axis with angle $\theta_x$ . . . . . . . . . . . . . . . . . . . . 177
A.3 Rotation about Y-axis with angle $\theta_y$ . . . . . . . . . . . . . . . . . . . . 178
A.4 Rotation about Z-axis with angle $\theta_z$ . . . . . . . . . . . . . . . . . . . . 179
A.5 Successive rotation of a solid body about its reference coordinates . . 180
A.6 Consecutive rotations of the solid . . . . . . . . . . . . . . . . . . . . . . 182

# List of Tables

2.1 Acceleration components difined for the acceleration of an arbitrary point on a rigid body . . . . . . . . . . . . . . . . . . . . . . . . . . . 19

3.1 Variation of track gauge type . . . . . . . . . . . . . . . . . . . . . . . . . 27

5.1 Mass and inertia properties of rigid bodies . . . . . . . . . . . . . . . . . . 126
5.2 Initial position vectors of the rigid bodies . . . . . . . . . . . . . . . . . . 127
5.3 Topology of the springs connecting the wheelsets with the bogie frames 128
5.4 Springs stiffness and Damping coefficients for elements connecting the wheelsets with the bogie frames . . . . . . . . . . . . . . . . . . . . . 129
5.5 Topology of the springs connecting the bogie frame with the car body 129
5.6 Springs stiffness and Damping coefficients for elements connecting the bogie frames with the car body . . . . . . . . . . . . . . . . . . . . . . 129
5.7 Geometry and contact parameters of the wheelset . . . . . . . . . . . . 130
5.8 Mass and inertia properties of a single bogie . . . . . . . . . . . . . . . . 133
5.9 Lateral shift of each wheelset relative to the track . . . . . . . . . . . 144
5.10 Yaw angle of each wheelset relative to the track . . . . . . . . . . . . 145
5.11 Forces at each wheel . . . . . . . . . . . . . . . . . . . . . . . . . . . . . . 149

B.1 Kalker's creepage and spin coefficients . . . . . . . . . . . . . . . . . . 189

# List of Symbols

## Convention

| | |
|---|---|
| $a, A, \gamma$ | Scalar; |
| $\mathbf{a}$ | Vector; |
| $\mathbf{A}$ | Matrix; |

## Over script

| | |
|---|---|
| $\bar{\mathbf{a}}$ | Vector represented in track frame of reference; |
| $\bar{\bar{\mathbf{a}}}$ | Vector represented in body frame of reference; |
| $\dot{\mathbf{a}}$ | First time derivative of a vector $\mathbf{a}$; |
| $\ddot{\mathbf{a}}$ | Second time derivative of a vector $\mathbf{a}$; |
| $\tilde{\mathbf{a}}$ | Skew-symmetric matrix; |

## Down script

| | |
|---|---|
| $\underline{\mathbf{a}}$ | Vector represented in Intermediate frame of reference; |

## Superscript

| | |
|---|---|
| $\mathbf{a}^{\mathrm{T}}$ | Transpose of a vector; |
| $\mathbf{A}^{\mathrm{T}}$ | Transpose of a Matrix; |

## Subscript

| | |
|---|---|
| $a_r$ | Quantity referred to the rail; |
| $a_w$ | Quantity referred to the wheel; |
| $a_c$ | Quantity referred to the contact; |
| $a_G$ | Quantity referred to center of mass; |

## Latin Symbols

| | |
|---|---|
| a,b | Longitudinal and transversal semi axis of the contact ellipse; |
| A,B | Geometrical functions related to the principle and transversal radii of curvature of the wheel and the rail; |
| $\mathbf{A}$ | Transformation matrix from track frame to fixed frame; |
| $\mathbf{B}$ | Transformation matrix from solid frame to track frame; |
| $\mathbf{B}_{zx}$ | Transformation matrix from intermediate frame to track frame; |
| $C_{11}, C_{22}, C_{23}, C_{33}$ | Creepage and spin coefficients from Kalker's theory; |
| $c$ | Damping coefficient; |
| $\mathbf{q}$, $\dot{\mathbf{q}}$, $\ddot{\mathbf{q}}$ | Vectors of generalized coordinate, velocities and acceleration; |
| $\mathbf{Q}$ | Generalized force vector; |
| $E$ | Young's modulus; |
| G | Track gauge; |
| $G$ | The combined shear modulus of rigidity of rail and wheel materials; |
| $\mathbf{k}$ | Spring stiffness; |
| $\mathbf{K}$ | Geometry parameter; |
| $\mathbf{I}$ | Identity matrix; |
| $\boldsymbol{J}$ | Inertia matrix; |
| $J_{xx}$ $J_{yy}$ $J_{zz}$ | Moments of inertia with respect to the principal axes of a rigid body; |
| $R$ | Radius of curvature; |
| X Y Z | Global reference frame; |
| $\mathrm{X_T Y_T Z_T}$ | Track reference frame; |
| $\mathrm{X_S Y_S Z_S}$ | Solid reference frame; |
| $\underline{\mathrm{X}}\ \underline{\mathrm{Y}}\ \underline{\mathrm{Z}}$ | Intermediate reference frame; |
| $\mathbf{M}$ | System mass matrix; |
| $\mathbf{M_c}$ | Moment at the contact patch; |
| $m$ | Rigid body mass; |
| $\boldsymbol{n}$ | Principal unit normal vector; |
| $\boldsymbol{l}$ | Principal unit longitudinal vector; |
| $\boldsymbol{t}$ | Principal unit lateral vector; |

## Greek Symbols

| | |
|---|---|
| $\delta$ | Indentation (or approach) during contact; |
| $\gamma$ | Conicity of the wheel profile; |
| $\boldsymbol{\omega}$ | Solid angular velocity in the global frame of reference; |
| $\boldsymbol{\tau}$ | Track angular velocity; |
| $\nu$ | Poisson's ratio; |
| $\kappa$ | Curvature; |
| $\xi_x$ | Longitudinal creepage; |
| $\xi_y$ | Lateral creepage; |
| $\xi_{sp}$ | Spin creepage; |
| $\phi$ | Roll angle; |
| $\phi_{eq}$ | Equilibrium cant angle; |
| $\theta$ | Pitch angle; |
| $\psi$ | Yaw angle; |

# Abbreviations

| | |
|---|---|
| **CM** | Centre of Mass; |
| **MBS** | MultiBody System; |
| **K.E** | Kinetic Energy; |
| **DAE** | Differential Algebraic Equations; |
| **DOF** | Degrees Of Freedom; |
| **ODE** | Ordinary Differential Equations; |
| **F.O.R** | Frame Of Reference; |
| **RHT** | Right Hand Term of the equation of motion; |
| **G.I.D.F** | General Input Data File; |
| **I.P** | Initial Position; |

# Chapter 1

# Introduction

## 1.1 Introduction

Modelling and simulation in the field of railway dynamics is a complex interdisciplinary topic. The necessity for the enhancement of the performance of the railway vehicles and obtaining more safety and comfort conditions of the railway vehicles leads to more complex definition and description for all parameters affecting the model simulation of the railway vehicle systems.

Then it was necessary to define a computational tool capable of the accurate description of such systems. The existing computational tools used in the dynamic analysis required not only in the purposes of enhancement of these systems, including also facing the fast progress in the other means of transportation systems, but also for the design purposes and maintenance operations of the railway systems in order to avoid the time and material loses used in making prototypes for the studying of the simulation of parts and systems under study.

Now it is easy to use the simulation solutions provided with the computational simulation programs to predict and make the necessary design modifications on the models before and during the operation of these parts in realistic working conditions of the railway systems [38]. The aim of the work, is to introduce a computational tool used for the dynamic analysis of the railway systems with in the multibody system formulations, that consider the railway vehicles and rail guided systems as a connection of rigid bodies.

In the presented work the dynamic analysis includes as a first stage, the track parameterizations and definition of the track geometry, the second stage is the dynamic analysis of the railway systems using the multibody formulations for rigid bodies, then a model of a railway vehicle is presented to validate the multibody program used in the dynamic simulation of the railway vehicle systems and the computational results are obtained.

## 1.2 Work motivation

The dynamic analysis of railway or other types of rail guided vehicles requires an accurate description of the track geometry. During the research and development of the new transportation solutions, the computational tools can be used to study problems related to the maintenance and operation of existing railway vehicles. The use of profiled- flanged steel wheels running on steel track in order to simultaneously support, guidance and traction was a brilliant concept in the early days in this industry. Nevertheless, the simplicity of the concept masked the complexity of the contact phenomenon [51, 52, 58].

The complex contact forces developed in the wheel-rail interface strongly influence the dynamic behaviour of the rail guided vehicle. Also the characteristics of the suspensions, the masses and inertia properties of the system elements and the geometry of the track play an important role in this issue. The previously mentioned reasons and more reasons related to the ride comfort, wheel-rail wear and vehicle stabilities were a strong motivation for making such work presented. The main objective is to develop a simulation tool capable of making the dynamic analysis of railroad vehicles regarding the following topics.

- Development of a parameterized track model that allows the realistic analysis of the railroad guided vehicles.
- Definition of the mathematical formulations that describe and characterize the wheel-rail contact model.
- Definition of the creepage and calculation of the creepage forces and moments affecting the wheel-rail interaction model.
- Dynamic analysis of a railroad vehicle using multibody relations.
- Dynamic simulation for a vehicle moving on the proposed track model in deferent operation scenarios.

## 1.3 Literature review

Simulation of the dynamic behaviour of railway vehicles is a complex topic in the railway dynamic field. Modern general-purpose softwares for the simulation of railway vehicle systems have included features that enable efficient dynamic analysis of the railway vehicles and vehicle-track interaction [3, 48, 65]. The dynamic behaviour of railway vehicles relates to the motion or vibration of all the parts of the vehicle and is influenced by the vehicle design, particularly the suspension and the track on which the vehicle runs. Due to this issue, several models of simulation schemes were developed in which all the factors affecting the dynamics of a railway vehicle were studied, such as the model developed by Iwinicki and Wickens [25], in which a Matlab computer program was developed in order to validate the results obtained by experimental measurements from a 1/5 scale roller rig used to evaluate the design change of the vehicle suspension system in Manchester Metropolitan University.

The model used in the simulation and implemented in the Matlab code was, a four-axel vehicle with a car body and two bogies have been used. Each bogie has a frame including two wheelsets. All the bogies and the wheelsets are assumed to be rigid bodies connected by mass less suspension elements. The instability in 1/5 roller rig has clearly been detected by the linear MATLAB program used and the model has provided more thorough re-examination of the effects of the errors due to the scaling and finite radius of the roller used, and usefulness of a roller rig analysis of railway behaviour.

During the last decades, the techniques using multibody approaches have evolved from manual graphics art to a highly specialized research field where the kinematics and dynamics of general mechanical systems are analyzed [48, 57, 61]. More efficient and reliable computer codes were developed to allow the formulation and the analysis of the dynamic behaviour of railway systems and solving the equations of motion of mechanical systems included with increasing the degree of complexity. Multibody computational methods can be used to simulate the dynamic effects of vehicle components and the track, and the use of multibody algorithms which allow for the analysis of the nonlinear models, linearization schemes currently employed in railroad vehicle-track can be evaluated [58].

J. Pombo and J. Ambrósio [48, 50] have developed and implemented a computational tool suitable to study the dynamic behaviour of rail guided vehicles in realistic operation conditions. An efficient multibody methodology was suggested and its computational implementation was discussed. The methodology proposed can be summarized in several points: the description of a three dimensional track model used for a roller coaster application [49, 50] and railway vehicle; obtaining realistic track conditions by definition and implementation of the track irregularities; development of a new methodology [51, 52] for the accurate prediction of the location of the contact points between the wheel and the rail surfaces; implementation of several creep force models in order to compute all the tangential forces at the contact patch defined in the wheel-rail interaction area; finally validation of the multibody code presented in this work with modelling of a railway vehicle used by Lisbon metro company, and its performance was studied in real operation conditions and in different operation scenarios.

The numerical results obtained from the computational tool proposed and the results obtained from ADAMS/RAIL computer package used to study and simulate the performance of two railway vehicles in real operation conditions, were compared with experimental tests made on the railway vehicles to validate the obtained results.

Shabana *et al.* [60] presented a nonlinear finite element formulation for modelling the rail structural flexibility in multibody railroad vehicle systems, it was considered to use two types of interpolations in the kinematic equations developed in the study;*the geometry interpolation* and the *deformation interpolation.* The coupling between the rail deformation and geometry, contact coordinates and nonlinear vehicle dynamics was considered.

The main aim of the analysis, was developing a new procedure that allows building complex track model which is used as an input to general purpose multibody computer program used in the dynamic analysis of railroad vehicle systems. This was achieved by the following consequence; first the track geometry was defined in a pre-processor computer program which produces an output *geometry file* including all information about the track elements of the space curve of the track and the left and right rail in terms of position coordinates and rotations defined at the selected nodal points; as a second step, making a finite element model of the track in a finite element pre-processor computer based on the track material properties and geometry and the output is a *finite-element*; finally the *geometry file* and the *finite-element* were used as an input to a general purpose multibody computer program in which the wheel-rail contact models are implemented to study the dynamic behaviour of the railroad vehicle.

E. Meli *et al.* [39] has developed a numerical model which reproduces the complete three-dimensional dynamics of a railway vehicle running on a generic track. The model has been developed with the objective of real-time implementation, in order to use the results to control the actuators of Hardware In the Loop (HIL) test rigs. The numerical model in the test rig has been realised in Matlab – Simulink$^{TM}$ environment. The module was applied to a Benchmark vehicle (The Manchester wagon). A comparison between the obtained results and the those obtained using a commercial multibody software package ADAMS/RAIL was shown. In the work presented by Meli, it was highlighted that the models used evaluate the deformation of the wheel and the rail in the contact zone by means of two different approaches. With respect to the existing models of railway multibody models, its features were more detailed modelling of wheel-rail contact problems. The track geometry description represents the first step in the solution of the dynamic analysis problem. In this step, the pre-processing operation for the track geometry is made using the input data provided by the manufacturing or the industry to be the input for the track geometry program. Afterwards the output data generated in such step provided to the next step which include the multibody dynamic analysis program used to simulate the behaviour of the rail guided vehicle.

The track model used in the current work for the dynamic simulation is presented as a parameterized track in order to obtain the required information of the track. All the kinematic and dynamic parameters are parameterized as a function of the parameter used here which is the distance covered by the vehicle or the track length. There are two main approaches used in the parameterization of the track centreline: the first one uses a combination of analytical segments, straight, transition and plane curve segments to form the track model used in the analysis. The second approach depends on the use of piece wise cubic interpolation schemes to make an interpolation between provided data points representing the track to find the parameterized track centreline curve.

In both approaches it was necessary to define the cant angle of the track to provide a complete definition of the track. In the methodology presented in the work, it is proposed to use analytical segments to form the designed track. The track model introduced in this work which consists of tangent or straight line segment, followed by transition curve segment, and finally the plane curve segment with constant radius $R$. The pre-processed data defined in the track geometry step was provided to a multibody program used for the dynamic analysis of the railroad vehicle, starting with the study and the analysis of a general solid moving along the proposed track. As a next step, the analysis of wheelset moving along the track and then the combination between the two solids in the step of the definition of the train vehicle model proposed in the work in the proceeding context.

J. Pombo [49, 50] developed an appropriate methodology for the accurate description of the track centreline geometry, in the frame work of multibody dynamics. A preprocessing step was made to achieve the computational efficiency for the definition of spatial geometry of the centreline based on the data given by the user. Starting with the roller coaster application, four different interpolation schemes were used in the definition of the spatial track centreline. All the information and the data of the right and left rail were stored in a tabulated manner in which interpolation between the entires were made to obtain the required information. The application was extended to be used in the definition of railway track application in which the rail irregularities were implemented and piecewise interpolation schemes were used to parameterize the track irregularities, as well as the input data, to obtain the track centreline as a function of the track length.

Shabana *et al.* [61] use an analytical track description defined by three step procedure: i)Projection, which defines the planar curve obtained by projecting the track centreline onto the horizontal plane; ii) Development, which defines an elevation angle; iii) Super-elevation, which defines the track cant angle. In his formulation, a relationship between the arc-length of actual curve and arc-length of the projected curve is stated.

Then, the track centreline is defined by providing information about the horizontal curvature as a function of the projected arc-length, the vertical development angle as a function of actual arc-length and the cant angle as a function of the projected arc-length. During the dynamic analysis, the rail space curve are obtained by means of absolute nodal coordinate formulation, leading to an isoperimetric beam element that can be conveniently used to describe curved rigid and flexible rails.

The method considers each rail as a separate body in order to account for relative motion. The method used by Shabana [60] in the definition of the track pre-processing step, basically depends on the definition of the *geometry file*, in which the input data for this program use the industry data such as the curvature, super-elevation and development. The output data of the pre-processing stage was used in the next stage which is the development of a finite element pre-processor computer program. Description of the rail deformation was discussed which based on the finite element floating frame of reference formulation [57]. The use of this formulation allows for arbitrary rigid body displacement of the track structure, it also allows treating the two rails as one body or two separate bodies.

The fundamental component common to all conventional railway vehicles is the wheelset [48]. The movement of the wheelset over the track is characterized by a complex interaction [3, 58] where lateral translation as well as yaw and roll rotations are observed. The formulation of the problem of contact between the wheel and the rail is complex task and has been the subject of several investigations which presented different solutions [51, 52, 59].

Two approaches can be used for solving the problem of wheel-rail contact [61] in railroad dynamics. The first is the commonly called constraint approach, in which non-linear kinematic contact constraint equations are introduced. In this approach, the contact surfaces are represented in a parametric form using the differential geometry methods. The coordinates of the contact points can be predicted online during the dynamic simulation by introducing surface parameters that describe the contact surface geometries.

The second is the elastic approach, in which the wheelset is assumed to have six degrees of freedom with respect to the rails. The local deformation of the contact surface at the contact point is allowed and the normal contact forces are defined using normal contact theories or in terms of assumed stiffness and damping coefficients. This type of approach allows the separation between the wheel and the rail and allows multiple contact points to be managed. One of the main problems related to this approach is the definition of the contact point location online.

In most elastic force models, the three-dimensional contact problem is reduced, for the sake of efficiency, to a two-dimensional problem when the location of the contact points is searched for. Both of these approaches allow the component of the contact force normal to the surfaces to be defined. In the constraint method these forces are calculated as the Lagrange multipliers that, together with the system generalized coordinates and the surface parameters time derivatives, constitute the unknown vector of the differential algebraic equation system that describes the vehicle dynamics.

In the elastic approach, the normal component of the contact force at the contact point is calculated as a function of the penetration between the surfaces. The contact problem can be divided into three distinct but related tasks: the contact geometry, the contact kinematics and contact mechanics. Contact geometry is the problem of defining the location of the contact point on the profiled surfaces taking into account the geometric contact constraints which impose constraints upon the relative displacements and orientations of the contacting bodies. Contact kinematics defines the creepages (normalized relative velocities) at the point of contact. Contact mechanics determines the tangential creep forces and spin moment on the basis of three-dimensional rolling contact theories.

Shabana *et al.* [59] developed a new elastic force contact formulation for the dynamic simulation of the wheel-rail interaction. In this contact formulation, four surface parameters are introduced in order to be able to describe the geometry of the surfaces of the two bodies that come in contact. The method developed in the mentioned investigation exploits features of multibody computational algorithms that allow adding arbitrary first order differential equations.

A differential equation, associated with the rail arc length and expressed in terms of the wheel generalized co-ordinates and velocity, is used to accurately predict the location of the points of contact between the wheel and the rail. This first order differential equation is integrated simultaneously with the dynamic equations of motion of the wheel-rail system, thereby defining the rail arc length travelled by the wheel. This arc length is used with an optimized search algorithm to determine all possible contact regions.

Pombo [51, 52] presented a new general formulation for the accurate prediction of the location of the contact points on the wheel and rail surfaces. The mentioned model has been proposed and implemented in a general multibody program used in the dynamic analysis of railway vehicles. The coordinates of the contact points are predicted online during the dynamic analysis by introducing the surface parameters that describe the geometry of the contact surfaces.

This method was applied to study specific problems inherent to the railway dynamics such as the two points of contact scenario. The methodology to look for the candidates for contact points is fully independent for the wheel tread and for the wheel flange. The used formulation also allowed for investigations related to hunting instability and prediction of wheel climbing, which are very important to study derailment phenomena. The methodology used [48] for the parameterization of the wheel and rail surfaces and for the description of the wheel-rail contact phenomenon was general, since it was able to represent any spatial configuration of the wheels and rails and any wheel and rail profiles, even the ones obtained from direct measurements. Because the wheels are treated separately, the used approach allowed dealing with railway vehicles either with conventional wheelsets, like trains, or with independent wheels, such as in many of the trams in operation.

In the contact model used by E. Meli *et al.* [39] the contact point position is calculated offline by means of a procedure based on the simplex method. This procedure was used to generate a three dimensional lookup table used in the real-time simulation to find the position of the contact points as a function of wheelset-rail relative displacement, described by three coordinates (the lateral wheelset displacement, the roll and yaw wheelset angle). The procedure was numerically sufficiently efficient and allows multiple contact points to be managed.

The method used in this thesis for solving the wheel-rail contact problem is based on the elastic approach, in which the wheel is considered to have six DOF with respect to the rail and the normal contact forces are defined in terms of the indentation between the surfaces and using Hertz contact theory. The main problem encountered when using the elastic approach, is the determination of the contact points. For the sake of efficiency, the three dimensional contact problem is usually reduced to a two dimensional problem [39] when searching for the contact points.

In the dynamic analysis of railway vehicles, the evaluation of the wheel-rail contact forces is repeated many times. Then, short calculation time algorithm should be used taking into account the computational cost of the model implemented in the multibody computer program used in the analysis. The method used in the presented work for calculating the tangential contact forces and moments is Kalker linear theory of rolling contact [30, 31, 33, 58], this theory based on the assumptions that the existence of small creepages and spin creep, and the area of slip is so small that its influence can be neglected. Under these assumptions, the adhesion zone is assumed to cover the entire area of contact. This method doesn't include the saturation effect of the friction force and, therefore, it is limited to contact problems with small creepage values.

Due to the simplicity and computational implementation easiness, Cartesian coordinates are used [61] in this work to formulate the equations of motion of the multibody systems. No kinematic constraints are added to the formulation, to avoid the complexity produced from the Differential Algebraic Equations (DAE) see [16], also the instabilities in the integration process, produced from the substitution of the algebraic equations of the system by their counterpart (ODE), are avoided.

The equations of motion developed in this work are set of Ordinary Differential Equations (ODE) solved by numerical integration algorithms. Two approaches are often used to formulate the dynamic equations of motion of a mechanical systems: the *Newtonian* and the *Lagrangian* approaches. In the *Newtonian* approach, vector mechanics is used to develop the dynamic equations, in this approach the equilibrium position of each body is first studied separately, and it can be used relatively for simple systems and is not suited for the analysis of complex systems such as railroad vehicles.

In the *Lagrangian* approach, scalar quantities such as the virtual work and the kinetic and potential energies are used to develop the equations of motion of the body. In this case there is no need to study the equilibrium of the bodies in the system separately [2, 61]. In this work the *Lagrangian* approach is used to develop the equations of motion of the multibody systems.

The concept of the generalized coordinates is fundamental in the Lagrangian formulation of the equations of motion. For unconstrained motion proposed here in the formulation, six degrees of freedom are used for each body used in the multibody system; three coordinate are used to describe the translation of a point on the body and the other three are used to describe the orientation of the body frame of reference. The parameterization of the finite rotation used in this work is the set of Euler angles, where the orientation of a point on the rigid body is defined using three successive rotations. To avoid singularity problems that may exist in the formulation, the final rotation in the successive rotations proposed was assigned to the higher values of rotation angles.

## 1.4 Scope and work organization

The main objective of the work is to develop an appropriate method using the multibody approach to realize dynamic analysis for the railway vehicle system. The developed computational tool is applied in different application scenarios using a general multibody program developed in MATLAB environment, to achieve the required tasks. The importance of the work can be illustrated in the demonstration of railway system application modelling and make the necessary analysis for the studied systems to analyze the dynamic behaviour of the railway vehicle. The multibody simulation tool developed in this work has some extra capabilities which include:

- The full description of the track configuration used in the simulation of railway applications.
- Including any modifications carried on the track configuration and the use of flexible track models.
- The accurate detection of the contact location of the contact points between the wheel and rail surfaces .
- Implementation of several creep force models to compute the tangential forces which develop in the wheel-rail interface

An important purpose of the developed work is the validation of the presented simulation tool. To achieve this goal, a procedure is followed to validate the results obtained by the simulation tool which includes the following steps: The first step is making a comparison between the results of the simulation tool and the results obtained by different simulation packages used to analyze the dynamic behaviour of the Manchester Benchmark vehicle; the second step is making a comparison between the analysis and results obtained by the developed simulation tool in this work and the results obtained by the commercial simulation package SIMPACK for TGV001 locomotive vehicle in different operation scenarios.

The work proposed here is presented in the following five chapters. The dynamic analysis of railway systems requires the construction of the equation of motion of the vehicle model and the accurate description of the vehicle kinematic structure. For this purpose, a multibody formulation using Cartesian coordinates is presented in Chapter (2). The formulation allows for general three dimensional unconstrained multibody systems to be modelled and the respective equation of motion to be assembled and solved.

Chapter (3) presents an overview of the information needed to perform design analysis of railway vehicles. The track issues and track terminologies are presented as well as the design requests for the track segments characterization including the cant design and the description of the transition curve modelling. The wheel rail contact problem plays an important role in the dynamic analysis of the railway vehicles. A discussion of the theories used to solve the geometrical contact problem is presented. Special emphasis are presented by three wheel-rail contact force models to solve the tangential contact problem, which include the Kalker linear theory, FASTSIM algorithm and finally Polach nonlinear creep force model. The three contact force models are implemented in the multibody simulation tool developed in this work.

Chapter (4) devoted the proposed methodology used to develop the equation of motion for railway multibody systems. Beginning with the definitions of the reference frames used in the formulation, followed by a description of the track model which is defined to be used in the simulation purposes. A wheel-rail contact model is implemented through the proposed algorithm in this work. The model detects the coordinates of the contact points between wheel-rail surfaces in such way that permits the detection of multi contact points. Afterwards, the normal contact forces are calculated at the detected contact areas, then the tangential contact forces are calculated using the creep force models explained in Chapter (3). The mathematical multibody model is presented in Chapter (4) which presents the base model for the developed simulation tool.

In Chapter (5), the main structure of the multibody simulation tool is presented. The simulation tool proposed by this work is used to analyze the dynamic behaviour of railway systems. In the early design of the tool, a simplified contact models are implemented to study the contact between the wheel and rail. This simplified contact model is used in the analysis of a single bogie of the TGV001 locomotive vehicle, negotiating a straight and curved tracks. Afterwards, the simulation is carried out on a complete vehicle with the same operating scenarios. The geometry of the contact profiles of the rail and the wheel is replaced from the simplified to the real geometry using the standard UIC60 rail profile and S1002 wheel profile in the contact model implemented in the multibody program. The simulation tool is then used to analyze the dynamic behaviour of the Manchester Benchmark vehicle. A comparison has been made between the obtained results by the tool proposed in this work and various commercial packages used in the simulation of the Benchmark. To validate the capability of the simulation tool in the analysis of railway systems, another comparison is made between the obtained results for the dynamic behaviour of TGV001 locomotive vehicle and the results obtained by SIMPACK commercial package for railway applications.

Finally, in Chapter (6), overall conclusions are presented and perspective future work in the railway dynamics that are a sequence of this work are suggested.

# Chapter 2

# Multibody system analysis

The mechanical systems included under the definition of multibodies comprise railway systems, robots, spacecraft, automobile suspensions and steering systems, graphic arts, machine tools and others. Normally, the mechanisms used in all these applications are subjected to large displacements, hence, their geometric configuration undergoes large variations under normal service conditions. Moreover, in recent years operating speeds have been increased, and consequently, there has been an increase in accelerations and inertia forces. These large forces inevitably lead to the appearance of dynamic problems that one must be able to predict and control.

Basic concept in any presentation of multibody mechanics is the understanding of the motion of subsystems (bodies or components). The need for a better design, in addition to the fact that many mechanical and structural systems operate in hostile environments, has made necessary the inclusion of many factors that have been ignored in the past. In the systems such as mentioned the neglect of the deformation effect, for example, when these systems are analyzed leads to a mathematical model that poorly represents the actual system

Railway vehicles and roads represent the most important types of the application of the multibody approach. A multibody system can be defined as a collection of rigid and/or flexible bodies interconnected by kinematic joints and/or force elements [48]. The relative motion between the bodies forming the multibody systems is controlled by the kinematic joints. On the other hand, the force elements represent the internal forces which are produced due to the relative motion between the connected bodies.

The dynamic analysis of the multibody systems [1, 2, 57] includes the formation as well as the solution of second order differential equations which present the equations of motion of the rigid or flexible body. The solution of the equations of motion set may involve the solution of a set of algebraic equations which can be formed due to the existence of kinematic constraints.

The number of degrees of freedom DOF is defined for the rigid bodies to be six. For flexible bodies, each body has six DOF plus the generalized flexible coordinates necessary to describe the deformation [48, 57]. The number of coordinates required may be lager than the number of DOF of the multibody system depending on the type of the modelled system as well as the type of the used coordinates.

In the presented work, Cartesian coordinates are used to facilitate the implementation of the developed methodology for the analysis of the multibody systems and to be implemented in the multibody simulation tool presented by the thesis. Lagrangian approach is used, which leads to a number of generalized coordinates equal to the number of DOF of the system, so there is no need to define constraint equations in the formulation of the proposed methodology. By this way, the solution an algebraic set of equations presenting the kinematic constraints, is avoided as well as the need of the stabilization techniques used for the solution of such system of equations [10]. In the presented work the connection between the car body and the bogies as well as the connection between the bogie and the wheelsets can be modelled realistic form by viscous elements without the need of any kinematic constraints.

In the following sections, the multibody basic concepts and formulations are presented. The formulations are adopted in specific form that supports the implementation of such formulations in the proposed methodology used to construct the simulation tool VIA which has been used to realize the dynamic simulation of railway systems.

## 2.1 Multibody systems and joints

A multibody system can be defined as an assembly of two or more rigid bodies joined together imperfectly. A kinematic pair or joint is defined as the imperfect part which is joining two rigid bodies. A joint in multibody system permits certain DOF of the relative motion and restricts or prevents others, based on the joint type. For example, a *revolute* joint allows only relative rotations, *prismatic* joint allows relative rotation and translation as well.

On the other hand, force elements such as spring damper systems can be used to interrelate internal forces between two bodies. Multibody systems can be divided into main branches *open-chain* systems and *closed chain* systems. For example, if a system is composed of bodies without branches, then it is called open-chain other wise it is called closed-chain [2].

## 2.2 Dependent and independent coordinates

For the description of the position and motion of a body, it is necessary to define a set of coordinates that will allow one to completely define the position, velocity and acceleration of the body at all times. The selection of the set of coordinates or parameters that can be used to define the system depending on the modelled system and type of coordinates used.

The selection of the type of the coordinates depends on the easiness of the implementation of the coordinates and whether it is efficient to be used as well as offers high computational. The different dynamic formulations may also benefit from the characteristics of a particular set of coordinates.

The selection of the coordinates type presents the solution of the first problem in a time modelling of multibody systems [26]. Existing two options for the coordinate selection:

- The first is the use of the independent coordinates, whose number coincides with the number of DOF of the multibody system.
- The second is the use of dependent coordinates, whose number is greater than the number of DOF of the multibody system. The selection of such type of coordinates requires the definition of a set of constraint equations equal to the difference between the number of dependent coordinate and the DOF of the system.

Independent coordinates can be very useful to describe with a minimum data set the actual velocities or accelerations and small variations in the position, with the unique limitations that they may lead to the highest computational efficiency. The independent coordinates are used in the presented work in the determination of the position, velocity and acceleration of a rigid bodies forming the multibody systems of railway vehicles.

## 2.3 Kinematic analysis of multibody systems

Kinematics is the study of position, velocity and acceleration of a system without the need of the forces definition. In principle, the analysis of complex systems that has N DOF, it is assumed to use a simple model to obtain realistic solutions. The rigid body concept is a good presentation of a body which doesn't deform under the influence of external forces. In the following sections, the kinematic quantities describing the motion of a rigid body are presented.

### 2.3.1 Frames of reference for a multibody system

In the description of a multibody system, measurable quantities are used to define the motion of the body. These quantities have to be measured with respect to a specific frame of reference [57]. The frame of reference is defined by three orthogonal coordinates rigidly connected in a point which defines the frame of reference origin.

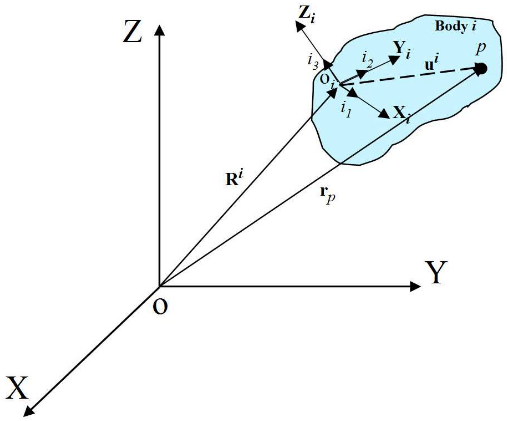

Figure 2.1. *Body corrdinate systems*

In figure (2.1), two types of coordinate systems are defined. The first is the fixed coordinate system (XYZ) which represents the unique standard frame for all the bodies used in a multibody system. The second is the body or the local frame of reference $(\mathrm{X}_i, \mathrm{Y}_i, \mathrm{Z}_i)$ defined for a body $i$. The local frame of reference of the body $i$ translates and rotates with the body; therfore its translation and orientaion with respect to the fixed frame is changing with time.

Assuming that $\mathbf{i}_1$, $\mathbf{i}_2$, $\mathbf{i}_3$ three unit vectors acting along the axes X, Y and Z, respectively. A vector $\mathbf{u}^i$ can be defined in the fixed frame by the following expression:

$$\mathbf{u}^i = u^i\,\mathbf{i}_1 + \mathrm{u}^i\,\mathbf{i}_2 + \mathrm{u}^i\,\mathbf{i}_3 \tag{2.1}$$

The same by defining $\boldsymbol{i}_1, \boldsymbol{i}_2, \boldsymbol{i}_3$ to represent three unit vectors acting along the axes $\mathrm{X}_i, \mathrm{Y}_i$ and $\mathrm{Z}_i$, the unit vector $\mathbf{u}^i$

$$\bar{\mathbf{u}}^i = \bar{u}^i\,\boldsymbol{i}_1 + \bar{u}^i\,\boldsymbol{i}_2 + \bar{u}^i\,\boldsymbol{i}_3 \tag{2.2}$$

By this way, we have two different representations for the same vector $\mathbf{u}^{\mathrm{i}}$ . Since it is easier to define a vector in the local frame of reference, so it is necessary to define the relationship between the local and global frame of reference. A transformation matrix $\mathbf{A}^i$ is defined to demonstrate the orientation of a local reference frame with respect to the fixed frame. So that a unit vector $\mathbf{u}^i$ in the fixed frame of reference can be defined in the local frame by using the following expression

$$\mathbf{u}^i = \mathbf{A}^i\,\bar{\mathbf{u}}^i \tag{2.3}$$

### 2.3.2 Transformation matrix

In many dynamical problems, especially in multibody dynamics [19, 53], it is useful to express the motion of rotating bodies, using a set of inertial frames attached to the bodies and a fixed frame. It is also known that any rotating frame fixed to a rigid body can be related to the fixed inertial frame by three successive rotations. The transformation matrix is obtained by the definition of consecutive rotations with the system rotation angles. So it is necessary to define the rotation matrix used in the formulation of the transformation matrix.

In the kinematic analysis of multibody systems, the bodies forming the system may undergo large relative displacements and rotations. The location of each point on a body $i$ for example forming a component of the multibody system, can be defined by three translational parameters representing the origin of the body $i$ with respect to the fixed frame as seen in figure (2.1), and three relative rotations representing the orientation of body $i$ with respect to the fixed frame.

To represent the concept of the transformation from a local frame to a fixed frame, we first assume that the two frame of references are parallel as seen in figure (2.2)

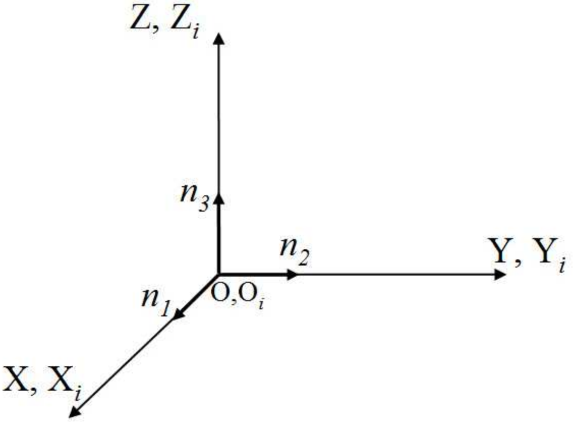

FIGURE 2.2. *Fixed and local frame of references*

A vector **n** is represented by its three orthogonal components along the inertia frame of reference as seen in the previous figure. Assuming that the body frame of reference $(\mathrm{X}_i, \mathrm{Y}_i, \mathrm{Z}_i)$ rotates with an angle $\phi$ about the $\mathrm{X_i}$ axes, so the vector **n** can be defined in the new reference frame $(\mathrm{X}_{i1}, \mathrm{Y}_{i1}, \mathrm{Z}_{i1})$ after the first rotation by the following expressions

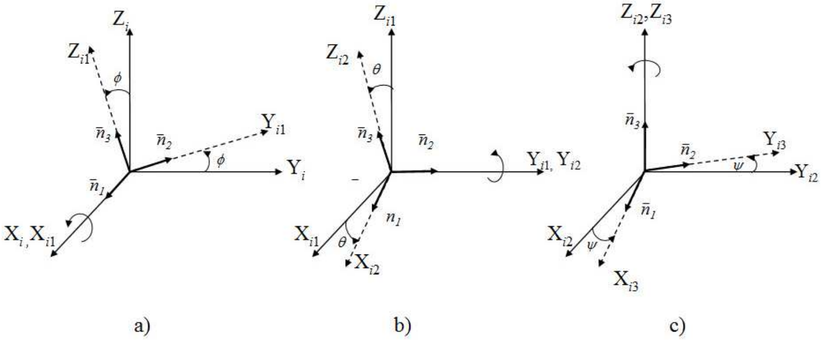
$Z_i$
$Z_{i1}$
$\phi$
$\bar{n}_3$
$\bar{n}_2$
$Y_{i1}$
$\phi$
$Y_i$
$\bar{n}_1$
$X_i, X_{i1}$
a)
$Z_{i1}$
$Z_{i2}$
$\theta$
$\bar{n}_3$
$\bar{n}_2$
$Y_{i1}, Y_{i2}$
$n_1$
$X_{i1}$
$\theta$
$X_{i2}$
b)
$Z_{i2}, Z_{i3}$
$\bar{n}_3$
$\bar{n}_2$
$Y_{i3}$
$\psi$
$Y_{i2}$
$\bar{n}_1$
$X_{i2}$
$\psi$
$X_{i3}$
c)

Figure 2.3. *Successive rotations about the inertial axes of the body*

$$\begin{aligned} n_1 &= \bar{n}_1 \\ n_2 &= \bar{n}_2 \cos\phi + \bar{n}_3 sin\phi \\ n_3 &= -\bar{n}_2 \sin\phi + \bar{n}_3 \cos\phi \end{aligned} \tag{2.4}$$

which can be written in a matrix form as follow:

$$\begin{bmatrix} n_1 \\ n_2 \\ n_3 \end{bmatrix} = \begin{bmatrix} 1 & 0 & 0 \\ 0 & \cos\phi & sin\phi \\ 0 & -sin\phi & \cos\phi \end{bmatrix} \begin{bmatrix} \bar{n}_1 \\ \bar{n}_2 \\ \bar{n}_3 \end{bmatrix} \tag{2.5}$$

which drive us to the following expression

$$\mathbf{n} = \mathbf{A}_\phi \bar{\mathbf{n}} \tag{2.6}$$

where $\mathbf{A}_\phi$ is the matrix of rotation about $X_i$ axis with an angle $\phi$, see figure (2.3a). The same is realized by making a rotation about the $Y_{i1}$ axis with an angle $\theta$ as seen in figure (2.3a), then we obtain

$$\mathbf{n} = \mathbf{A}_\theta \bar{\mathbf{n}} \tag{2.7}$$

where $\mathbf{A}_\theta$ is the rotation matrix defined by the following expression:

$$\mathbf{A}_\theta = \begin{bmatrix} \cos\theta & 0 & -sin\theta \\ 0 & 1 & 0 \\ sin\theta & -sin\phi & \cos\theta \end{bmatrix} \tag{2.8}$$

and finally by making the last rotation about $Z_{i2}$, a new reference fram $(X_{i3}, Y_{i3}, Z_{i3})$ as seen in figure (2.3c) is defined and the vector n can be represented by

$$\mathbf{n} = \mathbf{A}_\psi \bar{\mathbf{n}} \tag{2.9}$$

where the rotation matrix $\mathbf{A}_\psi$is defined by

$$\mathbf{A}_\psi = \begin{bmatrix} \cos\psi & sin\psi & 0 \\ -sin\psi & \cos\psi & 0 \\ 0 & 0 & 1 \end{bmatrix} \tag{2.10}$$

Finally the transformation matrix produced from the successive rotations, explained in figure (2.3), can be obtained by

$$\mathbf{A} = \mathbf{A}_\phi \mathbf{A}_\theta \mathbf{A}_\psi \tag{2.11}$$

where the three angles $\phi$, $\theta$ and $\psi$ are the rotation angles that define the orientation of the frame of reference. The concept of Euler angles is used in the presented work in the way that the rotation sequences are selected by special way explained in Chapter (4) that avoid the singularity problems.

## 2.4 Rigid body kinematics

The term rigid body implies that the deformation of the body under consideration is assumed small such that the body deformation has no effect on the gross body motion. Hence, for a rigid body, the distance between any two of its particles remains constant at all times and all configurations [26, 53, 57]. The motion of a rigid body in space can be completely described by using six generalized coordinates.

In the formulations presented by this work, only rigid bodies are considered. When dealing with rigid body systems, the kinematics of the body is completely described by the kinematics of its coordinate system because the particles of a rigid body do not move with respect to a body-fixed coordinate system. The local position of a particle on the body can then be described in terms of fixed components along the axes of this moving coordinate system.

### 2.4.1 General displacement

The spatial transformation used in this work is expressed by three independent coordinates which present the orientation of a body $i$ that forms a part of the multibody system, with respect to the fixed reference frame. The general displacement of a body $i$ in the multibody system is described by rotation and translation. As seen by figure (2.1), if the body undergoes pure rotation, then a vector $\mathrm{u}^i$ of a point $p$ on the body can be defined by equation (2.3).

If the body $i$ translates in addition to rotation. Then the complete definition of the body motion is described by: the definition of the translation of the body which is defined by the vector $\mathbf{R}^i$ that presents the global position vector of the local reference frame origin; in addition, the definition of the orientation described by the transformation matrix $\mathbf{A}^i$. The global position vector of an arbitrary point on a generic body $i$ is definced by $\mathbf{r}_p$, given by

$$\mathbf{r}_p = \mathbf{R}^i + \mathbf{A}^i\,\bar{\mathbf{u}}^i \tag{2.12}$$

## 2.4.2 Velocity analysis

The absolute velocity vector on a point on a rigid body is obtained by differentiating the position vector with respect to time. From equation (2.12), the velocity vector of an arbitrary point $p$ on the rigid body $i$ is obtained by

$$\dot{\mathbf{r}}_p = \dot{\mathbf{R}}^i + \dot{\mathbf{A}}^i\,\bar{\mathbf{u}}^i \tag{2.13}$$

where $\dot{\mathbf{r}}_p$ is the absolute velocity vector of a point $p$ and $\dot{\mathbf{R}}^i$ is the absolute velocity vector of the origin of the body reference frame.

From the orthogonality property defined for the transformation matrix [57] the following expression can be used

$$\dot{\mathbf{A}}\,\mathbf{A}^{\mathrm{T}} = -\mathbf{A}\,\dot{\mathbf{A}}^{\mathrm{T}} \tag{2.14}$$

A matrix which is equal to the negative of its transpose must be skew symmetric matrix then we find that:

$$\dot{\mathbf{A}}\,\mathbf{A}^{\mathrm{T}} = \tilde{\boldsymbol{\omega}} \tag{2.15}$$

where $\tilde{\omega}$ is a skew symmetric matrix that defines the absolute angular velocity vector of the body in the fixed frame of reference. Equation (2.15), provides another definition of the time derivative of the transformation matrix given by

$$\dot{\mathbf{A}} = \mathbf{A}\,\bar{\tilde{\boldsymbol{\omega}}} \tag{2.16}$$

where $\bar{\tilde{\boldsymbol{\omega}}}$ is a skew symmetric matrix defines the angular velocity vector in the local frame of reference of the body

From both equations (2.15)and (2.16) the absolute angular velocity of the system is given by

$$\tilde{\boldsymbol{\omega}} = \mathbf{A}\,\bar{\tilde{\boldsymbol{\omega}}}\,\mathbf{A}^{\mathrm{T}} \tag{2.17}$$

Substituting the vector $\dot{\mathbf{A}}^i\,\bar{\mathbf{u}}^i$ defined in equation (2.13) by the obtained expressions for the time derivative of the transformation matrix

$$\begin{gathered}\dot{\mathbf{r}}_p = \dot{\mathbf{R}}^i + \tilde{\boldsymbol{\omega}}\boldsymbol{A}^i\,\bar{\mathbf{u}}^i \\ \dot{\mathbf{r}}_p = \dot{\mathbf{R}}^i + \mathbf{A}\,\bar{\tilde{\boldsymbol{\omega}}}\,\bar{\mathbf{u}}^i\end{gathered} \tag{2.18}$$

### 2.4.3 Acceleration analysis

The absolute acceleration of an arbitrary point on a rigid body in multibody systems can be obtained by differentiating the velocity vector obtained by equation (2.13) which can be given by

$$\ddot{\mathbf{r}}_p = \ddot{\mathbf{R}}^i + \boldsymbol{\omega}^i \times \left(\boldsymbol{\omega}^i \times \mathbf{u}^i\right) + \boldsymbol{\alpha}^i \times \mathbf{u}^i \tag{2.19}$$

where $\ddot{\mathbf{R}}^i$ is the absolute acceleration of the origin of the body reference, $\omega^i$ and $\alpha^i$ are, respectively, the angular velocity and angular acceleration vectors defined in the global coordinate system, and $\mathbf{u}^i$ can be replaced by the expression given by equation (2.3) then we find that

$$\ddot{\mathbf{r}}_p = \ddot{\mathbf{R}}^i + \mathbf{A}^i \left[\bar{\boldsymbol{\omega}}^i \times \left(\bar{\boldsymbol{\omega}}^i \times \bar{\mathbf{u}}^i\right)\right] + \mathbf{A}^i \left(\bar{\boldsymbol{\alpha}}^i \times \bar{\mathbf{u}}^i\right) \tag{2.20}$$

where $\bar{\boldsymbol{\omega}}^i$ and $\bar{\boldsymbol{\alpha}}^i$ are, respectively, the angular velocity vector and angular acceleration vector defined in the body coordinate system.

The vector $\ddot{\mathbf{r}}_p$ representing the acceleration of an arbitrary point on a rigid body in multibody system can be written on the form

$$\ddot{\mathbf{r}}_p = \mathbf{a_l} + \mathbf{a_c} + \mathbf{a_t} + \mathbf{a_n} \tag{2.21}$$

where

$$\begin{aligned} \mathbf{a_l} &= \mathbf{A^i}\,\ddot{\mathbf{r}}_\mathbf{p} \quad ; \quad \mathbf{a_c} = \mathbf{2}\,\boldsymbol{\omega}^\mathbf{i} \times \mathbf{v_G} \\ \mathbf{a_t} &= \boldsymbol{\alpha}^\mathbf{i} \times \mathbf{r_p} \quad ; \quad \mathbf{a_n} = \bar{\boldsymbol{\omega}}^\mathbf{i} \times \left(\bar{\boldsymbol{\omega}}^\mathbf{i} \times \mathbf{r_p}\right) \end{aligned} \tag{2.22}$$

$a_l$ represents the local acceleration defined in the global coordinate system. $a_c$ is the *Coriolis* acceleration, $a_t$ is the *tangential* acceleration and $a_n$ is the normal acceleration. $\mathbf{v}_G$ is the velocity vector of the centre of mass of the body.

By the definition of the previous acceleration components, we can get the magnitudes and the direction of each acceleration from the following table

| **Component** | **Magnitude** | **Direction** |
|---|---|---|
| $\mathbf{a_n}$ | $\dot{\theta}^2 r$ | Along the vector $(-\mathbf{r})$ |
| $\mathbf{a_t}$ | $\ddot{\theta}\, r$ | Perpendicular to both $\boldsymbol{\alpha}$ and $\mathbf{r}$ |
| $\mathbf{a_c}$ | $2\,\dot{\theta}\, v_G$ | Perpendicular to both $\boldsymbol{\omega}^i$ and $\mathbf{v}_G$ |

TABLE 2.1. *Acceleration components difined for the acceleration of an arbitrary point on a rigid body*

where $v_G$ is the norm of the velocity vector $\mathbf{v_G}$ and $r$ is the length of the vector $\mathbf{r}$.

## 2.5 Dynamic analysis of multibody systems

The dynamic analysis of multibody systems consists in the study of their motion as a response to external applied forces and moments. The motion of the system is generally not prescribed. The calculation of the body motion is one of the principle objectives of the dynamic analysis. This type of analysis also provides a process to estimate external forces which depends on the relative position between the system components, such as those generated by springs, dampers and actuators. Also external forces which generated as a consequence of the system interaction with the surrounding environment, such as contact and friction forces, are considered. Another significant result provided by this type of analysis, is the calculation of the internal reaction forces, generated in the kinematic pairs.

### 2.5.1 Generalized coordinates

The generalized coordinates are defined as the set of variables that define the multibody system configuration. A rigid body in the space is defined by using three coordinates that describe the translation of the particle with respect to the three axes of the fixed frame. In addition to the translational set of coordinates, it is important to define other three coordinates that define the orientation of the body with respect to the fixed frame of reference. Once the set of coordinates defining the six independent coordinates for the rigid body is identified, the global position of an arbitrary point on the body can be expressed in terms of these coordinates.

A multibody system as shown in figure (2.1), which consists of $n_b$ interconnected rigid bodies, requires $6\,n_b$ coordinates in order to describe the system configuration in space. To understand and control the motion of the multibody system, it is important to identify a set of independent generalized coordinates called degrees of freedom (DOF).

For convenience, we will use the notation $\mathbf{q}^i$ to denote the generalized coordinates of the body reference, that is

$$\mathbf{q}^i = \begin{bmatrix} \mathbf{R}^{i\,\mathrm{T}} & \boldsymbol{\theta}^{i\,\mathrm{T}} \end{bmatrix}^{\mathrm{T}} \tag{2.23}$$

where $\mathbf{R}^i$ represents the set of the translational generalized coordinates, and $\theta^i$ defines the set of the generalized rotational coordinates of the rigid body

### 2.5.2 Virtual work

In the following section, the generalized forces are introduced by the definition of the principle of the virtual wok in both static and dynamic analysis

In case of static equilibrium, we assume a system composed of $n_p$ particles in three dimensional space. A force vector $\mathbf{F^i}$ represents the sum of the external and constraint forces affecting particle $i$.

$$\mathbf{F}^i = \mathbf{F}_e^i + \mathbf{F}_c^i \tag{2.24}$$

In the presented work, no kinematic constraint is used, so that the term of the constraint forces is null then $\mathbf{F}^i = \mathbf{F}_e^i$. In case of static equilibrium we find that

$$\mathbf{F}_e^{i\,\mathrm{T}}\, \delta\mathbf{r}^i = 0 \tag{2.25}$$

then the virtual work of the external applied forces is calculated by

$$\delta W = \mathbf{F}_e^{i\,\mathrm{T}}\, \delta\mathbf{r}^i = 0 \tag{2.26}$$

Equation (2.26) is the principle of virtual work for static equilibrium.

The displacement of a particle $i$ can be defined by means of the particle generalized coordinates as

$$\mathbf{r}^i = \mathbf{r}^i\left(\mathbf{q}^i\right) \tag{2.27}$$

where $\mathbf{q}^i$ is the set of generalized coordinates defined for the system. Then the virtual work of an arbitrary point $i$ can be written on the form

$$\delta\mathbf{r}^i = \sum_j^n \frac{\partial \mathbf{r}^i}{\partial q_j}\, \delta q_j \tag{2.28}$$

where $n$ is the number of the generalized coordinates of the system. by substituting in equation (2.26), then the virtual work can be defined as

$$\delta W = \sum_i^{n_p} \sum_j^n \mathbf{F}_e^{i\,\mathrm{T}}\, \frac{\partial \mathbf{r}^i}{\partial q_j}\, \delta q_j \tag{2.29}$$

In the case of dynamic equilibrium, according to Newton's second law. The resultant force applied on a particle $i$ is equal to the rate of change in the momentum of the particle, that is,

$$\mathbf{F}^i - \dot{\mathbf{P}}^i = 0 \tag{2.30}$$

where $\mathbf{P}^i$ is the momentum of a particle $i$. When the particle is assumed to be in equilibrium, then

$$\sum_i^{n_p} \left(\mathbf{F}^i - \dot{\mathbf{P}}^i\right)^{\mathrm{T}} \delta\mathbf{r}^i = 0 \tag{2.31}$$

The force vector $\mathbf{F}^i$ is replaced with the external forces only applied to the system as the constraint forces term is null

$$\sum_{i}^{n_p} \left(\mathbf{F}_e^i - \dot{\mathbf{P}}^i\right)^{\mathrm{T}} \delta \mathbf{r}^i = 0 \tag{2.32}$$

substituting with the virtual displacement value obtained by equation (2.28) we find that

$$\delta W = \sum_{i}^{n_p} \sum_{j}^{n} \left(\mathbf{F}_e^i - \dot{\mathbf{P}}^i\right) \frac{\partial \mathbf{r}^i}{\partial q_j} \delta q_j \tag{2.33}$$

The generalized forces are introduced by applying the principle of virtual work in both cases of static and dynamic analysis. The virtual work and generalized forces can also be derived for rigid body systems with constraints. This can be achieved by identifying the system-independent coordinates, and try to determine the generalized forces associated with these coordinates. A systematic approach that can be followed is to develop firstly the virtual work in terms of the system Cartesian coordinates that can be written, from both equations (2.29) and (2.33), in vector form as

$$\delta W = \mathbf{Q}^{\mathrm{T}} \delta \mathbf{q} \tag{2.34}$$

where $\mathbf{q}$ is the vector of system independent coordinates or degrees of freedom and $\mathbf{Q}$ is the vector of generalized forces associated with the coordinates $\mathbf{q}$.

### 2.5.3 Equations of motion of multibody system

Lagrange introduced the Lagrange function which depends on a set of generalized coordinates and velocities of a system [56]. The general work of Euler and Lagrange also led to the principle of least action, where differential equations are obtained by minimizing the action over an interval of time. The Lagrange equations represent a set of nonlinear $n$ second-order differential equations known as equations of motion. Lagrange's equation of motion can be written as

$$\frac{d}{dt}\left(\frac{\partial T^i}{\partial \dot{\mathbf{q}}^i}\right) - \frac{\partial T^i}{\partial \mathbf{q}^i} - \mathbf{Q}^{\mathrm{T}} = 0 \tag{2.35}$$

where $T^i$ is the total kinetic energy of the system, which can be defined by the following expression

$$T^i = \frac{1}{2} (\dot{\mathbf{q}}^i)^{\mathrm{T}} \, \mathbf{M}^i \, \dot{\mathbf{q}}^i \tag{2.36}$$

where the mass matrix $\mathbf{M}^i$ is given by

$$\mathbf{M}^i = \begin{bmatrix} \mathbf{m}^i_{RR} & \mathbf{m}^i_{R\theta} \\ \text{Symmetric} & \mathbf{m}^i_{\theta\theta} \end{bmatrix} \tag{2.37}$$

where the matrix $\mathbf{m}^i_{RR}$ associated with the translation of the body reference is a constant diagonal matrix, the matrix $\mathbf{m}^i_{R\theta}$ represents the inertia coupling between the translation and rotation of the body reference and the matrix $\mathbf{m}^i_{\theta\theta}$ associated with the rotational coordinates of the body reference

In the special case in which the origin of the coordinate system of the rigid body is rigidly attached to the centre of mass, the sub-matrix $\mathbf{m}^i_{R\theta}$ is the null matrix and the body $i$ mass matrix reduces to

$$\mathbf{M}^i = \begin{bmatrix} \mathbf{m}^i_{RR} & 0 \\ 0 & \mathbf{m}^i_{\theta\theta} \end{bmatrix} \tag{2.38}$$

by substituting with the value of the generalized coordinate vector expressed by equation (2.23), the total kinetic energy of the system can be written on the form

$$T^i = \frac{1}{2}(\dot{\mathbf{R}}^i)^{\mathrm{T}}\,\mathbf{M}^i\,\dot{\mathbf{R}}^i + \frac{1}{2}(\dot{\boldsymbol{\theta}}^i)^{\mathrm{T}}\,\mathbf{M}^i\,\dot{\boldsymbol{\theta}}^i \tag{2.39}$$

substituting in the Lagrange's equation of motion, then we can define the quadratic velocity vector as

$$\frac{\partial T^i}{\partial \dot{\mathbf{q}}^i} = [(\dot{\mathbf{R}}^i)^{\mathrm{T}}\,\mathbf{m}^i_{RR} \quad (\dot{\boldsymbol{\theta}}^i)^{\mathrm{T}}\,\mathbf{m}^i_{R\theta}] \tag{2.40}$$

which can be written on the form

$$\frac{d}{dt}\left(\frac{\partial T^i}{\partial \dot{\mathbf{q}}^i}\right) = [(\ddot{\mathbf{R}}^i)^{\mathrm{T}}\,\mathbf{m}^i_{RR} \quad \left((\ddot{\boldsymbol{\theta}}^i)^{\mathrm{T}}\,\mathbf{m}^i_{\theta\theta} + (\bar{\boldsymbol{\omega}}^i)^{\mathrm{T}}\bar{\mathbf{I}}^i_{\theta\theta}\,\dot{\bar{\mathbf{G}}}^i\right)] \tag{2.41}$$

where $\bar{\boldsymbol{\omega}}^i$ is the angular velocity vector defined in the body coordinate system and $\bar{\mathbf{G}}^i$ is the matrix that relates the angular velocity vector to the time derivatives of the orientation coordinates[1] and $\bar{\mathbf{I}}^i_{\theta\theta}$ is the mass moment of inertia matrix.

The derivative of the kinetic energy with respect to the generalized coordinates $\mathbf{q}^i$ is

$$\frac{\partial T^i}{\partial \mathbf{q}^i} = \frac{1}{2}\frac{\partial}{\partial \mathbf{q}^i}\left[(\dot{\boldsymbol{\theta}}^i)^{\mathrm{T}}\,\mathbf{m}^i_{\theta\theta}\dot{\boldsymbol{\theta}}^i\right] \tag{2.42}$$

Substituting with equation(2.41) and equation (2.42) in the Lagrange's equation (2.35), we obtain two uncoupled matrix equations. The first equation associated to the translation of the rigid body $i$ centre of mass which can be defined by the following equation

---

[1] Appendix **A**

$$\mathbf{m}^i_{RR}\ddot{\mathbf{R}}^i = \bar{\mathbf{Q}}^i_R \tag{2.43}$$

while the second equation associated with the rotation of the body, is obtained by the following expression

$$\mathbf{m}^i_{\theta\theta}\ddot{\theta}^i = \bar{\mathbf{Q}}^i_\theta - 2\,\dot{\bar{\mathbf{G}}}^i\,\bar{\mathbf{I}}^i_{\theta\theta}\,\bar{\boldsymbol{\omega}}^i \tag{2.44}$$

where subscripts $R$ and $\theta$ refer, respectively, to the body translation and rotation. The set of equations (2.43) and (2.43) represent the deferential equation of motion of a rigid body in the multibody system.

The multibody formulation is introduced using a general approach for the dynamic analysis of non constrained multibody system. The formulation presented in this chapter is detailed for the type of coordinates adopted. The mathematical modelling of multibody systems presented in this chapter is used in the development of the mathematical model of the methodology proposed in chapter (4) for the dynamic analysis of railway systems.

# Chapter 3

# Dynamics of railway systems

## 3.1 Introduction

The study of the railroad vehicle systems and the dynamic analysis of railway vehicle systems generally divided into two main stages. The first stage is a pre-processing stage at which the track geometry and the wheel and rail profiles are defined. The second stage is developing the equations of motion of the multibody vehicle system, in this stage all the parameters required to define the wheel and rail surfaces are defined as well as the track geometry parameters which enter the formulations of the contact conditions and the system equations of motion.

The first stage in the methodology proposed for the analysis of a railroad vehicle, is to define the track geometry and make modeling for the track to provide the required data in the next step of the dynamic analysis of the problem [61]. The introduction of the track irregularities is not considered here in the current work. The track models for multibody analysis must be in the form of parameterized curves, where the nominal geometry is obtained as a function of a parameter associated to the track curve length [48].

The parameterizations of the track can be done by two approaches. The first approach is the use of analytical segments for the track parametrization including the definition of the track. This is generally done by putting together straight and circular curves interconnected by transition track segment that ensure the continuity of the first and second derivatives of the railway in the transition points. The transition curve definition and popular curves used in the mathematical representation of the transition curve are presented in this Chapter. In railway dynamics, solving the problem of wheel-rail contact constitutes a key step in obtaining results in relation to the vehicle's dynamic behaviour. Precise calculation of wheel-rail contact parameters requires a high computational cost, since this calculation has to be made in each step of the time integration.

The localization of the contact point presents the first step in the solution of the contact problem, followed by the determination of the contact kinematics in which the creepages are calculated at the contact area located at the wheel rail interface. Finally, the contact force determination presents the final step in the solution of the contact problem, by finding the normal and tangential contact forces affecting the contact patch.

A description of the solution of geometrical contact problem can be presented by three different methods, namely, *The visible profile method* [36, 37], *Contact points detection using geometric relational properties* [48] and finally *the wheel rail differential contact method* [39], are included in this chapter to highlight the importance of the precise determination of the contact problem in the railway dynamic analysis. The solution of the geometrical contact problem in the presented work is defined in Chapter (4) by means of contact algorithm based on the virtual penetration between the contact surfaces.

The solution of dynamic contact problem is presented in this Chapter by the definition of normal contact force determination which in our case is presented by Hertz normal contact model. Finally, the tangential contact forces in the current work are solved by means of three different algorithms implemented in the dynamic multibody code used to realize the dynamic simulation of the railway vehicles.

In the early stages of the development of the proposed multibody methodology presented in Chapter (4), kalker linear contact theory is used to calculate the tangential forces between the wheel and rail contact profiles. The FASTSIM algorithm is implemented in the multibody simulation tool proposed in the current work. FASTSIM is a simple and fast program that calculates the total force in rolling contact from given creepages and spin.

The last algorithm used is Polach nonlinear creep force law which is used to study the tangential contact problem. The method is used to analyze the contact forces produced in the interaction between the wheel and rail. It also allows the determination of nonlinear creep forces taking into account the effect of the spin creepage. Moreover, it offers lower computational cost compared with FASTSIM algorithm. This method has been tested and used in different programs and simulation tools with good results in the dynamic analysis of railway systems. Polach method is implemented in the current work and the main characteristics and theoretical development of the algorithm are presented in this Chapter.

## 3.2 Track geometric description

The accurate description of the track is essential for the dynamic analysis of railway systems. The dynamic behaviour of the railway vehicles is dependent on the track conditions, also the loads transmitted to the vehicle from the track and the corresponding forces transmitted from the vehicle to the track are mainly depending on the track geometry. The track pre-processor uses industry input data such as the curvature, super -elevation and development [60]. Then all the necessary data required as input informations for the track model are provided in a separated input data file, and then the output data of the track geometry programs will be provided to the dynamic simulation program. In the following section, some of the physical aspects relevant to the design geometry of the track are presented.

## 3.2.1 Terminology of railway tracks

In this section, the basic definitions and terminology used in the railway systems are discussed as well as the design issues required for the common track systems

### 3.2.1.1 Track gauge

Generally the track gauge G figure (3.1) is defined as the distance between the two rails, more specifically the distance between the inside railheads measured 14 mm below the surface of the rail [15]. The measure of the track gauge was taken 14 mm below so that the measurement is less influenced by lateral wear on the rail head.

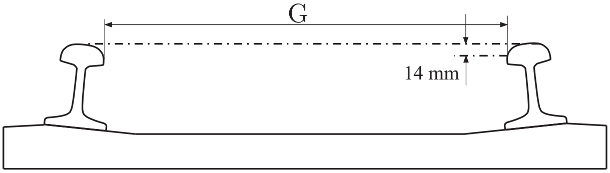

Figure 3.1. *Track gauge description*

The following table presents a summary for the track gauge types and the countries where they are applied:

| Track Gauge Type | Measured Value (mm) | Examples for countries where it is found |
|---|---|---|
| Narrow Gauge | 750 | Parts of Indonesia |
| | 1000 | Switzland |
| | 1067 | Suoth Africa - Japan -Indonesia |
| Standard Gauge | 1435 | Most commonly used |
| Broad Gauge | 1524 | Russia - Finland |
| | 1600 | Ireland - Australia |
| | 1668 | Spain - Portugal |

Table 3.1. *Variation of track gauge type*

#### 3.2.1.2 Horizontal curves

The railway tracks are in general composed of straight (or tangent) sections, transition curves and circular curves. The horizontal curves have constant radius and are defined in the tracks described in the horizontal plane. The radius of the curve used is defined with respect to the track centreline as shown in figure (3.2).

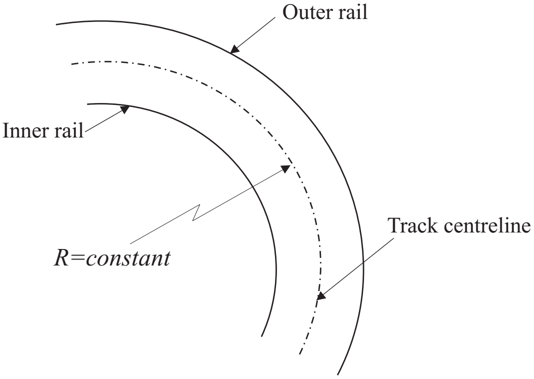

Figure 3.2. *Horizontal circular curve*

#### 3.2.1.3 Track width

Track width $D$ figure (3.4), is defined as the distance between the points of contact of the mean wheel circles with the rails, the nominal value for the track width is 1500 mm.

#### 3.2.1.4 Super-elevation

Track super-elevation $h_t$ is defined as the vertical distance between the right and left rail as shown in figure (3.4)

#### 3.2.1.5 Track grad

Track grad is defined as the ratio between the vertical elevation and the longitudinal distance.

### 3.2.2 Cant angle definition in the track model

When travelling in horizontal curves, railway vehicles are influenced by centrifugal forces, which act in a direction away from the centre of the curve to over turn the

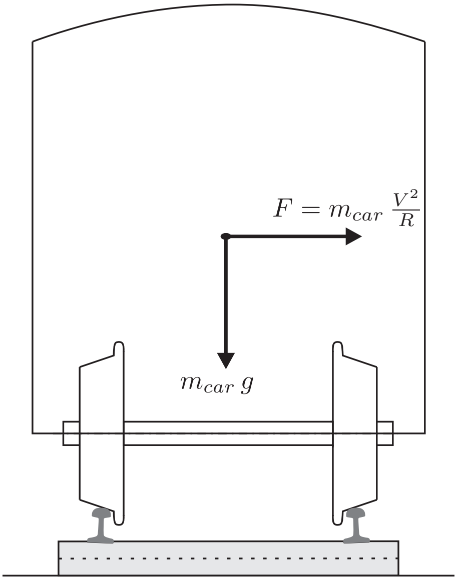

Figure 3.3. *Centrifugal force affecting a circulating railway vehicle*

vehicle. The sum of a vehicle weight and its centrifugal forces produced a resultant force directed to the outer rail see figure (3.3). When exceeding the friction force limit acting in the opposite direction, additional load is added on the outer rails due to contact between the wheel flange and the interior face of the rail producing the following risks:

- Derailment risks.
- Railway track ripping.
- Premature wear of rails specially the outer rail profile.
- Affecting the passengers ride comfort.

In order to counteract this force, the outer rail in a curve is raised [24, 48, 61]. The difference in height between the outer and the inner rail plane is called the cant or the super elevation $h_t$, which can be defined as shown in figure (3.4).

Then the cant angle $\phi$ as shown in the figure can be defined as [48, 61]

$$\phi = \arcsin\left(\frac{h_t}{D}\right) \tag{3.1}$$

The cant angle for zero track plane acceleration, at a given radius of curvature $R$ and vehicle speed $V$ can be defined as equilibrium cant angle [48] which can be found by

$$\phi_{eq} = \arctan\left(\frac{V^2}{R\,g}\right) \tag{3.2}$$

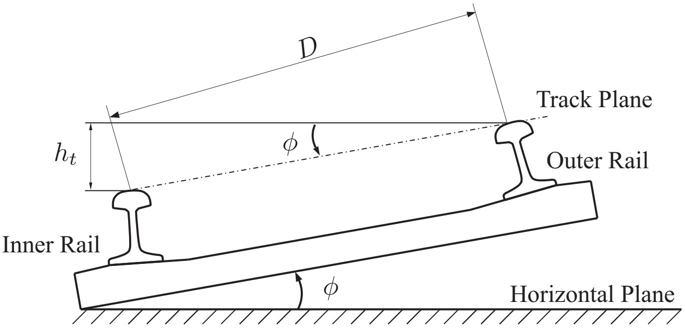

Figure 3.4. *Cant and Cant angle*

To define the track cant angle, we have first to define the plane at which the cant angle is defied in. So in the case of the flat tracks, the horizontal plane is the plane at which the cant angle is defined. But in case of the full spatial geometry track model, it is proposed to use the osculating plane Fig.(3.5), to be the reference plane at which the cant angle should be defined [50, 51].

### 3.2.3 Spatial track centreline

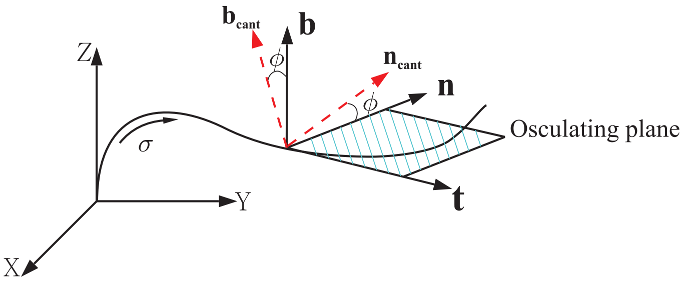

Figure 3.5. *Frenet Principle vectors and spatial definition of the cant angle*

In this section we may use the definitions of the principle vectors $(\mathbf{t} \ \mathbf{n} \ \mathbf{b})$ [39, 50], which are the tangent, normal, and binormal vector, respectively, defining Frenet frame that is attached to the spatial curve presenting the track centreline and we find the tangent, normal and binormal unit vectors. Finding the relations between them after the rotation with the cant angle ($\phi$), the vectors will be defined as $(\mathbf{t}_{\mathbf{cant}} \ \mathbf{n}_{\mathbf{cant}} \ \mathbf{b}_{\mathbf{cant}})$. It has to be said that if piecewise cubic interpolation was used to make the parameterization of the spatial curve then the user must set the cant angle corresponds to each one of the nodal points which is used to parameterize the track. If it supposed to use the analytical representation of the track model using analytical functions, the user must set the cant angle at the extremities of each track segment [48, 51]. In our case, the cant angle can be defined by the angle of rotation of the track frame of reference about the $X_T$-axis pointing to the direction of motion of the railway vehicle figure (3.6).

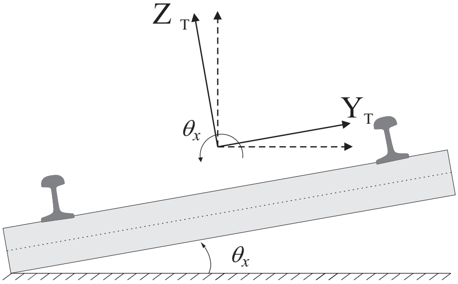
$Z_T$
$Y_T$
$\theta_x$
$\theta_x$

Figure 3.6. *Railway track cant angle*

### 3.2.4 Transition curves and super-elevation ramps

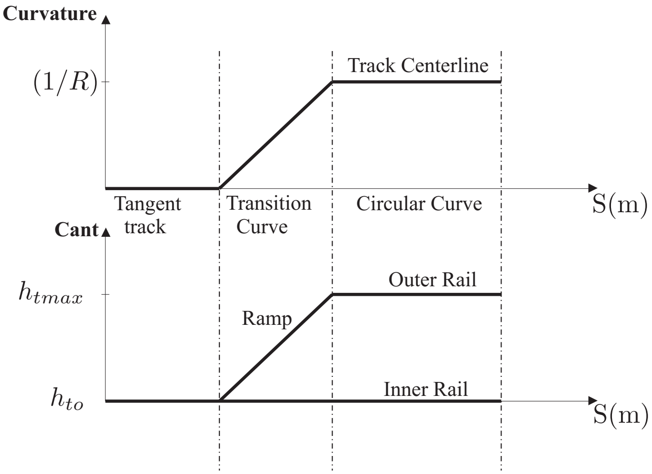
Curvature
$(1/R)$
Track Centerline
Tangent track
Transition Curve
Circular Curve
S(m)
Cant
$h_{tmax}$
Outer Rail
Ramp
$h_{to}$
Inner Rail
S(m)

Figure 3.7. *Transition Curves and Super-elevation Ramps*

When trains operated at normal speeds, a circular curve with cant cannot be followed directly by a tangent track, and vice-versa [48]. A transition curve is needed to guarantee the curvature continuity and minimize the change in the lateral acceleration of the vehicle. In general transition curves and super-elevation ramps figure (3.7), have the same start and the same end points.

The curvature and the cant in transition curves corresponds to each other. The length of the transition curves varies directly with the amount of curve super-elevation required. The maximum allowable rate of change of the super-elevation determines the minimum length of the transition for a given vehicle speed and curve super-elevation.

Figure (3.7) illustrates the main stages used in the simulation proposed in the current work, where a track composed of three stages is used. The track proposed in the thesis presents a simple configuration which composed of a straight track segment followed by a transition curve connecting the straight track with a circular curve with constant radius. $R$ is the radius of curvature used in each stage which has an infinite value for the straight track and increases during the transition stage until it reaches the constant value at the circular curve stage as shown. $h_{to}$ and $h_{tmax}$ are the height of the track in the straight stage and the final or circular curve stage respectively

#### 3.2.4.1 Transition curves

The transition curves can be defined as the curves adopted to change the track radius of curvature between the straight track to circular curves. The curvature radius of transition curves decreases from infinity value at the straight track stage to the value of the circular curve radius $R$ in the form that the cant height is changing according to the following relation

$$h = \frac{D}{g}\frac{V^2}{R} \tag{3.3}$$

where $h$ is the cant height. $D$ is the track width. $V$ is vehicle velocity. The transition curves should have the following properties when used in the connection between straight and circular curves as well as the change from circular to straight curve:

- The transition curve has to be tangent to both straight line and circular curve arc.
- The curvature value of transition curve is null at the straight stages.
- The curvature value of transition curve should equal to the curvature value of the circular curve stage ($1/R$).
- The transition curve should have a progressive curvature between straight and circular curve stages.

#### 3.2.4.2 Transition curves in the space

Figure (3.8) depicts a curve in the space. The curve can approximately be replaced by its projection in the plane ($OXY$). This means taking the projection $OA1$. The radius of curvature takes the corresponding value of curvatures at this point. The plane ($OXZ$) is considered to be the elevation and the plane ($OXY$) is considered to be the top plane. In the presented curve in figure(3.8), the circular curve starts at the point $A$. At the point B the equilibrium conditions are always verified between the centrifugal force and the cant height calculated by equation (3.3).

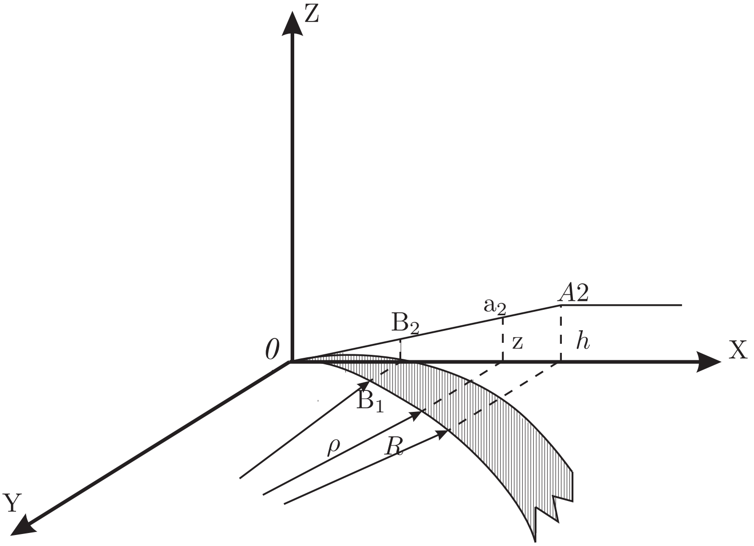

Figure 3.8. *Spatial presentation of the transition curve*

### 3.2.4.3 Mathematical definition of the transition curves

Existing various forms to define the transition curves used to connect the different track segments. In the following section, the popular curves used to define the transition curves are presented.

I) Clothoid curves

The equation that presents the planer definition of the Clothoid can be written in the form

$$\frac{y''}{(1+y'^2)^{\frac{3}{2}}}K_1 = s = \int_0^x \left(1+y'^2\right)^{\frac{1}{2}}dx \tag{3.4}$$

By solving the previous equation we can obtain:

$$\begin{aligned} y &= \tfrac{s^3}{6K_1} - \tfrac{1}{336}\tfrac{s^7}{K_1^3} + \tfrac{1}{6240}\tfrac{s^{11}}{K_1^5} - \ldots\ldots.. \\ x &= s - \tfrac{1}{40}\tfrac{s^5}{K_1^2} + \tfrac{1}{3456}\tfrac{s^9}{K_1^5} - \ldots.. \end{aligned} \tag{3.5}$$

If only the first term in the equations presenting the cubic term is selected, the following expression is obtained

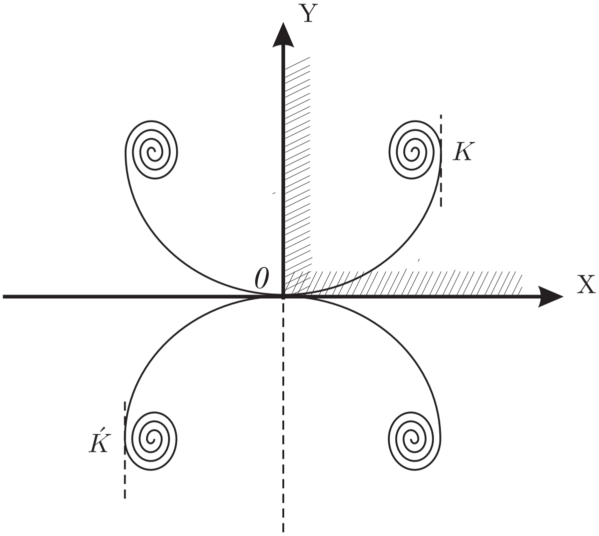

Figure 3.9. *Planar definition of the Clothoid curve*

$$y = \frac{x^3}{6K_1} \tag{3.6}$$

II) Oval curves

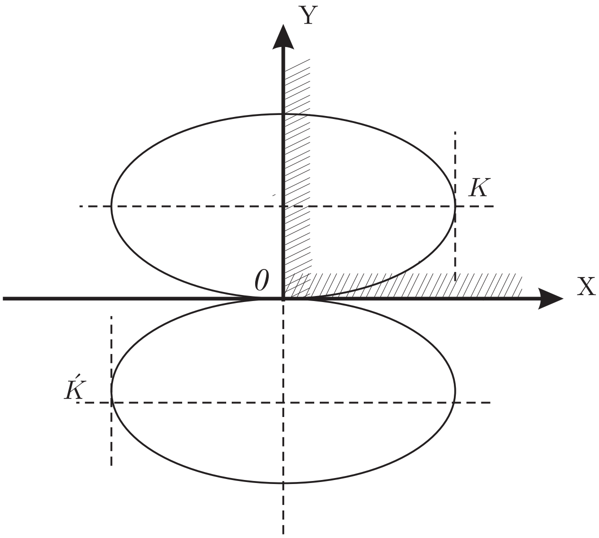

Figure 3.10. *Planar definition of Oval curve*

This type of curves can be represented by the following equation

$$\frac{y''}{\left(1+y'^2\right)^{3/2}}K_2 = x \tag{3.7}$$

substituting with the following variables in the previous equation

$$Y = \frac{y}{\sqrt{2}K_2} \qquad ; \qquad X = \frac{x}{\sqrt{2}K_2} \tag{3.8}$$

we get the following

$$Y = \frac{X^3}{3}\left(1 + \frac{1}{2}\frac{3}{4}X^4 + ...... + \frac{1.3.....(2n-3)(2n-1)}{1.4....(2n-2)\,2n\,(4n+3)}X^{4n}\right) \tag{3.9}$$

The same as explained in the previous sections, the first term is selected only giving the expression

$$y = \frac{x^3}{6K_2} \tag{3.10}$$

III) Lemniscate curves

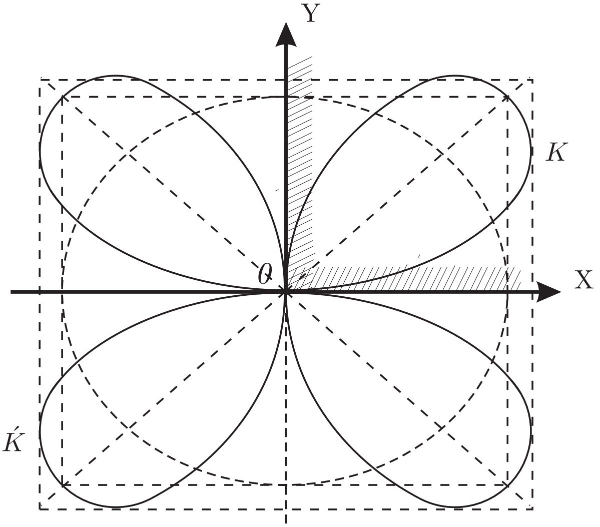

Figure 3.11. *Planar definition of Lemniscate curve*

This type of curves used in the planer definition of the transition curves as seen in figure (3.11) is represented mathematically by the following equation

$$\frac{y''}{(1+y'^2)^{\frac{3}{2}}}K_3 = \left(x^2+y^2\right)^{\frac{1}{2}} \tag{3.11}$$

by substituing with the following expressions in the previous equation

$$Y = \frac{y}{(2K_3)^{\frac{1}{2}}} \qquad ; \qquad X = \frac{x}{(2K_3)^{\frac{1}{2}}} \tag{3.12}$$

we get the following expression

$$Y = \frac{X^3}{3}\left(1 + 2\frac{X^4}{9} + 9\frac{X^8}{9^2} + 52\frac{X^{12}}{9^3} + 343\frac{X^{16}}{9^4} + ..\right) \tag{3.13}$$

The same for the Lemniscate curve, we take the first term in the equation, then the curve is defined by

$$y = \frac{x^3}{6K_3} \tag{3.14}$$

After the definition of the different types of the transition curves, it is necessary to highlight that the selected transtion curve in the presented work is the Clothoid curve. By the complete definition of the track used in the multibody code implemented in the program used in simulation purpposes of the rail way vehicles, it was necessay to define the wheel interaction phenomenon which presents one of the important steps in the study of the dynamics of railroad vehicles. In the following section, a definition of the contact problem is presented as well as the proposed methodologies used to solve both normal and tangential contact problems.

## 3.3 Wheel-rail interaction phenomenon

The importance of the modelling of the contact problem has a great influence on the vehicle dynamics because all the forces produced of reaction on the vehicle are transmitted through the contact forces. The simulation results are affected by the procession of the contact model. The dynamic behaviour of the railway vehicle is totally affected by the solution of the contact problem.

The exact definition of the contact problem leads to better results for the simulation of critical cases such as: Derailment process [11]; Dynamic instability problems; Wear process for the wheel-rail surfaces[27]; Squeal noise problems. The determination of the rolling contact problem [28] requires the definition of the relations between the deformation, pressure distribution and creepages.

Since all the forces supporting and guiding the railway vehicle result from the interaction between the wheel and rail. A good contact model must provide an accurate description of the global and local contact phenomena and a general handling of the multiple contact situations. The model has also to assure high numerical efficiency (in order to be implemented directly online within multibody models) as well as a good compatibility with multibody simulation tools.

The solution of the contact problem is divided into three different but correlated tasks: the solution of the geometrical contact problem; the solution of the normal contact problem and the solution of the tangential contact problem. The first task involves the determination of the contact points locations on the interface between the wheel and rail surfaces. The second task is related with the contact kinematics and consists in the calculation of the velocity vector and creepages values at the contact points. The last step is the accurate definition of the contact mechanics by the calculation of the wheel-rail contact forces.

The required data for solving the contact problem can be summarized in the following points:

- The contact geometry: requires the definition of the transversal geometry of the track as well as the geometrical properties of the wheel and rail surfaces.
- The mechanical properties of the surfaces in contact.
- The relative displacements of the wheelset with respect to the track.
- The kinematics of the contact: this includes the determination of the contact velocity vector at each contact point as well as the determination of the creepages by knowing the value of the forward velocity of the vehicle.

According to the used theory for the solution of the contact problem, the extracted data from the contact problem solution are:

- Number of contact areas.
- Shape and size of the contact area.
- Position vector of the contact points.
- The main principle unit vectors acting at the contact area which are calculated by the definition of the conicity value at each contact patch.
- Normal contact forces, tangential contact forces and spin creep moment at each contact area.

### 3.3.1 Classification of the wheel-rail contact theories

During the past decades, Kalker developed a number of wheel-rail contact theories that can be used to determine the tangential forces and spin moment between the wheel and the rail. The most important classification procedure for the contact problem was that used by Kalker[32, 33]. In the following section, a general classification for the wheel rail contact theories is presented.

- According the applied elasticity theory; the contact models are classified into exact and simplified. The exact theory is based on the infinite half space at which the displacement at a certain point depends on all applied forces at all the points of the belonging to the same domain [30], and this can be explained by the following expression

  $$\mathbf{u}(x, y) = \int_{\Omega} \mathbf{H}\,(\xi, \eta)\,\mathbf{p}\ (\xi, \eta)\ d\xi\, d\eta \tag{3.15}$$

  where **u** is the displacement vector produced from the elastic deformation at the *(x ,y)* point. **H** is the flexibility matrix. **p** is the contact traction distribution. Both magnitudes are function of the local coordinates $(\xi, \eta)$ inside the generic domain $\Omega$ defining the contact area.

  On the other hand, the simplified contact theory assumes that the displacement at a certain point is directly produced by the application of the forces at the same point.

- According to the consideration of the dynamic effects at the contact; the contact theories are classified into dynamic and quasi-static theories. The dynamic theories include the inertial effects in formulating the contact problem. But in the quasi-static theories, the inertial effects are not included in the contact solution.

- According to the dimensions used in the model; the theories can be classified according to the dimension into two dimensional and three dimensional contact theories. In the three dimensional contact theories, the displacement and the pressure distribution in the contact zone depend on three coordinates $x, y$ and $z$. On the other hand, the two dimensional contact theories are independent of the variable $y$. For this reason the two dimensional contact theories have a limited application in the dynamic analysis of railway vehicles.

- According to the saturation conditions of the contact forces; the existing theories are divided into linear an non-linear theories. In the linear contact theory, it was assumed that the tangential forces at the contact areas are linear with respect to the creepage values. For non-linear theory, the Coulomb law of saturation was considered which indicates that the tangential force is limited by the normal contact force and the coefficient of friction at the contact points.

## 3.4 Geometrical contact problem

The determination of the contact points at the wheel-rail interface is a complicated task since both surfaces are profiled. The large amount of parameters that involve the shape of surfaces in contact, relative contact velocities, contact forces, and physical properties of the materials, lead to complex algorithm for solving the wheel-rail contact problem[48, 52]. The first problem faced in the solution of the contact is the accurate prediction of the contact points location. Once the location of the contact points is determined, then the normal and tangential contact forces can be calculated at the detected contact points.

In the following section, all the aspects related to the wheel-rail contact geometry are presented. For the proposed wheel rail surface, the solution of the geometric contact problem consists of obtaining the following data:

- The number of contact areas between the wheel and rail surfaces.
- Position vector of each contact point representing each area of contact.
- Conicity value of the wheel and rail profiles at each contact point.
- Geometrical properties for both surfaces in contact in order to be used in the solution of the normal contact problem, such as the curvature values of both surfaces at the contact point.

### 3.4.1 Proposed solutions for the geometric contact problem

In the literature, existing various methods proposed by many authers to deal with the wheel rail interaction as well as finding the contact geometrical properties at the wheel rail interface. In the following section, the most effective models used to solve the geometrical contact problem are presented.

### 3.4.2 The visible profile method

The method was presented by Kik et al. [37]. The method was used to study the effect of the angle of attack on the contact parameters [11]. For a given value of the wheelset angle of attack $\psi$, the wheel profile is substituted by the projection of the three dimensional wheel surface along the direction parallel to the track centreline. The projected profile is obtained as the envelope of n ellipses (n being the number of points that define the wheel profile) that are the traces of n circumferential sections of the wheel in the plane orthogonal to the rails as shown in figure (3.12).

By the change in the angle of attack of the wheel, the visible wheel profiles are computed. In the next step, by changing the values of the lateral displacement the corresponding roll angle $\phi$ is computed by equating the profile distance on the left wheel $u_l$ to the profile distance of the right wheel $u_l$

$$u_l\left(\psi, y_{rel}, \phi\right) = u_r\left(\psi, y_{rel}, \phi\right) \tag{3.16}$$

where $y_{rel}$ is the relative lateral displacement of the wheel profile. The profile distance is measured in the vertical direction representing the minimum distance between the visible wheel profile and the rail.

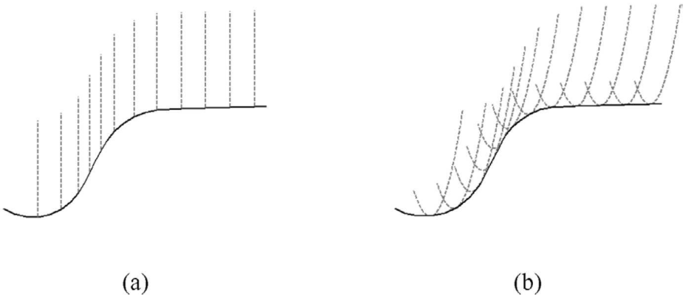

Figure 3.12. *Wheel profile projection: (a) $\psi$=0 (b) $\psi \neq 0$*

Solving the above nonlinear equation presented by equation (3.16), the roll rotation $\phi$ of the wheelset is determined. Then, the wheelset is displaced in vertical direction by an amount equal to the previously computed profile distances $u_l$=$u_r$, so that the two visible wheel profiles come into contact with the rail without any compenetration, and a single contact point (called 'geometric' contact point) is obtained on the left and right profiles. Finally, a search is performed for other points along the profiles that might enter into contact due to the elastic deformation of wheel and rail surfaces in the contact patch. These are the locations of potential multiple contacts between the wheel and the rail. In order to detect these locations, the distance between the visible wheel profile and the rail along the normal direction is computed, and a potential multiple contact point is associated with each position where a local minimum of this distance occurs, in association with a value of the normal distance lower than the maximum elastic deformation allowed for the contacting bodies. For all the contact points, the following contact parameters relevant to the computation of wheel-rail forces obtained :

- The difference between the rolling radius for the left and right wheel in the contact point and the nominal rolling radius of the wheel.
- The inclination of the contact with respect to the railhead plane.
- The undeformed distance between the wheel and rail surfaces.
- The longitudinal displacement $d$ of the contact point with respect to the vertical plane of the wheelset

As seen in figure (3.13), r is the distance in lateral direction between the longer semi-axis of the contacting ellipse and the contact point $P$ in the projection plane.

The method provides a reasonable results for the applications in the simulation tools as it was mentioned in the presented work of F. Braghin et al. [11], where the method was used to generate bidimensional contact table as function of the relative wheel-rail lateral displacement $y_{rel}$ and of the wheelset angle of attack $\psi$.

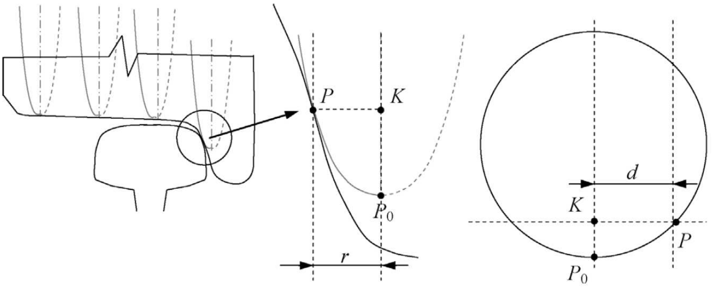

FIGURE 3.13. *Contact point forward movement; extracted from [11]*

### 3.4.3 Contact points detection using geometric relational properties

The method was used by J. Pombo et al. [52]. The methodology proposed depends on finding the contact points between two parametric surfaces by knowing the geometric relational properties between the two surfaces.

The methodology composed of two steps to find the coordinates of the contact points between the two surfaces: The first is to find the coordinates of the possible candidate points that may be in contact on both surfaces, that was found by solving a set of geometric equations for the surfaces; The second is to calculate the minimum distance between the candidate points and make the check whether penetration exists or not.

The solution of the problem can be illustrated by figure (3.14), where two generic surfaces $i$ and $j$ are defined by two parametric functions $\mathbf{p}(u,w)$ and $\mathbf{q}\ (s,t)$.

The vector of the minimum distance between the two surfaces can be defined as:

$$\mathbf{d} = \mathbf{p}(u,w) - \mathbf{q}\ (s,t) \tag{3.17}$$

By defining the normal vectors $\mathbf{n}_i$ and $\mathbf{n}_j$ as well as the tangent vectors $\mathbf{t}_i^u$, $\mathbf{t}_i^w$ for the surface $i$ and $\mathbf{t}_j^s$ and $\mathbf{t}_j^t$ for the surface $j$, respectively. The vector of normal distance $\mathbf{d}$ has to be parallel to the normal vectors of both surfaces, which is represented by the following equations

$$\mathbf{d} \times \mathbf{n}_i = 0 \tag{3.18}$$

$$\mathbf{d} \times \mathbf{n}_j = 0 \tag{3.19}$$

Finding the minimum distance between the two surfaces is not sufficient to determine all the possible candidate points for all the situations that can be found in the wheel-rail contact which can be presented as shown in figure (3.15)

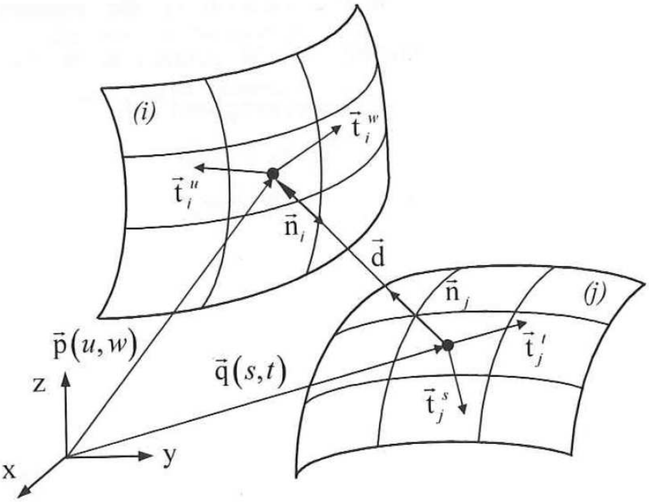
(i)
$\vec{t}_i^w$
$\vec{t}_i^u$
$\vec{n}_i$
$\vec{d}$
$\vec{n}_j$
(j)
$\vec{p}(u,w)$
$\vec{q}(s,t)$
$\vec{t}_j^t$
$\vec{t}_j^s$
z
y
x

Figure 3.14. *Candidate points for contact between two parametric surfaces, extracted frome [52]*

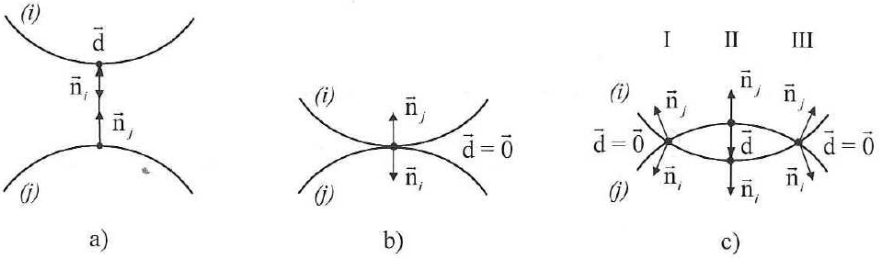
(i)
$\vec{d}$
$\vec{n}_i$
$\vec{n}_j$
(j)
a)
(i)
$\vec{n}_j$
$\vec{d}=\vec{0}$
$\vec{n}_i$
(j)
b)
I
II
III
(i)
$\vec{n}_j$
$\vec{n}_j$
$\vec{n}_j$
$\vec{d}=\vec{0}$
$\vec{d}$
$\vec{d}=\vec{0}$
(j)
$\vec{n}_i$
$\vec{n}_i$
$\vec{n}_i$
c)

Figure 3.15. *Candidate points for contact between two parametric surfaces, extracted from [52]*

Existing three possible situations for the wheel rail contact points detection secnario as shown in the previous figure:

a) There is no penetration between the two surfaces, means that the wheel is lifted.

b) Contact exists in one single point.

c) Amount of penetration is found between the wheel and rail surfaces and the contact points are selected with in the interpenetration volume.

The contact points are these points that have the maximum elastic deformation measured in the normal direction to the contact patch. Two sets of equations are added to completely present the possible contact situations between wheel and rail to detect all candidate points for contact between the two surfaces:

$$\left.\begin{aligned}\mathbf{n}_j^T \times \mathbf{t}_i^u &= 0\\ \mathbf{n}_j^T \times \mathbf{t}_i^w &= 0\end{aligned}\right\} \tag{3.20}$$

$$\left.\begin{aligned}\mathbf{d}^T\ \ \mathbf{t}_i^u &= 0\\ \mathbf{d}^T\ \ \mathbf{t}_i^w &= 0\end{aligned}\right\} \tag{3.21}$$

Equation (3.20) means that the two normal vectors for both surfaces are parallel. On the other hand, equation (3.21) means that the minimum distance vector has to be parallel to the normal vector of the surface $i$.

As mentioned in the first step in the methodology proposed, the two sets of equations (3.20) and (3.21) are solved to find the coordinates of the candidates contact points to be stored out.

The second step in the methodology is presented here by the search for the minimum distance $d$ defined by equation (3.22) between the candidate points

$$\mathbf{d} = \|\mathbf{d}\| \tag{3.22}$$

Afterwards, check was made to find whether there is penetration or not by verifying the condition presented by the equation (3.23)

$$\mathbf{d}^{\mathrm{T}}\mathbf{n}_j \ \leq 0 \tag{3.23}$$

If there is no penetration between the two surfaces, the candidate points are eliminated from the selection process. By this way the location of the contact point between the two generic surfaces is determined. This method was applied for the wheel-rail contact problem with the only condition that the parameterized wheel and rail surfaces must be convex [48, 52].

### 3.4.4 The wheel-rail differential contact method

The method was presented by Meli et al. [39], where a 3D differential contact model was used to solve the geometrical contact problem.

The wheel and rail surfaces are defined as seen in figure (3.16). Two reference frames are used in the formulation: the first $(O_{\mathrm{w}}, X_{\mathrm{w}}, Y_{\mathrm{w}}, Z_{\mathrm{w}})$ is attached to the wheel profile while the second reference frame $(O_{\mathrm{r}}, X_{\mathrm{r}}, Y_{\mathrm{r}}, Z_{\mathrm{r}})$ is attached to the rail profile. The model was presented as a closed box with input and output data

The input data to the model are the following :

- The relative position vector between the wheel and rail $\mathbf{O}_{\mathrm{w}}^{\mathrm{r}}$.
- The relative orientation between the wheel and rail $\mathbf{R}_{\mathrm{w}}^{\mathrm{r}}$.
- The absolute velocity vector $\dot{\mathbf{O}}_{\mathrm{w}}^{\mathrm{r}}$.

- The absolute angular velocity of the wheel system $\boldsymbol{\omega}_{\mathrm{w}}^{\mathrm{r}}$.

The output data of the contact model are:

- The contact patches $A_{\mathrm{wC}}$ and $A_{\mathrm{rC}}$.
- The contact forces $F_{\mathrm{wC}}$ and $F_{\mathrm{rC}}$.
- The contact stresses $\sigma_{\mathrm{w}}$ and $\sigma_{\mathrm{r}}$.
- The displacement of the wheel $\mathbf{u}_{\mathrm{w}}$ as well as the displacement of the rail $\mathbf{u}_{\mathrm{r}}$.

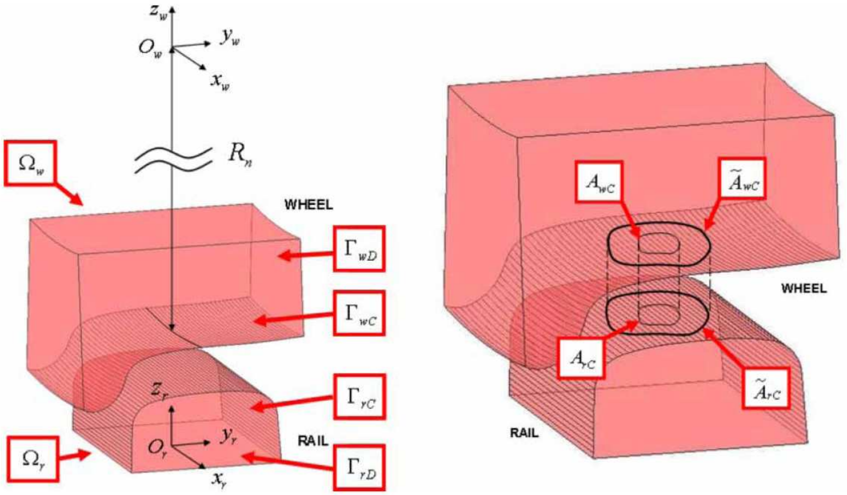

Figure 3.16. *Domains, boundaries and contact areas, extracted from [39]*

In the model proposed, the wheel and rail bodies are presented as elastic bodies $\Omega_{\mathrm{w}}$ and $\Omega_{\mathrm{r}}$. The size contact patch is considered to be small compared with the wheel and rail dimensions [64].

The boundaries of the wheel and rail are split into two disjoint regions. The contact boundaries $\Gamma_{\mathrm{wC}}$ and $\Gamma_{\mathrm{wD}}$ are defined for the wheel profile. The boundaries $\Gamma_{\mathrm{rC}}$ and $\Gamma_{\mathrm{rD}}$ are defined for the rail profile.

The position of the undeformed configurations is determined by knowing the wheel-rail kinematics as well as the location of the Dirichlet boundaries. In case of contact, by defining the geometrical intersection between $\Gamma_{\mathrm{wC}}$ and $\Gamma_{\mathrm{rC}}$ allows us to determine the penetration areas $\tilde{A}_{\mathrm{wC}}$ and $\tilde{A}_{\mathrm{rC}}$ which can be considered as a first estimation for the real contact areas $A_{\mathrm{wC}}$ and $A_{\mathrm{rC}}$.

By this way, the real contact areas are known for the model and have to be calculated. For this issue a contact map $\Phi$ is defined. Considering the wheel profile as a master surface, a generic point on the wheel surface $X_{\mathrm{w}}^{\mathrm{r}}$ is connected with a point on the rail surface $\Phi\left(X_{\mathrm{r}}\right)$. So the distance between the undeformed contact surfaces can be defined as:

$$\mathbf{d}\left(X_{\mathrm{w}}^{\mathrm{r}}\right)=\left(\mathbf{u}_{\mathrm{w}}^{\mathrm{r}}-\mathbf{u}_{r}\right)\cdot\mathbf{n}_{\mathrm{w}}^{\mathrm{r}}-\left(\Phi\left(X_{\mathrm{w}}^{\mathrm{r}}\right)-X_{r}\right)\cdot\mathbf{n}_{\mathrm{w}}^{\mathrm{r}} \tag{3.24}$$

where

- $X_{\mathrm{w}}^{\mathrm{r}}$ is the relative position vector between wheel and rail profiles.
- $\mathbf{u}_{\mathrm{r}}$ is the displacement of the rail.
- $\Phi\left(X_{\mathrm{w}}^{\mathrm{r}}\right)$ is a generic point on the wheel surface.
- $X_{\mathrm{r}}$ generic point on the rail profile.
- $\mathbf{n}_{\mathrm{w}}^{\mathrm{r}}$ is the normal versor to the surface $\Gamma_{\mathrm{WC}}$.

In the case of penetration between the wheel and rail surfaces, the distance $d$ takes a positive value. Then by this way the real contact areas $A_{\mathrm{w}C}$ and $A_{\mathrm{r}C}$ are defined by knowing the wheel rail relative kinematics as well as the wheel and rail displacements. According to that, the contact geometrical problem was solved by knowing the penetration value as well as the contact patch location on the wheel-rail interface.

## 3.5 Normal contact problem

Generally in the wheel-rail interaction problem, if there is no penetration between the wheel and the rail, the contact forces are assumed to be null. The occurrence of the penetration is used as the basis to develop a procedure to evaluate the local deformation of the bodies in contact. These forces are calculated as being equivalent to those that would appear if the bodies in contact were pressed against each other by external static force [48, 60]. This means that the contact forces are treated as elastic forces expressed as functions of the co-ordinates and velocities of the two bodies.

Existing two different models for the calculation of the normal contact force. The first deals with the theoretical contact point and the second is based on the virtual interpenetration between the surfaces. The Hertz model for the calculation of the normal contact problems is considered to be one of the models that uses the theoretical contact point to estimate all the characteristics of the contact area.

The procedure proposed here in the current work for the calculation of the normal contact force depends on Hertz contact model for calculating the normal force applied at the contact point between the wheel and the rail. The direction of the normal force is determined from the normal vector to the wheel and rail surfaces at the point of contact.

### 3.5.1 Hertz normal contact force

The Hertz theory [18] is used for the solution of the normal contact force between contact bodies under the following assumptions [28, 44]:

- All the produced deformations in the contact zone are considered to be elastic.
- The size of the contact patch is very small compared with the radius of curvature of the contact surfaces. If this condition is applied, the Boussinesq equations can be used in the definition of the pressure displacement relation.
- Frictionless contact is assumed between the contact surfaces, so the normal and tangential contact problems can be solved independently.
- All the bodies in contact are assumed to have a smooth surfaces without surface roughness.
- The undeformed distance between the contact bodies can be represented by a quadratic function:

$$h\left(x,y\right)=C_1x^2+C_2y^2 \tag{3.25}$$

Under these conditions, the contact area is defined by an ellipse and the normal contact pressure distribution is considered to have ellipsoidal shape as well. It is necessary to highlight that the Hertz solution is used in most of the railway simulators as it offers a good estimation of the normal contact force with small computational cost.

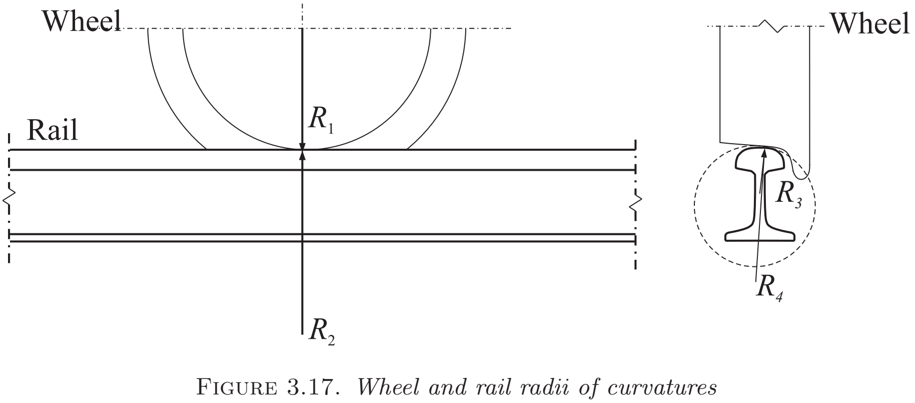

Figure 3.17. *Wheel and rail radii of curvatures*

Figure (3.17), shows the interaction between the rail and the wheel, and the radius of curvature of both the wheel and the rail is defined as shown in the same figure. The principle rolling radius of the wheel is $R_1$, $R_3$ is the transversal radius of curvature of the wheel at the point of contact, $R_2$ is the transversal radius of curvature of the rail which usually has infinity value, and $R_4$ is the principal rolling radius of the rail at point of contact. The normal contact force produced at the point of contact can be calculated through the following expression

$$F_z = \frac{\delta^{\frac{3}{2}}}{\sqrt{r^3 \left(\frac{3}{4}\ (K_{\mathrm{w}} + K_{\mathrm{r}})\right)^2 \left(\frac{A-B}{2}\right)}} \tag{3.26}$$

where $F_z$ is the normal contact force, $\delta$ is the amount of indentation or the penetration between the wheel and the rail, $K_{\mathrm{w}}$ and $K_{\mathrm{r}}$ are the material parameters of the wheel and the rail respectively, and can be calculated through the expression

$$K_{\mathrm{w}} = \frac{1-\nu_{\mathrm{w}}^2}{E_{\mathrm{w}}} \quad ; \quad K_{\mathrm{r}} = \frac{1-\nu_{\mathrm{r}}^2}{E_{\mathrm{r}}} \tag{3.27}$$

where $\nu_{\mathrm{w}}$ and $\nu_{\mathrm{r}}$ are the poisson's ratio for the wheel and rail materials respectively, $E_{\mathrm{w}}$ and $E_{\mathrm{r}}$ are young's modulus of elasticity of the wheel and rail materials. The parameter $r$ in equation (3.26) can be found from Hertz's table [2], by interpolation between the values of the angular parameter $\Theta$ [48, 61], which can be calculated by the following expression

$$\Theta\ =\ \arccos\left(\frac{B-A}{B+A}\right) \tag{3.28}$$

where $A$ and $B$ are geometrical functions related to the principle and transversal radii of curvature of the wheel and the rail, which can be found by

$$\left.\begin{aligned} A &= \frac{1}{2}\left(\kappa_1 + \kappa_2\right) \\ B &= \frac{1}{2}\left(\kappa_3 + \kappa_4\right) \end{aligned}\right\} \tag{3.29}$$

Where $\kappa$ is the curvature which can be calculated through the following equation

$$\kappa = \frac{1}{R_n} \quad ; \ n =\ 1, 2, 3 \text{ and } 4 \tag{3.30}$$

### 3.5.2 Size and shape of the contact patch

When two elastic bodies are pressed against each other by normal force, a contact region is formed around the point of contact. The shape and size of the contact patch between the two bodies are given by Hertz contact theory [17, 24, 33, 48]. In this section we will describe the necessary expressions required to calculate the size of the contact patch. In most of the railway applications the contact ellipse is a good approximation of the real contact patch, and in the current simulation it was sufficient to use Hertz theory in the analysis of the normal contact problem. The contact patch takes the shape of an ellipse shown in figure (3.18)

---

[2] Appendix **B**

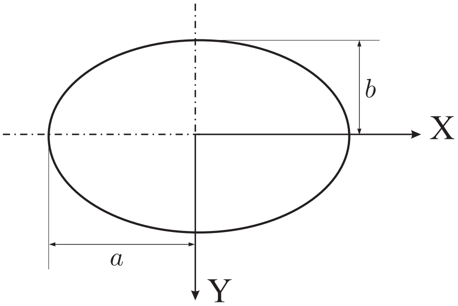

Figure 3.18. *Longitudinal and transversal semi axes of the contact ellipse*

The longitudinal and transversal semi axis of the contact ellipse can be calculated by knowing the radii of curvature, the properties of the both wheel and the rail, and the normal contact force between them. The formulations used in the bibliography [12, 24], to calculate the contact ellipse semi axes can be written as

$$a = m \sqrt[3]{\frac{3}{4} F_z \left( \frac{K_\mathrm{w} + K_\mathrm{r}}{A + B} \right)} \tag{3.31}$$

$$b = n \sqrt[3]{\frac{3}{4} F_z \left( \frac{K_\mathrm{w} + K_\mathrm{r}}{A + B} \right)} \tag{3.32}$$

where $m$ and $n$ are constants can be found by the interpolation between the values illustrated in Hertz table [2], for the corresponding values of the angle $\Theta$ which vary from 0 to 180 °.

## 3.6 Tangential contact problem

The last step in the complete definition of the contact problem is the solution of the tangential contact problem. In the study of the wheel rail interaction phenomenon, it was found that lateral instability, hunting motion, ride quality and derailment problems are directly affected by the creep forces that occur at the contact patch. Many theories have been described in the literature presenting the different ways used to deal with the tangential forces.

---

[2] Appendix **B**

Some of the theories are used in the case where the contact area take the form of ellipse or circular shape, and others deal with any shape of the contact areas. Other differences can be illustrated between such theories, where some theories permit the use of variable coefficient of frictions and others use only constant value for the friction coefficient. On the other hand, some algorithms are designed to be used with high values for the creepages and others deal with small values of the creepages.

The selection between the tangential theories depends mainly on the case where the theory is applied whether existing multi point contact cases and determining whether the calculated values of the creepages are high or small. The precision of the solution obtained as well as the computational cost are considered to have an important effect in the selection of the tangential contact theory.

In the proceeding section, a three dimensional rolling contact model is illustrated, to present the wheel rail interaction and used to calculate the creep forces at the contact patch [48]. According to Hertz theory, an elliptical contact area was produced due to the contact between the wheel and the rail, normal stress distribution was formed. Due to the rotation of the wheel over the rail, a friction is presented in addition to the normal stress. Shear stress may occur in the contact area which results a longitudinal and lateral tangential forces. The rotation axis of the wheel is not required to be parallel to the rail lateral axis, so a relative angular velocity about the normal axis is produced. So the contact interface tends to twist which produces tangential stress and slip, due to the spin produced by angular velocity at the contact area [58].

In the presented work, three different methods are defined to be used in the solution of the tangential problem. The used theories are:

- The Linear Theory of rolling contact
- FASTSIM algorithm
- Polach nonlinear creep force model

### 3.6.1 Creepage phenomenon

The creep phenomenon, also known as creepage, exists when two bodies are pressed against each other with normal forces and are allowed to roll over each other. Creep may be described as a part elastic and part frictional behaviour in which an elastic body, rolls over another elastic body, shares an area of contact where both slip and adhesion occur simultaneously. Therefore, a creep region of contact may be regarded as transition state between pure rolling and pure sliding. The creepages are crucial in the calculation of the creep forces and moments which develop in the wheel rail contact interface, for this purpose the accurate description of the creep phenomenon associated to the wheel-rail interaction is essential. In railway vehicle dynamics, the creep is used to characterize the relative difference in velocities between ideally rolling wheel [23, 40], having no slip in the contact, and the real one. The slip velocity between the wheel and the rail can be defined as a function of the longitudinal, lateral and spin creep which known as the creepages. For better understanding of the creep phenomenon, a wheel rolling over a rail is presented in the figure below, illustrating the longitudinal and lateral creepages as shown in figure (3.19)

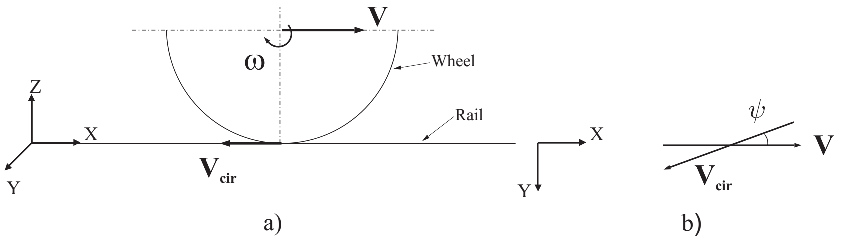

Figure 3.19. *Wheel rolling over rail:a) Longitudinal creepage; b) Lateral creepage*

### 3.6.1.1 Longitudinal Creepage

In case of rolling without slipping, the distance travelled by the wheel in one revolution is equal to the circumference of the wheel. But when torque is applied to the wheel, the distance travelled by the wheel in the forward direction is less than the circumference. Since the wheel profile is coned, then the longitudinal creep is arised when there is a difference in the rolling radii of the two wheels of the wheelset. The longitudinal creepage can be defined as [60].

$$\xi_x = \frac{Forward\ \ velocity\ \ of\ \ the\ \ wheel\ \ \text{-}\ Forward\ \ velocity\ \ of\ \ the\ \ rail}{Pure\ \ rolling\ \ forward\ \ velocity} \tag{3.33}$$

by finding the contact point velocity vector. The longitudinal creepage can be written as

$$\xi_x = \frac{\mathbf{V}_c^{\mathrm{T}}\boldsymbol{l}}{V} \tag{3.34}$$

where $\mathbf{V}_c$ is the velocity vector of the contact point represented in the intermediate system of reference associated with the wheelset, $V$ is the rolling velocity [40], $\boldsymbol{l}$ is the principle vector in the longitudinal direction at the point of contact on the wheel profile as shown in figure (3.20).

### 3.6.1.2 Lateral Creepage

The lateral creepage $\xi_y$ occurs when the wheelset is forced to move in a direction that makes a yaw angle $\psi$ with respect to the rolling plane Figure (3.19), it is defined as the quotient between the lateral component of the relative velocity of the contact

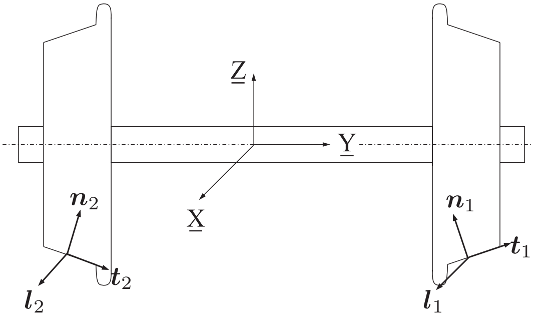

Figure 3.20. *The principle tangent, normal, and longitudinal vector at the left wheel represented by number(1) and at the right wheel represented by number(2)*

points, i.e the lateral slip velocity, and the wheel forward velocity [48], lateral creepage generally can be defined as:

$$\xi_y = \frac{\textit{Lateral velocity of the wheel - Lateral velocity of the rail}}{\textit{Pure rolling forward velocity}} \tag{3.35}$$

Lateral creepage has a significant influence on the rails corrugations caused by the lateral creepage forces. Furthermore, the stick -slip phenomenon can be supposed to be induced between a resultant of mainly lateral and longitudinal creepage forces [20]. Lateral creepage is thus likely to exist in combination with longitudinal creepage and the influence of longitudinal creepage on the mechanism of squeal noise behaviour, specifically the creepage/creep force relationship, is of interest [40]. To calculate the lateral creepage in the current model in the dynamic simulation of the wheelset system, the following expression is used

$$\xi_y = \frac{\mathbf{V}_c^{\mathrm{T}} \boldsymbol{t}}{V} \tag{3.36}$$

where $\boldsymbol{t}$ is the tangential unit vector at the point of contact on the wheel profile as shown in figure (3.19).

### 3.6.1.3 Spin Creepage

The spin creepage is due to the component of the relative angular velocity of the two bodies normal to the contact surfaces. The angular velocity of a wheel relative to the rail can be decomposed into three components; one of them is perpendicular to the contact plane, while the other two are tangent to the plane of contact [58]. However pure rolling occurred when the rolling occurs without sliding or spin [48]. The normal angular velocity is the instantaneous rate at which the wheel turns on the contact plane relative to rail, the normal component of the relative angular velocity acting through the normal direction to the contact surface represented by the unit normal vector $\vec{\mathbf{n}}$ shown in figure (3.21), causes the spin.

Since the wheel profiles are coned, the rolling angular velocity of the wheel $\vec{\boldsymbol{\omega}}$ is not perpendicular to the vector normal to the contact area $\vec{\mathbf{n}}$ as shown in figure (3.21) the consequence is that the wheel has an angular velocity $\vec{\boldsymbol{\omega}}_n$ relative to the rail in the contact patch. The spin creepage is given by the angular velocity of the wheel, about the normal to the contact region and can be defined by the following equation

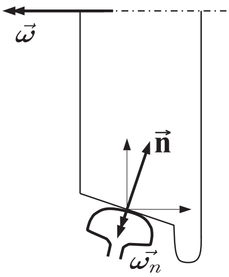

Figure 3.21. *Spin creepage*

$$\xi_{sp} = \frac{\textit{Wheel angular velocity -Rail angular velocity}}{\textit{Pure rolling forward velocity}} \tag{3.37}$$

which can be written as:

$$\xi_{sp} = \frac{\boldsymbol{\omega}^{\mathrm{T}}\,\boldsymbol{n}}{\mathbf{V}} \tag{3.38}$$

Where $\underline{\boldsymbol{\omega}}$ is the angular velocity of the wheelset represented in the intermediate reference frame and $\underline{\boldsymbol{n}}$ is the unit normal vector at the contact point. Longitudinal and lateral creepages are dimensionless, but the spin creep has the dimension of $\left(length^{-1}\right)$. The longitudinal creepage $\xi_x$ is related with the difference between the rolling forward velocity and the circumferential velocity $|\mathbf{V} - \mathbf{V_{cir}}|$, the lateral creepage $\xi_y$ characterizes the non alignment of the wheel with respect to the rail, while the spin creepage $\xi_{sp}$ is related with the concity of the wheel [32].

### 3.6.2 The Linear Theory of rolling contact

In addition to the normal contact forces acting on the contact patch, the tangential forces acting at the contact area must be determined. The creep forces and the spin creep moment are resulting from the tangential motion of the wheel relative to the rail in the contact region, therefore they depend on the creepages. The dimension of the contact ellipse and the normal contact force calculated by Hertz formulation expressed by equation(3.26), are required to calculate the creep forces. The relationship between the creepages quantities, longitudinal creepage $\xi_x$, lateral creepage $\xi_y$ and the spin creep moment $\xi_{sp}$ and the creep forces can be determined by the creep force law [23, 30, 33].

It was proposed to use the *linear theory of rolling contact* proposed by Kalker [29] to calculate the tangential contact forces at the contact patch, the name linear is directly joined to the application of Coulomb's law and the application of the conditions of Coulomb's theory for the saturation of the tangential stress. Then the linear theory is an approximation, because for large creepages, the tangential traction expressed by Coulomb's law can be violated[33, 40, 48]. For small creepages $\xi_x$ , $\xi_y$ and spin $\xi_{sp}$, the area of slip is so small that its influence can be neglected. The adhesion zone, therefore, can be assumed to cover the area of contact. Kalker's linear creep force-creepages relation [12, 23, 30] are given for the longitudinal creep force as

$$F_x = -f_{33}\,\xi_x \tag{3.39}$$

and for the lateral creep force

$$F_y = -f_{11}\,\xi_y - f_{12}\,\xi_{sp} \tag{3.40}$$

finally for the spin creep moment can be expressed as

$$M_{sp} = f_{12}\,\xi_y - f_{22}\,\xi_{sp} \tag{3.41}$$

The minus sign indicates that the creep force acts in the opposite direction to the creepages [33, 40], where the coefficients appeared in equations(3.39), (3.40) and (3.41), $f_{11}$, $f_{12}$, $f_{22}$ and $f_{33}$ are Kalker's creep coefficient which can be determined by the following expressions.

$$\left.\begin{array}{ll} f_{11} = G a\, b\, C_{22} & f_{12} = G\sqrt{a^3 b^3}\, C_{23} \\ f_{22} = G a^2 b^2\, C_{22} & f_{33} = G a\, b\, C_{11} \end{array}\right\} \tag{3.42}$$

Then the creep force law can be written in matrix form as

$$\left\{\begin{array}{c} F_x \\ F_y \\ M_{sp} \end{array}\right\} = -G\,a\,b \begin{bmatrix} C_{11} & 0 & 0 \\ 0 & C_{22} & \sqrt{a\,b}\,C_{23} \\ 0 & -\sqrt{a\,b}\,C_{23} & a\,b\,C_{33} \end{bmatrix} \left\{\begin{array}{c} \xi_x \\ \xi_y \\ \xi_{sp} \end{array}\right\} \tag{3.43}$$

Where $G$ is the combined shear modulus of rigidity of rail and wheel materials, $c_{ij}$ are the creepage and spin coefficients which are calculated for the exact theory can be obtained from Kalker's table, and these coefficients depend on the combined poisson's ratio and the ratio between the longitudinal and transversal axis $(a/b)$ of the contact

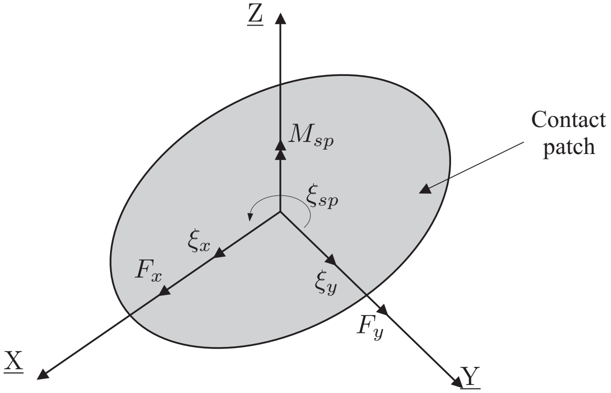

FIGURE 3.22. *Creepages velocities and tangential forces on the contact patch*

ellipse[2]. All these forces are acting in local normal and tangential coordinate directions defined by the orientation of the contact ellipse figure (3.22). By appropriate transformations they may be expressed as acting and counter acting forces on the wheel and the rail in their interference systems. Finally the contact loads can mainly be divided into contact forces and contact moments shown in the equation of motion for the wheel set and the track [3].

---

[2] Appendix **B**

### 3.6.3 FASTSIM algorithm

FASTSIM algorithm was developed by Kalker [32]. The main principle of the algorithm is the use of the relation between the tangential stresses and the displacement based on the simplified elasticity theory instead of the use of the elasticity theory developed by Cerruti.

In Cerruti's equations, the displacement at a specific point in the contact area in a determined direction depends, not only, on the pressure applied at the point, but also, on all pressure values applied on the rest of the points of the contact area in all directions.

In the simplified elasticity theory [33], it is assumed that the displacement at a specific point in the contact area is produced only due to the pressure applied at this point in the deformation direction. Also, the theory proposed that existing linear relation between the pressure applied and the produced displacement, and the proportionality parameter that relates the displacements and the stresses at the contact patch is the flexibility parameter $L$.

FASTSIM algorithm has a low computational cost compared with CONTACT [33], with an acceptable degree of precision that is permitted in the analysis and simulation of railway systems. In addition to the simplifications proposed by the linear elasticity theory, the following assumptions are used in the analysis presented by the algorithm:

- The normal and tangential contact problem are treated independently [28].
- The contact area has an elliptic shape, this is applied only when the Hertz conditions are verified.
- The friction coefficient is constant all over the contact area

#### 3.6.3.1 Mathematical development of FASTSIM algorithm

To solve the tangential contact problem, the following equation has to be solved

$$\mathbf{S}\left(x,y\right) = \mathbf{N}\left(x,y\right) - \frac{\partial}{\partial x}\mathbf{u}\left(x,y\right) \tag{3.44}$$

where $\mathbf{N}\left(x,y\right)$ is the dimensionless rigid slip vector. The previous equation can be written in the form

$$\begin{bmatrix} S_x \\ S_y \end{bmatrix} = \begin{bmatrix} \xi_x - \xi_{sp} y \\ \xi_y + \xi_{sp} x \end{bmatrix} - \frac{\partial}{\partial x}\begin{bmatrix} u_x \\ u_y \end{bmatrix} \tag{3.45}$$

where

* $S_x$ : relative slip in the rolling direction $x$.

- * $S_y$ : relative slip in the lateral direction $y$.
- * $\xi_x$: longitudinal creepage.
- * $\xi_y$: lateral creepage.
- * $\xi_{sp}$: spin creepage.
- * $u_x$: deformational displacement in the longitudinal direction.
- * $u_y$: deformational displacement in the lateral direction.

By the definition of the tangential stress values in the contact zone $\mathbf{P}_{\text{tan}}$, the equations are applied with the following conditions

$$\left.\begin{array}{llll} \text{Adehsion zone} & |\mathbf{P}_{tan}| < \mu\,\mathbf{P}_{norm} & and & |\mathbf{S}\,(x,y)| = 0 \\ \text{Slip zone} & |\mathbf{P}_{tan}| = -\,\mu\,\mathbf{P}_{norm}\,\frac{\mathbf{S}(x,y)}{|\mathbf{S}(x,y)|} & and & |\mathbf{S}\,(x,y)| \neq 0 \end{array}\right\} \tag{3.46}$$

By applying the simplified elasticity equations presented to relate the tangential stresses with the displacements, we find that:

$$\mathbf{u}\,(x,y) \;=\; L\,\mathbf{P}_{tan} \tag{3.47}$$

substituting in equation (3.45) then we get :

$$\begin{bmatrix} S_x \\ S_y \end{bmatrix} = \begin{bmatrix} \xi_x - \xi_{sp} y \\ \xi_y + \xi_{sp} x \end{bmatrix} - L\,\frac{\partial}{\partial x}\begin{bmatrix} P_x \\ P_y \end{bmatrix} \tag{3.48}$$

$$\frac{\partial}{\partial x}\begin{bmatrix} P_x \\ P_y \end{bmatrix} = \frac{1}{L}\begin{bmatrix} \xi_x - \xi_{sp}\, y \\ \xi_y + \xi_{sp}\, x \end{bmatrix} - \frac{1}{L}\begin{bmatrix} S_x \\ S_y \end{bmatrix} \tag{3.49}$$

The tangential stress at a point $x + dx$ can be found by the following expression

$$\begin{bmatrix} P_x\,(x+dx) - P_x\,(x) \\ P_y\,(x+dx) - P_y\,(x) \end{bmatrix} = \frac{dx}{L}\begin{bmatrix} \xi_x - \xi_{sp} y \\ \xi_y + \xi_{sp} x \end{bmatrix} - \frac{dx}{L}\begin{bmatrix} S_x \\ S_y \end{bmatrix} \tag{3.50}$$

Both equations (3.45) and (3.50) are used to calculate the tangential stress as well as the slip value at a specific point in the contact area by means of the value stresses at a known point. In our case, the known point at which the tangential stress, is the point $(x + dx)$.

For solving both equations, it is assumed that the point $x$ initially located in the adhesion zone. Under this assumption, the tangential pressure is known as $\mathbf{P}_{adh}$. In the case of adhesion at the pint $x$, then the relative slip is null at this point and equation (3.50) can be written as

$$\begin{bmatrix} P_{x,adh} \\ P_{y,adh} \end{bmatrix} = \begin{bmatrix} P_x\,(x+dx) \\ P_y\,(x+dx) \end{bmatrix} - \frac{dx}{L} \begin{bmatrix} \xi_x - \xi_{sp}\, y \\ \xi_y + \xi_{sp}\, x \end{bmatrix} \tag{3.51}$$

Once the tangential stress at the point $x$ is calculated, then a check has been made for the tangential stress value if it is less than the saturation limit as defined by the following equation

$$\mathbf{P}_{adh} < \mu\,\mathbf{P}_{norm} \tag{3.52}$$

If the condition is verified, then the tangential stress at the point $x$ is replaced by the value of the adhesion tangential stress. If the last condition is not verified, then the point $x$ is defined to be located in the slip zone.

In the case of slipping, the algorithm assumes that the direction of the tangential stress is the same direction of the adhesion stress $\mathbf{P}_{adh}$. The absolute value of the tangential stress should be equal to the product of the frication coefficient by the normal pressure as it was established by Columb's law [4]

$$\mathbf{P}_{tan} = \mu\,\mathbf{P}_{norm} \cdot \frac{\mathbf{P}_{adh}}{|\mathbf{P}_{adh}|} \tag{3.53}$$

#### 3.6.3.2 Calculation of the flexibility parameter

For obtaining the flexibility parameter $L$ used in equation (3.48), the results obtained by FASTSIM algorithm for small slip values, defined as exact values, should be equated to results obtained by the linear theory [29]

The tangential force vector obtained by the linear theory can be written in the following form [4, 12]

$$\mathbf{F}_{Linear\,Theory} = \begin{bmatrix} G\,a\,b\,C_{11}\xi_x \\ G\,a\,b\left(C_{22}\xi_y + \sqrt{a\,b}\right)C_{23}\xi_{sp} \end{bmatrix} \tag{3.54}$$

To obtain the value of the tangential forces at the contact zone at small slip values where the area of contact can be completely in adhesion, the tangential stress equation (3.48) can be written in the form:

$$\begin{bmatrix} \xi_x - \xi_{sp} y \\ \xi_y + \xi_{sp} x \end{bmatrix} - L\,\frac{\partial}{\partial x}\,\mathbf{P}_{tan} = \begin{bmatrix} 0 \\ 0 \end{bmatrix} \tag{3.55}$$

Then the tangential forces are found by

$$\mathbf{F}_{FASTSIM} = \begin{bmatrix} \frac{8\,a^2 b\,\xi_x}{3\,L} \\ \\ \frac{8\,a^2 b\,\xi_y}{3\,L} + \frac{\pi\,a^2 b\,\xi_{sp}}{4\,L} \end{bmatrix} \tag{3.56}$$

By equating both equations (3.54) and (3.56) the flexibility parameters can be found as :

$$\left.\begin{aligned} L_1 &= \frac{8\,a}{3\,C_{11} G} \\ \\ L_2 &= \frac{8\,a}{3\,C_{22} G} \\ \\ L_3 &= \frac{\pi\,a^{3/2}}{4\,\sqrt{b}\,C_{23} G} \end{aligned}\right\} \tag{3.57}$$

### 3.6.4 Polach nonlinear creep force model

The method was proposed by O. Polach [47]. The objective of the presented work was the development of a new algorithm used to calculate the tangential contact forces, with a computational cost lower than that offered by FASTSIM. In spite of the simplifications used in the formulation, the spin effect has been taken into account in the work presented by Polach.

The mathematical development of the proposed algorithm was explained in details, in addition he presented a FORTRAN code and some test results were included to facilitate the implementation of the code.

#### 3.6.4.1 Mathematical development of Polach algoritm

In the method presented, the contact area is assumed to be elliptical with semi axes $a$ and $b$. The normal pressure distribution has an ellipsoidal shape according to Hertz theory as seen in figure (3.23).

The friction coefficient is assumed to be constant in the whole contact area. Then, the maximum tangential stress can be obtained according to Coulumb's law by the following:

$$\mathbf{P}_{tan} = \mu\,\mathbf{P}_{norm} \tag{3.58}$$

Freibauer has calculated the for this case, the force displacement curve using a proposed transformation for the ellipsoidal distribution of the tangential stresses to spherical distribution. This transformation can be realized by the following expressions

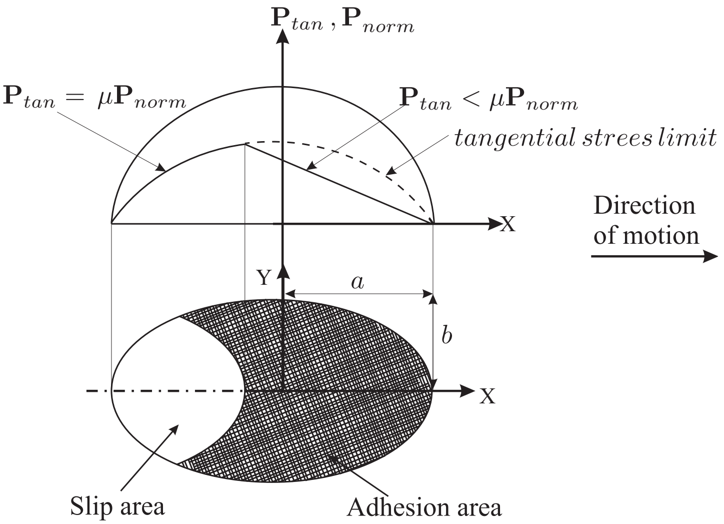
$\mathbf{P}_{tan}$ , $\mathbf{P}_{norm}$
$\mathbf{P}_{tan} = \mu\mathbf{P}_{norm}$
$\mathbf{P}_{tan} < \mu\mathbf{P}_{norm}$
tangential strees limit
X
Direction of motion
Y
a
b
X
Slip area
Adhesion area

FIGURE 3.23. *Normal and tangential stress destribution in the contact area according to Polach model [47]*

$$\left.\begin{aligned} y^* &= \tfrac{a}{b}\, y \\ \mathbf{P}^*_{tan} &= \tfrac{a}{\mu\ \mathbf{P}_{norm}|_{\max}} \mathbf{P}_{tan} \end{aligned}\right\} \tag{3.59}$$

The tangential stresses are proportional to the trailing edge distance as well as the slip value at the centre of the contact area. The proportionality coefficient is presented by the parameter $C$, and the tangential stress gradient is known as $\varepsilon_p$, which can be found by the following expression

$$\varepsilon_p = C\,\frac{a}{\mu\ \mathbf{P}_{norm}|_{\max}}\,\xi \tag{3.60}$$

According to Polach approach, The resultant tangential force caused by the longitudinal and lateral creepages can be obtained by integrating the tangential stress equation on the whole contact area obtaining the following expression

$$\mathbf{F} = -\frac{2\mu F_z}{\pi}\left(\frac{\varepsilon_p}{1+\varepsilon_p} + \arctan\,\varepsilon_p\right) \tag{3.61}$$

where $F_z$ is the normal contact force calculated by Hertz theory. To obtain the tangential forces in $x$ and $y$ directions, the following formulation is used

$$\left.\begin{aligned} F_x &= \mathbf{F}\,\tfrac{\xi_x}{\xi} \\ F_y &= \mathbf{F}\,\tfrac{\xi_y}{\xi} \end{aligned}\right\} \tag{3.62}$$

where $\xi_x$ and $\xi_y$ are the creepages in the longitudinal and lateral direction, respectively. $\xi$ represents the resultant translational creepage which can be defined by the following expression

$$\xi = \sqrt{\xi_x^2 + \xi_y^2} \tag{3.63}$$

Once the tangential problem is solved without taking into account the spin creepage. The wheel rail contact is now solved when the spin effect considered to be used in Polach method. Then the creepage value at the contact area, is now modefied to include the effect of spin creepage as follow

$$\xi_c = \sqrt{\xi_x^2 + \xi_{yc}^2} \tag{3.64}$$

where $\xi_c$ is the modefied translational creepage, and $\xi_{yc}$ is the modefied lateral creepage defined as

$$\xi_{yc} = \begin{cases} \xi_y & ;\ |\xi_y + \xi_{sp}\,a\,| \leq |\xi_y\,| \\ \xi_y + \xi_{sp}\,a & ;\ |\xi_y + \xi_{sp}\,a\,| > |\xi_y\,| \end{cases} \tag{3.65}$$

The spin effect is accounted by considering the lateral tangential force given by:

$$F_{ys} = -\frac{9}{16} a\,\mu\,F_z\,K_M\,\left(1 + 6.3\left(1 - e^{-a/b}\right)\right) \tag{3.66}$$

where $K_M$ is a constant calculated by

$$K_M = |\varepsilon_s|\left(\frac{\delta_s^3}{3} - \frac{\delta_s^2}{2} + \frac{1}{6}\right) - \frac{1}{3}\left(1 - \delta_s^2\right)^{3/2} \tag{3.67}$$

where $\delta_s$ defined as

$$\delta_s = \frac{\varepsilon_s^2 - 1}{\varepsilon_s^2 + 1} \tag{3.68}$$

in case of including the spin influence, then the tangential gradient $\varepsilon_s$ is obtained by

$$\varepsilon_s = \frac{2}{3} \frac{C_s\, \pi\, a^2\, b}{\mu\, F_z} \frac{\xi_{yc}}{1 + 6.3\left(1 - e^{-a/b}\right)} \tag{3.69}$$

The rigidity parameters $C$ and $C_s$ are calculated for both cases in which the spin effect is not taken into account as well as the case where the spin effect is included, respectively. The logival form used to obtain the values of $C$ and $C_s$ is equating the obtained results from Polach mehtod at small creepage values with the results obtained by Klaker linear theory as it can be shown by the following

- In case that the longitudinal and lateral creepages are only included the rigidity parameter can be calculated by:

$$C = \frac{3}{8} \frac{G}{a} \sqrt{\left(C_{11} \frac{\xi_x}{\xi}\right)^2 + \left(C_{22} \frac{\xi_y}{\xi}\right)} \tag{3.70}$$

- In case that the spin effect is considered, then the following expression is used:

$$C_s = \frac{4}{\pi} \frac{G\sqrt{b}}{\sqrt{a^3}} C_{23} \tag{3.71}$$

Finally Polach model can be written in the form

$$\left.\begin{aligned} F_x &= F \tfrac{\xi_x}{\xi_c} \\ F_y &= F \tfrac{\xi_y}{\xi_c} + F_{ys} \tfrac{\xi_{sp}}{\xi_c} \end{aligned}\right\} \tag{3.72}$$

According to Polach, the creep moment caused by the spin creepage or the lateral creepage is too small compared with the moment affecting the vehicle, so it can be neglected and the spin creep moment is obtained as

$$M_{sp} \approx 0 \tag{3.73}$$

# Chapter 4

# Multibody methodology for railway analysis

## 4.1 Introduction

Multibody methodologies are not widely used despite the fact that such methodologies can be applied to develop more detailed and general models for railroad vehicle-track systems [58]. In the proceeding context of this chapter, the geometric, kinematics and dynamic aspects of a general rigid body moving along parameterized track representing the railroad are discussed. Equations of motion presenting the multibody systems are formulated for a system consists of multiple rigid bodies each with six DOF [57, 61].

The use of any kinematic constraint on the motion is avoided in order to overcome the difficulties produced when using such constraints. These difficulties appear in the need of solving a set of differential algebraic equations [48, 50] or the transformation of the system of differential algebraic equations (DAE) to ordinary differential equations (ODE), and then the use of stabilization techniques for the constraint equations in the solution is avoided.

In this chapter, the multibody formulations used in the dynamic analysis of railway systems are presented in order to be used in the computational tool developed to carry out the simulation for the railway vehicles. Starting with the definition of the reference frames used in the multibody model, a complete description of the reference frames is presented in order to give a detailed definition for all the variables and identities used in the mathematical model used in the dynamic simulation of the railway systems.

Each reference frame is clearly defined, starting from the fixed frame of reference, the track frame of reference which represents the frame that follows the motion of the body [50, 61] and finally the body reference frame. The local coordinate frame for each body is introduced to identify the position and orientation of each point on the body with respect to each local frame. The origin of each locale frame is attached to the body center of mass. The transformation between the reference frames is defined by calculating the necessary transformation matrix required, using Euler angles with a specified rotation sequence that avoid the singularity problem [19, 61].

Track geometry plays an important rule in the dynamic analysis of railway vehicles. The track models for multibody analysis must be in the form of parameterized curves, where the nominal geometry is obtained as a function of a parameter associated to the track curve length [50, 51].

The parameterizations of the track can be done by two approaches, the first approach is the use of analytical segments where the track definition is generally done by putting together straight and circular curves interconnected by transition track segment that ensure the continuity of the first and second derivatives of the railway in the transition points. The second approach depends on the parameterization of the track using piecewise cubic interpolation schemes. These methods require the definition of control points representing the track and provide the interpolation between these points to represent the parameterized track path.

Undesired oscillations produced by using the mentioned interpolation schemes which can be avoided in such case of the horizontal track geometry for railway application. In the work presented, the track parameterization is done by using analytical segments. As an example for the track comfiguration possibility offered by the wrk here, the proposed track is defined as a straight line segment, followed by a transition curve connecting the straight line stage with the final stage presented by a plane curve with a constant radius. The methodology defined in the presented work permits any track configuaration to be used in the dynamic simulation purposes.

The fundamental component common to all conventional railway vehicles is the wheelset. In general, it consists of two wheels rigidly fixed to a common axle. The movement of the wheelset over the track is characterized by a complex interaction where appreciable lateral translations as well as yaw and roll rotations are observed. The simulation of railroad vehicle-track systems using Multibody computer algorithms requires the use of a module for the wheel-rail interaction [3, 34]. This interaction, which is due to the rolling and slipping contact between the profiled surfaces of the rail and the wheel, has a significant effect on the vehicle dynamics and stability [58].

The determination of the contact point position is a crucial part in the solution of the geometrical contact problem. In the work presented a reliable model is used to accurately detect the position vector of the contact points by knowing the relative position and orientation between the wheel and rail profiles. The contact model used by the investigation group showed a satisfactory results in the detection of the contact patch at the wheelrail interface. The procedure used can be summarised in the way that the wheel surface is assumed to be formed by a small conical segments formed by the revolution of the straight segments, defined between the wheel profile points, around the transversal axis perpendicular to the direction of motion of the wheelset.

The rail profile is assumed to be produced by the extrusion of the rail profile points measured in the longitudinal direction. The contact patch is defined by longitudinal strips which define the intersection between the conical segment representing the wheel profile with the rail straight line. The strips forming intersection area, which are produced by the virtual interpenetration between the two contact bodies, are characterized by: the position vector defining the entrance and exit points; strip length; strip thickness; conicity value at each strip; rolling and indentation radius and the maximum penetration.

The contact model used permits multi points of contact detection, between the wheel and rail surfaces. This advantage allows us to define each contact patch separately. The position vector of each contact point on left and right wheel profile is detected in the formulation presented in this chapter. The velocity vector of the contact point is calculated and then the creepages introduced at the wheel-rail contact point are determined.

Lagrangian approach is used to determine the system equations of motion. The method mainly depends on the definition of the system generalized coordinates, then determining the generalized force vector affecting the body under study. Kinematic analysis of a general rigid body is presented followed by the dynamic analysis of such body, and then the formulations extended to include the kinematic and dynamic analysis of the wheelset.

## 4.2 Reference frames description

In this section, the complete description of the reference frames is presented in order to give a detailed definition for all variables and identities used in the mathematical formulation of the models used in the dynamic simulation of the railway multibody systems. The main reference frames used in the analysis are presented in the following section. An important remark in the present work, is the use of an intermediate frame of reference in case of dealing with the wheelset analysis. The use of such frame of reference permits the precise definition of the contact point position as it will be shown in the definiton and analysis of the wheelset.

Cartesian coordinates are supposed to be used in the formulation used due to the simplicity of its implementation in the multibody program used in the railway vehicles dynamic analysis. Rotation sequences are defined for the track frame of reference, as a successive rotation about Z-axis, followed by rotation about Y-axis and finally a rotation about X-axis. But the rotation sequences used for general rigid body is defined as a successive rotation about Z-axis, then about X-axis and finally, the pitch motion with a rotation about Y-axis.

### 4.2.1 Reference frames

In this section all the frame of references used in the formulations are defined, giving more details about each reference frame used as well as its combination with the overall system. Starting with the description of the system used in the analysis of rigid body as shown figure (4.1). Three main reference frames are used, the first one is the fixed frame of reference (X Y Z), the second one is the track frame of reference ($X_T$ $Y_T$ $Z_T$) identefied by the subindex T and the third frame of reference is the rigid body frame of reference ($X_S$ $Y_S$ $Z_S$) identefied by the subindex S.

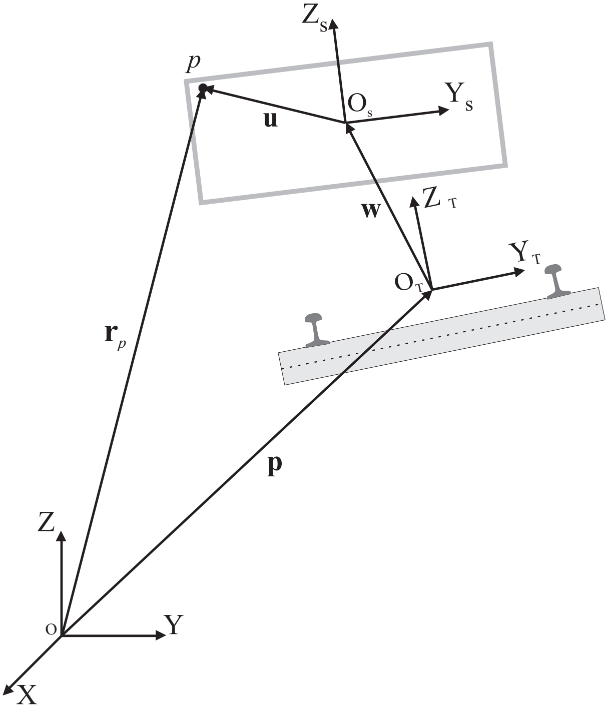

Figure 4.1. *Reference frames combination*

### 4.2.2 Fixed reference frame

A system that can be located at any fixed point with respect to the systems and bodies used in the analysis. The frame is defined by three orthogonal axes X, Y and Z, that are rigidly connected in one point called the origin O. In this reference frame, all the measurable quantities that can define the configuration of the body are represented with respect to the fixed fram such as: displacements, velocities and accelerations.

Figure (4.2) shows a combination of three orthogonal coordinates defining the fixed frame. The Z-axis is pointing to the vertical direction, X and Y-axis forming the horizontal plane. The vector **u** can be written in terms of its components in the fixed fram of reference as follow:

$$\mathbf{u} = \begin{bmatrix} u_x & u_y & u_z \end{bmatrix}^{\mathrm{T}} \tag{4.1}$$

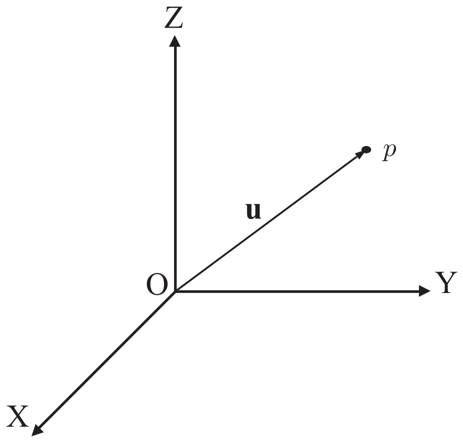

FIGURE 4.2. *Fixed Reference Frame*

### 4.2.3 Track reference frame

Track reference frame is defined with three orthogonal coordinates axis $X_T$ ,$Y_T$ , and $Z_T$ as shown in figure (4.3). The track reference frame is located at the track centreline between the left and right rail profiles and moves at the nominal vehicle velocity. The direction of the $X_T$-axis is pointing to the longitudinal direction referring to the rolling direction of the moving body along the track, $Z_T$-axis pointing to the vertical direction normal to the track horizontal plane and the Y-axis located normal to ($Z_T$ $X_T$) plane. The number of the track reference frame is selected to be equal to the number of the wheelsets in the vehicle model. Each wheelset has its own track system of reference, by this way the small displacements and rotations of each wheelset with respect to the track frame are detected to determine the contact problem with high precision.

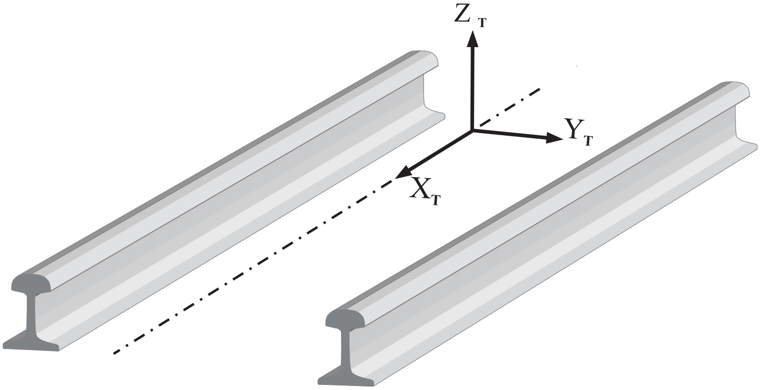

Figure 4.3. *Track Reference Frame*

A point $p$ located in the track reference frame has a position vector $\bar{\mathbf{u}}$ which can be expressed in the local track frame of reference as shown in figure (4.4).

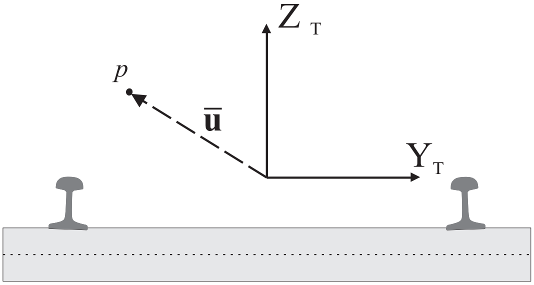

Figure 4.4. *Local position of point p in Track reference frame*

$$\bar{\mathbf{u}} = \begin{bmatrix} \bar{u}_x & \bar{u}_y & \bar{u}_z \end{bmatrix}^{\mathrm{T}} \tag{4.2}$$

The upper bar sign means that the vector is presented in the track reference frame. This notation is used to distinguish the difference between the vectors presented in the track frame of reference and the fixed frame of reference.

### 4.2.4 Body reference frame

The same as the track reference frame is defined in the previous section, the body reference frame is represented in this section by defining three orthogonal coordinate axes $\mathrm{X_S}$, $\mathrm{Y_S}$, and $\mathrm{Z_S}$ coinciding with the axes of inertia of the body. The body frame of reference attached to the center of mass of the rigid body figure (4.5). The local position vector of a point $p$ located in the body reference frame can be defined as:

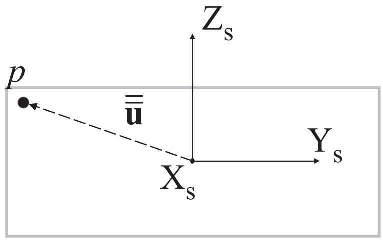

Figure 4.5. *Local position of point p in the body reference frame*

$$\bar{\bar{\mathbf{u}}} = \begin{bmatrix} \bar{\bar{u}}_x & \bar{\bar{u}}_y & \bar{\bar{u}}_z \end{bmatrix}^{\mathrm{T}} \tag{4.3}$$

The double upper bar sign means that the vector is presented in the body frame.

## 4.3 Reference frame transformations

In this section, it was necessary to define how to make the transformation from one reference system to another in order to present the necessary formulations used in the frames transformation in the proceeding context.

### 4.3.1 Transformation from track to fixed reference frame

Figure (4.6) shows the combination of the track frame ($\mathrm{X_T}$ $\mathrm{Y_T}$ $\mathrm{Z_T}$) with the fixed reference frame (X Y Z). The global reference frame can be located at any fixed point selected by the user. The track reference frame is located as seen in the same figure at the track centerline between the right and left rail.

A point $p$ in the track reference frame can be defined by the position vector $\mathbf{r}_{\mathrm{p}}$, which represents the location of point $p$ with respect to the fixed reference frame (X Y Z) as follow

$$\mathbf{r}_p = \mathbf{p} + \mathbf{u} = \mathbf{p} + \mathbf{A}\,\bar{\mathbf{u}} \tag{4.4}$$

where $\mathbf{p}$ is the global position vector of the of origin $\mathrm{O_T}$ of the track reference frame. $\mathbf{u}$ is the global position vector of the point $p$ with respect to the fixed frame of reference. $\bar{\mathbf{u}}$ is the position vector of the point $p$ with respect to the track frame of reference. $\mathbf{A}$ is the transformation matrix form the track frame of reference ($\mathrm{X_T}$ $\mathrm{Y_T}$ $\mathrm{Z_T}$) to the fixed frame (X Y Z). This matrix can be written as [57]:

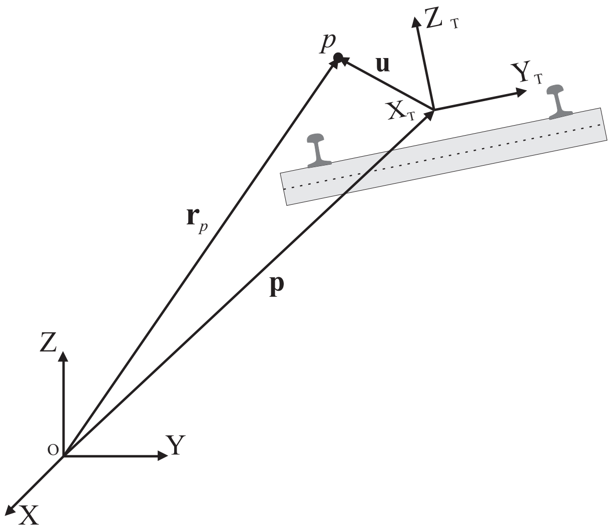

Figure 4.6. *Transformation from Solid to Track reference frame*

$$\mathbf{A} = \mathbf{A}_z \, \mathbf{A}_y \, \mathbf{A}_x \tag{4.5}$$

The selected sequence of rotations was achieved by making three consecutive rotations about Z-axis and then rotation about Y-axis and finally rotation about X-axis. For large rotation angles, the use of Euler angles in the calculation of the transformation matrix may cause singularity problems [3, 61]. To avoid these problems, the selection of the rotation sequence for the track frame is chosen by making the largest rotation values at the extremes of the rotation sequence. In the present case, the rotation about Z-axis is selected in the beginning and the rotation about X-axis presenting the roll rotation or the cant angle of the track [19, 57] was selected in the end of the rotation sequence. The expression of the transformation matrix **A** illustrated in details in the included appendix[1].

### 4.3.2 Transformation from body to fixed reference frame

The description of the transformation from the fixed reference frame to the body frame is illustrated by defining the three main reference frames required to present the general rigid body which rather than the wheelset. Figure (4.7) shows the sequence of the transformation, from the body to the track frame of reference. Afterwards, transformation from track to global frame of reference. The point $p$ located on the rigid body can be defined by defining the position vector with respect to the global reference frame as:

---

[1] Appendix **A**

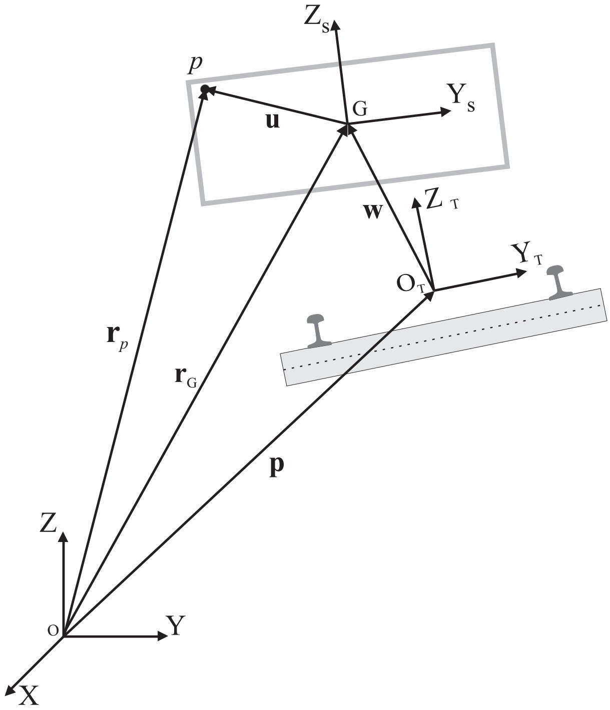

Figure 4.7. *Transformation from Body reference frame to Fixed reference frame*

$$\begin{aligned} \mathbf{r}_p &= \mathbf{r_G} + \mathbf{u} \\ &= \mathbf{p} + \mathbf{A}\,\bar{\mathbf{w}} + \mathbf{A}\,\mathbf{B}\,\bar{\bar{\mathbf{u}}} \end{aligned} \tag{4.6}$$

where $\mathbf{r}_G$ is the global position vector of the center of mass of the body which coincides with the origin of the body reference frame. $\bar{\mathbf{w}}$ is the position vector of the reference frame origin G with respect to the track reference frame. $\mathbf{B}$ is the transformation matrix required to define the orientation of the rigid body reference frame ($X_S$ $Y_S$ $Z_S$) with respect to the track reference frame. $\bar{\bar{\mathbf{u}}}$ is the position vector of the point $p$ with respect to the rigid body reference frame.

The transformation matrix $\mathbf{B}$ is obtained by three consecutive rotations using Euler angles principle, but with the difference that the rotation sequence in our case includes: rotation about Z-axis with an angle $\theta_z$, then a rotation about X-axis with an angle $\theta_x$, and finally as the largest value for the rotation angles used in the transformation is the rotation about Y-axis with an angle $\theta_y$ which represents the rotation of the wheelset. The selection of the rotation sequence here is used to avoid the singularity problems that may be appeared in case of dealing with high values for the rotation angles used during the motion.

To conclude the previous idea for the transformation frome a system of refrence to another, Figure (4.8) is demonestrating transformation matrices requiered for the identities used in the formulations applied to the the multibody methodology proposed for making dynamic simulation for railway vehicles.

It is appeared from the figure shown, the matrix **A** is used to define the orientation of the track reference frame with respect to the fixed reference frame. The matrix **B** is used to define the orientation of the rigid body reference frame with respect to the track reference frame. To define the orientation of the rigid body reference frame with respect to the global reference frame, it was necessary to represent two successive transformation represented by the multiplication of the two matrices **A** and **B** respectively.

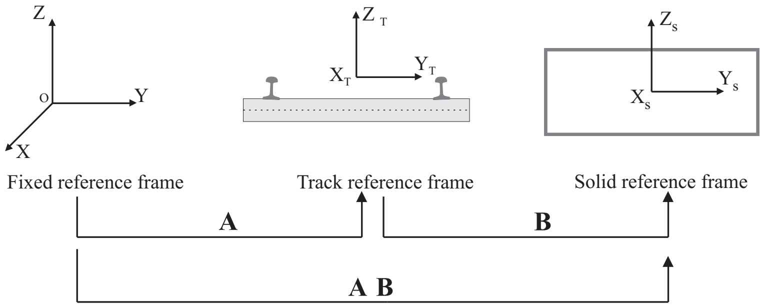

Figure 4.8. *Successive transformations between frame of references*

## 4.4 Track model

The first step used in the track centerline parameterization is the selection of the approach used in the parameterization. One of the most common approaches used is the parameterization using the analytical segments [49, 50] for representation of the track parameters. In this procedure the track is built using a combination of tangent track, transition curve and circular curve segments. The second approach that can be used is the parameterization of the track centreline using cubic splines [41, 50], between the control points that can be used as an input data, defined by the user and the corresponding cant angle at each control point.

Once we have clearly defined the approach that will be used to make the parameterization, the centreline can be easily parameterized as a function of the parameter $\sigma$, which represent the point that define the location of the wheelset along the track centerline. The cant angle is parameterized as function of the track distance covered by the vehicle $\sigma$ and the frame of reference associated to the track centreline after the cant angle rotation can be calculated. so the procedure followed is summarized in the following steps:

- Definition of the approach used for parameterization of the track centreline whether it is analytical segments or cubic splines, this part is defined by the user.

- The track centreline is parameterized as function of the parameter $\sigma$.
- The cant angle is parameterized as a function of the parameter $\sigma$. Then, the orientation of the track frame of reference is completely defined by the determination of the cant angle.
- The output data is defined to all the necessary parameters required to define the track centreline geometry. This data is used online during the dynamic analysis of the multibody systems.

The method used in the current work for parameterization of the track centreline is the analytical segments approach [39, 48, 49] . The track is defined by using a combination of tangent or straight line segment, followed by transition curve segment to ensure the smooth transition between the tangent part and the circular curve segment.

### 4.4.1 Track modelling using analytical segments

In this section, a detailed description is provided for designed track used in the dynamic simulation. The mathematical presentation of the track at each point is represented in the section below to give position vector and then all the kinematic variables at each distance $\sigma$ on the track. In the work, presented the track segments are selected to form special case-without loss of generality-for the designed path used in the simulation presented in the following order:

1. Straight line track.
2. Transition curve.
3. Circular curve with constant radius $R$.

The proposed methodology in the definition of the track configuration can be applied for any path designed for the track as well as including the track defects and irregularities. The track reference frame represented by the three orthogonal axes ($\mathrm{X_T}$ $\mathrm{Y_T}$ $\mathrm{Z_T}$) will be assigned to the centreline between the left rail and the right rail as shown in Figure (4.9). The $\mathrm{X_T}$ axis is pointing to the rolling direction, as seen in section (4.2.3) which can be shown in figure (4.10)

### 4.4.2 Straight line stage

The track presented is started with a straight segment as shown in Figure (4.11). The starting point of the straight segment of the track is the distance point $\sigma = 0$. The end point of the straight segment is the point $\sigma = l_1$. This can be represented by the simple straight line equation of first order as

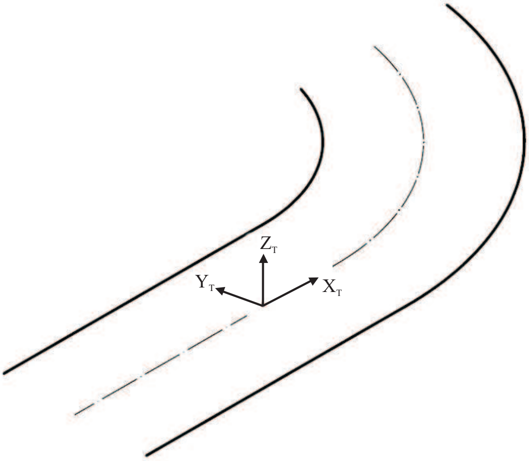

Figure 4.9. *Track model used in the dynamic simulation*

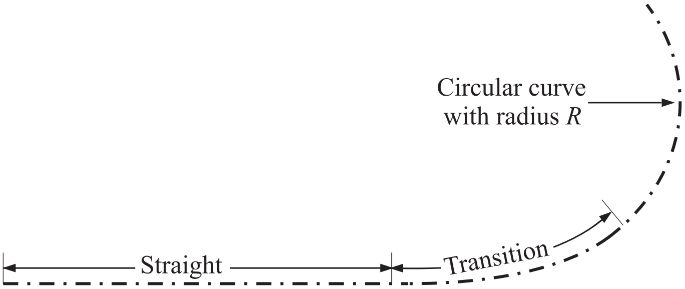

Figure 4.10. *Track segments definitions*

$$x(\sigma) = a_s\sigma + b_s \tag{4.7}$$

where $a_s$ ,$b_s$ are constants of the straight line equation. This stage is considered to be the first stage in the track simulation. Then the track can be parameterized as a function of the track distance covered as

$$\mathbf{p}(\sigma) = \begin{bmatrix} x(\sigma) \\ y(\sigma) \\ z(\sigma) \end{bmatrix} \tag{4.8}$$

substituting with the values of $\sigma = 0$ at the beginning of the straight stage and $\sigma = l_1$ at the end of the straight stage, also by substituting with the value of the cant height $h_{to}$ for obtaining the $z$ position at the straight track stage, we find that

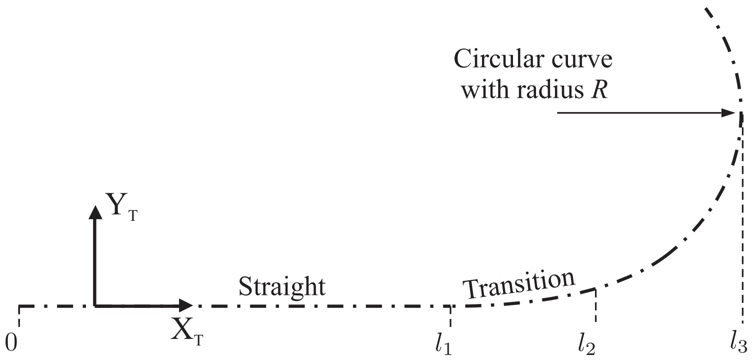

Figure 4.11. *Track segment lengths*

$$x(\sigma) = \sigma \tag{4.9}$$

$$z(\sigma) = h_{to} \tag{4.10}$$

then the position vector of a point on the track in the straight line stage can described by

$$\mathbf{p}(\sigma) = \begin{bmatrix} \sigma \\ 0 \\ h_{to} \end{bmatrix} \tag{4.11}$$

### 4.4.3 Transition curve stage

The transition curve is known mathematically as Euler spiral, fitted between a straight line and circular curve. The transition curve starts with a radius equal to the infinity and ends with a radius equal to the radius of curvature of the adjacent curve. In the proposed track model, a transition curve of the type Clothoid as shown in the Figure (4.12) is used to define the transition curve stage.

The transition curve is presented by the Clothoid curve connects the straight and circular tracks to ensure the continuity in the first and second derivatives of the railway in the transition points. The transition curves are responsible for smooth variation of the lateral acceleration of the vehicle, when it moves from a straight track to a circular track or between two track segments of the same type with different radius or orientation [50].

To represent the transition between the straight line stage and the circular curve stage a Clothoid is defined. The tracing method used for the transition curve used is the conserved radius method, which leads to the parabolic equation of the Clothoid obtained given by the following expression

$$y(\sigma) = \frac{x^3(\sigma)}{6\, l_{clo}\, R} \tag{4.12}$$

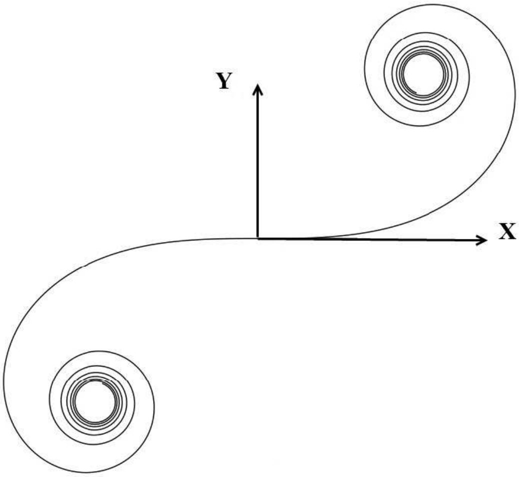

Figure 4.12. *Transition curve presented by Clothoid curve*

where $l_{clo}$ is the Clothoid length, and $R$ is the radius of the circular curve of the following stage. Using Fresnel integral, we can represent the coordinates of the Clothoid as a function of the distance $\sigma$ as follow:

$$x\left(\sigma\right) = \sigma - \frac{1}{10}\frac{\sigma^5}{\pi^2}K^2 \tag{4.13}$$

$$y\left(\sigma\right) = \frac{1}{6}\sigma^3\,K - \frac{1}{84}\frac{\sigma^7}{\pi^2}K^3 \tag{4.14}$$

where $K$ is a constant can be calculated as:

$$K\; = \frac{1}{l_{clo}\,R} \tag{4.15}$$

The transition curve in our simulation is started at the point $\sigma = l_1$ and is ended at the point of connection to the constant radius curve at the point $\sigma = l_1 + l_2$, where $l_2$ is the Clothoid length $l_{clo}$.

It is necessary to define the cant value at the starting and at the end of each stage. So for the transition cure stage here represented by the Clothoid, the hight at the beginning is $h_{to}$ and at the end of the stage is $h_{tmax}$. By assuming linear cant through the transition stage we find that the elevation of any point on the track can be found by

$$z\left(\sigma\right) = h_{to} + \frac{h_{tmax} - h_{to}}{l_{clo}}\,\sigma \tag{4.16}$$

The value of $h_{to}$ is equal to zero in case of the straight track, then the position vector of any point on the Clothoid curve can be written in matrix form in the planer representation as follow

$$\mathbf{S}(\sigma) = \begin{bmatrix} \sigma - \frac{1}{10}\frac{\sigma^5}{\pi^2}K^2 \\ \\ \frac{1}{6}\sigma^3 K - \frac{1}{84}\frac{\sigma^7}{\pi^2}K^3 \\ \\ \frac{h_{tmax} - h_{to}}{l_{clo}}\sigma \end{bmatrix} \tag{4.17}$$

### 4.4.4 Circular curve stage

This is the third stage in the proposed track geometry. In this stage, the track take a circular path with a constant radius of curvature $R$, the stage is started at the end point of the Clothoid which can be assigned to the point $\sigma = l_1 + l_2$, and is ended at the point at which $\sigma = l_1 + l_2 + l_3$, where $l_3$ is the circular curve length . By defining the Clothoid angle that can be written as:

$$\Phi(\sigma) = \arctan\left(\frac{dy/d\sigma}{dx/d\sigma}\right) \tag{4.18}$$

We can ratiocinate that the initiation angle of the circular curve is the angle of the Clothoid when the value of $\sigma$ is equal to the Clothoid length $l_{clo}$ and this can be calculated by the following expression:

$$\Phi(\sigma) = \Phi(\sigma = l_{clo}) \tag{4.19}$$

then the angle of the circular curve segment at any point $\sigma$ on the circular curve, can be calculated by the expressions:

$$\Phi_P = \Phi(\sigma) + \frac{\sigma}{R} \tag{4.20}$$

where $R$ is the circular segment radius of curvature. The position vector of the of the circular curve initiation point is indicated by the subscript $i$, can be written as:

$$x_i(\sigma) = x(l_{clo}) \tag{4.21}$$

$$y_i(\sigma) = y(l_{clo}) \tag{4.22}$$

Finally the components of the position vector of a point on the circular curve indicated by the subscript $cir$ are found through the next expression:

$$x_{cir}(\sigma) = \sin\left(\frac{\sigma}{R} + \Phi_i\right) - \sin(\Phi_i)\ R + x_i \tag{4.23}$$

$$y_{cir}(\sigma) = -\cos\left(\frac{\sigma}{R} + \Phi_i\right) + \cos(\Phi_i)\ R\ +\ y_i \tag{4.24}$$

$$z_{cir}(\sigma) = h_{tmax} \tag{4.25}$$

then the position vector of any point on the palne curve can be written in matrix as:

$$\mathbf{S}(\sigma) = \begin{bmatrix} x_{cir}(\sigma) \\ y_{cir}(\sigma) \\ z_{cir}(\sigma) \end{bmatrix} \tag{4.26}$$

## 4.5 Theoretical development of the proposed methodology

In the following section, the main formulations for the proposed simulation tool are presented in order to obtain the equations that permit the modelling of the railway vehicle using multibody technique. This technique permits the precise simulation of grand displacements of the rigid bodies, without the simplifications associated to the linearization methods such as in vibration. The developed methodology considers various configurations of the railway vehicle and different designs for the track segments. The bibliographic revision shows a great work done by various investigation groups and earlier development was developed by A. Shabana [61], P. Fisette [55] and J. Pombo [48]. The mentioned authors developed other techniques based on dependent coordinate systems using ( Euler parameters and Rodriguez formula), which have a principle advantage that there is no singular configuration can be obtained. In this work:

- Singularity problems were solved by the selection of the rotation sequence, taking into account that only the roll angle of the wheelset and the rotation of the curve may reach or exceed 90°.
- Intermediate reference frame was used to define the contact with better precise.

### 4.5.1 Kinematic analysis of rigid body system

The kinematic analysis deals with the study of the system motion independently of the forces that cause such motion of the body. The kinematic analysis is done to obtain the system position and velocity vectors as well as determination of the system generalized coordinates [2, 57]. Reaching to this point, we can define the position vector of a point located on the rigid body as shown in figure (4.7) using equation (4.6). Taking the first time derivative for the position vector, we can obtain the velocity vector of an arbitrary point located on the rigid body as

$$\dot{\mathbf{r}}_p = \dot{\mathbf{p}} + \dot{\mathbf{A}}\,\bar{\mathbf{w}} + \mathbf{A}\,\dot{\bar{\mathbf{w}}} + \left(\dot{\mathbf{A}}\,\mathbf{B} + \mathbf{A}\,\dot{\mathbf{B}}\right)\,\bar{\bar{\mathbf{u}}} \tag{4.27}$$

where $\dot{\mathbf{r}}_p$ is the velocity vector of an arbitrary point $p$. $\dot{\mathbf{p}}$ is the velocity of the origin of the track reference frame. $\dot{\mathbf{A}}$ first time derivative of the transformation matrix required to transform from the track frame to the fixed reference frame[1]. $\dot{\bar{\mathbf{w}}}$ is the relative velocity of the of body reference frame coincides with the body inertial frame of reference located in G. $\dot{\mathbf{B}}$ is first time derivative of the transformation matrix required to transform from the body frame of reference to the track frame of reference[1].

### 4.5.2 Total kinetic energy of the system

The kinetic energy of a general rigid body can be found by the form [57]

$$T = \frac{1}{2}\dot{\mathbf{q}}^{\mathrm{T}}\,\mathbf{M_s}\,\dot{\mathbf{q}} \tag{4.28}$$

where $\mathbf{q}$ is the vector of the generalized coordinates of the rigid body given by the equation:

$$\mathbf{q} = \begin{bmatrix} \bar{\mathbf{w}}^{\mathrm{T}} & \boldsymbol{\theta}^{\mathrm{T}} \end{bmatrix}^{\mathrm{T}} \tag{4.29}$$

where $\bar{\mathbf{w}}$ is the vector of displacements of the body reference frame. $\boldsymbol{\theta}$ is the vector of the rotation angles determining the orientation of the body. According to the portioning of the generalized coordinates of the rigid body, the kinetic energy can be found by the following equation

$$T = T_{\bar{\mathrm{w}}\bar{\mathrm{w}}} + T_{\bar{\mathrm{w}}\,\theta} + T_{\theta\theta} \tag{4.30}$$

where $T$ is total kinetic energy of the body. $T_{\bar{\mathrm{w}}\bar{\mathrm{w}}}$ is the translational kinetic energy term, $T_{\bar{\mathrm{w}}\theta}$ represents the coupling between the translational kinetic energy and the rotational kinetic energy term. $T_{\theta\theta}$ is the rotational kinetic energy term. For the rigid body system we have in our case, the term that represents the coupling between the translational and rotational kinetic energy $T_{\bar{\mathrm{w}}\theta}$, is null because the rigid body frame of reference ($\mathrm{X_S}$ $\mathrm{Y_S}$ $\mathrm{Z_S}$) is located at center of mass of the rigid body. Then the total kinetic energy of the system in this case will be written as

$$T = T_{\bar{\mathrm{w}}\bar{\mathrm{w}}} + T_{\theta\theta} \tag{4.31}$$

---

[1] Appendix **A**

### 4.5.3 Translational kinetic energy of the system

The translational kinetic energy term of the rigid body can be written as

$$T_{\bar{\mathrm{w}}\bar{\mathrm{w}}} = \frac{1}{2}\,\dot{\mathbf{r}}_G^{\mathrm{T}}\,\mathbf{M}_s\,\dot{\mathbf{r}}_G \tag{4.32}$$

where $\mathbf{r}_G$ is the position vector of the center of mass of the rigid body figure (4.7) which can be found by

$$\mathbf{r}_G = \mathbf{p} + \mathbf{A}\,\bar{\mathbf{w}} \tag{4.33}$$

and $\mathbf{M}_s$ is the mass matrix of the rigid body[1] can be written as

$$\mathbf{M}_s = m_s\,\mathbf{I}_{3\times 3} \tag{4.34}$$

where $m_s$ is the mass of the rigid body. The vector representing the velocity of the center of mass is found by calculating the time derivative for the position vector of the body mass center presented by the equation (4.33) as shown:

$$\dot{\mathbf{r}}_G = \dot{\mathbf{p}} + \dot{\mathbf{A}}\,\bar{\mathbf{w}} + \mathbf{A}\,\dot{\bar{\mathbf{w}}} \tag{4.35}$$

substituting in the translational kinetic energy term we obtain

$$\begin{aligned} T_{\bar{\mathbf{w}}\bar{\mathbf{w}}} = {} & \tfrac{1}{2}\dot{\mathbf{p}}^{\mathrm{T}}\,\mathbf{M}_s\,\dot{\mathbf{p}} + \left(\dot{\mathbf{p}}^{\mathrm{T}} + \tfrac{1}{2}\,\dot{\bar{\mathbf{w}}}^{\mathrm{T}}\,\mathbf{A}^{\mathrm{T}} + \bar{\mathbf{w}}^{\mathrm{T}}\,\dot{\mathbf{A}}^{\mathrm{T}}\right)\mathbf{M}_s\,\mathbf{A}\,\dot{\bar{\mathbf{w}}} \\ & + \left(\dot{\mathbf{p}}^{\mathrm{T}} + \tfrac{1}{2}\bar{\mathbf{w}}^{\mathrm{T}}\,\dot{\mathbf{A}}^{\mathrm{T}}\right)\mathbf{M}_s\,\dot{\mathbf{A}}\,\bar{\mathbf{w}} \end{aligned} \tag{4.36}$$

### 4.5.4 Rotational kinetic energy of the system

The rotational kinetic energy of the rigid body can be written as

$$T_{\theta\theta} = \frac{1}{2}\bar{\bar{\boldsymbol{\omega}}}^{\mathrm{T}}\,\boldsymbol{J}_{\theta\theta}\,\bar{\bar{\boldsymbol{\omega}}} \tag{4.37}$$

where $\boldsymbol{J}_{\theta\theta}$ is the inertia matrix of the rigid body[1], $\bar{\bar{\boldsymbol{\omega}}}$ is the angular velocity of the rigid body represented in the rigid body reference frame which can be written as

$$\bar{\bar{\boldsymbol{\omega}}} = \bar{\bar{\boldsymbol{\tau}}} + \bar{\bar{\boldsymbol{L}}}\,\dot{\boldsymbol{\theta}} \tag{4.38}$$

where $\bar{\bar{\boldsymbol{\tau}}}$ is the track angular velocity vector represented in the body reference frame. The term $\bar{\bar{\boldsymbol{L}}}\,\dot{\boldsymbol{\theta}}$ represents the relative angular velocity of the rigid body with respect to the track frame of reference. $\boldsymbol{L}$[2] represents the matrix that relates the angular velocity vector of the rail to the time derivatives of the orientation parameters [60]. By substitution in the rotational kinetic energy equation (4.37) it is found that

---

[1] Appendix **A**

$$T_{\theta\theta} = \frac{1}{2}\,\bar{\bar{\boldsymbol{\tau}}}^{\mathrm{T}}\,\boldsymbol{J}_{\theta\theta}\,\bar{\bar{\boldsymbol{\tau}}} + \left(\bar{\bar{\boldsymbol{\tau}}}^{\mathrm{T}} + \frac{1}{2}\dot{\boldsymbol{\theta}}^{\mathrm{T}}\,\bar{\bar{\boldsymbol{L}}}^{\mathrm{T}}\right)\boldsymbol{J}_{\theta\theta}\,\bar{\bar{\boldsymbol{L}}}\,\dot{\boldsymbol{\theta}} \tag{4.39}$$

By substitution with equation (4.36) and equation (4.39), the total kinetic energy term represented can be found by

$$\begin{aligned} T = {} & \tfrac{1}{2}\dot{\mathbf{p}}^{\mathrm{T}}\,\mathbf{M}_s\,\dot{\mathbf{p}} + \left(\dot{\mathbf{p}}^{\mathrm{T}} + \tfrac{1}{2}\,\dot{\bar{\mathbf{w}}}^{\mathrm{T}}\,\mathbf{A}^{\mathrm{T}} + \bar{\mathbf{w}}^{\mathrm{T}}\,\dot{\mathbf{A}}^{\mathrm{T}}\right)\mathbf{M}_s\,\mathbf{A}\,\dot{\bar{\mathbf{w}}} \\ & + \left(\dot{\mathbf{p}}^{\mathrm{T}} + \tfrac{1}{2}\bar{\mathbf{w}}^{\mathrm{T}}\,\dot{\mathbf{A}}^{\mathrm{T}}\right)\mathbf{M}_s\,\dot{\mathbf{A}}\,\bar{\mathbf{w}} + \tfrac{1}{2}\,\bar{\bar{\boldsymbol{\tau}}}^{\mathrm{T}}\,\boldsymbol{J}_{\theta\theta}\,\bar{\bar{\boldsymbol{\tau}}} + \left(\bar{\bar{\boldsymbol{\tau}}}^{\mathrm{T}} + \tfrac{1}{2}\dot{\boldsymbol{\theta}}^{\mathrm{T}}\,\bar{\bar{\boldsymbol{L}}}^{\mathrm{T}}\right)\boldsymbol{J}_{\theta\theta}\,\bar{\bar{\boldsymbol{L}}}\,\dot{\boldsymbol{\theta}} \end{aligned} \tag{4.40}$$

### 4.5.5 Dynamic analysis of rigid body system

The dynamic analysis of multibody systems consists of the study of their motion as response to the external applied forces as well as the moments [1, 26, 57]. The motion of the system is generally not prescribed, being its calculation one of the principle objectives of the dynamic analysis. This type of analysis also provides a process to estimate external forces that are dependent on the relative position between the system components, such as those type of forces generated by springs, dampers and actuators. Also the external forces generated as a consequence of the interaction between the system and its surrounding environment, such as contact and friction forces are considered.

The primary stage in setting up a computer model for the railway dynamic analysis is to prepare the mathematical equations that represent the vehicle-track system. These set of equations are called the equation of motion and they are usually a second order differential equations. The equations of motions are prepared depending on the complexity of the vehicle model and the components of the system. The railway system is considered to be a connection of rigid bodies and mass less elements, this is called MBS [24] and the degree of complexity of the simulation carried out on the system varies depending on the required results. In the proceeding context, the equation of motions of the MBS used in the computer model were developed assuming that all the bodies are rigid bodies with 6 DOF.

#### 4.5.5.1 Lagrangian approach for calculating the equations of motion

In this section, the dynamic equation of motion of rigid body is derived. To determine the configuration of the rigid body system, it was first necessary to define generalized coordinates $\mathbf{q}$ [61], as defined in the previous section of the kinematic analysis as defined in equation (4.29), that specifies the position and orientation of each point of any body in the multibody system shown by figure (4.7).

---

[2] Appendix **A**

In the *Lagrangian* approach, scalar quantities such as the virtual work and the kinetic and potential energies are used to develop the equations of motion of the body and in this case there is no need to study the equilibrium of the bodies in the system separately [43, 61]. Due to the linear independency of the generalized coordinates, the application of *D'Alembert- lagrange's* equation leads to *Lagrange's* Equation which is given by the equation

$$\left(\frac{d}{dt}\left(\frac{\partial T}{\partial \dot{\mathbf{q}}}\right)-\frac{\partial T}{\partial \mathbf{q}}\right)^{T}-\mathbf{Q}=0 \tag{4.41}$$

where $\mathbf{q}$, $\dot{\mathbf{q}}$ are vectors of generalized coordinate and velocities respectively. $\mathbf{Q}$ is the generalized force vector associated to the generalized coordinate vector [57, 61], which can be written as follow

$$\mathbf{Q}=\begin{bmatrix}\mathbf{Q}_{\bar{\mathrm{w}}}\\ \mathbf{Q}_{\boldsymbol{\theta}}\end{bmatrix} \tag{4.42}$$

#### 4.5.5.2 Quadratic velocity vector

By definition of the time derivative of the generalized coordinates vector $\dot{\mathbf{q}}$ associated to the rigid body, we can find that the coordinates are the time derivative of the displacements included in the vector $\dot{\bar{\mathbf{w}}}$ and the time derivatives of the rotation angles of the rigid body included in the vector $\dot{\boldsymbol{\theta}}$.

Starting with the translational component of the generalized coordinate vector, we get the derivative of the kinetic energy with respect to the velocity vector $\dot{\bar{\mathbf{w}}}$ so

$$\frac{\partial T}{\partial \dot{\bar{\mathbf{w}}}}=\left(\dot{\mathbf{p}}^{\mathrm{T}}+\dot{\bar{\mathbf{w}}}^{\mathrm{T}}\,\mathbf{A}^{\mathrm{T}}+\bar{\mathbf{w}}^{\mathrm{T}}\,\dot{\mathbf{A}}^{\mathrm{T}}\right)\mathbf{M}_s\,\mathbf{A} \tag{4.43}$$

by finding the time derivative term for the previous equation

$$\begin{aligned}\frac{d}{dt}\left(\frac{\partial T}{\partial \dot{\bar{\mathbf{w}}}}\right)=&\ddot{\bar{\mathbf{w}}}^{\mathrm{T}}\,\mathbf{A}^{\mathrm{T}}\,\mathbf{M}_s\,\mathbf{A}+2\,\dot{\bar{\mathbf{w}}}^{\mathrm{T}}\,\dot{\mathbf{A}}^{\mathrm{T}}\,\mathbf{M}_s\,\mathbf{A}+\dot{\bar{\mathbf{w}}}^{\mathrm{T}}\,\mathbf{A}^{\mathrm{T}}\,\mathbf{M}_s\,\dot{\mathbf{A}}+\\&\ddot{\mathbf{p}}^{\mathrm{T}}\,\mathbf{M}_s\,\mathbf{A}+\dot{\mathbf{p}}^{\mathrm{T}}\mathbf{M}_s\,\dot{\mathbf{A}}+\bar{\mathbf{w}}^{\mathrm{T}}\,\ddot{\mathbf{A}}^{\mathrm{T}}\,\mathbf{M}_s\,\mathbf{A}+\bar{\mathbf{w}}^{\mathrm{T}}\,\dot{\mathbf{A}}^{\mathrm{T}}\mathbf{M}_s\,\dot{\mathbf{A}}\end{aligned} \tag{4.44}$$

The same by finding the time derivative term for rotational component of the generalized coordinate vector, we can get the derivative of the kinetic energy with respect to $\dot{\boldsymbol{\theta}}$

$$\frac{\partial T}{\partial \dot{\boldsymbol{\theta}}}=\left(\dot{\boldsymbol{\theta}}^{\mathrm{T}}\,\bar{\bar{\boldsymbol{L}}}^{\mathrm{T}}+\bar{\bar{\boldsymbol{\tau}}}^{\mathrm{T}}\right)\boldsymbol{J}_{\theta\theta}\,\bar{\bar{\boldsymbol{L}}} \tag{4.45}$$

by finding the time derivative term for the previous equation

$$\frac{d}{dt}\left(\frac{\partial T}{\partial \dot{\boldsymbol{\theta}}}\right) = \left(\ddot{\boldsymbol{\theta}}^{\mathrm{T}}\,\bar{\bar{\boldsymbol{L}}}^{\mathrm{T}} + \dot{\boldsymbol{\theta}}^{\mathrm{T}}\,\dot{\bar{\bar{\boldsymbol{L}}}}^{\mathrm{T}} + \dot{\bar{\bar{\boldsymbol{\tau}}}}^{\mathrm{T}}\right) \boldsymbol{J}_{\theta\theta}\,\bar{\bar{\boldsymbol{L}}} + \left(\dot{\boldsymbol{\theta}}^{\mathrm{T}}\,\bar{\bar{\boldsymbol{L}}}^{\mathrm{T}} + \bar{\bar{\boldsymbol{\tau}}}^{\mathrm{T}}\right) \boldsymbol{J}_{\theta\theta}\,\dot{\bar{\bar{\boldsymbol{L}}}} \tag{4.46}$$

#### 4.5.5.3 Derivatives of the K.E with respect to generalized coordinates

Finding the derivative of the kinetic energy of the system with respect to the displacement $\bar{\mathbf{w}}$ vector, it is found that

$$\frac{\partial T}{\partial \bar{\mathbf{w}}} = \left(\dot{\mathbf{p}}^{\mathrm{T}} + \bar{\mathbf{w}}^{\mathrm{T}}\,\dot{\mathbf{A}}^{\mathrm{T}} + \dot{\bar{\mathbf{w}}}^{\mathrm{T}}\,\mathbf{A}^{\mathrm{T}}\right) \mathbf{M}_s\,\dot{\mathbf{A}} \tag{4.47}$$

In the rotational kinetic energy equation, the term $\bar{\bar{\boldsymbol{\tau}}}$ is represented in the rigid body frame of reference. The same term can be written in the track frame of reference using the relations defined in Chapter (4.2) as

$$\bar{\bar{\boldsymbol{\tau}}} \,=\, \mathbf{B}^{\mathrm{T}}\,\bar{\boldsymbol{\tau}} \tag{4.48}$$

Then the kinetic rotational energy can be found by

$$T_{\theta\theta} = \frac{1}{2}\,\bar{\boldsymbol{\tau}}^{\mathrm{T}}\,\mathbf{B}\,\boldsymbol{J}_{\theta\theta}\,\mathbf{B}^{\mathrm{T}}\,\bar{\boldsymbol{\tau}} + \bar{\boldsymbol{\tau}}^{\mathrm{T}}\,\mathbf{B}\,\boldsymbol{J}_{\theta\theta}\,\bar{\bar{\boldsymbol{L}}}\,\dot{\boldsymbol{\theta}} + \frac{1}{2}\dot{\boldsymbol{\theta}}^{\mathrm{T}}\,\bar{\bar{\boldsymbol{L}}}^{\mathrm{T}}\,\boldsymbol{J}_{\theta\theta}\,\bar{\bar{\boldsymbol{L}}}\,\dot{\boldsymbol{\theta}} \tag{4.49}$$

The same for the rotational part, finding the derivative of the kinetic energy of the system with respect to the rotation angles vector $\boldsymbol{\theta}$. The rotation angles are included only in both matrices $\mathbf{B}$ and $\bar{\bar{\boldsymbol{L}}}$ corresponding to the rotation sequence of the rigid body, then

$$\frac{\partial T}{\partial \theta_i} = \bar{\boldsymbol{\tau}}^{\mathrm{T}}\frac{\partial \mathbf{B}}{\partial \theta_i}\left(\boldsymbol{J}_{\theta\theta}\,\bar{\bar{\boldsymbol{\tau}}} + \boldsymbol{J}_{\theta\theta}\,\bar{\bar{\boldsymbol{L}}}\,\dot{\boldsymbol{\theta}}\right) + \left(\bar{\bar{\boldsymbol{\tau}}}^{\mathrm{T}} + \dot{\boldsymbol{\theta}}^{\mathrm{T}}\,\bar{\bar{\boldsymbol{L}}}^{\mathrm{T}}\right) \boldsymbol{J}_{\theta\theta}\frac{\partial \bar{\bar{\boldsymbol{L}}}}{\partial \theta_i}\dot{\boldsymbol{\theta}} \tag{4.50}$$

### 4.5.6 Generalized forces associated to the generalized coordinates

The generalized forces are introduced by application of the principle of virtual work [2, 57] in both cases of static and dynamic analysis

#### 4.5.6.1 Virtual displacement

From equation (4.6) describing the position vector of an arbitrary point on the rigid body body, the virtual displacement can be written as

$$\delta \mathbf{r}_p = \mathbf{A}\delta\,\bar{\mathbf{w}} + \mathbf{A}\,\frac{\partial \mathbf{B}}{\partial \boldsymbol{\theta}}\;\bar{\bar{\mathbf{u}}}\,\delta\boldsymbol{\theta} \tag{4.51}$$

#### 4.5.6.2 Generalized force corresponding to generic force vector applied on the body

Assuming that there is a generic force vector $\boldsymbol{F}$ affecting the rigid body. This type of forces can be friction forces, external or internal forces generated by force elements such as springs or dampers. This force vector can be written with respect to the track reference frame as

$$\bar{\boldsymbol{F}} = \mathbf{A}^{\mathrm{T}}\boldsymbol{F} \tag{4.52}$$

#### 4.5.6.3 Virtual work

The virtual work produced from the application of the external force vector can be written as follow

$$\delta W = \boldsymbol{F}^{\mathrm{T}}\,\mathbf{A}\,\delta\bar{\mathbf{w}} + \boldsymbol{F}^{\mathrm{T}}\mathbf{A}\,\frac{\partial \mathbf{B}}{\partial \boldsymbol{\theta}}\;\bar{\bar{\mathbf{u}}}\,\delta\boldsymbol{\theta} \tag{4.53}$$

substituting from equation (4.52) in equation (4.53), then the virtual work can be calculated through the following expression:

$$\delta W = \bar{\boldsymbol{F}}^{\mathrm{T}}\,\delta\bar{\mathbf{w}} + \bar{\boldsymbol{F}}^{\mathrm{T}}\,\frac{\partial \mathbf{B}}{\partial \boldsymbol{\theta}}\;\bar{\bar{\mathbf{u}}}\,\delta\boldsymbol{\theta} \tag{4.54}$$

#### 4.5.6.4 Generalized force

Comparing this expression with the definition of the virtual work [57, 61] that can be expressed as

$$\delta W = \begin{bmatrix} \mathbf{Q}_{\bar{\mathrm{w}}}^{\mathrm{T}} & {\mathbf{Q}_{\theta}}^{\mathrm{T}} \end{bmatrix} \begin{bmatrix} \delta\bar{\mathbf{w}} \\ \delta\boldsymbol{\theta} \end{bmatrix} \tag{4.55}$$

where $\mathbf{Q}_{\bar{\mathrm{w}}}$ is called the generalized force vector associated to the translational vector $\bar{\mathbf{w}}$, and $\mathbf{Q}_{\theta}$ is the generalized coordinate vector associated to the rotational angles vector $\boldsymbol{\theta}$. Furthermore the generalized forces associated to the mentioned generalized coordinates can be written as:

$$\mathbf{Q}_{\bar{\mathrm{w}}} = \bar{\boldsymbol{F}} \tag{4.56}$$

$$Q_{\theta_x} = \bar{\boldsymbol{F}}^{\mathrm{T}} \frac{\partial \mathbf{B}}{\partial \theta_x} \bar{\bar{\mathbf{u}}} \tag{4.57}$$

$$Q_{\theta_y} = \bar{\boldsymbol{F}}^{\mathrm{T}} \frac{\partial \mathbf{B}}{\partial \theta_y} \bar{\bar{\mathbf{u}}} \tag{4.58}$$

$$Q_{\theta_z} = \bar{\boldsymbol{F}}^{\mathrm{T}} \frac{\partial \mathbf{B}}{\partial \theta_z} \bar{\bar{\mathbf{u}}} \tag{4.59}$$

## 4.6 Equations of motion development

Once the contribution of the translational and rotational kinetic energy has been determined, then the corresponding equations of motion could be found by the implementation of the Lagrangian techniques as shown in details in the next section

### 4.6.1 Translational equation of motion

From equations (4.44) and (4.47) in Lagrange's formula we get that

$$\ddot{\bar{\mathbf{w}}}^{\mathrm{T}}\, \mathbf{A}^{\mathrm{T}}\, \mathbf{M}_s\, \mathbf{A} + 2\, \dot{\bar{\mathbf{w}}}^{\mathrm{T}}\, \dot{\mathbf{A}}^{\mathrm{T}}\, \mathbf{M}_s\, \mathbf{A} + \ddot{\mathbf{p}}^{\mathrm{T}}\, \mathbf{M}_s\, \mathbf{A} + \bar{\mathbf{w}}^{\mathrm{T}}\, \ddot{\mathbf{A}}^{\mathrm{T}}\, \mathbf{M}_s\, \mathbf{A} - \mathbf{Q}_{\bar{\mathrm{w}}} = 0 \tag{4.60}$$

using the identities explained in the appendix, we replace the first and second time derivative of the track transformation matrix[1], also the mass matrix replaced with its value, we get that

$$m_s \left( \ddot{\bar{\mathbf{w}}} + \mathbf{A}^{\mathrm{T}}\, \ddot{\mathbf{P}} + 2\, \tilde{\bar{\boldsymbol{\tau}}}\, \dot{\bar{\mathbf{w}}} + \tilde{\bar{\boldsymbol{\tau}}}\, \tilde{\bar{\boldsymbol{\tau}}}\, \bar{\mathbf{w}} + \dot{\bar{\bar{\boldsymbol{\tau}}}}\, \bar{\mathbf{w}} \right) - \mathbf{Q}_{\bar{\mathbf{w}}} = 0 \tag{4.61}$$

### 4.6.2 Rotational equation of motion

The same for the rotational angles vector, from equations (4.45) and (4.50) in Lagrange's formula we get that

$$\bar{\bar{\bar{\boldsymbol{L}}}}^{\mathrm{T}} \boldsymbol{J}_{\theta\theta} \bar{\bar{\bar{\boldsymbol{L}}}}\, \ddot{\boldsymbol{\theta}} + \bar{\bar{\bar{\boldsymbol{L}}}}^{\mathrm{T}} \boldsymbol{J}_{\theta\theta}\, \dot{\bar{\bar{\bar{\boldsymbol{\tau}}}}} + \dot{\bar{\bar{\bar{\boldsymbol{L}}}}}^{\mathrm{T}} \boldsymbol{J}_{\theta\theta} \bar{\bar{\bar{\boldsymbol{\tau}}}} + \bar{\bar{\bar{\boldsymbol{L}}}}^{\mathrm{T}} \boldsymbol{J}_{\theta\theta}\, \dot{\bar{\bar{\bar{\boldsymbol{L}}}}}\, \dot{\boldsymbol{\theta}} + \dot{\bar{\bar{\bar{\boldsymbol{L}}}}}^{\mathrm{T}} \boldsymbol{J}_{\theta\theta}\, \bar{\bar{\bar{\boldsymbol{L}}}}\, \dot{\boldsymbol{\theta}} - \frac{\partial T}{\partial \theta_i} - \mathbf{Q}_{\boldsymbol{\theta}} = 0 \tag{4.62}$$

where the value of the term $\frac{\partial T}{\partial \theta_i}$ can be obtained from equation.(4.50)

---

[1] Appendix **A**

### 4.6.3 Equations of motion of wheelset

The application for studying a rigid body moving on the track, can be represented here by a wheelset system moving along the track model designed for the simulation of the movement for general rigid body system defined in the previous section. The wheelset system should be defined and all the forces acting on the wheelset system including all the contact forces, moments and all forces transmitted from the suspension elements conecting the wheelset to the bogie frame and conecting the bogie frame with the car body.

#### 4.6.3.1 Wheelset

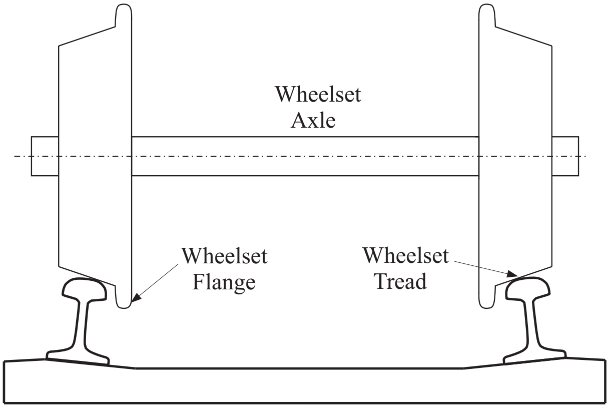

Figure 4.13. *Conventional wheelset*

The fundamental component common in all conventional railway vehicles is the wheelset, it consists of two wheels rigidly fixed to a common axle [58], as shown in figure (4.13). Since the wheels are not free to rotate independently, they have the same rotational speed and a constant distance between the two wheels. The wheels treads are conical and profiled, in order to allow them to negotiate curves without slipping. The wheelsets have steering capabilities and are one of the most components that affect the vehicle stability and its curving performance [24, 48]. The wheel profile is composed of two parts, the wheel tread and the wheel flange. The wheel tread is usually conned at 1/20 or 1/40 and is in contact with the rail head. The wheel flange is provided on the inside edge of the tread. For lateral displacement, it becomes in contact with the rail edge, limiting the wheel lateral motion and reducing the probability to derailment.

#### 4.6.3.2 Wheelset frame of reference

For the wheelset system represented, it is considered to use an intermediate system of reference represented before making the final rotation about the Y- axis which is the axis of rotation of the wheelset. The considered intermediate system of reference will be defined after two consecutive rotations about Z-axis and X-axis respectively. The importance of the use of the intermediate system of reference appeared in the definition of the contact forces and the angular velocity vectors before making the rotation of the wheelset about Y-axis to provide the simplicity of the representation of the angular velocity vector[57], in the intermediate reference frame. Figure (4.14) shows a description of the intermediate reference frame, which consists of three orthogonal coordinates ($\underline{X}$ $\underline{Y}$ $\underline{Z}$). The $\underline{Z}$-axis is pointing to the vertical direction, $\underline{Y}$-axis is parallel to the axis of rotation of the wheelset, and finally the $\underline{X}$-axis is normal to the two other axes and pointing to the direction of motion of the wheelset.

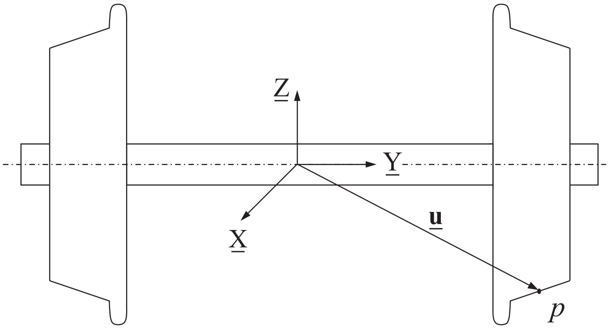

FIGURE 4.14. *Intermediate reference system associated to wheelset system*

For an arbitrary point located on the wheel profile, the position vector be written as follow

$$\underline{\mathbf{u}} = \begin{bmatrix} \underline{\mathrm{u}}_x & \underline{\mathrm{u}}_y & \underline{\mathrm{u}}_z \end{bmatrix}^{\mathrm{T}} \tag{4.63}$$

The lower bar sign means that the quantity represented in the intermediate frame of reference. Then by defining the wheelset frame of reference in combination with the track and fixed reference frames figure (4.15), all the kinematic and dynamic quantities calculated for the wheelset can be represented in the global reference frame as well as the track reference frames.

Contact problem for the wheel rail interaction forms a crucial part in the simulation of the MBS representing the wheelset and this problem can be divided in three distinct but related tasks [39]. The first is the contact geometry which is the problem of finding the location of the contact points on the profiled surfaces taking into account the relative displacements and orientation of the contact bodies. The second is the contact kinematics in which the creepages are defined at the point of contact. Finally the contact mechanics in which the contact tangential creep forces and spin moments are calculated.

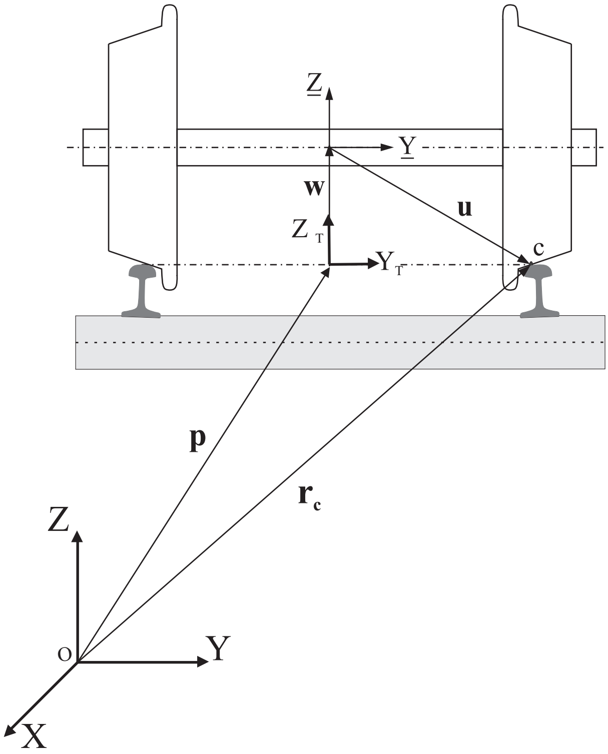

Figure 4.15. *Representation of the Wheelset, Track and Fixed reference frame combination*

### 4.6.3.3 Kinematic analysis of wheelset system

The kinematic analysis means the determination of the system position and velocity vectors as well as the definition of the generalized coordinates of the system under study. Reaching to this point, we can define the position vector of a point located on the wheelset system. The most important points when dealing with wheelset systems are the contact points between the wheel and rail interface, where all the contact forces and moments are defined.

The position vector of the contact points can be determined only after the solution of the geometrical contact problem. The velocity vector at the contact points will be determined by obtaining the first derivative for the contact position vector. In the following section the selected point for the analysis is the contact point located on the wheel tread as demonstrated in figure (4.15). The geometrical contact problem is solved in the current work by using a special procedure explained in the next section for detecting the contact points between the wheel and rail.

## 4.7 Wheel-rail contact model

In the presentation of the wheel and rail models used in the formulations. Both of them is considered to be a rigid body, so that the contact zone could be reduced to a contact point. In reality when two bodies are in contact, the elastic deformation of both surfaces causes the contact to be spread over a finite area, rather than to be concentrated in a point. This finite area is known as the contact patch. In railway vehicle dynamics, when a wheel rolls over the rails exists a micro-slip in the contact zone, which is called creep.

This micro-slip together with the normal contact forces, cause the tangential contact forces, known as creep forces [12, 17, 48]. In the wheel-rail contact problem, the dimension of the contact area is small when compared with the typical dimensions of the contacting bodies. Hence, the normal contact force developed in the contact area can be reduced to a single normal force. According to Hertz theory proposed here to study the wheel-rail contact problem, the dimension of the contact area are only dependent of the normal force, the material properties and the surface curvature of the contact bodies, being independent of the tangential forces that developed in the contact interface. The normal and tangential contact problems are decoupled and their solutions are treated sequentially.

### 4.7.1 Contact geometric problem

The procedure followed to solve the geometrical contact problem will be presented. The main requests, that should be found in the model used for the determination of the geometrical contact problem are summarised in the following points:

I) Having high computational efficiency; as the application of the procedure used in solving the contact problem is the implementation of the model used in the dynamic simulation of the railway vehicles. The computational cost should be minimized as the contact problem is solved at each time step during the numerical integration used in the simulation.

II) Neglecting the transitory effects in the contact model; due to the main use of the contact model in the simulation program. And including the transitory effects will slow down the solution and then the simulation time will increase.

III) Capable of estimation of the contact area with high precision; by the precise determination of the number of contact area at each time step, the shape and size of the contact patch and the amount of penetration produced during the simulation of the wheel-rail contact phenomena.

#### 4.7.1.1 Procedure used in the solution of the geometrical contact problem

The steps used in the solution of the geometrical problem are explained in the following steps:

I) Definition of the wheel and rail surfaces, by the definition of the profiles in the transversal plane of the track. The wheel surface is defined by the rotation of the wheel profile around the axis parallel to the contact plane and the rail surface is defined by means of the extrusion of the points forming the rail profile along the longitudinal direction.

II) Calculating the intersection area between the wheel and rail surfaces in contact, resulting from the relative position of the two contact bodies.

III) Obtaining the amount of the maximum penetration at the each contact area, and determination of the local position of the point of the maximum penetration value.

IV) Calculating the pressure distribution in the contact area that follows the elliptical pressure distribution used by Hertz.

#### 4.7.1.2 Assumptions

I) The model used is based on the virtual interpenetration between the wheel and rail profiles; the use of the virtual interpenetration method instead of the use of the models based on the theoretical point of contact has the following advantages:

    - The use of the method offers better estimation for the contact area as the real geometries of the contact bodies are considered in all the domain of the potential contact area.
    - High computational efficiency, this can be shown by the precise results obtained for the same computational cost offered by the methods based on the theoretical point of contact.
    - The methods based on the virtual interpenetration between surfaces in contact are more reliable as the contact characteristics are estimated by means of the definition of the intersection area.

II) The distribution of the normal pressure in the contact area follows Hertz model; after the definition of the contact ellipse semi axis as the same procedure followed in Hertz normal theory. The normal pressure distribution takes ellipsoidal shape as in Hertz model. The model offers low computational cost with acceptable precision in the obtained results compared with those obtained analytically.

The solution of the geometrical contact problem starts by the definition of the relative position between the two bodies in contact. In the current case, the relative displacements are defined between the wheel and the rail to find the interpenetration between the wheel and rail surfaces as well as the number of contact areas.

For the modelling of the wheel-rail contact problem, two reference systems are used: the first one is the track system of reference ($X_T\, Y_T\, Z_T$) and the second is the wheel-set system of reference ($\underline{X}\,\underline{Y}\,\underline{Z}$) as it was shown in section (4.2).

To solve the geometrical contact problem, the next steps have to be followed:

- Defining the contact surfaces for the wheel and the rail.
- Defining an appropriate method that finds the intersection between the two contact surfaces.
- Defining the mathematical model defining the intersection between a straight line with a cone segment.
- Defining the interpenetration areas defined by strips.

#### 4.7.1.3 Contact surfaces definitions

The interpenetration areas can be obtained by the intersection between the wheel and rail surfaces. These surfaces are obtained by the definition of the wheel and rail profiles. The rail surface is obtained by the intersection of the rail surface with the plane ($Y_T\, Z_T$), and the wheel profile is defined by the intersection of the wheel surface with the plane($\underline{X}\,\underline{Y}$).

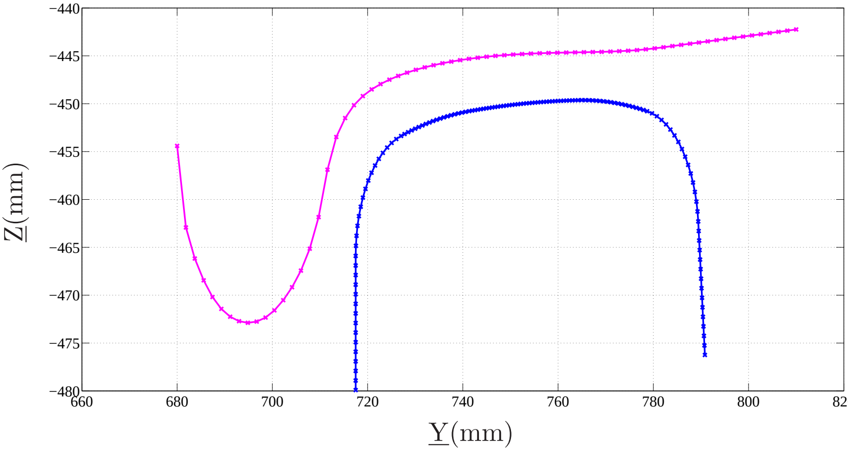

FIGURE 4.16. *Measured Wheel and Rail profiles*

By the definition of the wheel and rail profiles in 2D as shown in figure (4.16), the wheel surface can be generated by the revolution of the wheel profile around the Y axis. On the other hand, the rail profile can be generated by the extrusion of the rail profile point along ($\mathrm{X_T}$) axis.

Once the wheel and rail surfaces are obtained, it is supposed that both of the contact bodies are considered as rigid bodies and existing a penetration between them. By this end, the geometrical contact problem is defined by the determination of the interpenetration between the wheel and rail surface by knowing the relative position between the two surfaces.

The interpenetration area is defined as the projection of the interpenetration volume in the tangential plane to the contact. The interpenetration area in this case represents the potential contact area, this assumption was used in the contact models used by Pitrowiski[35, 45, 46] and Ayasse and Chollet [5], respectively. Once we have defined the surfaces in contact, it is necessary to establish suitable procedure to obtain the intersection between them.

#### 4.7.1.4 Procedure used to obtain the intersection between contact surfaces

According to the model used in this work to define the contact surfaces, it was explained in the previous section that the wheel surface is obtained by the revolution of the wheel profile about the axis parallel to the contact plane. Therefore, each segment on the wheel profile will define a conical segment forming the wheel surface. Each point on the rail profile will define a straight line in the longitudinal ($\mathrm{X_T}$) direction. To obtain the interpenetration area starts by obtaining the intersection between the straight lines presenting the rail surface with the conical segments presenting the wheel surface as seen in figure (4.17).

Simulating the rail surface with straight line even in the curved tracks doesn't introduce excessive errors in the solution, taking into account that the the contact area dimension and the radius of curvature of curved tracks.

By this end, the geometrical contact problem between the wheel and rail surfaces is reduced to a problem where we search for the intersection between a straight line presenting the rail, and a conical segment presenting the wheel as shown in figure (4.18) with the following characteristics:

- Each point of the rail profile represented in the ($\underline{\mathrm{Y}}\,\underline{\mathrm{Z}}$) plane, defines a longitudinal straight line $i$. A point belongs to the straight line $i$ has the coordinates $(x, y_i^r, z_i^r)$ . The sub index $r$ indicates that the point belongs to the rail profile. $x$ parameter indicates the position of the point along the straight line.
- A conical segment $j$ is defined by two consecutive points on the wheel profile presented in the wheelset system of reference that have the coordinates $(0, y_j^w, z_j^w)$ and $(0, y_{j+1}^w, z_{j+1}^w)$ . The super index $w$ indicates that the point belongs to the wheel profile. An important parameter $\zeta$ is defined to present the angle of the wheel profile segment about $\underline{\mathrm{Y}}$ axis, and its value vary from 0 to $2\pi$.

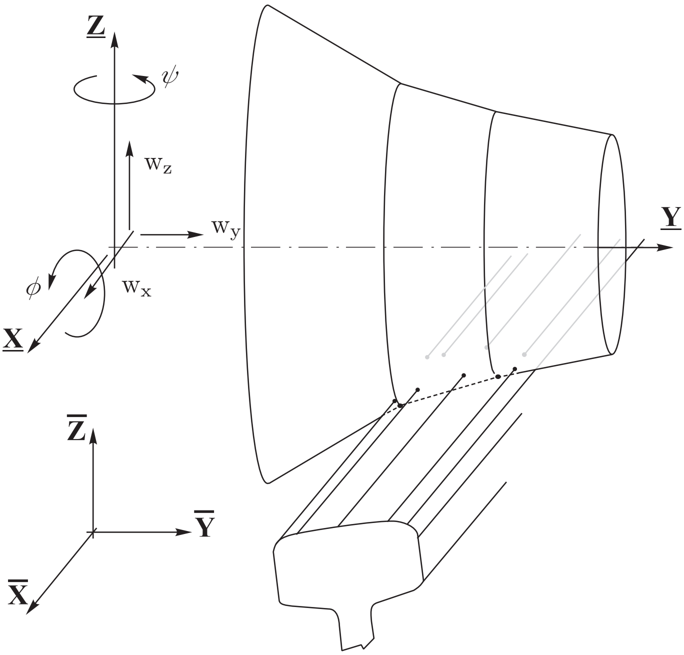

FIGURE 4.17. *System of references of the wheel and rail surfaces used in the definition of the contact geometry problem*

- By defining the relative position between the wheel and rail surfaces, the position of a conical segment belongs to the rigid body presenting the wheel profile, is determined by three translational coordinates $(\mathrm{w_x}, \mathrm{w_y}, \mathrm{w_z})$: in the longitudinal, transversal and vertical direction respectively; and three rotational coordinates: roll angle $\phi^w$ , pitch angle $\theta^w$ and finally yaw angle $\psi^w$.

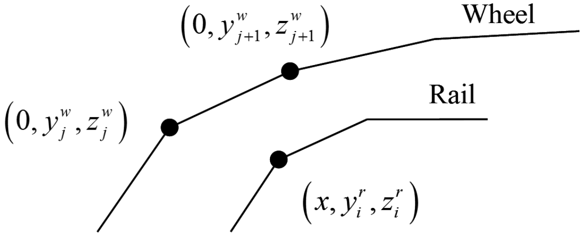

FIGURE 4.18. *Wheel and rail segments used to find the intersection between the wheel-rail surfaces*

#### 4.7.1.5 Intersection between straight line and conical segment

In this section, a system of nonlinear equations will be defined to solve the intersection between a straight line and a conical segment in the space and the solution of these equations will be presented.

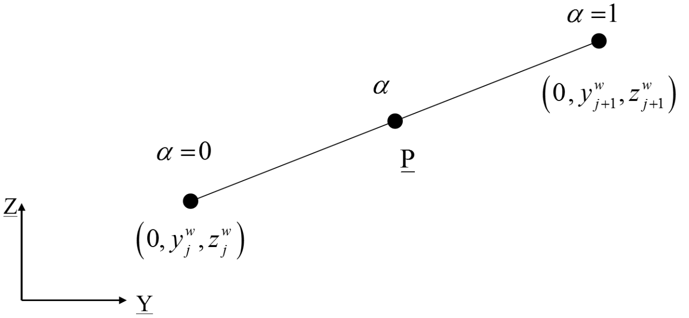

FIGURE 4.19. *Determination of a generic point on a segment on the wheel profile*

Figure (4.19), presents a segment on the wheel profile defined by two consecutive points $(0, y_j^w, z_j^w)$ and $(0, y_{j+1}^w, z_{j+1}^w)$ which defines a conical part by the revolution of the segment about $\underline{\mathrm{Y}}$ axis to form the wheel surface. A new parameter $\alpha$ was defined to generally describe a point on the wheel segment. The value of $\alpha$ is varying from $\alpha = 0$ to $\alpha = 1$ at the extreme points of the segment. A point $\underline{\mathbf{P}}$ on the segment presenting a generic point on the wheel profile can be defined in the wheelset reference system by the following expression

$$\underline{\mathbf{P}} = \mathbf{B}_{\underline{\mathrm{Y}}} \begin{bmatrix} 0 \\ \alpha y^w_{j+1} + (1-\alpha)\, y^w_j \\ \alpha z^w_{j+1} + (1-\alpha)\, z^w_j \end{bmatrix} \tag{4.64}$$

where $\mathbf{B}_{\underline{\mathrm{Y}}}$ is the transformation matrix produced from rotation about the transversal axis $\underline{\mathrm{Y}}$ with an angle $\zeta$. By pre multiplying the last expression by the transformation matrix $\mathbf{B}_{\mathrm{zx}}$, the point $\mathbf{P}$ can be represented in the track system of reference as mentioned in chapter (4.2)

$$\underline{\mathbf{P}} = \mathbf{B}_{\mathrm{zx}}\, \mathbf{B}_{\underline{\mathrm{Y}}} \begin{bmatrix} 0 \\ \alpha y^w_{j+1} + (1-\alpha)\, y^w_j \\ \alpha z^w_{j+1} + (1-\alpha)\, z^w_j \end{bmatrix} \tag{4.65}$$

The modifications made on the model mark a significant modefication which can be noted here by taking the variation in the longitudinal direction as an additional coordinate for the wheelset to add a new degree of freedom to the problem that was not included in the model.

The intersection problem between the wheel and rail can be presented by finding the intersection between the conical segment forming part of the wheel and the straight line presenting the extruded point on the rail profile taking into account the displacement $(\mathrm{w_x}, \mathrm{w_y}, \mathrm{w_z})$ of the wheelset in X, Y and Z direction respectively as well as the rotations $\alpha$ and $\psi$. The intersection can be found by equating the position vector of a generic point on the conical segment $j$ with a point on the straight line $i$ on the rail profile. And by this way a system of three nonlinear equations with three unknown parameters $(x, \zeta, \alpha)$

$$\begin{bmatrix} x \\ y_i^r \\ z_i^r \end{bmatrix} = \mathbf{B}_{zx}\,\mathbf{B}_{\underline{\mathrm{Y}}} \begin{bmatrix} 0 \\ \alpha y^w_{j+1} + (1-\alpha)\, y^w_j \\ \alpha z^w_{j+1} + (1-\alpha)\, z^w_j \end{bmatrix} + \begin{bmatrix} \mathrm{w_x} \\ \mathrm{w_y} \\ \mathrm{w_z} \end{bmatrix} \tag{4.66}$$

The solution of this system of equations will give intersection points between the conical segment and straight line in the space as shown in figure (4.20)

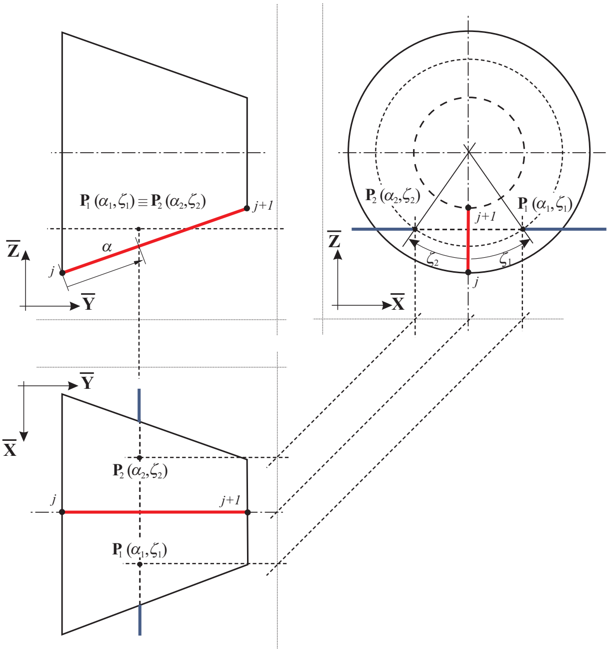

$P_1(\alpha_1,\zeta_1) \equiv P_2(\alpha_2,\zeta_2)$
$j+1$
$\alpha$
$j$
$\overline{Z}$
$\overline{Y}$
$P_2(\alpha_2,\zeta_2)$
$P_1(\alpha_1,\zeta_1)$
$j+1$
$\zeta_2$
$\zeta_1$
$j$
$\overline{Z}$
$\overline{X}$
$\overline{Y}$
$\overline{X}$
$P_2(\alpha_2,\zeta_2)$
$j$
$j+1$
$P_1(\alpha_1,\zeta_1)$

Figure 4.20. *3D view for the intersection between a straight line $i$ with a conical segment $j$*

Existing three possible solutions for the given system of equations:

- No solution existing; in this case the line doesn't intersect with the conical segment.
- Existing one double solution; in case that the line is tangent to the conical segment.

- Existing two solutions; this represents the general case in which the two points of intersection will represent the entrance and exit points of the line with the conical segment.

The solution of the system of nonlinear algebraic equations will reach the following expression

$$A\cos(\zeta)+B\sin(\zeta)+C=0 \tag{4.67}$$

solving the previous equation 4.67, we can obtain the value of the parameter $\zeta$

$$\begin{pmatrix}\zeta_1\\ \zeta_2\end{pmatrix}=\begin{bmatrix}2\arctan\left(\frac{-B+\sqrt{B^2-A^2-C^2}}{C-A}\right)\\ \\ 2\arctan\left(\frac{-B-\sqrt{B^2-A^2-C^2}}{C-A}\right)\end{bmatrix} \tag{4.68}$$

taking the positive value for $\zeta_1$ and the negative value for $\zeta_2$. The three possible solutions can be obtained by solving equation (4.68)

- If the discriminant is negative, this means that there is no real solution and this case presents the case where no intersection can be found because the wheel surface is located above the rail surface.
- If the discriminant is equal to zero, this means that the straight line presenting the rail is tangent to conical segment and in this case $\zeta_1=\zeta_2$.
- In the general case, existing two real solutions representing the entrance and exit points giving two values for $\zeta_1$ and $\zeta_2$ .

For each value of $\zeta$, a new value for the parameter $\alpha$ has to be calculated which indicates the longitudinal position where the straight line $i$ intersects with the conical segment $j$. The values of $\alpha$ can be calculated from equation (4.66) by solving the equation in Y or Z directions giving two values $\alpha_y$ and $\alpha_z$ as follow

$$\alpha_y=\frac{a_1\sin(\zeta)+a_2\cos(\zeta)+a_3}{a_4\sin(\zeta)+a_5\cos(\zeta)+a_6} \tag{4.69}$$

where:

$$\begin{aligned}
a_1&=\sin(\psi)z_j^w\\
a_2&=-\cos(\psi)\sin(\phi)z_j^w\\
a_3&=-y_i^r+\cos(\psi)\cos(\phi)y_j^w+\mathrm{w_y}\\
a_4&=\sin(\psi)\left(z_j^w-z_{j+1}^w\right)\\
a_5&=\cos(\psi)\sin(\phi)\left(z_{j+1}^w-z_j^w\right)\\
a_6&=\cos(\psi)\cos(\phi)\left(y_j^w-y_{j+1}^w\right)
\end{aligned}$$

The same we can obtain the value of $\alpha_z$

$$\alpha_z = \frac{b_1 \sin(\zeta) + b_2 \cos(\zeta) + b_3}{b_4 \sin(\zeta) + b_5 \cos(\zeta) + b_6} \tag{4.70}$$

where:

$$\begin{array}{lcl} b_1 = 0 & ; & b_2 = \cos(\phi) z_j^w \\ b_3 = \sin(\phi) y_j^w - z_i^r + \mathrm{w_z} & ; & \mathrm{b_4} = 0 \\ b_5 = \cos(\phi) \left( z_j^w - z_{j+1}^w \right) & ; & b_6 = \sin(\phi) \left( y_j^w - y_{j+1}^w \right) \end{array}$$

The value of $\alpha_y$ is measured in the horizontal projection, on the other hand the value of $\alpha_z$ is measured in the vertical projection. Generally in the case that the conical segment is located in a vertical direction, this means that the denominator in the expression of $\alpha_y$ will be zero and the value $\alpha$ can be found by the expression of $\alpha_z$. The same as if the conical segment is located in the horizontal direction , this means that the denominator in $\alpha_z$ expression will be null then the value of $\alpha$ will be found by the equation representing $\alpha_y$.

If the value of $\alpha$ within the defined limits $0 \leq \alpha \leq 1$ this means that the straight line $i$ is in intersection with the cone segment $j$. If $\alpha < 0$ this means that it will search for the intersection between the line $i$ with the con segment $j - 1$. If $\alpha > 1$ this means that it will search for the intersection between the line i with the segment $j + 1$.

Finally each of the entrance and exit points produced from the intersection between the line with the conical segment can be found depending on the obtained values of the parameter $\zeta$ and can be determined from equation (4.66) as follow:

$$\begin{aligned} x = & \left(\sin(\psi)\cos(\phi)\,\cos(\zeta) + \cos(\psi)\sin(\zeta)\right)\left(\alpha\, z_{j+1}^w + (1-\alpha)\, z_j^w\right) \\ & - \sin(\psi)\cos(\phi)\,\left(\alpha\, y_{j+1}^w + (1-\alpha)\, y_j^w\right) + \mathrm{w_x} \end{aligned} \tag{4.71}$$

#### 4.7.1.6 Strip definition

The intersection between the wheel profile and the rail profile is presented by means of longitudinal strips resulted from the interpenetration between the two contact surfaces of the wheel and rail respectively. The produced strip figure (4.21) can be defined by the following characteristics:

I) Position vector of the leading intersection point $(x_{iL}, y_{il}, z_{iL})$ and trailing intersection point $(x_{iT}, y_{iT}, z_{iT})$ resulting from the intersection between a conical segment with the straight line segment presenting the rail

II) The strip length $l_s$

The strip length can be defined as the distance between the trailing and leading intersection points

$$l_s = |x_{iL} - x_{iT}| \tag{4.72}$$

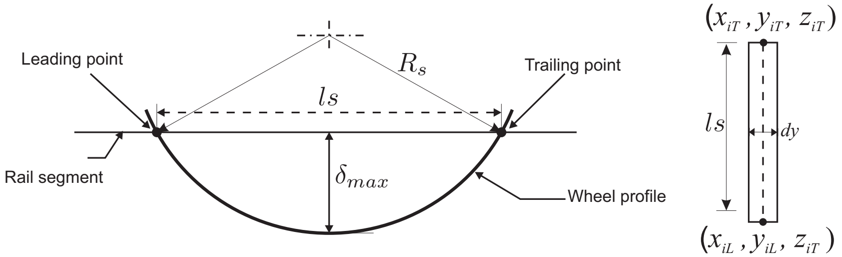

Figure 4.21. *Definition of a strip forming the interpenetration area*

III) Strip thickness $dy$

The strip thickness $dy$ can be calculated by knowing the coordinates of the strip $i$ and the strip $i+1$.

IV) Strip conicity $\gamma_s$

The value of the conicity taken to be the value of the conicity at the wheel profile figure (4.22) at the wheel conical segment intersecting with the rail and can be calculated as follow

$$\gamma_s = \arctan\left(\frac{z_{j+1} - z_j}{y_{j+1} - y_j}\right) \tag{4.73}$$

V) Rolling radius passing through the strip $r_s$

To calculate the rolling radius corresponding to the strip $s$, the parameter $\alpha$ will be used to linearly interpolate the values of the rolling radius at the extreme points of the cone segment

$$r_{\mathrm{s}}(\alpha) = (\alpha\, r_{j+1} - (1-\alpha)\, r_j) \tag{4.74}$$

where $r_j$, $r_{j+1}$ are the values of the rolling radius at the extreme points of the conical segment$j$. In case of the entrance and the exit of the straight segment $i$ is not at the same conical segment $j$, then the value of the rolling radius will be taken as the mean value of the rolling radius that calculated by equation (4.74)

VI) Indentation radius $R_s$

The indentation radius can be calculated by knowing the values of the rolling radius and the conicity at the corresponding strip [24]

$$R_s(\alpha) = \frac{r_{\mathrm{s}}(\alpha)}{\cos(\gamma_s)} \tag{4.75}$$

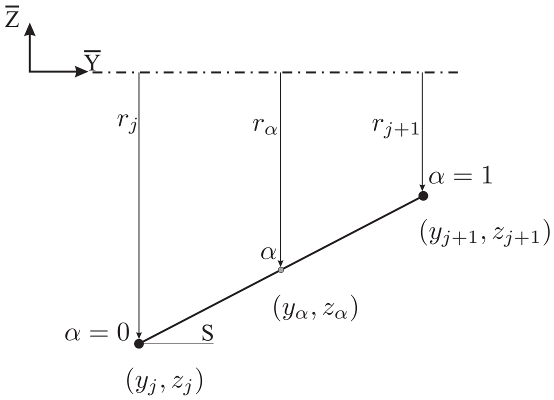
$\bar{Z}$
$\bar{Y}$
$r_j$
$r_\alpha$
$r_{j+1}$
$\alpha = 1$
$(y_{j+1}, z_{j+1})$
$\alpha$
$(y_\alpha, z_\alpha)$
$\alpha = 0$
S
$(y_j, z_j)$

FIGURE 4.22. *Determination of the rolling raduis of each strip*

VII) Maximum penetration of the strip $\delta_{max}$

The value of the maximum indentation is calculated by the assumption that the wheel is making a circular indentation with a radius $R_s$ for each strip figure (4.23)

$$\delta_{\max}{=}R_s(\alpha) - \sqrt{R_s^2(\alpha) - \left(\frac{l_s}{2}\right)^2} \tag{4.76}$$

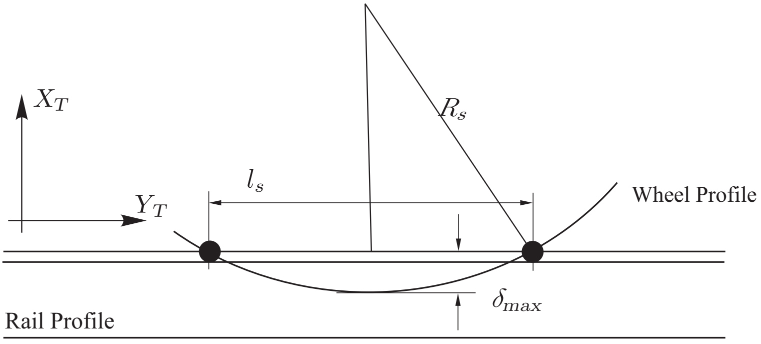
$X_T$
$R_s$
$l_s$
Wheel Profile
$Y_T$
$\delta_{max}$
Rail Profile

FIGURE 4.23. *Determination maximum penetration between wheel and rail profiles*

## 4.7.2 Position vector of the contact point

The contact model implemented in the simulation tool to solve the geometric contact problem is capable of detecting multiple contact point cases. Each contact area can be separately defined by its own strips forming the intersection between the wheel and rail profiles. By the determination of the interpenetration area between the contact surfaces, the contact point is selected at the strips having the maximum penetration values between the wheel and rail profiles. The point of contact is identified as the mid point between the extreme points which characterize the strips with the maximum penetration value. Then the local position vector having the coordinates of the contact can be defined by

$$\bar{\bar{\mathbf{u}}}_{\mathbf{c}} = \frac{\bar{\bar{\mathbf{u}}}_{LP} + \bar{\bar{\mathbf{u}}}_{TP}}{2} \tag{4.77}$$

where $\bar{\bar{\mathbf{u}}}_{\mathbf{c}}$ is the local position vector of the contact point. $\bar{\bar{\mathbf{u}}}_{LP}$ is the position vector of the leading intersection point. $\bar{\bar{\mathbf{u}}}_{TP}$ is the position vector of the trailing intersection point of the strip with the maximum penetration value, all defined in the wheelset reference frame.

The position vector of the point of contact can be written with respect to the global reference frame as

$$\mathbf{r}_c = \mathbf{p} + \mathbf{A}\,\bar{\mathbf{w}} + \mathbf{A}\,\mathbf{B}_{zx}\,\underline{\mathbf{u}}_c \tag{4.78}$$

where $\mathbf{B}_{zx}$ is the intermediate transformation matrix required to transform from the intermediate to track reference frame, it is the matrix produced from two successive rotations about Z-axis and X-axis respectively. $\underline{\mathbf{u}}_c$ is the position vector of the contact point with respect to the intermediate reference frame. By defining the overall motion of the wheelset by realising the final rotation about $\underline{\text{Y}}$-axis. The transformation from the intermediate transformation reference frame to the general rigid body reference frame can defined by introducing the transformation matrix $\mathbf{B}_y$. Now all the transformation matrices are introduced between all the system of references used in the formulation of the wheelset system, and these can be explained by the figure (4.24).

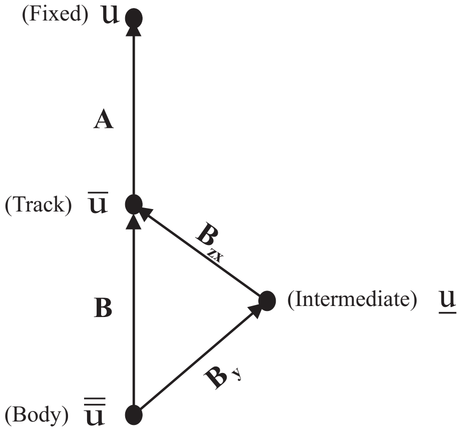
(Fixed) $\mathbf{u}$
**A**
(Track) $\bar{\mathbf{u}}$
$\mathbf{B}_{zx}$
**B**
(Intermediate) $\underline{\mathbf{u}}$
$\mathbf{B}_y$
(Body) $\bar{\bar{\mathbf{u}}}$

FIGURE 4.24. *Transformation schem between the different reference frames*

Figure(4.24) indicates that, it is necessary to define the transformation matrix **A** to transform from the track reference frame to the fixed reference frame. To transform from the rigid body reference frame to the track reference frame the matrix **B** was defined. The transformation from the rigid body to track reference frame was achieved by two steps in which the intermediate reference system is defined. The first step is to make a transformation from rigid body to intermediate by defining the transformation matrix $\mathbf{B}_y$ and then the second step is defined in the definition of the matrix $\mathbf{B}_{zx}$ required to transform from intermediate to track reference frame. Finally the position vector of the contact point can be expressed by the equation:

$$\mathbf{r}_c = \mathbf{p} + \mathbf{A}\,\bar{\mathbf{w}} + \mathbf{A}\,\mathbf{B}\,\bar{\bar{\mathbf{u}}}_{\mathbf{c}} \tag{4.79}$$

### 4.7.3 Velocity vector of the contact point

By making the first time derivative for the position vector equation (4.78), we can obtain the velocity vector of the contact point as:

$$\dot{\mathbf{r}}_c = \dot{\mathbf{p}} + \dot{\mathbf{A}}\,\bar{\mathbf{w}} + \mathbf{A}\,\dot{\bar{\mathbf{w}}} + \left(\dot{\mathbf{A}}\,\mathbf{B} + \mathbf{A}\,\dot{\mathbf{B}}\right)\,\bar{\bar{\mathbf{u}}}_c \tag{4.80}$$

The velocity of a point on the wheel profile consists of the summation of the total wheelset velocity and the circumferential contact point velocity. The wheelset total velocity which represents the velocity of the wheelset reference frame origin, it can be written as:

$$\dot{\mathbf{r}} = \dot{\mathbf{p}} + \dot{\mathbf{A}}\,\bar{\mathbf{w}} + \mathbf{A}\,\dot{\bar{\mathbf{w}}} \tag{4.81}$$

The circumferential velocity of a point on the wheel profile can be written as

$$\dot{\mathbf{r}}_{Cir} = \left(\dot{\mathbf{A}}\,\mathbf{B} + \mathbf{A}\,\dot{\mathbf{B}}\right)\,\bar{\bar{\mathbf{u}}}_c \tag{4.82}$$

$$\dot{\mathbf{r}}_{Cir} = \left(\mathbf{A}\,\tilde{\bar{\bar{\boldsymbol{\tau}}}}\,\mathbf{B} + \mathbf{A}\,\dot{\mathbf{B}}_{zx}\,\mathbf{B}_y + \mathbf{A}\,\mathbf{B}_{zx}\,\dot{\mathbf{B}}_y\right)\,\bar{\bar{\mathbf{u}}}_c \tag{4.83}$$

$$\dot{\mathbf{r}}_{Cir} = \mathbf{A}\,\tilde{\bar{\bar{\boldsymbol{\tau}}}}\,\mathbf{B}_{zx}\,\underline{\mathbf{u}}_c + \mathbf{A}\,\dot{\mathbf{B}}_{zx}\,\underline{\mathbf{u}}_c + \mathbf{A}\,\mathbf{B}_{zx}\,\dot{\mathbf{B}}_y\,\bar{\bar{\mathbf{u}}}_c \tag{4.84}$$

By recalling the identities used in the calculation of the time derivative of the transformation matrices **A** and $\mathbf{B}_{zx}$ [1], the global velocity vector of the contact point can be written as

---

[1] Appendix **A**

$$\dot{\mathbf{r}}_c = \dot{\mathbf{p}} + \mathbf{A}\,\tilde{\bar{\boldsymbol{\tau}}}\;\bar{\mathbf{w}} + \mathbf{A}\,\dot{\bar{\mathbf{w}}} + \mathbf{A}\,\tilde{\bar{\boldsymbol{\tau}}}\,\mathbf{B}_{zx}\,\underline{\mathbf{u}}_c + \mathbf{A}\,\dot{\mathbf{B}}_{zx}\,\underline{\mathbf{u}}_c + \mathbf{A}\,\mathbf{B}_{zx}\,\frac{\partial\,\mathbf{B}_y}{\partial\,\theta_y}\,\dot{\theta}_y\,\mathbf{B}_y^{\mathrm{T}}\,\underline{\mathbf{u}}_c \tag{4.85}$$

The contact point velocity is represented in the intermediate reference frame in the form

$$\dot{\mathbf{r}}_c = \mathbf{B}_{zx}^{\mathrm{T}}\,\mathbf{A}^{\mathrm{T}}\dot{\mathbf{p}} + \mathbf{B}_{zx}^{\mathrm{T}}\,\tilde{\bar{\boldsymbol{\tau}}}\;\bar{\mathbf{w}} + \mathbf{B}_{zx}^{\mathrm{T}}\,\dot{\bar{\mathbf{w}}} + \mathbf{B}_{zx}^{\mathrm{T}}\,\tilde{\bar{\boldsymbol{\tau}}}\,\mathbf{B}_{zx}\,\underline{\mathbf{u}}_c + \mathbf{B}_{zx}^{\mathrm{T}}\,\dot{\mathbf{B}}_{zx}\,\underline{\mathbf{u}}_c + \frac{\partial\,\mathbf{B}_y}{\partial\,\theta_y}\,\dot{\theta}_y\,\mathbf{B}_y^{\mathrm{T}}\,\underline{\mathbf{u}}_c \tag{4.86}$$

## 4.8 Wheelset dynamic analysis

The same as the dynamic analysis for a rigid body explained in section.(4.5.5) we can find the equations of motion for the wheelset defined in the previous section, the only difference is the values of the generalized force associated to the wheelset generalized coordinates. For calculating the generalized force, it was supposed to use the virtual work principle [2, 57, 61] as it was explained, in the previous sections, for the calculations of the generalized forces associated to the generalized coordinates of the rigid body. The virtual work can be found for a wheelset system by determining the virtual displacement of a point on the wheel profile, then the calculation of the force applied at this point. Reaching to the end of the determination of the contact forces and moments at the contact patch resulting from wheel-rail interaction, also the force applied to the wheelset system due to the spring element mounted between the wheel axle and the bogie, one can find the virtual work due to these types of forces as it can be illustrated in the following sections.

### 4.8.1 Generalized forces corresponding to contact forces

For the contact forces applied at the contact patch, including the normal contact force, longitudinal and lateral creepage forces, by knowing the virtual displacement that can be calculated from the position vector of the contact point represented by equation (4.78) which can be written as

$$\delta\,\mathbf{r}_{\mathrm{c}} = \frac{\partial\,\mathbf{r}_{\mathrm{c}}}{\partial\,\bar{\mathbf{w}}}\;\delta\,\bar{\mathbf{w}} + \frac{\partial\,\mathbf{r}_{\mathrm{c}}}{\partial\,\boldsymbol{\theta}}\;\delta\,\boldsymbol{\theta} \tag{4.87}$$

Then the virtual work due to the contact force can be found by

$$\delta W = \boldsymbol{F}_c^{\mathrm{T}}\,\delta\,\mathbf{r}_{\mathrm{c}} \tag{4.88}$$

$$\delta W = \boldsymbol{F}_c^{\mathrm{T}}\,\mathbf{A}\,\delta\,\bar{\mathbf{w}} + \boldsymbol{F}_c^{\mathrm{T}}\,\mathbf{A}\,\frac{\partial\,\mathbf{B}_{zx}}{\partial\,\boldsymbol{\theta}}\,\underline{\mathbf{u}}_{\mathrm{c}}\,\delta\,\boldsymbol{\theta} \tag{4.89}$$

by defining the contact force vector resulting from the wheel-rail interaction and determined by equation (3.39), equation (3.40) and equation (3.26), which can be written as

$$\boldsymbol{F}_c = \begin{bmatrix} F_x & F_y & F_z \end{bmatrix}^{\mathrm{T}} \tag{4.90}$$

where $F_x$ is the longitudinal creep force, $F_y$ lateral creep force and $F_z$ is the normal contact force. From equation.(4.55), the generalized forces due to the contact force can be written as

$$\mathbf{Q}_{\bar{\mathrm{w}}} = \bar{\boldsymbol{F}}_c \tag{4.91}$$

$$Q_{\theta_x} = \bar{\boldsymbol{F}}_c^{\ \mathrm{T}}\,\frac{\partial\,\mathbf{B}}{\partial\,\theta_x}\,\bar{\bar{\mathbf{u}}} \tag{4.92}$$

$$Q_{\theta_y} = \bar{\boldsymbol{F}}_c^{\ \mathrm{T}}\,\frac{\partial\,\mathbf{B}}{\partial\,\theta_y}\,\bar{\bar{\mathbf{u}}} \tag{4.93}$$

$$Q_{\theta_z} = \bar{\boldsymbol{F}}_c^{\ \mathrm{T}}\,\frac{\partial\,\mathbf{B}}{\partial\,\theta_z}\,\bar{\bar{\mathbf{u}}} \tag{4.94}$$

where $\underline{\boldsymbol{F}}_c$ is the contact force vector represented in the intermediate coordinate system associated to the wheelset and $\mathbf{B}_{zx}$ is the transformation matrix from intermediate to fixed or global frame of reference.

### 4.8.2 Generalized forces corresponding to the spin contact moment

The contact moment at the contact patch is produced from the spin creepage moment $\boldsymbol{M}_{sp}$. The virtual work due to this moment $\boldsymbol{M}_c$ may be replaced by an equivalent pair of forces, $\boldsymbol{f}_1$ and $\boldsymbol{f}_2$, of equal magnitudes and opposite direction, acting on a plane perpendicular to the direction of $\boldsymbol{M}_c$ [26] and both supposed to be acting through the longitudinal direction defined by the unit vector $\underline{\boldsymbol{l}}$, and separated by the lateral unit vector $\underline{\boldsymbol{t}}$, figure (4.25) which represents the lateral vector. If the two forces applied at the contact point can be found by:

$$\left.\begin{aligned} \underline{\boldsymbol{f}}_1 &= -f\,\underline{\boldsymbol{l}} \\ \underline{\boldsymbol{f}}_2 &= \ \ f\,\underline{\boldsymbol{l}} \end{aligned}\right\} \tag{4.95}$$

Then the moment at the contact point can be found by

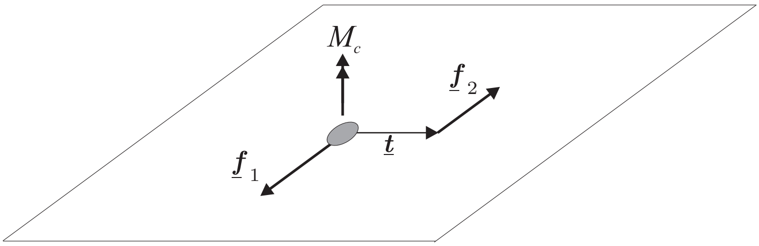
$M_c$
$\underline{\boldsymbol{f}}_2$
$\underline{\boldsymbol{t}}$
$\underline{\boldsymbol{f}}_1$

Figure 4.25. *Concentrated contact moment* $\boldsymbol{M}_c$ *acting on contact area*

$$\underline{\boldsymbol{M}}_c = \underline{\boldsymbol{t}} \times \underline{\boldsymbol{f}}_2 \tag{4.96}$$

Furthermore, the virtual work due to the contact moment can be now found by the following expression

$$\delta W = \underline{\boldsymbol{f}}_1 \delta \mathbf{r}_{f1} + \underline{\boldsymbol{f}}_2 \delta \mathbf{r}_{f2} \tag{4.97}$$

From equation (4.96), we find that

$$\underline{\boldsymbol{f}}_2 = -M \underline{\boldsymbol{l}} \tag{4.98}$$

but we know that $\boldsymbol{f}_1 = -\boldsymbol{f}_2$, then the virtual work due to these forces reduced to

$$\delta W = -M \underline{\boldsymbol{l}}^{\mathrm{T}} \mathbf{B}_{zx}^{\mathrm{T}} \frac{\partial \mathbf{B}_{zx}}{\partial \boldsymbol{\theta}} \underline{\mathbf{t}}_c \, \delta \boldsymbol{\theta} \tag{4.99}$$

$$Q_{\theta_x} = -M \underline{\boldsymbol{l}}^{\mathrm{T}} \mathbf{B}_{zx}^{\mathrm{T}} \frac{\partial \mathbf{B}_{zx}}{\partial \theta_x} \underline{\mathbf{t}}_c \tag{4.100}$$

$$Q_{\theta_y} = -M \underline{\boldsymbol{l}}^{\mathrm{T}} \mathbf{B}_{zx}^{\mathrm{T}} \frac{\partial \mathbf{B}_{zx}}{\partial \theta_y} \underline{\mathbf{t}}_c \tag{4.101}$$

$$Q_{\theta_z} = -M \underline{\boldsymbol{l}}^{\mathrm{T}} \mathbf{B}_{zx}^{\mathrm{T}} \frac{\partial \mathbf{B}_{zx}}{\partial \theta_z} \underline{\mathbf{t}}_c \tag{4.102}$$

### 4.8.3 Generalized forces corresponding to internal forces

The internal forces that may affect the wheelset such as the spring element forces acting on the wheelset connection with the bogie frame through the primary suspension springs. These Springs are elements capable of storing elastic potential energy, as well as, exerting forces that are a function of their positions[26]. In addition, springs play an important role in all but the kinematic problems. Modelling of the suspension element is a crucial part in the multibody dynamic program used for the simulation of the railway vehicle. To represent the forces transmitted by the suspension element we have to define the amount of change in the relative position vector between the two connection points which represent the amount of change between the undeformed and deformed spring length, and for this issue we use the model shown in figure (4.26), which represent a suspension element connecting two rigid bodies $i$ and $j$.

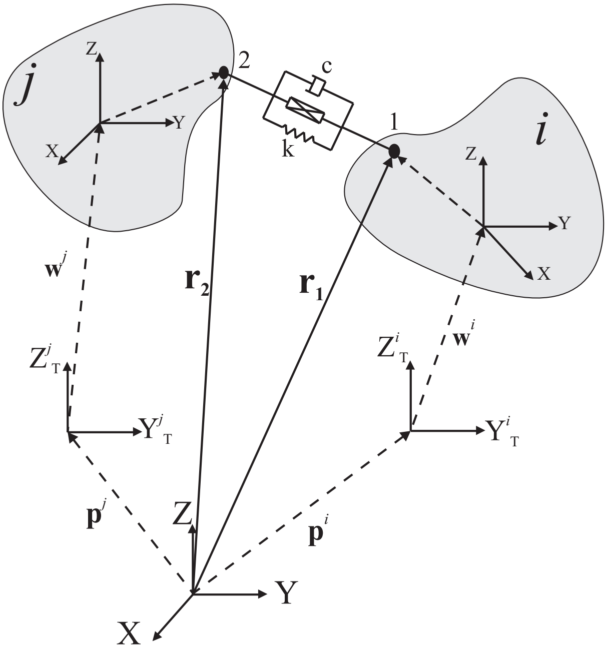

Figure 4.26. *Position vector of two connection points of a spring element between two bodies $i$ and $j$.*

The suspension is attached to the body $i$ at the point **1** and to the body $j$ through the point **2**. By defining the position vector of the reference frame of each body we found that, the position vector of the origin of the frame of reference of the rigid body $i$ can be found by the following expression

$$\mathbf{r}^i_G = \mathbf{p}^i + \mathbf{A}^i\,\bar{\mathbf{w}}^i \tag{4.103}$$

and the position vector of the origin of the reference frame of the rigid body $j$ can be written as follow

$$\mathbf{r}^j_G = \mathbf{p}^j + \mathbf{A}^j\,\bar{\mathbf{w}}^j \tag{4.104}$$

The position vector of the first connection point of the spring with the rigid body $i$ can be written as

$$\mathbf{r}_1 = \mathbf{r}_G^i + \mathbf{A}^i\,\mathbf{B}^i\,\bar{\bar{\mathbf{u}}}_1^i \tag{4.105}$$

The position vector of the first connection point of the spring with the rigid body $j$ can be written as

$$\mathbf{r}_2 = \mathbf{r}_G^j + \mathbf{A}^j\,\mathbf{B}^j\,\bar{\bar{\mathbf{u}}}_2^j \tag{4.106}$$

the relative position vector representing the deformed length of the spring element from point **1** to point **2** can be written as

$$\mathbf{r}_{12} = \mathbf{r}_2 - \mathbf{r}_1 \tag{4.107}$$

$$\mathbf{r}_{12} = \mathbf{r}_G^j - \mathbf{r}_G^i + \mathbf{A}^j\,\mathbf{B}^j\,\bar{\bar{\mathbf{u}}}_2^j - \mathbf{A}^i\,\mathbf{B}^i\,\bar{\bar{\mathbf{u}}}_1^i \tag{4.108}$$

where $\mathbf{A}^i$ and $\mathbf{A}^j$ are the transformation matrices required to transform from the track frame corresponding to the body $i$ and body $j$ respectively, to the fixed frame of reference. $\mathbf{B}^i$ and $\mathbf{B}^j$ are the transformation matrices required to transform from the local frame of of body $i$ and body $j$ to each corresponding track frame of reference. $\bar{\bar{\mathbf{u}}}_1^i$ is the position vector of the first connection point **1** with respect to the local frame of reference of body $i$. $\bar{\bar{\mathbf{u}}}_2^j$ is the position vector of the second connection point **2** with respect to the local frame of reference of body $j$. By the relative position vector between the spring connection points with respect to the local frame of reference of the first body $i$ the we find that it can be written as

$$\bar{\bar{\mathbf{r}}}_{12}^i = \mathbf{B}^{i\,\mathrm{T}}\,\mathbf{A}^{i\,\mathrm{T}}\left(\mathbf{r}_G^j - \mathbf{r}_G^i + \mathbf{A}^j\,\mathbf{B}^j\,\bar{\bar{\mathbf{u}}}_2^j\right) - \bar{\bar{\mathbf{u}}}_1^i \tag{4.109}$$

The relative vector between the two connection points can be written with respect to the second body $j$ as follow

$$\bar{\bar{\mathbf{r}}}_{21}^j = \mathbf{B}^{j\,\mathrm{T}}\,\mathbf{A}^{j\,\mathrm{T}}(\mathbf{r}_G^i - \mathbf{r}_G^j + \mathbf{A}^i\,\mathbf{B}^i\,\bar{\bar{\mathbf{u}}}_1^i) - \bar{\bar{\mathbf{u}}}_2^j \tag{4.110}$$

From equation (4.105) the velocity vector of the point **1** can be written as

$$\dot{\mathbf{r}}_1 = \dot{\mathbf{r}}_G^i + \dot{\mathbf{A}}^i\,\mathbf{B}^i\,\bar{\bar{\mathbf{u}}}_1^i + \mathbf{A}^i\,\dot{\mathbf{B}}^i\,\bar{\bar{\mathbf{u}}}_1^i \tag{4.111}$$

The same from equation (4.106) the velocity vector of the point **2** can be written as

$$\dot{\mathbf{r}}_2 = \dot{\mathbf{r}}_G^j + \dot{\mathbf{A}}^j\,\mathbf{B}^j\,\bar{\bar{\mathbf{u}}}_2^j + \mathbf{A}^j\,\dot{\mathbf{B}}^j\,\bar{\bar{\mathbf{u}}}_2^j \tag{4.112}$$

Also, the relative velocity vector between the two connection points can be expressed with respect to the local frame of reference of body $i$ as follow

$$\dot{\bar{\bar{\mathbf{r}}}}^{i}_{12} = \mathbf{B}^{i^{\mathrm{T}}}\, \mathbf{A}^{i^{\mathrm{T}}} \left( \dot{\mathbf{r}}^{j}_{2} - \dot{\mathbf{r}}^{i}_{1} \right) \tag{4.113}$$

The same can be found with respect to the reference frame of the second rigid body $j$ as

$$\dot{\bar{\bar{\mathbf{r}}}}^{j}_{21} = \mathbf{B}^{j^{\mathrm{T}}}\, \mathbf{A}^{j^{\mathrm{T}}} \left( \dot{\mathbf{r}}^{i}_{1} - \dot{\mathbf{r}}^{j}_{2} \right) \tag{4.114}$$

By knowing the undeformed vector between the two connection points $\bar{\bar{\mathbf{r}}}_{12\mathrm{O}}$, the force vector of the spring element can be calculated at the first connection point on the body $i$, by knowing the stiffness vector $\mathbf{k}$ and the damping coefficient vector $\mathbf{c}$ of the spring element which will have constant values if the spring and the damper are linear, in addition to the force vector representing the actuator force $\mathbf{f_a}$, as follow

$$\bar{\bar{\boldsymbol{F}}}^{i}_{\mathrm{s}} = \mathbf{k} \left( \bar{\bar{\mathbf{r}}}^{i}_{12} - \bar{\bar{\mathbf{r}}}_{12\mathrm{O}} \right) + \mathbf{c} \left( \dot{\bar{\bar{\mathbf{r}}}}^{i}_{12} \right) + \mathbf{f}_{\mathrm{a}} \tag{4.115}$$

and the same for the force vector of spring element affecting the body $j$ can be written with respect to its local frame as

$$\bar{\bar{\boldsymbol{F}}}^{j}_{\mathrm{s}} = \mathbf{k} \left( \bar{\bar{\mathbf{r}}}^{j}_{21} - \bar{\bar{\mathbf{r}}}_{21\mathrm{O}} \right) + \mathbf{c} \left( \dot{\bar{\bar{\mathbf{r}}}}^{j}_{21} \right) - \mathbf{f}_{\mathrm{a}} \tag{4.116}$$

Then, after the calculation of the element forces. We can apply the same virtual work principle defined by equation (4.53) to calculate the generalized force vector coressponding to to the spring element force

$$\delta W = \bar{\boldsymbol{F}}_{s}{}^{\mathrm{T}}\, \delta \bar{\mathbf{w}} + \bar{\boldsymbol{F}}_{s}{}^{\mathrm{T}}\, \frac{\partial \mathbf{B}}{\partial \boldsymbol{\theta}}\, \bar{\bar{\mathbf{u}}}\, \delta \boldsymbol{\theta} \tag{4.117}$$

$$\mathbf{Q}_{\bar{\mathrm{w}}} = \bar{\boldsymbol{F}}_{s} \tag{4.118}$$

$$\mathbf{Q}_{\boldsymbol{\theta}} = \bar{\boldsymbol{F}}_{s}{}^{\mathrm{T}}\, \frac{\partial\, \mathbf{B}}{\partial\, \boldsymbol{\theta}}\, \bar{\bar{\mathbf{u}}} \tag{4.119}$$

The proposed multibody methodlogy presented in this works permits grand displacement values and the main contribution of the method that it allows the replacement of the contact model by advanced contact models without any changes in the main structure of the methodology.

# Chapter 5

# Simulation results

## 5.1 Introduction

The importance of simulation is increased in the last decades as it can be used as part of the vehicle acceptance process and vehicle testing purposes. Modern multibody software packages are used as an essential part of the design process for new vehicles and for investigating service problems with existing vehicles. So it is necessary to build a reliable simulation tool to perform the dynamic analysis for railway vehicles, as well as testing the developed simulation tool to ensure that the obtained results are valid and optimized.

In this chapter, the main construction of the simulation tool Vehicle track Interaction Analysis "VIA" is explained starting from the data entry to the program and ending by the steps followed to run the program and extract the required results. The vehicle model used in the multibody program developed in the current work is described and its dynamic behaviour is studied in different operation scenarios. Afterwards the flow chart of the multibody program implemented in MATLAB environment is described.

A procedure is used to test and validate the obtained results from VIA program. Starting with a simplified model for the contact problem known in the bibliography as *Knife edge* model, the multibody simulation tool VIA is used to analyze the behaviour of a single bogie as well as a complete vehicle running in different simulation scenarios. As a second step after using the simplified model for the contact problem, the contact model is replaced by real contact model. The model is implemented to be used in the analysis of the Manchester Benchmark vehicle 1 negotiating the track case number 1. The obtained results are compared with those obtained by the different simulation packages used to analyze the Benchmark [21].

The analysis of the results depicts a good agreement between the results obtained by the VIA program and SIMPACK program [54]. As a continuation for the procedure used to validate the simulation tool, a comparison is made between results obtained by VIA and SIMPACK programs for TGV 001 vehicle. The model is built in SIMPACK environment for the vehicle model during the exchange period realised during the formation of the presented work in the mechanical engineering department, Politecnico di Milano. The results demonstrate an agreement between both analysis achieved by the simulation tools VIA and SIMPACK.

The contact problem plays an important role in the dynamic analysis of railway vehicles and the computation of wheel- rail contact forces is repeated many times. A methodology is used in the construction of the designed simulation tool presented in this work that permits the change of the contact model and contact calculation method without making any change on the main structure of the program. By this way the Kalker's FASTSIM model [32] used in the calculation of the tangential contact forces, is substituted by Polach model presented in [47]. The main objective is to test the ability of the simulation tool proposed in the current work to achieve such changes in fundamental parts of the multibody model like the changes made in the contact model. A comparison is made between the simulation analysis realised by the VIA program, using FASTSIM model to calculate the tangential forces at the contact patch, and that analysis realised using Polach contact model. The quality of the obtained results presented in this chapter conclude the validity of the implementation of the developed multibody methodology to be used in the dynamic analysis of railway vehicle systems in different operation conditions.

## 5.2 General description of the simulation tool

Using modern simulation packages, it is possible to carry out realistic simulation of the dynamic behaviour of railway vehicles. In most of the simulation tools used, the theoretical basis of the mathematical modelling is mature and reliable. User friendly graphical interfaces are used nowadays in the simulation packages to allow the users to test the effect of making changes on the dynamic analysis of the railway systems. For the developed simulation tool in the presented work, the code is written in Matlab environment and text-based interface is used to describe all the data and output parameters of the simulation realised. The program is designed in a flexible form that permits the implementation of different models for the contact problem as well as incorporating the models developed by the group fo the analysis of railway vehicles. The description of the simulation tool is illustrated in the following points below.

### 5.2.1 Data entry to the simulation tool

In this part of the program, all the required simulation data are entered to program in form of text that defines the following:

- **Track data**

Starting with the information regarding the track data; the type of the track used is defined in this stage whether a rigid or flexible track is used. In the proposed simulation tool, only rigid tracks are used to study the interaction between the railway vehicle and the track. The parameterization method used, is the analytical segments method. Where the track in the presented work here is completely defined as:

I *Straight line stage parameters*

Where the length of the straight line stage is introduced as well as the cant height. The coordinates of the beginning and the end points of the straight track are defined with respect to the global frame of reference.

II *Transition curve stage parameters*

In this section, the type of transition curve is clearly defined as a clothiod curve. The value of the cant height at the start of the transition curve is equal to that value in the straight curve stage and the Clothoid length $l_{clo}$. The cant height at the transition curve stage id defined to be equal to the maximum cant height at the beginning of the plane curve stage. The staring point coordinates of the clothiod stage is assigned to the same point of the end of the straight line stage. Also the end point coordinates coincide with starting point of the full curve stage.

III *Plane curve stage parameters*

The stage length is defined as well as the radius of curvature of the stage $R$ is presented as it is considered to use a constant radius curve.

- **Vehicle model components**

Regarding the vehicle data entry, starts by the definition of specific numbers that determine: the number of the rigid bodies used in the vehicle model including the car bodies, bogie frames and wheelsets; the number of suspension elements in each stage including the primary suspensions and the secondary suspensions; the number of the reference frames used in the simulation which related to the number of the moving track reference frames. The number of reference frames used in the current work is taken equal to the number of the wheelsets in the vehicle model. For the definition of the vehicle model, we have to distinguish between the both main components in the vehicle: the body components and the suspension components.

I *The body components*

The definition of the body components which hold the mass of the vehicle are of interest. As a second stage in the data entry, is the definition of the solids inertia properties (mass and moment of inertia), followed by the coordinates of the points where each track reference frame used in the simulation is located.

The third step, is to assign the solids to the track frame of reference taking into account the selection of the nearest track frame in order to avoid the leaks in the calculations of the relative displacements between the connecting bodies. The centre of mass coordinates for each rigid body is defined with respect to its corresponding track frame of reference.

The fourth step, is the determination of the external forces and torques affecting the rigid bodies presented in the global reference frame and the forces affecting the rigid bodies in the track frame of references.

II *The suspension components*

The suspension elements play important roles in reducing the bogie frame and car body accelerations as well as the dynamic wheel-rail forces. They also allow for proper curve negotiation, but a too soft suspension causes problems with the vehicle gauging and instability. Traction rods attaching the bogie frame to the car body are treated as longitudinal springs to transfer the longitudinal forces during the acceleration and deceleration.

The proposed suspension models used in the simulation purposes in the present work, are passive models, so the suspension forces are only related to the relative motion at the interface with the connected bodies. The spring models used are linear spring models consist of 3D model of three perpendicular linear springs [13].

The last step in the vehicle model data entry is to describe the models of the suspension elements used in the vehicle model. The suspensions used in the simulation are of the type of linear suspension elements composed of spring and viscous dampers. The suspension elements properties are organized as follow:

a) The definition of the suspension topology, where the springs connecting the bodies are defined by assigning each spring to the corresponding bodies connected by this spring as it will be illustrated in section (5.3.2).

b) The definition of the spring stiffness and damping coefficients for the primary spring system as well as the secondary spring system.

c) The definition of the position vector of spring connection points, on both bodies connected, with respect to the rigid frame of reference which in the simulation model here coincides with the body centre of mass.

d) The preload for the suspensions are predefined by calculating the amount of the normal load carried by each spring. The values of the preload forces are initially calculated in the pre-processing stage before the simulation beginning.

- **Contact model data entry**

  In the current work, two types of contact profiles have been used in the simulation, beginning with the simplified model used in the early design of the simulation tool presented, and ending with the standard contact profiles for the wheel and rail geometries, where the UIC60 rail profile is used for the rail and S1002 profile is used for the wheels. For each geometry used in the simulation, a special pre-processing function is used as to prepare the geometry used in the simulation before the program run. This can be illustrated for the standard wheel rail profiles mentioned. In the pre-processing step, the contact surfaces is first entered from the measured points of the rail and wheel profile as shown in figure (5.1). Then both profiles are brought to be in touch by putting the wheel profile just in touche with the rail profile as shown in the following figure.

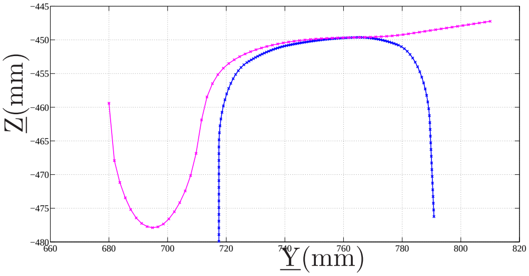

Figure 5.1. S1002 wheel profile in contact with UIC60 rail profile

In the pre-processing stage, the curvature value at all points of the wheel and rail is defined for both surfaces. The calculated curvature values for the left and right wheel profiles can be presented as shown in the figure below:

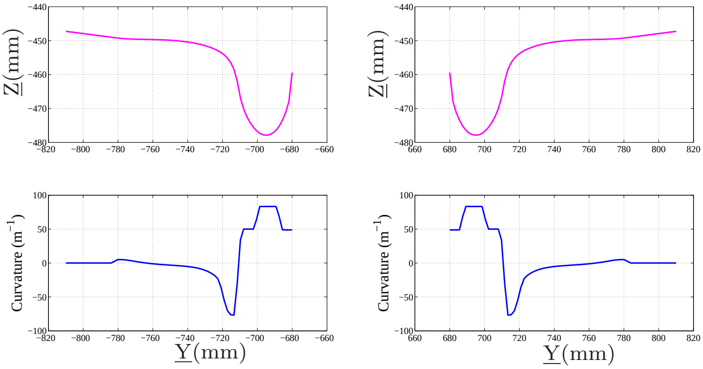

Figure 5.2. *Curvature values for the left and right wheel profile*

Figure (5.2) shows the values of the curvature for both left and right wheel. The *convex* surface of the wheel profile has a *positive* radius of curvature and *negative* sign is assigned to *concave* surface on the wheel profile [28].

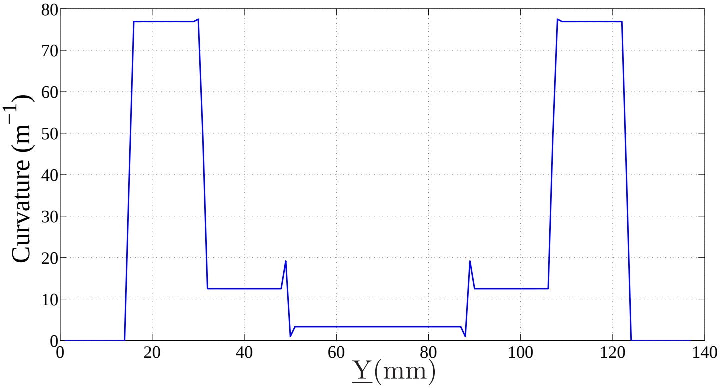

FIGURE 5.3. *Curvature values for the* UIC60 rail profile

For the UIC60 rail profiles, the curvature values for the rail profile points can be obtained as shown in figure (5.3). The sudden change in the radius of curvature of the rail head and rail corner causes sharp change in the curvature values. The change in the radius of curvature causes a numerical problems in the calculation of the normal contact forces using Hertz theory because of the change in the curvature values in these regions is not smooth enough to ensure the continuity in solution. This problem can be solved by using techniques for smoothing the curvature values of the rail at the zones where the sharp change occurs. The curvature values used in the simulation are plotted by the dashed line as seen in figure 5.4.

The contact model data entry process includes the definition of the procedure used in the solution of the normal and tangential contact problems. The normal contact problem is solved in the proposed methodology explained in chapter 4, based on Hertz theory. The required Hertz table is entered and registered to the input data in the pre-processing step.

The tangential contact problem is solved by using three different methods: the first method used in the simulation is the Kalker's linear method [30], the method is based on linear creep force-creepages relation and the results obtained by the method can be shown in the simulation results of the simplified *Knife edge* model; the second method is based on the determination of the tangential contact forces using FASTSIM algorithm [32], the model is used in the simulation of Manchester Benchmark and the simulation of TGV 001 model as it will be shown in the proceeding context; The last method used in the simulation purposes in the presented work here is the algorithm proposed by Polach [47].

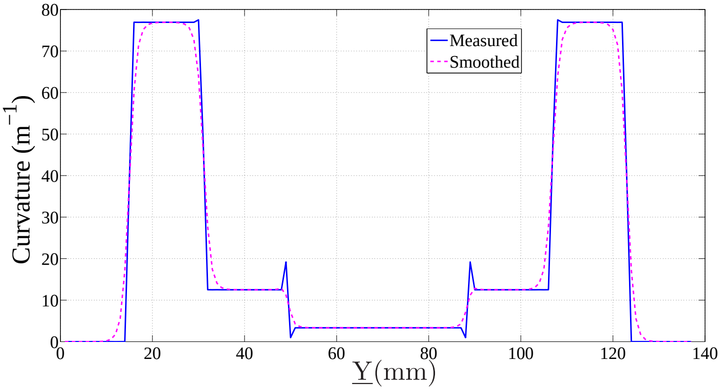

Figure 5.4. *Smoothed curvature values for the* UIC60 rail profile

The use of different contact models shows the flexibility in the simulation tool proposed in this work that permits the changes that made on the contact model without making any changes in the main structure of the program.

### 5.2.2 Program flow chart

In the following figure (5.5), the general flow chart of the multibody program developed in this thesis is explained. Starting with the input data for the model figure (5.5-a) all the required data for the program is entered and registered in organized structural way that permits the easy access to the data when it is necessary. As a second stage the track parameterization step is defined as seen in figure (5.5- b), in which the track segment if defined and all the kinematic parameters of the track are provides depending on the position of the selected vehicle body. The rigid body analysed is distinguished whether it is a wheelset or a bogie frame or a car body figure (5.5- c) and search for the type of connection between them and calculate the corresponding force associated to the connection type. The contact geometry is defined during the calculation of the contact forces at the wheel-rail interface (5.5- d). The forces associated to the coneection between each two rigid body is calculated in the next step, figure (5.5- e). Finally the system of ODE is solved and the response of the system is obtained (5.5- f).

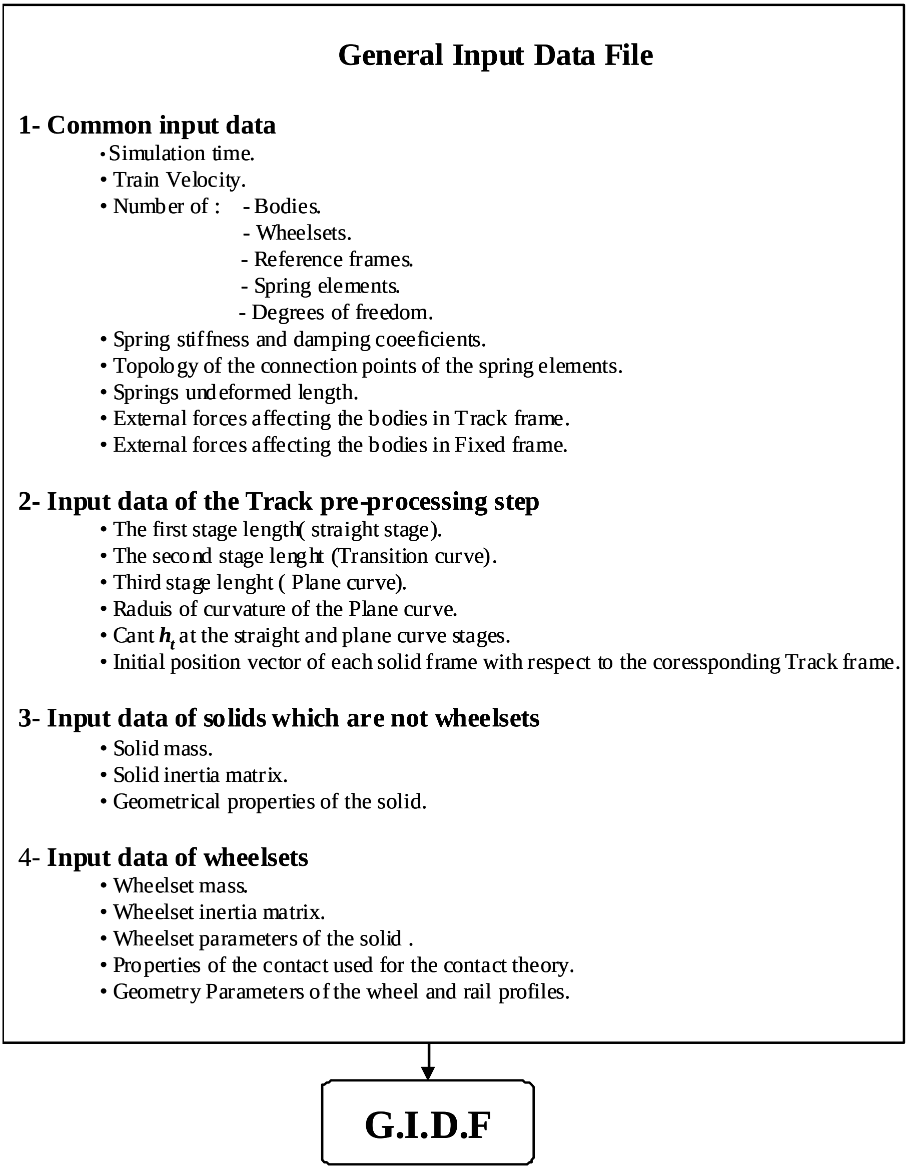

**General Input Data File**

**1- Common input data**

- Simulation time.
- Train Velocity.
- Number of : - Bodies.
  - Wheelsets.
  - Reference frames.
  - Spring elements.
  - Degrees of freedom.
- Spring stiffness and damping coeeficients.
- Topology of the connection points of the spring elements.
- Springs undeformed length.
- External forces affecting the bodies in Track frame.
- External forces affecting the bodies in Fixed frame.

**2- Input data of the Track pre-processing step**

- The first stage length( straight stage).
- The second stage lenght (Transition curve).
- Third stage lenght ( Plane curve).
- Raduis of curvature of the Plane curve.
- Cant $h_t$ at the straight and plane curve stages.
- Initial position vector of each solid frame with respect to the coressponding Track frame.

**3- Input data of solids which are not wheelsets**

- Solid mass.
- Solid inertia matrix.
- Geometrical properties of the solid.

**4- Input data of wheelsets**

- Wheelset mass.
- Wheelset inertia matrix.
- Wheelset parameters of the solid .
- Properties of the contact used for the contact theory.
- Geometry Parameters of the wheel and rail profiles.

FIGURE 5.5. *Multibody program flow chart- a*

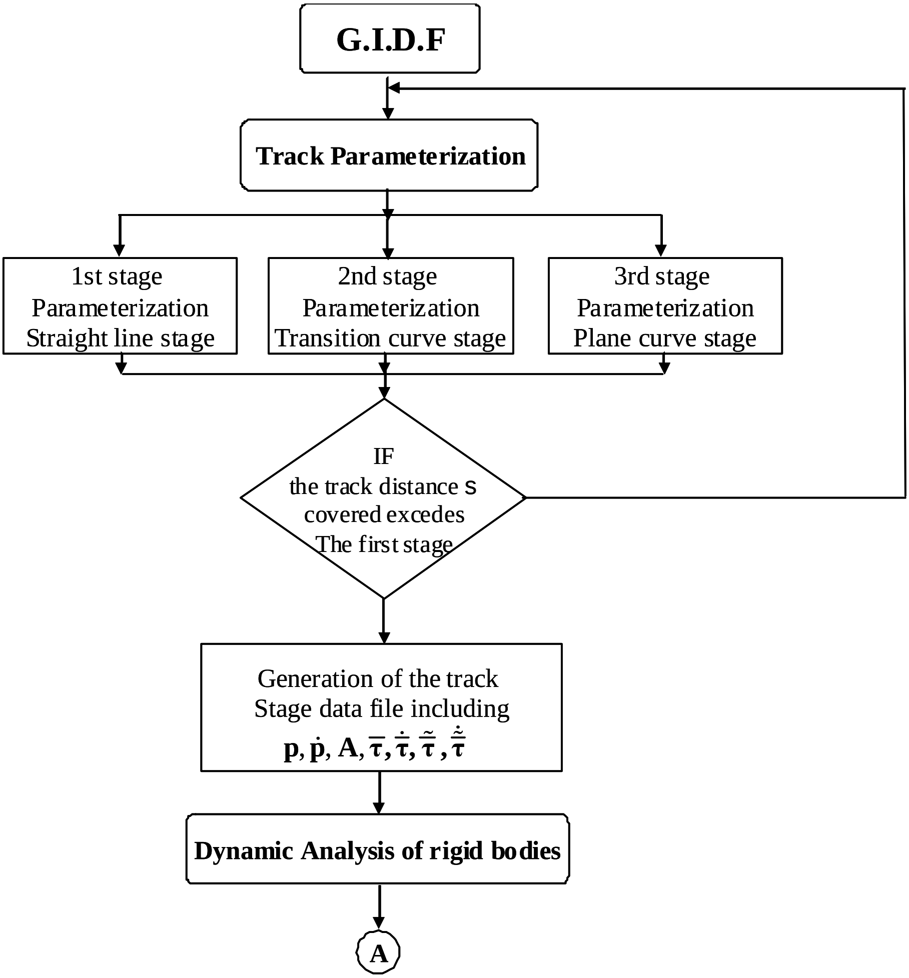
G.I.D.F
Track Parameterization
1st stage Parameterization Straight line stage
2nd stage Parameterization Transition curve stage
3rd stage Parameterization Plane curve stage
IF the track distance s covered excedes The first stage
Generation of the track Stage data file including
$\mathbf{p}, \dot{\mathbf{p}}, \mathbf{A}, \bar{\boldsymbol{\tau}}, \dot{\bar{\boldsymbol{\tau}}}, \tilde{\bar{\boldsymbol{\tau}}}, \dot{\tilde{\bar{\boldsymbol{\tau}}}}$
Dynamic Analysis of rigid bodies
A

*Multibody program flow chart- b*

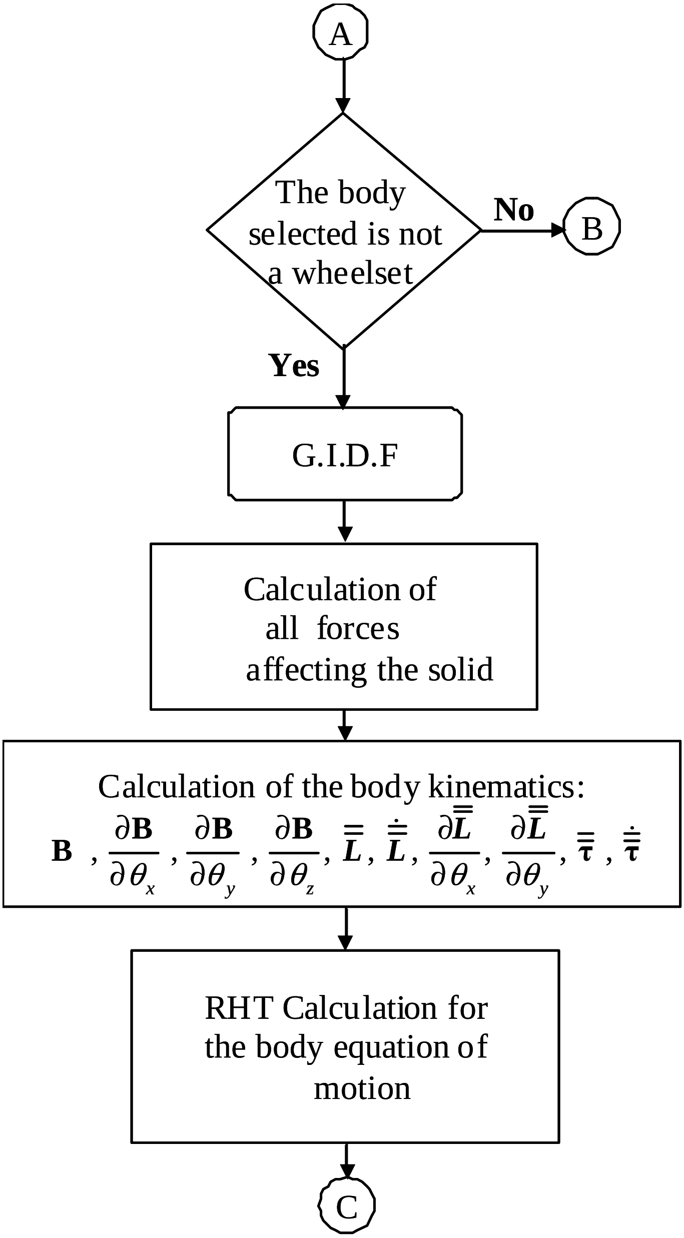
A
The body selected is not a wheelset
No
B
Yes
G.I.D.F
Calculation of all forces affecting the solid
Calculation of the body kinematics:
$\mathbf{B}\ ,\frac{\partial \mathbf{B}}{\partial\theta_x},\frac{\partial \mathbf{B}}{\partial\theta_y},\frac{\partial \mathbf{B}}{\partial\theta_z},\bar{\bar{\boldsymbol{L}}},\dot{\bar{\bar{\boldsymbol{L}}}},\frac{\partial\bar{\bar{\boldsymbol{L}}}}{\partial\theta_x},\frac{\partial\bar{\bar{\boldsymbol{L}}}}{\partial\theta_y},\bar{\bar{\boldsymbol{\tau}}}\ ,\dot{\bar{\bar{\boldsymbol{\tau}}}}$
RHT Calculation for the body equation of motion
C

*Multibody program flow chart- c*

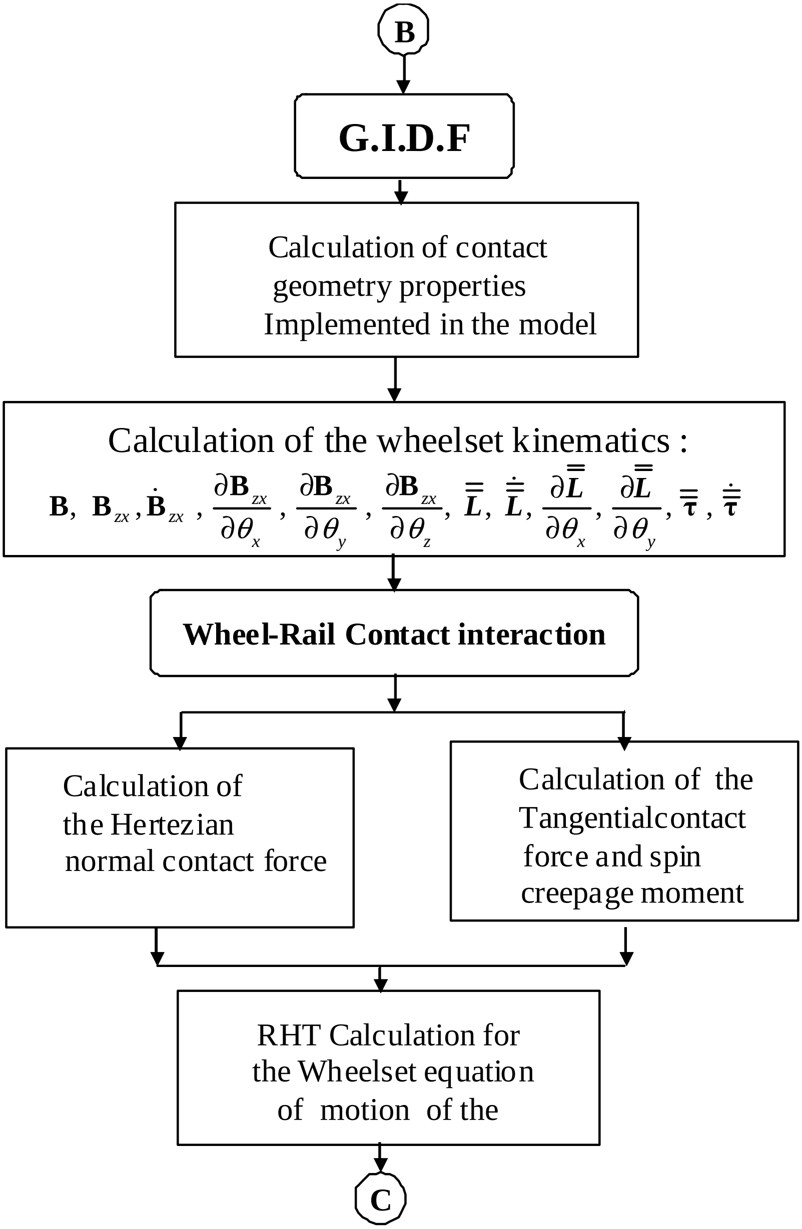
B
G.I.D.F
Calculation of contact geometry properties Implemented in the model
Calculation of the wheelset kinematics :
$\mathbf{B}, \mathbf{B}_{zx}, \dot{\mathbf{B}}_{zx}, \frac{\partial \mathbf{B}_{zx}}{\partial \theta_x}, \frac{\partial \mathbf{B}_{zx}}{\partial \theta_y}, \frac{\partial \mathbf{B}_{zx}}{\partial \theta_z}, \bar{\bar{L}}, \dot{\bar{\bar{L}}}, \frac{\partial \bar{\bar{L}}}{\partial \theta_x}, \frac{\partial \bar{\bar{L}}}{\partial \theta_y}, \bar{\bar{\tau}}, \dot{\bar{\bar{\tau}}}$
Wheel-Rail Contact interaction
Calculation of the Hertezian normal contact force
Calculation of the Tangentialcontact force and spin creepage moment
RHT Calculation for the Wheelset equation of motion of the
C

*Multibody program flow chart- d*

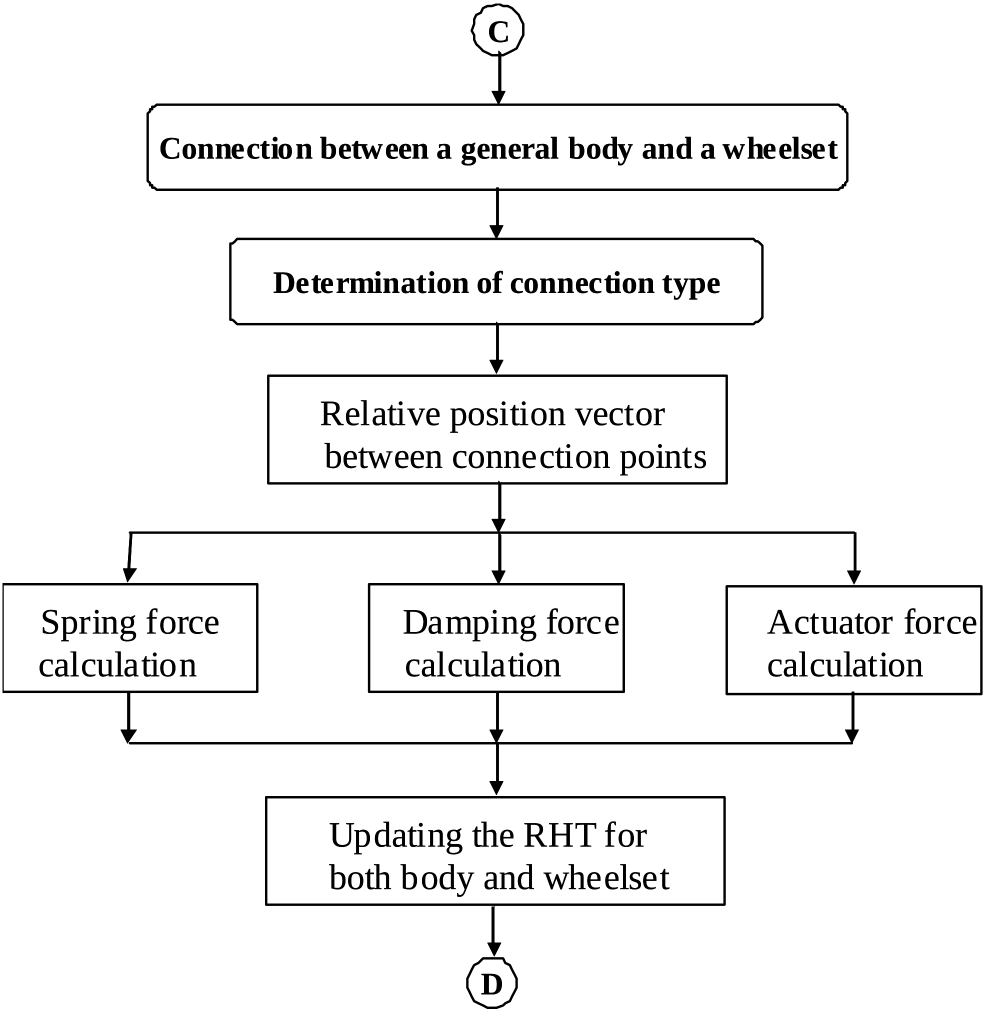
C
Connection between a general body and a wheelset
Determination of connection type
Relative position vector between connection points
Spring force calculation
Damping force calculation
Actuator force calculation
Updating the RHT for both body and wheelset
D

*Multibody program flow chart- e*

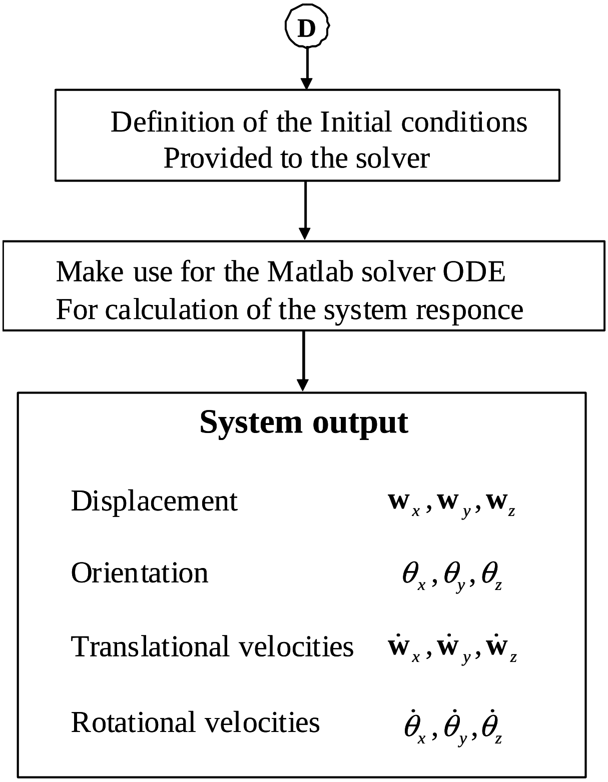
D
Definition of the Initial conditions
Provided to the solver
Make use for the Matlab solver ODE
For calculation of the system responce
System output
Displacement $\mathbf{w}_x, \mathbf{w}_y, \mathbf{w}_z$
Orientation $\theta_x, \theta_y, \theta_z$
Translational velocities $\dot{\mathbf{w}}_x, \dot{\mathbf{w}}_y, \dot{\mathbf{w}}_z$
Rotational velocities $\dot{\theta}_x, \dot{\theta}_y, \dot{\theta}_z$

*Multibody program flow chart- f*

### 5.2.3 Program run and extracted data

This section demonstrates the way that the dynamic analysis for a railway vehicle is achieved by the developed simulation tool including the procedure used to introduce the initial conditions before the program run. The analysis starts by the definition of the data file, from where the program reads the model data. The initial conditions were defined before the program runs. The velocity and the simulation time as well as the time step for the integration are defined for starting the analysis. Velocity and simulation time are provided to the intergrated solver of the program and the solution is obtained in vector form providing the displacements and velocities for the Multibody model of the analyzed vehicle. The extracted data from the simulation tool include a vector containing the displacements and rotations of each rigid body in the multibody model as well as the translational velocities and rotational velocities. In the current work, the number of the rigid bodies are seven bodies, each body has six D.O.F. As a sample of the extracted data from VIA simulation tool, we can define the following output:

I **Displacements**
  a) Longitudinal displacement in X-direction.
  b) Lateral displacement in Y-direction.
  c) Vertical displacement in Z-direction.

II **Rotations**
  a) Roll angle presenting the rotation about X-axis.
  b) Pitch angle presenting the rotation about Y-axis.
  c) Yaw angle presenting the rotation about Z-axis.

III **Velocities**
  a) The time derivative of the coordinates in the X, Y and Z direction.
  b) The time derivative of the rotation angle of the bodies.

IV **Compenetrations**
  a) Compenetration at the left wheel.
  b) Compenetration at the right wheel.

V **Normal contact forces**
  a) Normal contact force value for the left wheel.
  b) Normal contact force value for the right wheel.

VI **Creepages**
  a) Longitudinal creep.

   b) Lateral creep.

   c) Spin.

VII **Tangential forces**

   a) Longitudinal creep forces.

   b) Lateral creep forces.

   c) Spin creepage moment.

VIII **Total lateral guiding force**

IX **Ratio between the Lateral and vertical forces for both wheels (Y/Q)**

## 5.3 Testing the simulation tool using simplified contact model

In the following section, the geometrical aspects of the track used in the simulation will be presented, then a full description for the multibody model for the French TGV 001 vehicle used in the simulation is defined. The simplified contact model used in the early testing of the simulation tool known in the bibliography as *Knife edge* model, is presented here to be used in the simulation purposes. Then the obtained results for a single bogie as well as the obtained results for a complete vehicle negotiating the proposed track model, were presented in different simulation scenarios.

### 5.3.1 Transversal geometry of the designed track

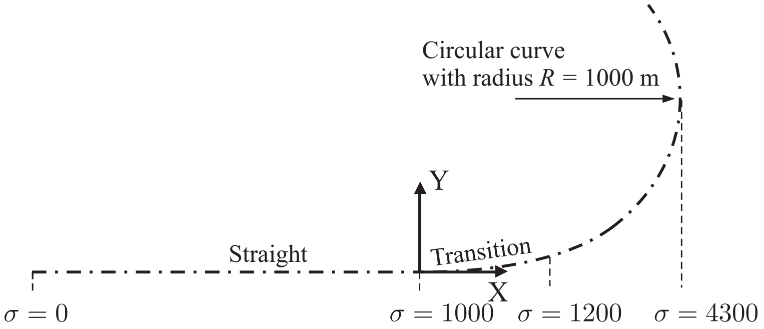

FIGURE 5.6. *Track segments data for the designed track*

According to the methods used in the characterization of the track centerline explained in Chapter (4), the model used in current work consists of a straight segmentwith a length of $1000\,m$, followed by a transition curve connecting the straight line stage to the plane curve stage, with a length of $200\,m$, then the plane curve stage which presents the final stage in the designed track model having a length of $3000\,m$. The fixed frame of reference is located at the starting point of the transition curve stage as it is illustrated in figure (5.6). For the complete definition of the track parameterization step in this part, it is necessary to define the cant angle at each track stage, for this issue we define the track height at the start and end of the track stage under study as shown in figure (5.7)

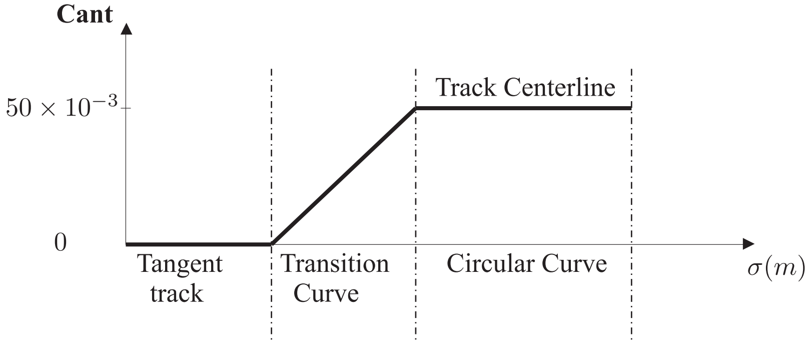

FIGURE 5.7. *Track Super-elevation Ramps*

The track height for the straight curve stage is defined as $h_{t,o} = 0$, and the maximum height of the track is defined as $h_{t,max} = 50 \times 10^{-3}$ m, taking into account that the value of the equilibrium cant angle can be obtained from the equation

$$\phi_{eq} = \arctan(\frac{V^2}{R\,g}) \tag{5.1}$$

Where $V$ is the velocity of the vehicle, $R$ is the radius of curvature of the plane curve stage, $g$ is the gravitational acceleration.

### 5.3.2 Multibody model for TGV 001 vehicle

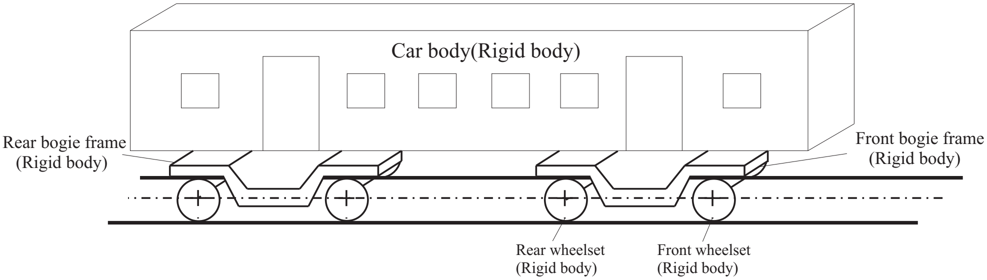
Car body(Rigid body)
Rear bogie frame (Rigid body)
Front bogie frame (Rigid body)
Rear wheelset (Rigid body)
Front wheelset (Rigid body)

FIGURE 5.8. *Three dimensional model of railway vehicle*

Generally, a railway vehicle consists of a collection of bodies and mechanical elements moving along the track. In the analysis proposed in this work, it is supposed to deal with only rigid bodies, then the car body, bogie frames, wheelsets figure (5.8) all are treated as rigid bodies due to their high structural stiffness. The rigid bodies are connected by means of spring elements. A schematic diagram shown in figure (5.9) represents the rigid bodies connection presenting the multibody vehicle model used in the dynamic analysis achieved in the developed work.

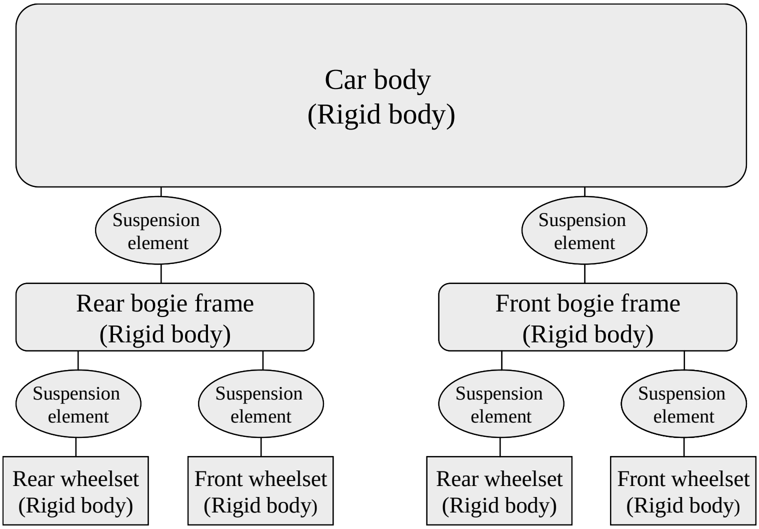
Car body
(Rigid body)
Suspension element
Suspension element
Rear bogie frame
(Rigid body)
Front bogie frame
(Rigid body)
Suspension element
Suspension element
Suspension element
Suspension element
Rear wheelset
(Rigid body)
Front wheelset
(Rigid body)
Rear wheelset
(Rigid body)
Front wheelset
(Rigid body)

FIGURE 5.9. *Schematic diagram of the rigid bodies used in the dynamic analysis*

According to the schematic diagram in figure(5.9), the car body is connected to the bogie frames by means of suspension elements usually known as the secondary suspensions. The bogie frames are connected to the wheelsets by means of other spring elements defined as the primary suspensions. The forces applied to the wheelset are transmitted upwards through the spring elements. The vehicle performance and dynamic behaviour are affected by the characteristics of these elements. According to the three-dimensional model presenting the vehicle proposed here figure (5.8), it can be shown that the model consists of 7 rigid bodies: one car body; couple of bogie frames; four wheelsets. Each rigid body has a 6 DOF, which means that there is no restrictions made for the movement of the body in whatever direction. The multibody model used in the dynamic analysis of 7 rigid bodies is a 42 DOF model.

The system of reference of each rigid ($X_s \, Y_s \, Z_s$) is attached to the CM of the rigid body. The number of the rigid body frame of reference used coincides with the number of the solids, and the number of track reference frames used is equal to the number of the wheelsets. The track reference frame of the bogie is selected to coincide with the track frame of the front wheelset of each bogie connection. For the car body, it is considered to be represented with respect to the track frame of the frontal wheelset attached to the front bogie frame. The position of each track frame is considered to be centred in the track between left and right rail at a height equal to the nominal radius of the wheel profile. Then the initial position of the each body is given by the location of its centre of mass CM with respect to the corresponding track frame of reference.

To represent the geometry properties and other inertia parameters for the solids used, each rigid body is identified with a number. This step is used to facilitate the analysis implemented in the multibody program, as shown in figure (5.10)

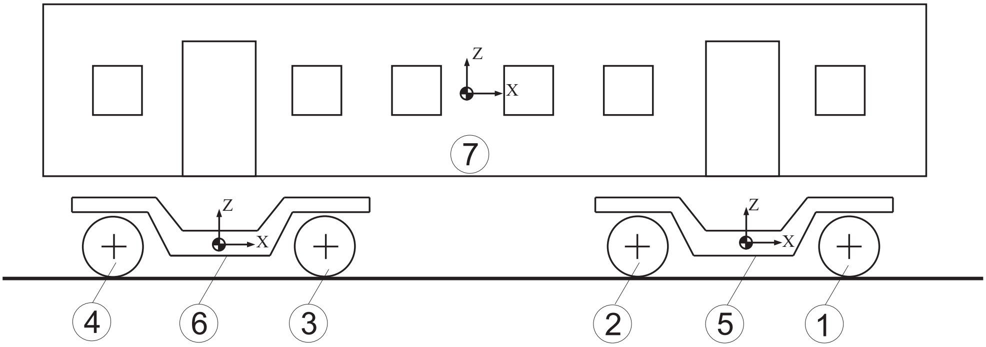

FIGURE 5.10. *Identification of the solids numbers*

Table (5.1) depicts the inertia properties of the solids used in the multibody model

| ID | Rigid body | Mass (kg) | Inertia properties ($kg.m^2$) | | |
|---|---|---|---|---|---|
| | | | $Roll(\boldsymbol{J}_x)$ | $Pitch\,(\boldsymbol{J}_y)$ | $Yaw\,(\boldsymbol{J}_z)$ |
| 1 | Front wheelset Front bogie | 1500 | 799,35 | 93,75 | 799,35 |
| 2 | Rear wheelset Front bogie | 1500 | 799,35 | 93,75 | 799,35 |
| 3 | Front wheelset Rear bogie | 1500 | 799,35 | 93,75 | 799,35 |
| 4 | Rear wheelset Rear bogie | 1500 | 799,35 | 93,75 | 799,35 |
| 5 | Front bogie frame | 3020 | 2130,912 | 4063,712 | 4063,712 |
| 6 | Rear bogie frame | 3020 | 2130,912 | 4063,712 | 4063,712 |
| 7 | Car body | 43200 | 69677,28 | 2430000 | 2430000 |

TABLE 5.1. *Mass and inertia properties of rigid bodies*

The initial position vector of each rigid body can be determined here by knowing the initial position vector of the moving track frame with respect to the fixed or the global frame of reference which assigned only the X-component representing the distance covered by the rigid body on the track ($\sigma$). The initial position vector of the rigid body frame of reference with respect to the corresponding track frame of reference as shown in table (5.2).

| ID | Corresponding Track F.O.R | I.P of the Track F.O.R w.r.t the Fixed F.O.R |  |  | I.P of the Solid F.O.R w.r.t the Track F.O.R |  |  |
|---|---|---|---|---|---|---|---|
|  |  | $(x)$ | $(y)$ | $(z)$ | $(x)$ | $(y)$ | $(z)$ |
| 1 | 1 | $\sigma_1$ | 0 | 0 | 0 | 0 | $r_o$ |
| 2 | 2 | $\sigma_2$ | 0 | 0 | 0 | 0 | $r_o$ |
| 3 | 3 | $\sigma_3$ | 0 | 0 | 0 | 0 | $r_o$ |
| 4 | 4 | $\sigma_4$ | 0 | 0 | 0 | 0 | $r_o$ |
| 5 | 1 | – | – | – | $x_1$ | 0 | $h_b$ |
| 6 | 3 | – | – | – | $x_2$ | 0 | $h_b$ |
| 7 | 1 | – | – | – | $x_3$ | 0 | $h_c$ |

Table 5.2. *Initial position vectors of the rigid bodies*

The values of $\sigma_1 \ldots \sigma_4$ indicate X-component of the position vector of the track frame of refrences used in the simulation with respect to the fixed frame of reference. $x_1$ is the X-component of the position vector of the front bogie frame with respect to the first track fram of reference. $x_1$ is the X-component of the position vector of the Rear bogie frame with respect to the third track fram of reference. $h_b$ represents the hight of the CM of each bogie frame measured from the track plane. $h_C$ is the hight of the CM of the car body measured from the track plane.

**Special elements**

In addition to the geometry problems and the definition of the bodies used in the model, there are some special elements that distinguish railway vehicle from other multibody system application. In this part, the spring elements existing in the model are selected, which presented by translational spring, damper and actuator. The coefficients used in the formulation define the type of these elements to be linear functions of the relative motion and velocity between the two connected bodies by the spring elements numbered with a sequence shown in figure (5.11). The stiffness and the damping coefficients are defined in table (5.4),for the spring elements connecting the wheelsets with the bogie frames as it can be shown by spring topology table .(5.3)

| Spring number | First body | Second body |
|---|---|---|
| 1 | 1 | 5 |
| 2 | 1 | 5 |
| 3 | 2 | 5 |
| 4 | 2 | 5 |
| 5 | 3 | 6 |
| 6 | 3 | 6 |
| 7 | 4 | 6 |
| 8 | 4 | 6 |

TABLE 5.3. *Topology of the springs connecting the wheelsets with the bogie frames*

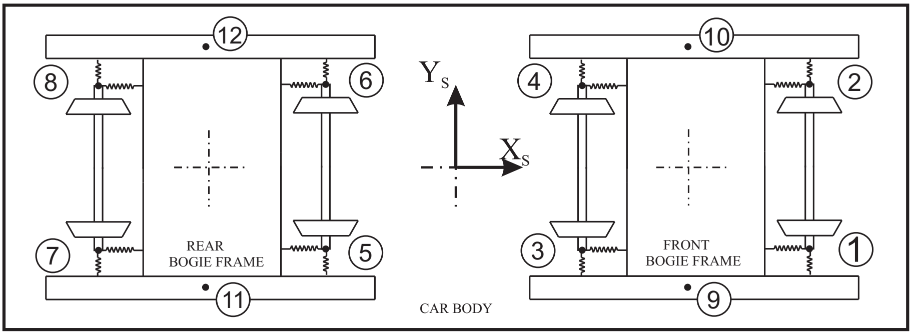

FIGURE 5.11. *Identification of the spring numbers connecting the rigid bodies forming the TGV 001 vehicle*

| Spring number | Stiffness (N.m) | | | Damping Coeff. (N.s.m$^{-1}$) | | |
|---|---|---|---|---|---|---|
| | $k_x$ | $k_y$ | $k_z$ | $c_x$ | $c_y$ | $c_z$ |
| 1 | $3.90 \times 10^7$ | $7.85 \times 10^6$ | $9.75 \times 10^5$ | 0 | 0 | $1.08 \times 10^4$ |
| 2 | $3.90 \times 10^7$ | $7.85 \times 10^6$ | $9.75 \times 10^5$ | 0 | 0 | $1.08 \times 10^4$ |
| 3 | $3.90 \times 10^7$ | $7.85 \times 10^6$ | $9.75 \times 10^5$ | 0 | 0 | $1.08 \times 10^4$ |
| 4 | $3.90 \times 10^7$ | $7.85 \times 10^6$ | $9.75 \times 10^5$ | 0 | 0 | $1.08 \times 10^4$ |
| 5 | $3.90 \times 10^7$ | $7.85 \times 10^6$ | $9.75 \times 10^5$ | 0 | 0 | $1.08 \times 10^4$ |
| 6 | $3.90 \times 10^7$ | $7.85 \times 10^6$ | $9.75 \times 10^5$ | 0 | 0 | $1.08 \times 10^4$ |
| 7 | $3.90 \times 10^7$ | $7.85 \times 10^6$ | $9.75 \times 10^5$ | 0 | 0 | $1.08 \times 10^4$ |
| 8 | $3.90 \times 10^7$ | $7.85 \times 10^6$ | $9.75 \times 10^5$ | 0 | 0 | $1.08 \times 10^4$ |

TABLE 5.4. *Springs stiffness and Damping coefficients for elements connecting the wheelsets with the bogie frames*

The same for the spring elements connecting the car body with the bogie frames. The connection topology and the coefficients values of the springs and dampers used can be shown in the following tables

| Spring number | First body | Second body |
|---|---|---|
| 9 | 5 | 7 |
| 10 | 5 | 7 |
| 11 | 6 | 7 |
| 12 | 6 | 7 |

TABLE 5.5. *Topology of the springs connecting the bogie frame with the car body*

| Spring number | Stiffness (N.m) | | | Damping Coeff. (N.s.m$^{-1}$) | | |
|---|---|---|---|---|---|---|
| | $k_x$ | $k_y$ | $k_z$ | $c_x$ | $c_y$ | $c_z$ |
| 9 | $1.73 \times 10^5$ | $1.73 \times 10^5$ | $5.3 \times 10^5$ | 0 | $3.5 \times 10^4$ | $1.50 \times 10^4$ |
| 10 | $1.73 \times 10^5$ | $1.73 \times 10^5$ | $5.3 \times 10^5$ | 0 | $3.5 \times 10^4$ | $1.50 \times 10^4$ |
| 11 | $1.73 \times 10^5$ | $1.73 \times 10^5$ | $5.3 \times 10^5$ | 0 | $3.5 \times 10^4$ | $1.50 \times 10^4$ |
| 12 | $1.73 \times 10^5$ | $1.73 \times 10^5$ | $5.3 \times 10^5$ | 0 | $3.5 \times 10^4$ | $1.50 \times 10^4$ |

TABLE 5.6. *Springs stiffness and Damping coefficients for elements connecting the bogie frames with the car body*

### 5.3.3 Simplified contact model

The most complex part in conventional railway vehicles is the wheelset. The wheelset used in the model is composed of two conical wheels rigidly connected by the wheel axle. The wheelset-rail interaction used in the simulation is the *Knife Edge* model defining the shape and type of the interaction between the two surfaces of the wheel and rail profiles as it can be shown in figure (5.12).

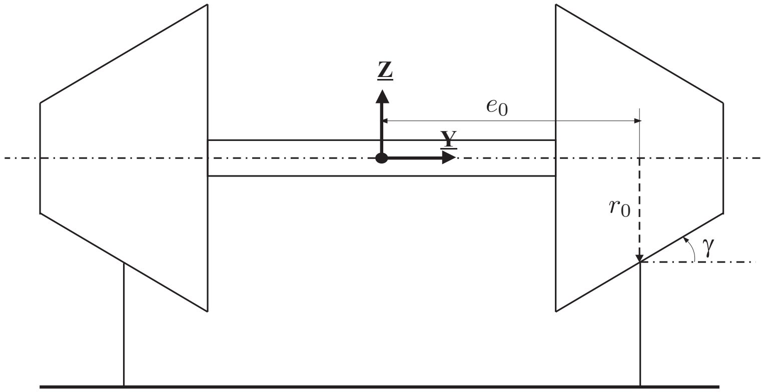

FIGURE 5.12. *Knife edge model of the wheel-rail interaction*

To represent the contact points and determine the geometry of the contact as an important step in the contact problem, the geometric parameter and contact parameters that represent the model used here in the simulation figure (5.13 ) can be obtained from the following table.

| **Parameter** | **Symbol** | **Value** | **Unite** |
|---|---|---|---|
| Conicity angle | $\gamma$ | 0.1 | rad |
| Semi distance | $e_0$ | 0.75 | m |
| Nominal radius | $r_0$ | 0.45 | m |
| Poisson's ratio of wheel material | $\nu_w$ | 0.25 | |
| Modulus of elasticity of wheel material | $E_w$ | $2.10 \times 10^{11}$ | Pa |
| Poisson's ratio of rail material | $\nu_r$ | 0.25 | |
| Modulus of elasticity of rail material | $E_r$ | $2.10 \times 10^{11}$ | Pa |

TABLE 5.7. *Geometry and contact parameters of the wheelset*

The simplified model as described in the figure having the reference frame ($\underline{X}$ $\underline{Y}$ $\underline{Z}$) in the centre of mass of the axle and the parameters illustrated on the figure can be defined as follow:

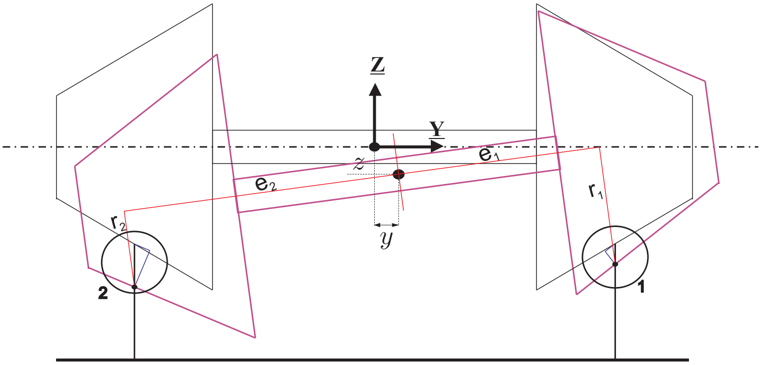

Figure 5.13. *Contact penetration produced from the movement of the wheelset*

- $e_0$: is the lateral distance from the wheelset reference associated to the centre of mass of the axle frame to the nominal contact point
- $r_0$: is the nominal radius of rotation.
- $\gamma$ : is the conicity angle of the wheel.
- $y$ : is the lateral displacement of the wheelset.
- $z$ : is the vertical displacement of the wheelset.
- $\delta$ : is the amount of the approach between the wheel and rail surfaces.
- $\phi$ : is the angle of rotation about the longitudinal x-axis
- $e_1$ : is the normal distance between the rolling radius $r_1$ and center of mass.
- $r_1$ : is the new left wheel rolling radius.
- $r_2$ : is the new right wheel rolling radius.

By shifting the wheelset with a lateral distance $y$ to the right, the position of the centre of mass of the axle is now changed and another point of contact produced due to the rotation of the axle about its centre with an angle of rotation $\phi$ about the x-axis. Producing a change in the rolling radius for the left and right wheel as shown in figure (5.13).

By this way the surfaces in contact are examined after making the lateral shift with a displacement y and the rotation angle $\phi$. By making a magnification for the contact zone for the left wheel contact at point **1** and also the same for the right wheel contact at point **2** as seen in figure (5.14).

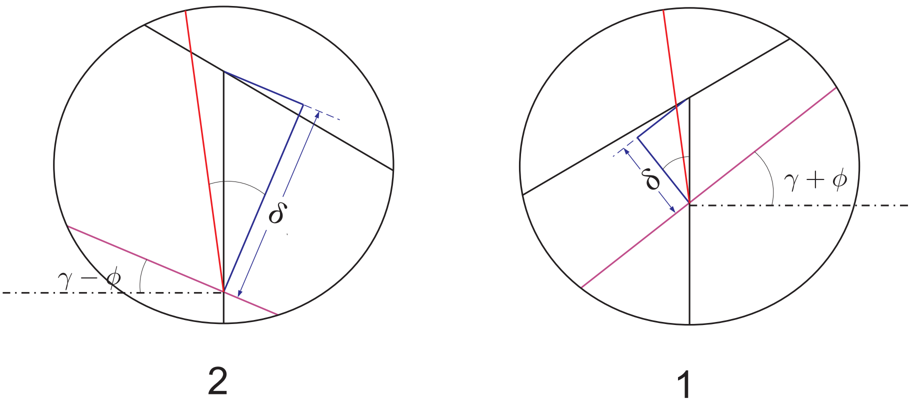

FIGURE 5.14. *Contact penetration calculation for the left and right wheel*

**Left wheel**

The contact geometry and amount of approach of the left wheel can be determined by the following equations

$$e_0 = \mathrm{y} + \mathrm{e}_1 \ \cos\phi + \mathrm{r}_1 \ \sin\phi \tag{5.2}$$

$$-\ r_0 = z + e_1 \ \sin\phi - \ r_1 \ \cos\phi \ + \ \delta \ \cos(\gamma + \phi) + \delta \ \tan(\gamma + \phi) \ \sin(\gamma + \phi) \tag{5.3}$$

$$\tan\gamma = \frac{r_1 - r_0}{e_0 - e_1} \tag{5.4}$$

**Right wheel**

The same as the left wheel, we can find the approach of the right wheel by solving the following set of equations

$$e_0 = \ y \ - e_2 \ \cos\phi + r_2 \ \sin\phi \tag{5.5}$$

$$-\ r_0 = \ z \ - e_2 \ \sin\phi - r_2 \ \cos\phi + \ \delta \ \cos(\gamma - \phi) + \delta \ \tan(\gamma - \phi) \ \sin(\gamma - \phi) \tag{5.6}$$

$$\tan\gamma = \frac{r_0 - r_2}{e_2 - e_0} \tag{5.7}$$

## 5.3.4 Simulation scenarios and obtained results

The bogie model used for the simulation, is a single bogie with two axels running through the proposed track explained in section (5.3.1). The following section demonstrates the multibody model that consists of three rigid bodies: bogie frame; front wheelset; rear wheelset. The primary suspensions connect the bogies to the wheelset figure (5.15) comprise the following elements:

1. Four springs.
2. Four dampers (vertical dampers).

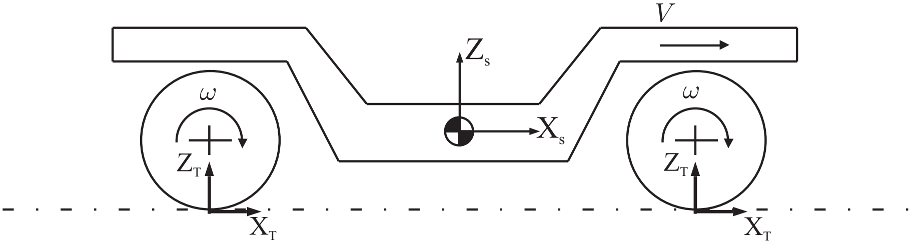

FIGURE 5.15. *Single bogie frame used in the simulation*

The following table shows the inertia properties of the bogie frame used in the simulation. The multibody model of the bogie frame is numbered as it can be seen n the table, where the ID number refers to identification of each rigid body as shown in table (5.8).

| ID | Rigid body | Mass | Inertia properties ($kg.m^2$) | | |
|---|---|---|---|---|---|
| | | (kg) | $Roll(\boldsymbol{J}_x)$ | $Pitch\,(\boldsymbol{J}_y)$ | $Yaw\,(\boldsymbol{J}_z)$ |
| 1 | Front wheelset | 1500 | 799,35 | 93,75 | 799,35 |
| 2 | Rear wheelset | 1500 | 799,35 | 93,75 | 799,35 |
| 3 | Bogie frame | 3020 | 2130,912 | 4063,712 | 4063,712 |

TABLE 5.8. *Mass and inertia properties of a single bogie*

#### 5.3.4.1 Single bogie negotiating a straight track

The simulation condition for the bogie frame can be defined primary by the description of the track geometry defined in section (5.3.1). The fixed frame of reference presenting the observer of the body is located at the point of the beginning of the transition curve. The bogie figure (5.15) including the bogie frame as a rigid body and two wheelsets, is located initially on the track without any initial misalignments or rotations that may develop any initial disturbance in the results.

The bogie frame is studied at the conditions of forward velocity 20 m/s. For the model shown of the bogie, a dynamic analysis is made to study the dynamic response of the bogie firstly moving through straight line section. The model exhibits stable response during the motion when it is moving with a velocity of 20 m/s. Then it is supposed to change the forward velocity to higher values to study the instability of the model and hunting motion produced during the simulation.

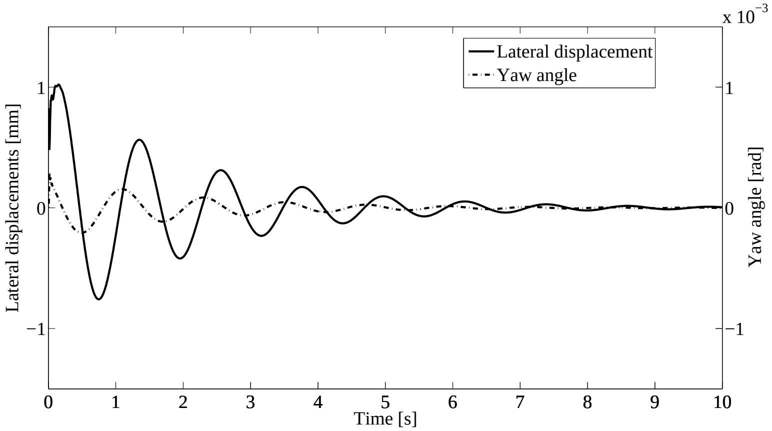

FIGURE 5.16. *Lateral displacement and yaw angle of front wheelset*

Figure (5.16) shows the lateral displacement and the yaw angle of the first wheelset of the bogie frame under study. An initial misalignment with a value of 1 mm is given to first wheelset, and it is noted that the system returns to its stable position after 10 seconds, also this can be noted in figure (5.17) representing the lateral displacements of front and rear wheelsets.

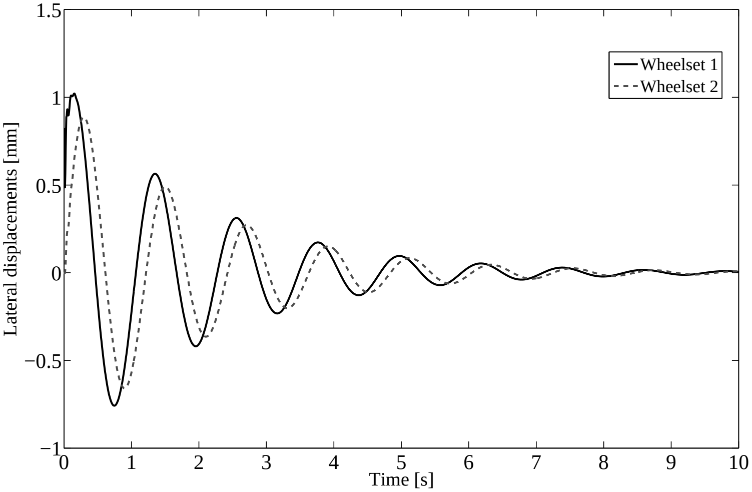

FIGURE 5.17. *Lateral displacement of the front and rear wheelset of the bogie*

It can be seen that the lateral displacement of the rear wheelset is shifted from the frontal one with an amount representing the distance between the centre of mass of the front wheelset and the rear wheelset.

To study the instability of the system of the wheelsets, it is considered to increase the velocity to 40 m/s with the same value of the initial misalignment.

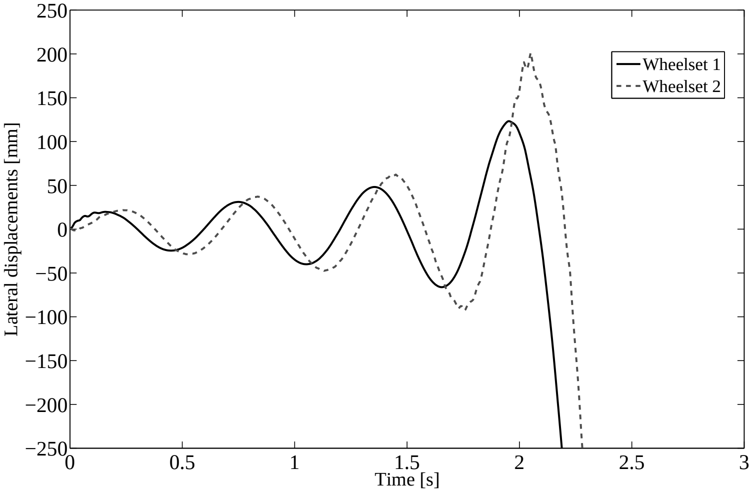

Figure 5.18. *Lateral displacement of front wheelset and rear wheelset*

In figure (5.18) the lateral displacement of first and second wheelset, is increasing with the time and doesn't return to its stable position. This means that the system exceeds the critical velocity entering to the instability stage.

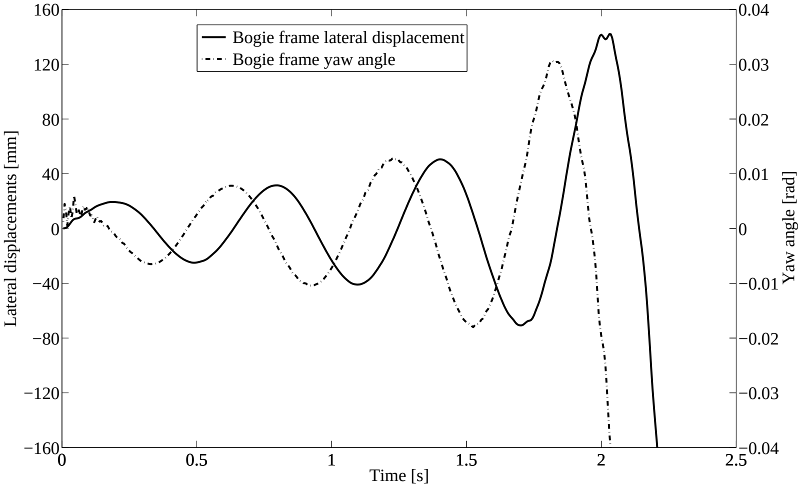

Figure 5.19. *Lateral displacement and yaw angle of the bogie frame*

Figure (5.19) shows the lateral displacement and the yaw angle change for the bogie frame as it represents a different type of analysis for a rigid body which is not wheelset.

#### 5.3.4.2 Single bogie negotiating a curved track

The second scenario here in the simulation is defined for a bogie frame moving through a curved track. It is necessary to define the transition curve stage connecting the tangent track to the constant radius circular track. The transition curve stage here taking the form of a clothoid curve with a length of 200 m. The transition curve in the current work is designed to connect the tangent track defined in the previous to a canted curve with a constant radius equal to 1000 m. The cant is designed here for a velocity of 100 m/s and the equilibrium cant angle can be defined by knowing this velocity using equation (3.2).

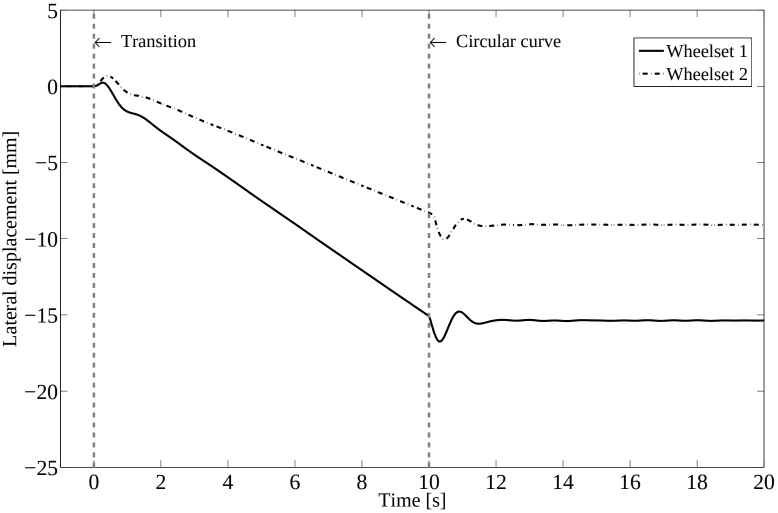

Figure 5.20. *Lateral displacement of front and rear wheelset negotiating transition curve stage*

Figure (5.20) shows that the wheelset displaced toward the outer rail during the motion of the through the transition curve stage. The wheelsets systems return to the stability positions after they enter the constant radius circular curve stage. Figure (5.21) and figure (5.22) show the change in the roll angle and the change in yaw angle, respectively of both wheelsets during the motion in the curved tracks provided by the used track segments in this work.

Figure (5.23) shows unstable response for the lateral displacement of the front wheelset of the frontal bogie presented in the vehicle model.

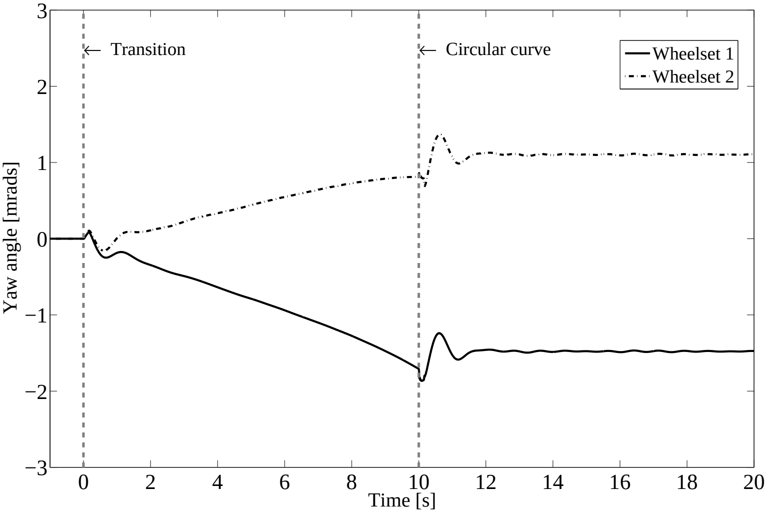

FIGURE 5.21. *Yaw angle of the front and rear wheelset of the bogie frame*

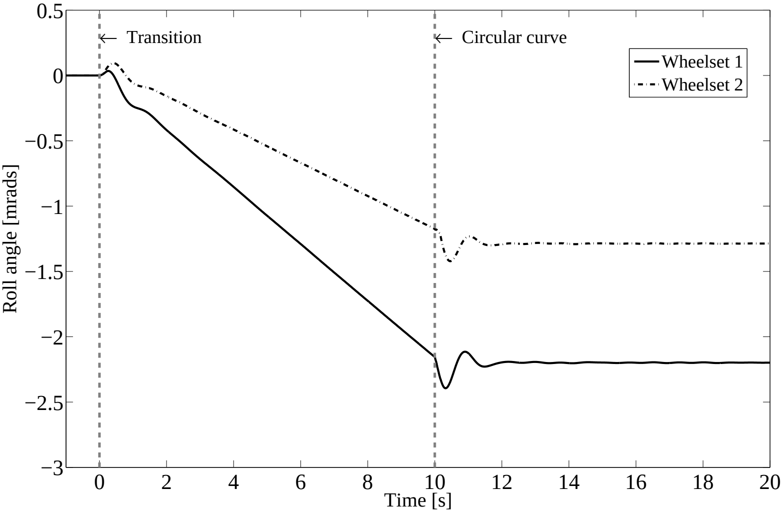

FIGURE 5.22. *Roll angle of the front and rear wheelset of the bogie frame*

#### 5.3.4.3 Complete vehicle negotiating straight track

The multibody program used for the simulation issue here, is applied for the case of a complete railway vehicle figure (5.8), composed as it is shown, of two bogie frames

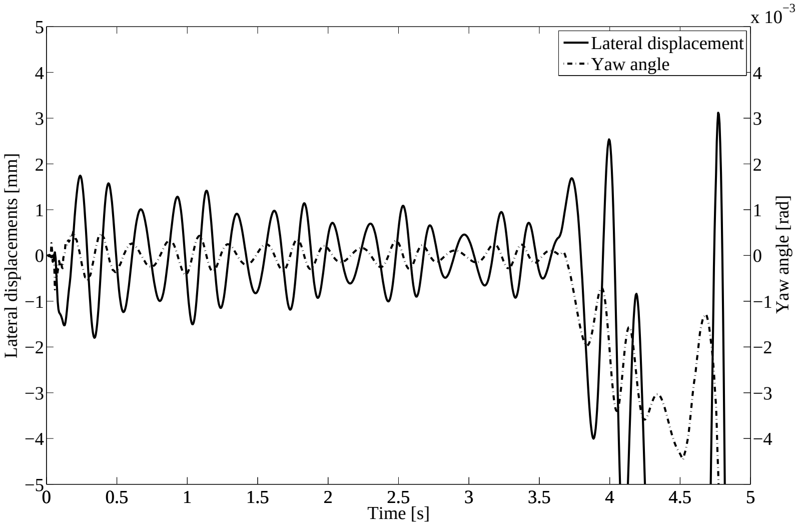

FIGURE 5.23. *Lateral displacement and yaw angle of the front wheelset of the front bogie frame of the complete vehicle model*

and a car body. Each bogie frame contains front and rear wheelset. The same analysis is defined here to represent the dynamic response of the complete vehicle in different simulation scenarios. Starting with the motion of the vehicle systems through tangent track stage. The stability conditions for the motion are studied and with the increase in the velocity produces unstable response of the vehicle.

#### 5.3.4.4 Complete vehicle negotiating curved track

The same analysis made for a single bogie frame along the transition curve stage, is applied here for the case of complete vehicle. The lateral displacements of the wheelsets is determined for the front and rear wheelset attached to both front and rear bogie frames. The behaviour of the $1^{st}$ wheelset of the front bogie exhibits is the same as the $3^{rd}$ wheelset which attached to the rear bogie frame. As well as both wheelset number 2 and wheelset number 4 of the vehicle, depict the same behaviour.

It is also clear that there is a shift between the response of each wheelset from the first wheelset, this is because the wheelset enters the curved track primary and then followed by the other wheelsets separated with the amount of time required to move from the origin of the system of reference of the first wheelset to the following one. The rear wheelset for the front and rear bogie frame, is shifted by a lower amount than the front wheelset toward the outer rail during the motion in the curved track traying to make the bogie centered to the track to stabilise the motion in curved sections of the track.

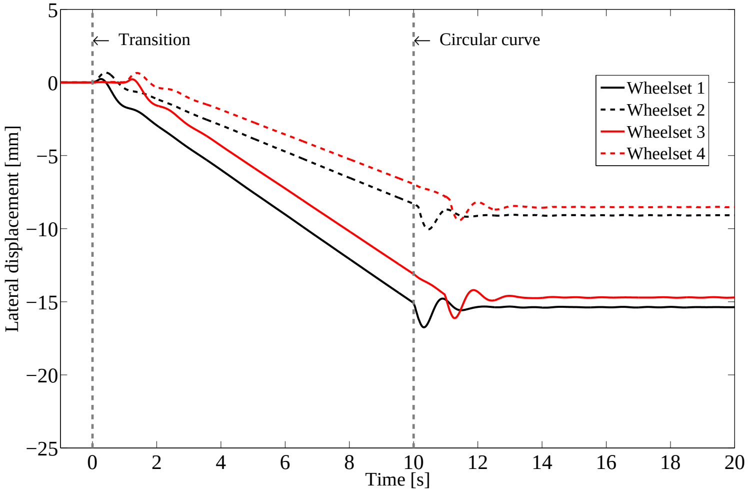

FIGURE 5.24. *Lateral displacement of the wheelsets attached to the front and rear bogie frames*

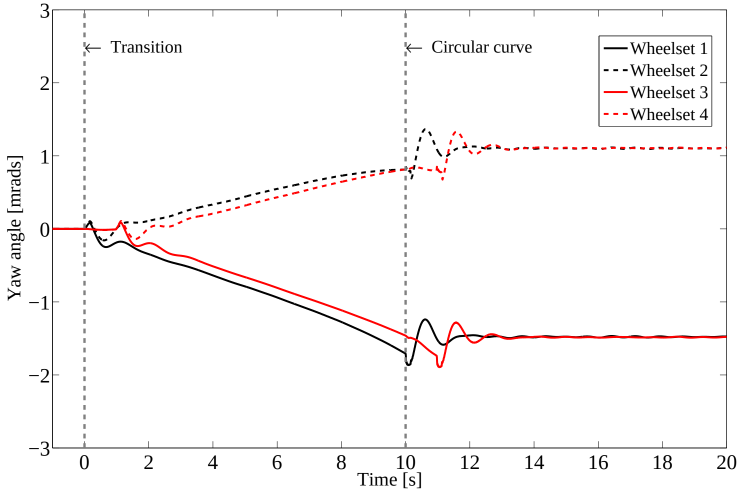

FIGURE 5.25. *Yaw angle variation of the wheelsets attached to the front and rear bogie frames*

Figure (5.24) and figure (5.25) depict the lateral displacement and the yaw angle change, respectively for the front and rear wheelset systems of the vehicle during the motion through the transition curve.

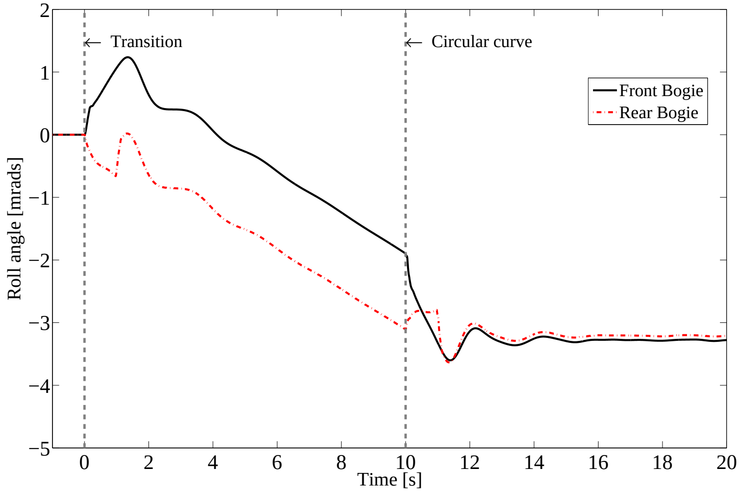

Figure 5.26. *Roll angle change of front and rear bogie frames*

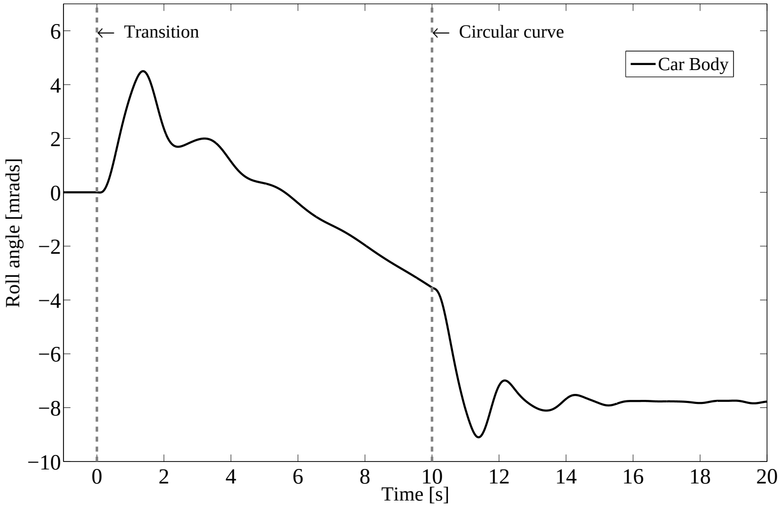

Figure 5.27. *Roll angle change of car body*

The same for the bogie frames and the car body, the change in the roll angle figure (5.26) and figure (5.27), can be shown for both systems during the period covered by the vehicle through the transition curve stage which extends to 10s, with a velocity of 20m/s.

## 5.4 Comparison with the Manchester Benchmark

The Manchester Benchmark was presented at the International Workshop Computer Simulation of Rail Vehicle Dynamics at Manchester Metropolitan university. The details of the vehicles and the track cases which form the Benchmark were presented in the work published in [21]. Where two simple vehicles and four matching track cases have been defined to allow the comparison between various computer simulation packages being used to model the dynamic behaviour of railway vehicles. The results of the simulation carried by these packages were presented afterwards in [22]. Simulations using the Benchmark were carried out with VAMPIRE, GENSYS, SIMPACK, ADAMS/Rail, MEDYNA and NUCARS.

In the presented work in this thesis, a comparison has been made between the results obtained by the developed simulation tool "VIA" and those obtained by the different packages used in modelling and simulation of the Manchester Benchmark.

**Objectives:**

- Investigating the capability and suitability of the VIA program to analyse the dynamic behaviour of railway vehicles.
- Study the possibility of the use of the developed simulation tool in various applications of the railway dynamic field.

In the following sections, a brief description for the vehicle used in the comparison will be provided as well as a complete definition of the selected track case used in the simulation.

### 5.4.1 Track case definition

In the Manchester Benchmark statement, four track cases were defined to run with the Benchmark vehicle models, providing real situations to allow the accurate behaviour to be seen in the simulation. The selected track case here, is the track case 1 [21, 22] which was used to study the following:

- Predict the quasi-static curving behaviour.
- Predicting the risk of derailment on curved twisted track for a simple bogie vehicle.

**Geometrical description of the track**

The chosen part of the track composed of straight track with a length of 50m, followed by a 30m linear transition into a curve of 150m radius with 100mm cant and lasts 60m as shown in figure (5.28).

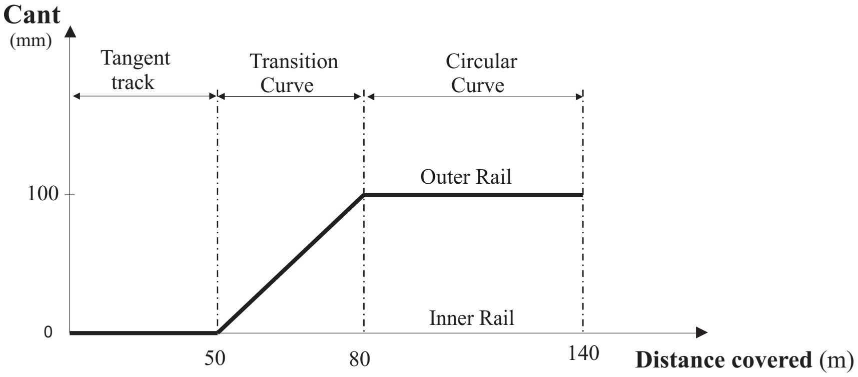

FIGURE 5.28. *Track case 1 for the Manchester Benchmark*

The wheel and rail profile are the common S1002 wheel profile and UIC60 rail profile. Track gauge is 1435mm and the inclination of the rail is 1:40.

The track input is specially designed to match the geometry of the Benchmark vehicle 1, and running with a constant velocity of 4.4m/s.

## 5.4.2 Benchmark Vehicle 1

There are two vehicle models defined by the Manchester Benchmark to present typical vehicles that designers and researchers are using. Both vehicles do not represent the actual vehicles and both models are as simple as possible in order to remove ambiguities that can appear during the use of the model by each simulation package.

The selected model for the simulation purposes presented in the current work is the Benchmark vehicle 1. The vehicle is a general passenger coach with two bogies and a simple primary suspension, without the asymmetry and without yaw dampers. Based on the ERRI B176 Benchmark vehicle, for more details about the vehicle specifications see [21].

The obtained results were presented for Benchmark vehicle 1, providing complete description of the dynamic behaviour of the vehicle during the run of the vehicle along the defined track case 1, previously mentioned.

The results obtained are compared with those presented in the Benchmark published results for the predicted behaviour of the vehicle 1 in the constant radius and super-elevation part of the track case 1 running at a speed of 4.4m/s.

In this section the movement of the vehicle number 1 of the Manchester Benchmark is analyzed, and a comparison has been made between the current results and those obtained by the different simulation packages which used to achieve the dynamic analysis for the Benchmark vehicle [22]

The results obtained by the simulation tool VIA in the present work are presented by the black colour line as seen in the following figures which show the results obtained by different commercial packages used in simulating the Benchmark.

The comparison starts with the analysis of the lateral shift figure (5.29), of the first wheelset attached to the front bogie. According to the results published in [22], there is a slight difference between the values obtained for the lateral displacement of the first wheelset by the different simulation packages, where it reaches a value of 7.818 mm by NUCARS program, towards the outside direction of the rails.

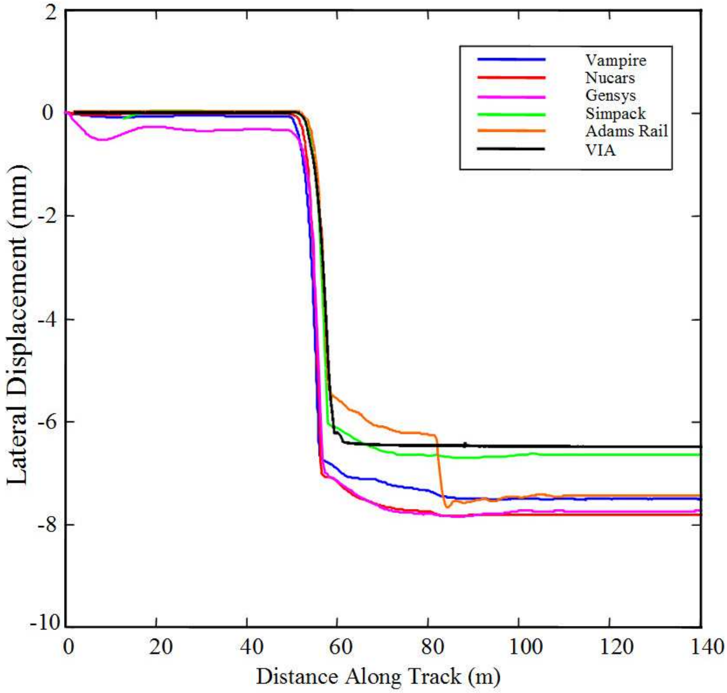

FIGURE 5.29. *Manchester Benchmark Vehicle 1, Case1 -Lateral displacement of Wheelset 1*

The value of the lateral shift obtained by VIA program for the first wheelset, in the straight line stage has a zero value like the values obtained by the other simulation packages. The lateral shift starts to increase toward the outside direction during the negotiation of the vehicle the transition curve stage until it reaches a constant value of 6.51mm in the quasi-static position reached in the constant radius curve stage. The obtained value by SIMPACK for the lateral displacement of the first wheelset 6.53mm as it can be seen in figure (5.29).

| | VIA | SIMPACK | VAMPIRE | GENSYS | ADAMS | NUCARS |
|---|---|---|---|---|---|---|
| Lateral shift/m | e-3 | e-3 | e-3 | e-3 | e-3 | e-3 |
| Wheelset 1 | -6.510 | -6.53 | -7.5097 | -7.747 | -7.189 | -7.818 |
| Wheelset 2 | 6.400 | 8.04 | 7.6397 | 8.003 | 7.402 | 8.030 |
| Wheelset 3 | -6.500 | -5.83 | -6.8079 | -6.974 | -6.408 | -7.141 |
| Wheelset 4 | 5.900 | 7.36 | 7.0069 | 7.315 | 6.458 | 7.388 |

Table 5.9. *Lateral shift of each wheelset relative to the track*

Table (5.9) shows the lateral shift values obtained by the different simulation packages used in the dynamic analysis of the Manchester Benchmark. The simulation results carried out by VIA program are highlighted by gray colour as shown in the table. The lateral displacement variation for the vehicle wheelsets obtained by VIA program are presented in the figure below

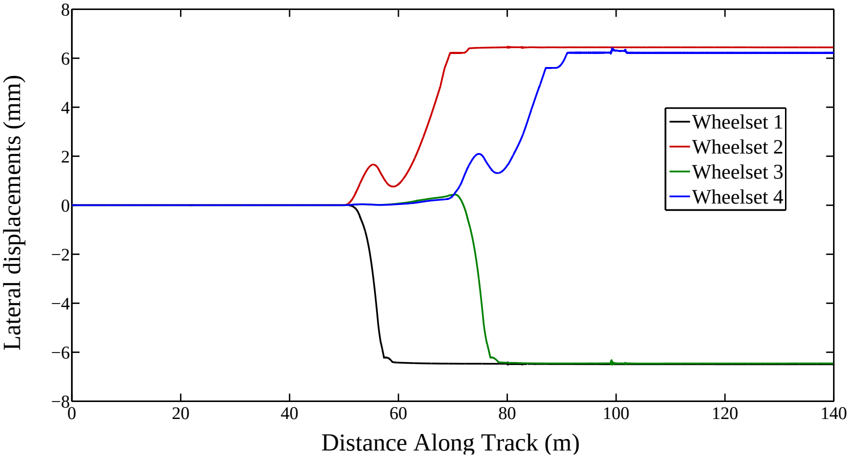

Figure 5.30. *Manchester Benchmark Vehicle 1, Case1 -Lateral displacement of the Wheelsets*

A comparison has been made between VIA program and the different simulation packages for the values of the yaw angle of the first wheelset as shown in figure (5.31). The obtained result shows a good agreement with the yaw angle value obtained by SIMPACK program and with in the same range of the other commercial packages values as it can be verified in table (5.10).

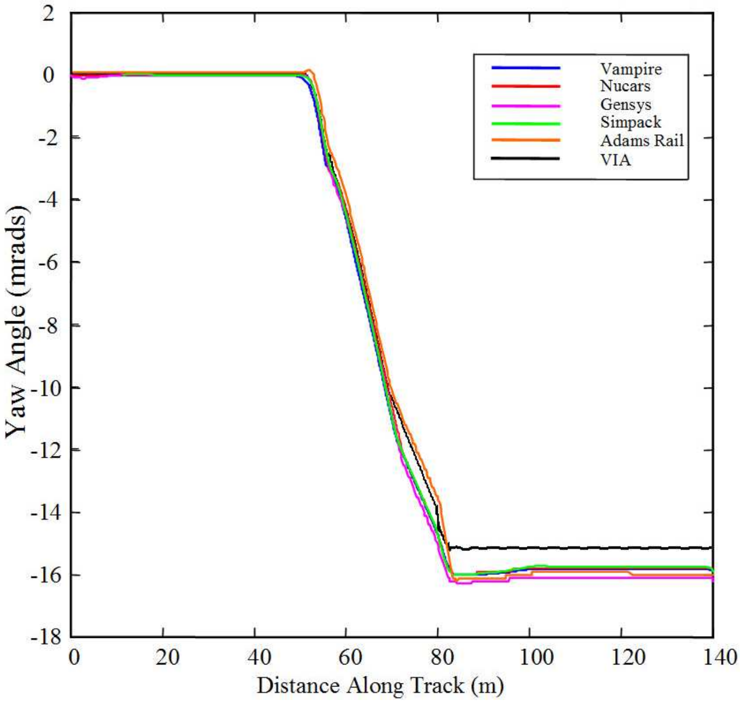

FIGURE 5.31. *Manchester Benchmark Vehicle 1, Case1 - Yaw angle Wheelset 1*

| | VIA | SIMPACK | VAMPIRE | GENSYS | ADAMS | NUCARS |
|---|---|---|---|---|---|---|
| Yaw angle/rad | e-3 | e-3 | e-3 | e-3 | e-3 | e-3 |
| Wheelset 1 | -15.10 | -15.740 | 15.8316 | -16.06 | -15.422 | -15.773 |
| Wheelset 2 | 1.30 | -0.830 | 0.7849 | 0.51 | 1.129 | 0.852 |
| Wheelset 3 | -12.40 | -13.790 | -13.8581 | -14.18 | -13.458 | -13.905 |
| Wheelset 4 | 2.00 | 2.781 | 2.7692 | 2.42 | 3.08 | 2.726 |

TABLE 5.10. *Yaw angle of each wheelset relative to the track*

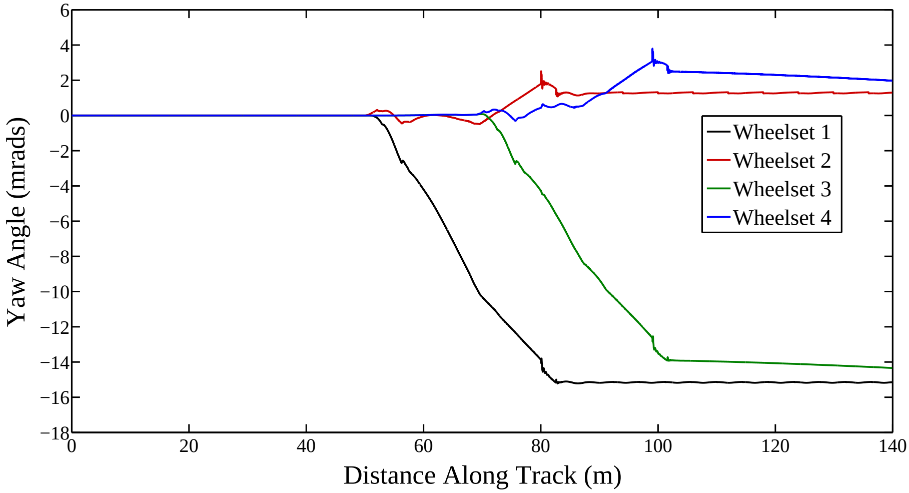

Figure 5.32. *Manchester Benchmark Vehicle 1, Case1 - Yaw angle for each wheelset*

The following figure (5.33) shows the variation of the roll angle for each wheelset in the selected track section of the Manchester Benchmark case 1

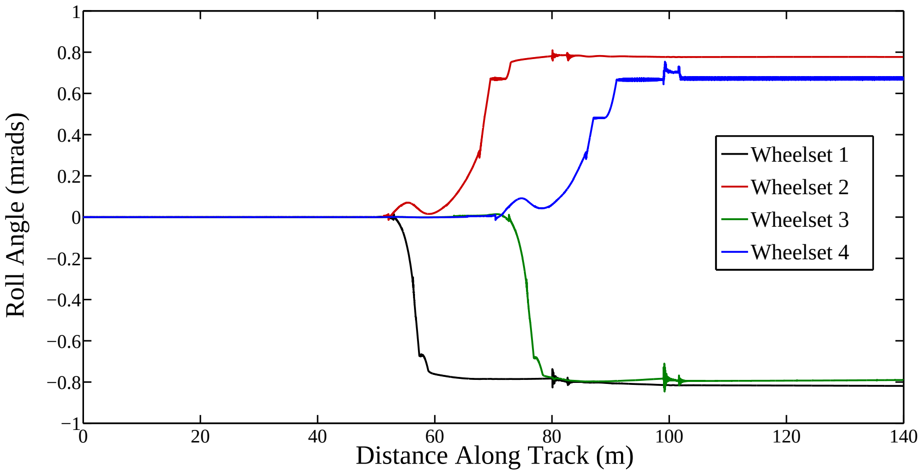

Figure 5.33. *Manchester Benchmark Vehicle 1, Case1 - Roll angle for each wheelset*

The comparison between the results of VIA program and the simulation packages used in the analysis of the Benchmark is extended to include the variation of the contact forces during the simulation time. Figures (5.34) and (5.35), show the variation of total lateral guiding forces affecting the left and right wheel of the first wheelset of the vehicle number 1 during the track negotiation. The oscillations appeared in the results in the beginning of the constant curve stage are due to the transitory effects produced from the exit from the transition curve to the constant radius curve where it can be seen that these oscillations were damped and disappeared in the rest of the stage and the vehicle reaches a quasi-static equilibrium condition.

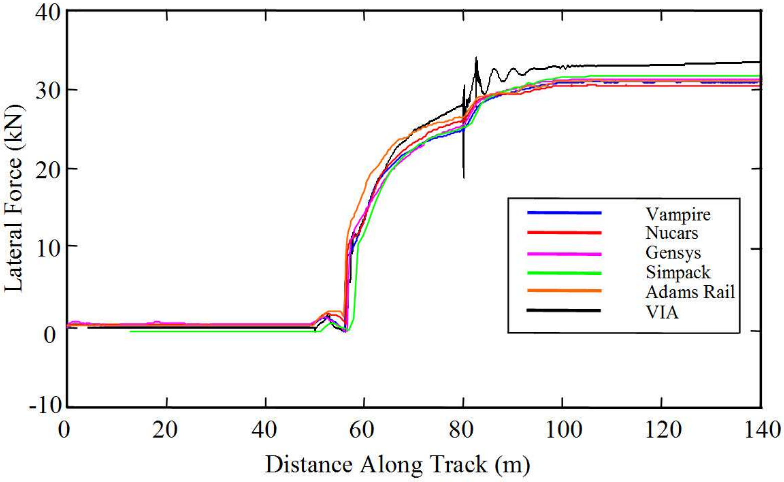

Figure 5.34. *Manchester Benchmark Vehicle 1, Case1 -Total Lateral Guiding Forces: Wheelset 1- Left wheel*

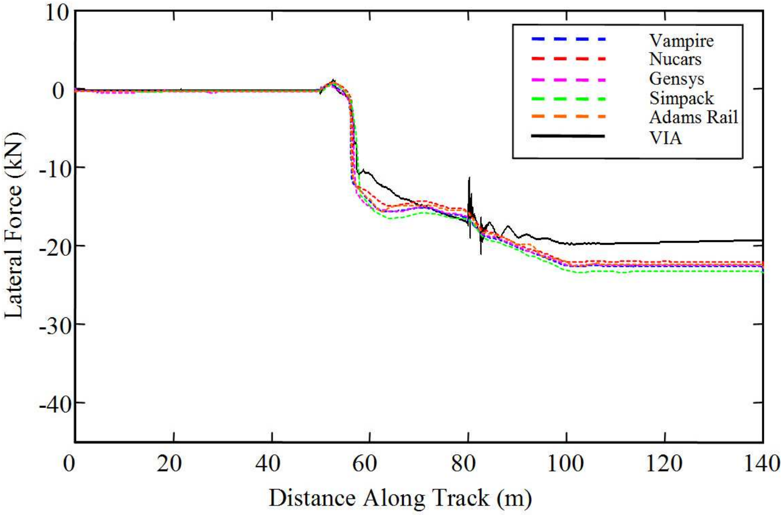

Figure 5.35. *Manchester Benchmark Vehicle 1, Case1 - Total Lateral Guiding Forces: Wheelset 1- Right wheel*

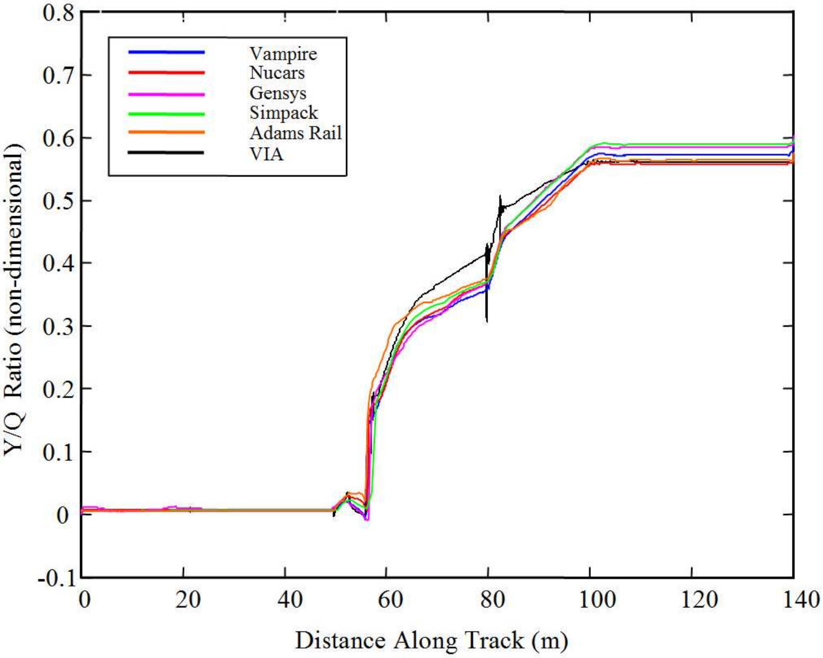

FIGURE 5.36. *Manchester Benchmark Vehicle 1, Case1 - Ratio of Lateral to Vertical Forces: Wheelset 1, Left Wheel*

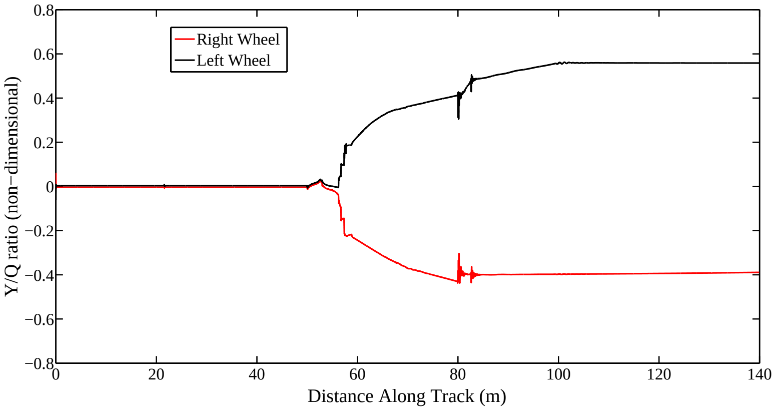

FIGURE 5.37. *Manchester Benchmark Vehicle 1, Case1 - Ratio of Lateral to Vertical Forces: Wheelset 1, Left and Right Wheel*

One of the most important indicators of the derailment potential is the lateral/vertical (Y/Q) force ratio at each wheel. Critical for the evaluation of the safety of a wheelset to derailment. It can be estimated by measurement, by numerical simulation, and also by an analytical quasi-static model [24]. This subject has been treated by many researchers whose work led, in particular, to some derailment criteria like those by Nadal [42], Weinstock [63] and Elkins and Wu [14]. Figure (5.36) depicts the Y/Q ratio for the outer wheel of the first wheelset of the vehicle number 1 of the Manchester Benchmark. The obtained results for the Y/Q ratio calculated by VIA program are identical to that calculated by the other simulation packages as it is illusterated in the presented comparison. While figure (5.37) shows the Y/Q ratio for the outer and inner wheel respectively of the first wheelset of the vehicle 1.

| | VIA | VAMPIRE | GENSYS | SIMPACK | ADAMS | NUCARS |
|---|---|---|---|---|---|---|
| Longitudinal force/N (Left wheel) | e3 | e3 | e3 | e3 | e3 | e3 |
| Wheelset 1 | 9.581 | 2.9643 | 2.357 | 2.87 | 4.6 | 2.652 |
| Wheelset 2 | -20.572 | -15.763 | -15.915 | -16.89 | -15.68 | -15.685 |
| Wheelset 3 | 10.487 | 1.5244 | 0.877 | 3.676 | 3.28 | 1.398 |
| Wheelset 4 | -20.142 | -16.799 | -16.958 | -18.39 | -17.13 | -16.856 |
| Longitudinal force/N (Right wheel) | | | | | | |
| Wheelset 1 | -11.950 | -3.0732 | -3.466 | -3.548 | -4.8 | -3.811 |
| Wheelset 2 | 20.109 | 15.2873 | 15.897 | 16.562 | 15.51 | 15.42 |
| Wheelset 3 | -12.261 | -1.6562 | -1.721 | 1.818 | -3.49 | -2.291 |
| Wheelset 4 | 10.950 | 16.5176 | 16.876 | 18.054 | 16.98 | 16.57 |
| Lateral force/N (Left wheel) | | | | | | |
| Wheelset 1 | 32.453 | 31.2595 | -31.330 | 32.667 | 29.68 | 30.538 |
| Wheelset 2 | 2.8694 | 1.5463 | 1.177 | 1.571 | 1.2 | 1.519 |
| Wheelset 3 | 19.860 | 18.9030 | 19.306 | -20.737 | 17.57 | 18.692 |
| Wheelset 4 | 5.448 | 4.1225 | 3.688 | -4.241 | 3.8 | 3.999 |
| Lateral force/N (Right wheel) | | | | | | |
| Wheelset 1 | -19.172 | -22.6180 | -22.480 | -23.312 | -21.93 | -22.055 |
| Wheelset 2 | -19.811 | -21.1322 | -21.340 | -22.247 | -20.38 | -21.269 |
| Wheelset 3 | -21.246 | -24.8774 | -24.724 | -25.400 | -23.99 | -24.526 |
| Wheelset 4 | -4.888 | -10.1868 | -20.195 | -11.535 | -9.28 | -9.856 |
| Vertical force/N (Left wheel) | | | | | | |
| Wheelset 1 | -59.987 | -54.4773 | -53.740 | 55.42 | -53.80 | -54.811 |
| Wheelset 2 | -45.606 | -39.8973 | -40.150 | -41.046 | -39.67 | -39.745 |
| Wheelset 3 | -54.146 | -49.3711 | -49.110 | 50.895 | -49.23 | -49.799 |
| Wheelset 4 | -47.203 | -44.0811 | -44.180 | 45.336 | -44.00 | -44.193 |
| Vertical force/N (Right wheel) | | | | | | |
| Wheelset 1 | -48.526 | -54.8336 | -55.530 | -53.728 | -55.25 | -54.506 |
| Wheelset 2 | -65.320 | -68.5845 | -68.62 | -67.597 | -69.14 | -69.399 |
| Wheelset 3 | -53.374 | -59.2295 | -59.530 | -57.989 | -59.66 | -59.34 |
| Wheelset 4 | -64.486 | -65.3854 | -64.930 | -63.778 | -64.95 | -64.804 |

TABLE 5.11. *Forces at each wheel*

Table (5.11) provides the obtained values by VIA program for the forces at each wheel, of the rest of the Manchester vehicle number 1 wheelsets, compared with the results obtained by the other packages. The following figures demonstrate the obtained results of the forces on the rest of the vehicle wheelsets.

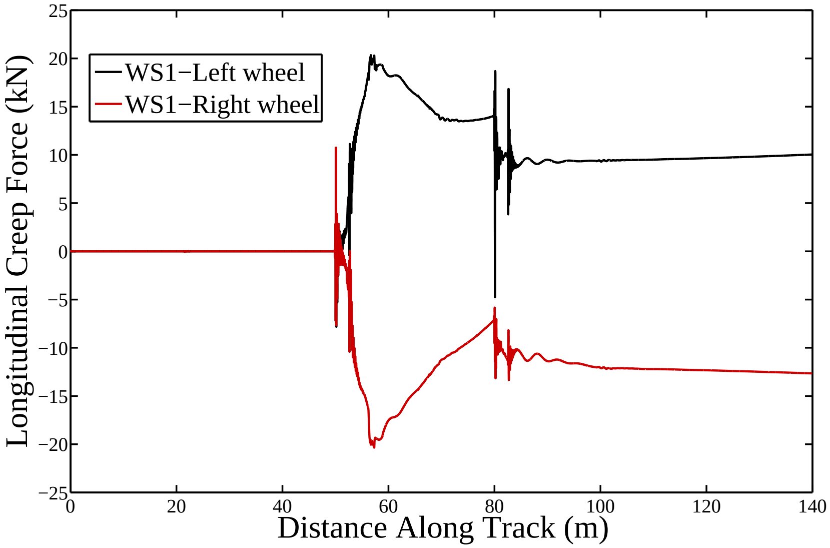

FIGURE 5.38. *Manchester Benchmark Vehicle 1, Case1 - Longitudinal force: Wheelset 1, Left and Right Wheel*

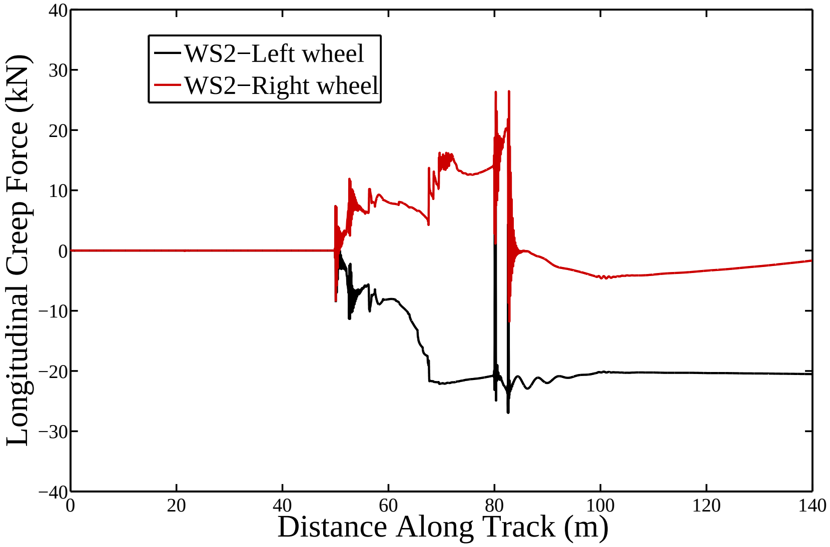

FIGURE 5.39. *Manchester Benchmark Vehicle 1, Case1 - Longitudinal force: Wheelset 2, Left and Right Wheel*

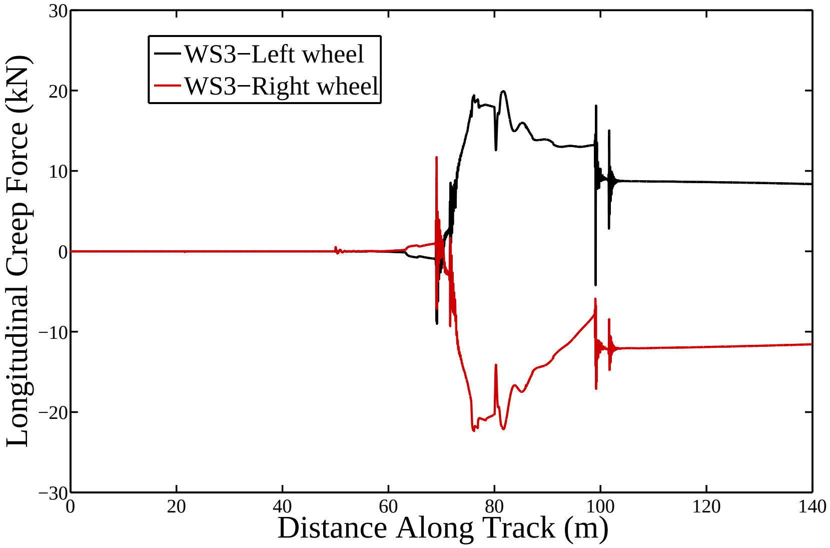

Figure 5.40. *Manchester Benchmark Vehicle 1, Case1 - Longitudinal force: Wheelset 3, Left and Right Wheel*

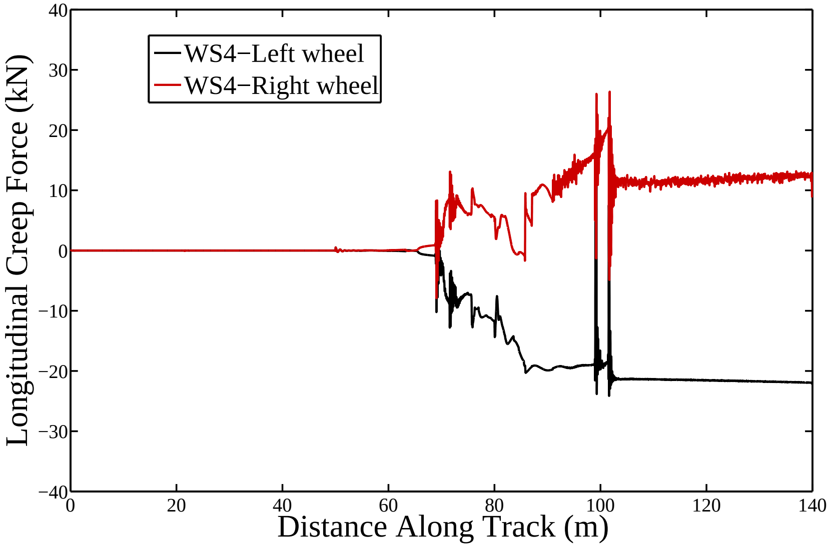

Figure 5.41. *Manchester Benchmark Vehicle 1, Case1 - Longitudinal force: Wheelset 4, Left and Right Wheel*

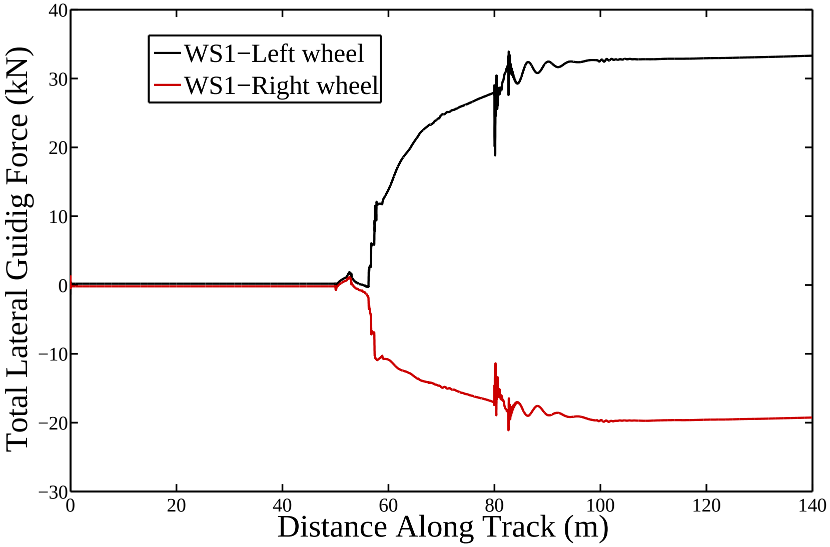

Figure 5.42. *Manchester Benchmark Vehicle 1, Case1 - Lateral force: Wheelset 1, Left and Right Wheel*

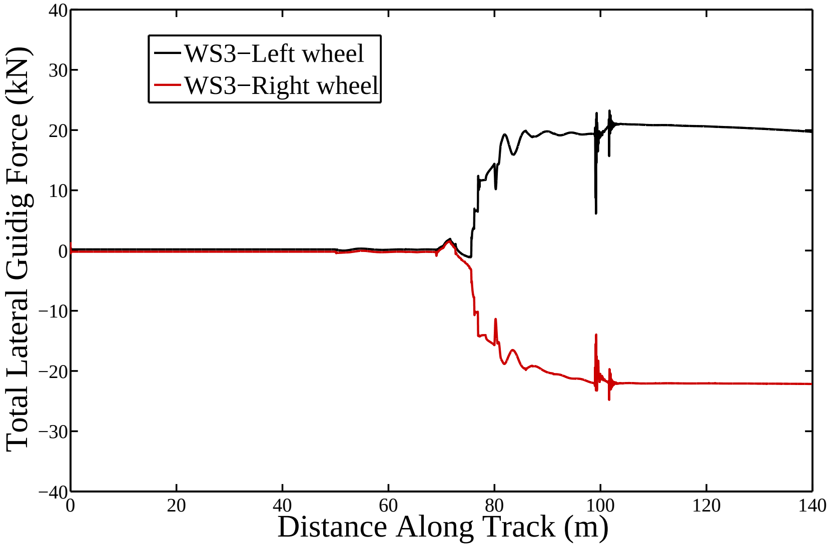

Figure 5.43. *Manchester Benchmark Vehicle 1, Case1 - Lateral force: Wheelset 3, Left and Right Wheel*

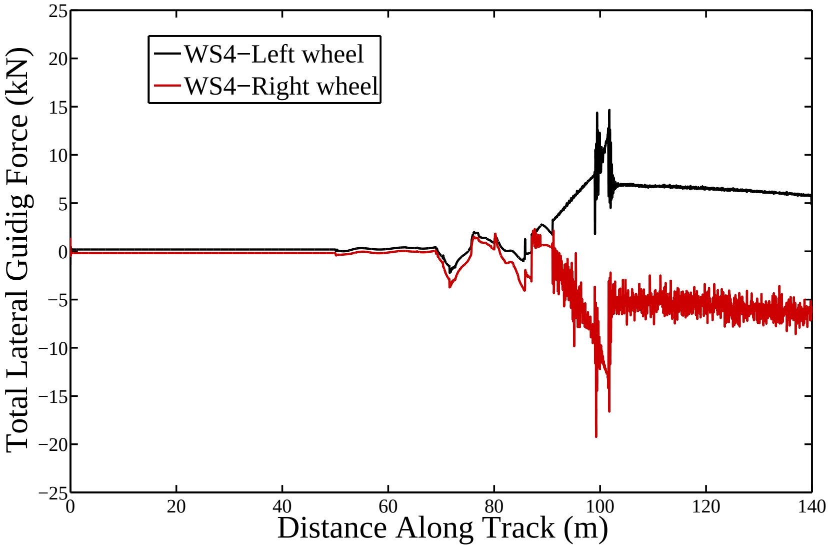

Figure 5.44. *Manchester Benchmark Vehicle 1, Case1 - Lateral force: Wheelset 4, Left and Right Wheel*

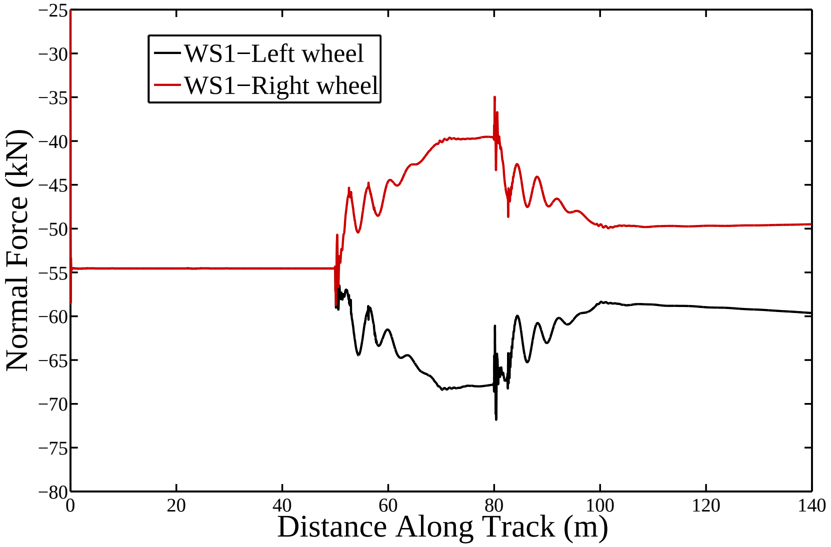

Figure 5.45. *Manchester Benchmark Vehicle 1, Case1 - Normal force: Wheelset 1, Left and Right Wheel*

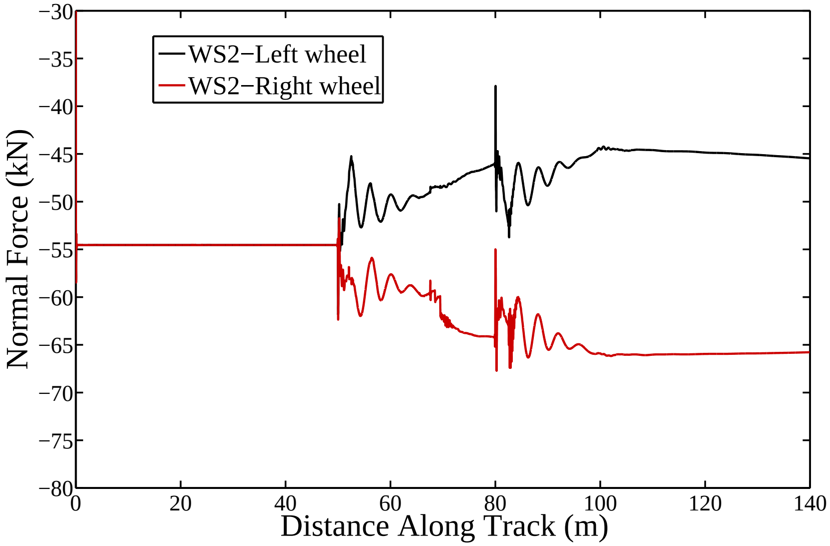

Figure 5.46. *Manchester Benchmark Vehicle 1, Case1 - Normal force: Wheelset 2, Left and Right Wheel*

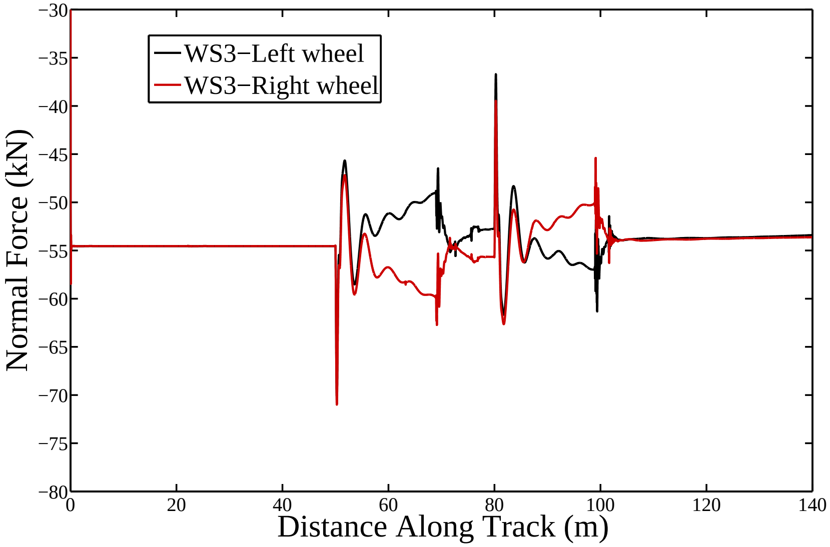

Figure 5.47. *Manchester Benchmark Vehicle 1, Case1 - Normal force: Wheelset 3, Left and Right Wheel*

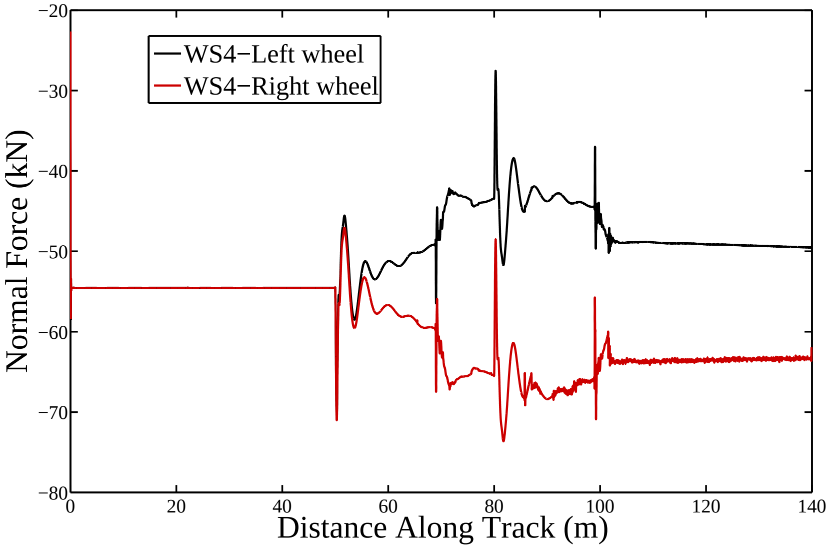

FIGURE 5.48. *Manchester Benchmark Vehicle 1, Case1 - Normal force: Wheelset 4, Left and Right Wheel*

## 5.5 Application and comparison with SIMPACK program

SIMPACK was developed by German Aerospace Research Organisation DLR and as it was intended for road vehicles and other systems as well as rail vehicles it allowed nonlinear kinematics from the start [24]. The equations of motion are formulated in terms of relative coordinates and can be generated symbolically and numerically in an implicit and explicit form. During the stay abroad distance realised in the Politecnico di Milano, as a part of the presented work and as a continuation for the procedure followed to validate the results of the simulation tool VIA.

Building the model by SIMPACK and realization of the simulation is achieved by following three main steps: 1) Pre-Processing; 2) Processing; 3) Processing. In the following context each process is explained separately in details

1) **Pre-Processing**

In the definition of the Pre-Processing step, a procedure is followed to define the model and the operating conditions before starting the simulation including the next points

- Track definition

An important step in the model building is the definition of the track. The

SIMPACK definition of track alignment modelling element is used to describe the geometry of railway or road vehicle tracks in three dimensional space. Standard track model number 13 is used for the designed track in the current work. The following data is provided to the program to completely define the track properties:

- Length of Straight Track.
- Length of Transition Track.
- Radius, End of Transition Track.
- Super-elevation, End of Transition Track.
- Reference Length for Super-elevation.
- Length of the Circular Arc.
- Total Track Length.

- Body Definition

  A complete model for the TGV 001 vehicle described in section (5.3.2). The model is built in SIMPACK environment as it can be shown in figure (5.49).

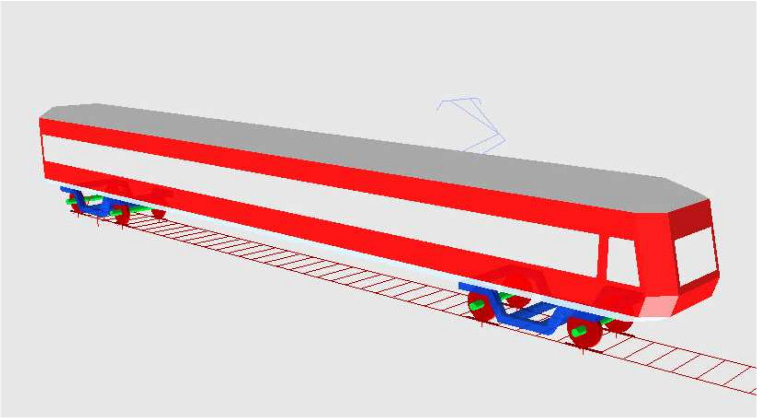

Figure 5.49. *TGV0 01 car model in SIMPACK environment*

All the inertia properties of the bodies forming the vehicle model are introduced to complete the body definition phase. The wheel and rail profiles are defined as the standard profile UIC60 for the rail and S1002 for the wheel for both left and right side. The wheel nominal radius is adjusted in according to the radius used for the model defined in VIA program, as well as the semi distance between the nominal contact points.

- Joints Definition

All the joints defined are associated to railway joint type. The solution of the contact problem includes the definition of the contact model and contact approach used in the simulation. The following figure (5.50) illustrates the main aspects of the definition of the contact models in SIMPACK program.

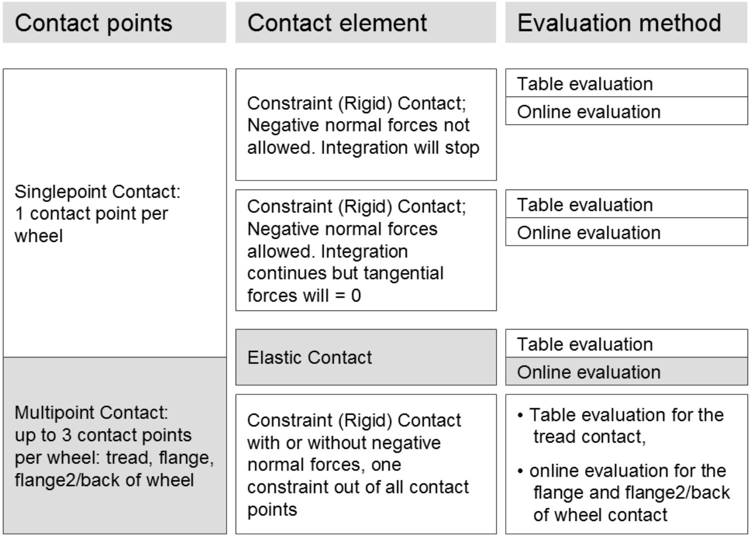

| Contact points | Contact element | Evaluation method |
|---|---|---|
| Singlepoint Contact: 1 contact point per wheel | Constraint (Rigid) Contact; Negative normal forces not allowed. Integration will stop | Table evaluation<br>Online evaluation |
| | Constraint (Rigid) Contact; Negative normal forces allowed. Integration continues but tangential forces will = 0 | Table evaluation<br>Online evaluation |
| | Elastic Contact | Table evaluation<br>Online evaluation |
| Multipoint Contact: up to 3 contact points per wheel: tread, flange, flange2/back of wheel | Constraint (Rigid) Contact with or without negative normal forces, one constraint out of all contact points | • Table evaluation for the tread contact,<br>• online evaluation for the flange and flange2/back of wheel contact |

FIGURE 5.50. *Contact Models in SIMPACK*

The selected contact model, as it is highlighted in the previous figure with gray colour, is a multipoint contact model that permits the definition of all possible contact points that can be detected during the simulation, up to 3 contact points per wheel: tread, flange and flange2/back of wheel as seen in figure (5.51)

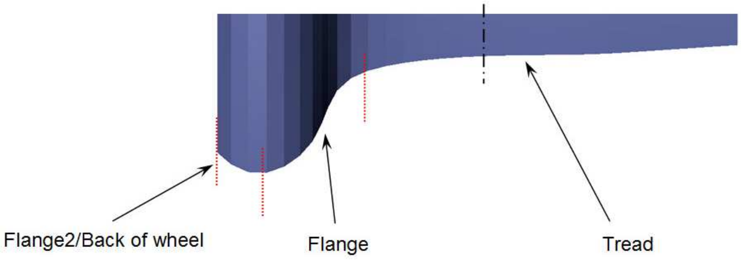

FIGURE 5.51. *Divisions of the wheel profile*

The elastic approach is selected to define the contact element type as it is illustrated in the previous figure (5.50). Finally the evaluation is selected to be on line evaluation to be in agreement with the procedure followed by VIA program. Finally and for the complete definition of the contact problem, the default method: Simplified theory of Kalker (FASTSIM) [32], is selected for the calculation of the tangential contact forces with a constant coefficient of friction equal to 0.45.

- Force Elements

  The force elements here refers to the primary and secondary suspension elements. The selected element type 05: spring/damper parallel compact (Cmp) is used for definition of the force type.

2) **Processing**

   Online time integration is used to solve the system equation of motion. The simulation time step is adjusted to $10^{-2}$s. The velocity is adjusted the same like the simulation speed of 25.6m/s provided to VIA program and the total simulation time is adopted to 15s, then the calculation started by the provided conditions.

3) **Processing**

   The processing step deals with the final result plotting and extracted data from the simulation. The SIMPACK program offers a detailed results for each body forming the multibody model in the railway vehicle. An important part in the extracted results related to the wheel-rail data which can be summarised in the following:

   - Wheelset lateral position in track
   - Wheelset yaw angle .
   - Creepage (longitudinal, lateral, spin).
   - Normal force N, traction forces.
   - Traction coefficients.
   - Wheel forces Y, Q.
   - Frictional power P.
   - Contact point coordinates on wheel/on rail.
   - Longitudinal contact point shift.
   - Semi-axes a, b of the Hertzian ellipse.
   - Area of the Hertzian ellipse.
   - Ratio of the semi-axes a/b.

- Current Kalker coefficients $C_{11}$, $C_{22}$, $C_{23}$.

As a continuation for the procedure followed to validate the obtained results from VIA simulation tool developed in the current work, a comparison is made for the simulation data obtained from VIA program and the data from SIMPACK commercial package for railway analysis, for a the TGV 001 vehicle model. The multibody model of the vehicle is built as it is explained in chapter (4). The results obtained for a vehicle model negotiating the designed track are explained in section (5.3.1). The vehicle wsa located on the track to run 100m of the straight line stage of, followed by a transition stage of 200m connecting the the straight stage to a plane curve stage with a constant radius of 1000m.

The obtained results form VIA program are presented in solid lines in the following figures and on the other hand the SIMPACK results are presented by means of dashed lines as seen in the following section.

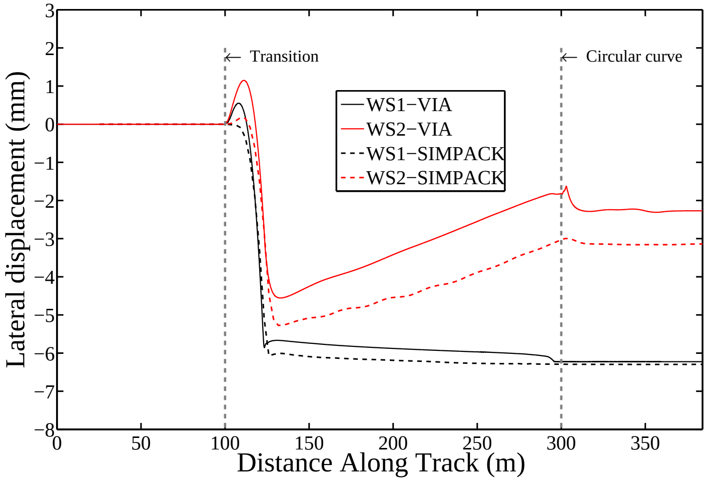

FIGURE 5.52. *Lateral shift of the leading and trailing wheelsets of the front bogie for a forward velocity of 25.6m/s, using VIA and SIMPACK simulation tools*

Figure (5.52) presents the comparison between the lateral shift value obtained by VIA and SIMPACK for the first and second wheel set of TGV 001 vehicle. The value of the lateral displacement of the first wheelset obtained by the developed simulation tool is very similar to that obtained by SIMPACK because the lateral shifting process is limited by the flange contact and it reaches a maximum value in the quasi-static position reached in the constant radius curve stage.

As shown in both figure (5.52) and figure (5.53), the lateral shift value for the trailer wheelset is always lower than the value reached by the leading wheelset as the trailing is always trying to keep the bogie frame centred to the track during the curve

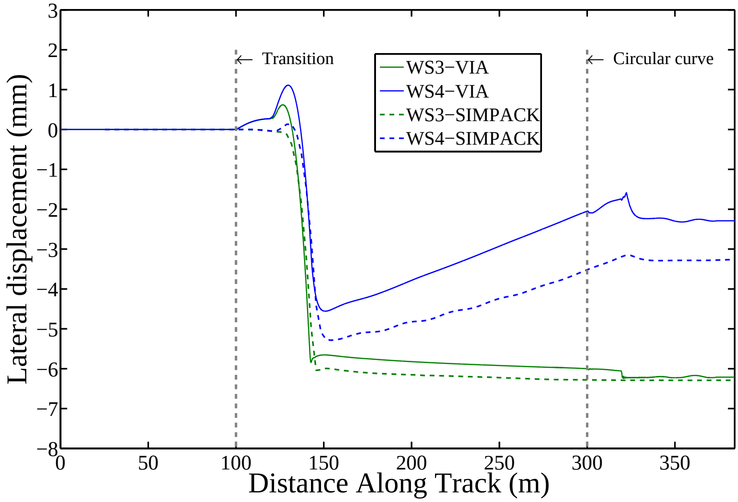

Figure 5.53. *Lateral shift of the leading and trailing wheelsets of the rear bogie for a forward velocity of 25.6m/s, using VIA and SIMPACK simulation tools*

negotiation.

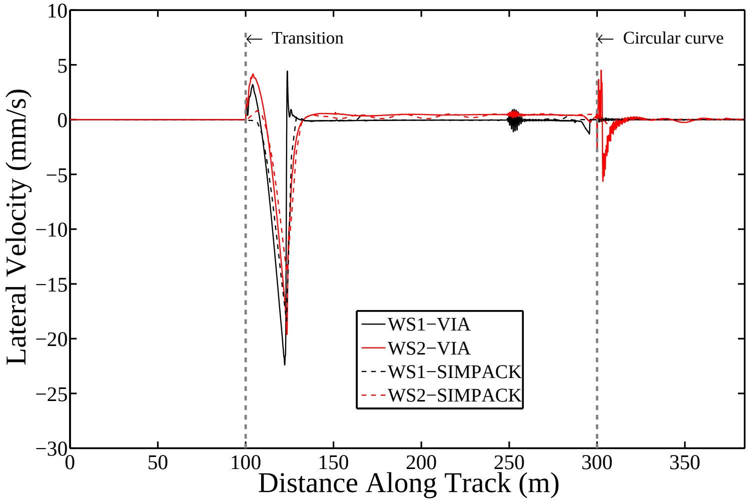

Figure 5.54. *Lateral velocity of the leading and trailing wheelsets of the front bogie, using VIA and SIMPACK simulation tools*

Figure (5.54) as well as figure (5.55) shows the lateral velocity of the leading and trailing wheelset conected the fornt and rear bogie frame, respictively. The obtained

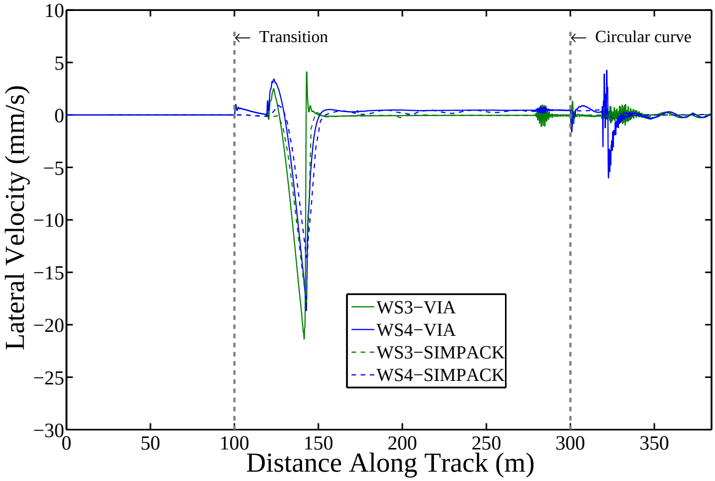

Figure 5.55. *Lateral velocity of the leading and trailing wheelsets of the rear bogie, using VIA and SIMPACK simulation tools*

results by VIA show a good agreement for the velocity values with that obtained by SIMPACK, Except for the oscilations produced in the exite from the transition curve stage to the constant curve stage due to the oscilation in the contact position detection in each stage.

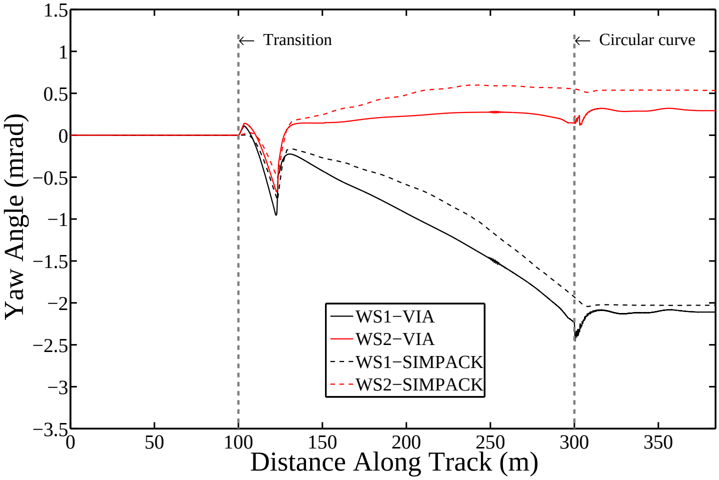

Figure 5.56. *Yaw angle variation for the leading and trailing wheelsets of the front bogie, using VIA and SIMPACK simulation tools*

In figure (5.56) a comparison between the obtained values for the yaw angle variation of the front and rear wheelset of the front bogie frame, is presented. These results obtained by both VIA and SIMPACK program for a forward velocities of 25.6m/s for a vehicle running through the track are presented in section (5.3.1).

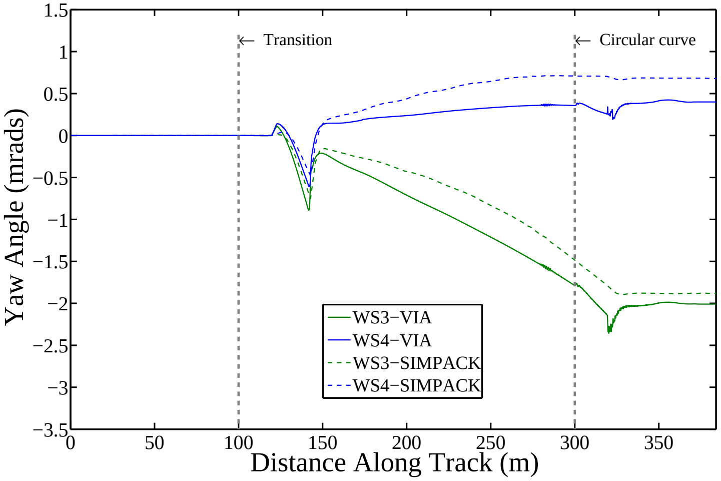

Figure 5.57. *Yaw angle variation for the leading and trailing wheelsets of the rear bogie, using VIA and SIMPACK simulation tools*

Figure (5.57) depicts the variation in the yaw angle for the font and rear wheelset of the rear bogie frame. Another aspect shown in both figures is that the values of yaw angle of the rear wheelsets is lower than the yaw angle for the front wheelsets. As it was mentioned that the rear wheelset keeps the bogie in stable running during the movment in curved tracks. It is evident that the leading wheelset reaches to a maximum value for the yaw angle in the constant curve stage as the motion is limited by the flange contact.

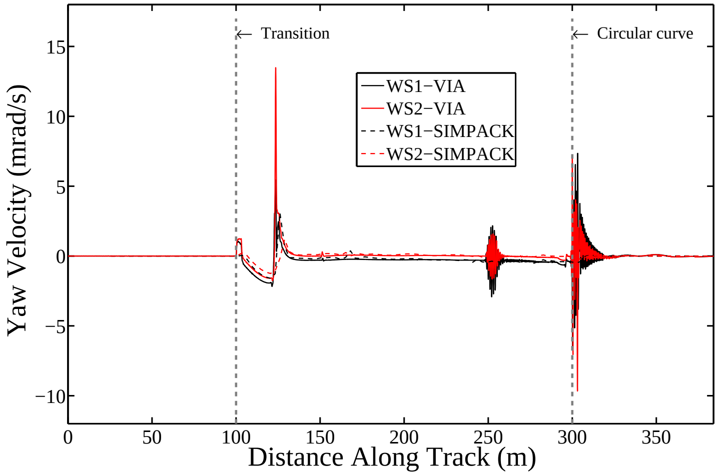

Figure 5.58. *Yaw velocity variation for the leading and trailing wheelsets of the front bogie, using VIA and SIMPACK simulation tools*

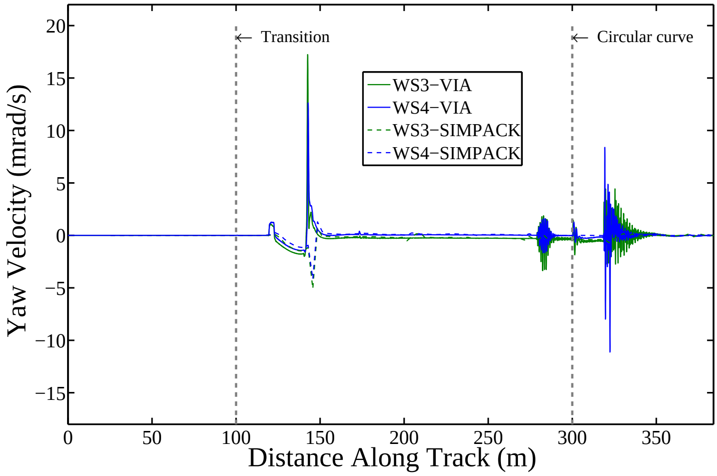

Figure 5.59. *Yaw velocity for both wheelsets attached to the rear bogie frame, using VIA and SIMPACK simulation tools*

Figures (5.58) and (5.59 ) present the change in the yaw velocity for the leading and trailing wheelsets of the front and rear bogie frames respectively.

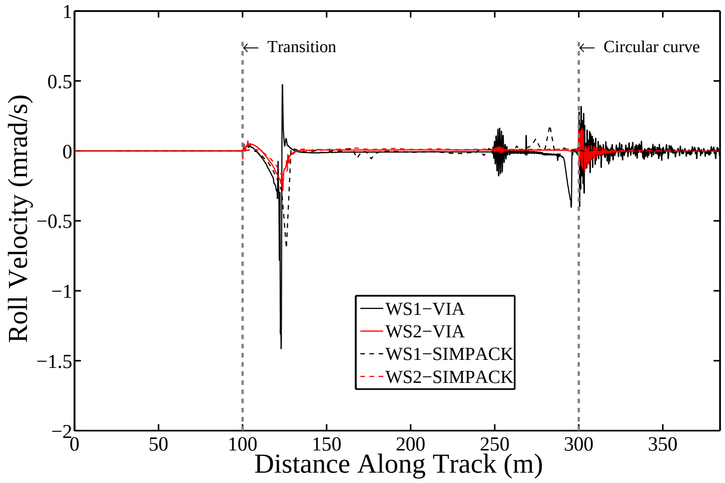

FIGURE 5.60. *Roll velocity for the first and second wheelsets*

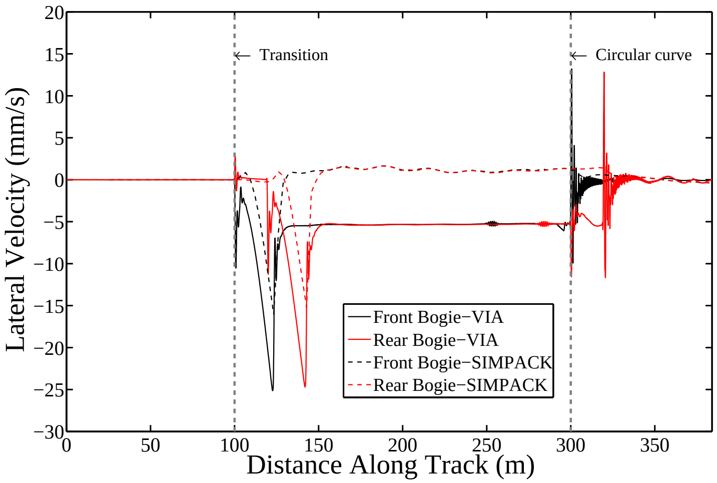

FIGURE 5.61. *Lateral velocity of the front and rear bogie frames*

The plots (5.61) and (5.62) correspond to the dynamic analysis performed with initial forward velocity of 25.6m/s. The figures present the variation in the yaw as well as tha roll velocity, respictively of both bogie frames of the TGV 001 vehicle.

In the beginning of the constant radius curve stage, decaying oscillations are observed during the oscillatory changes of the contact forces. The oscillations are decreased directly as a result of the vehicle stability by reaching quasi-static equilibrium in the constant curve stage.

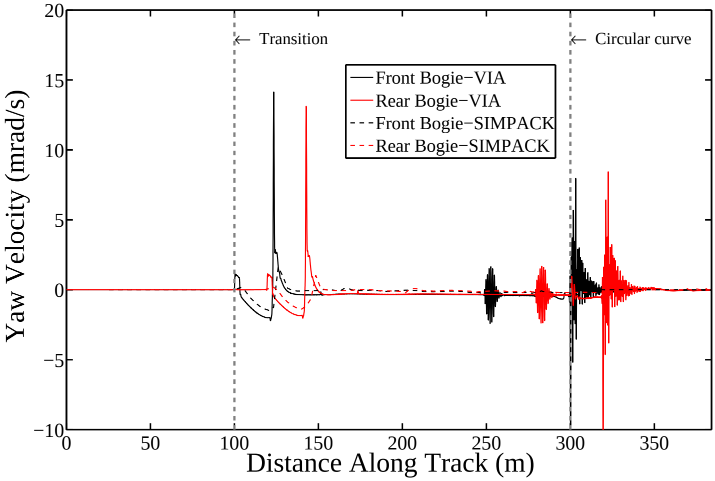

Figure 5.62. *Yaw velocity of the front and rear bogie frames*

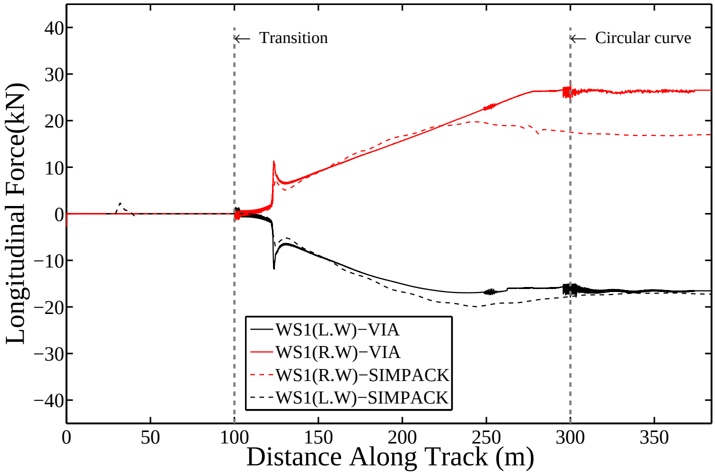

Figure 5.63. *Longitudinal creep forces on the left and right wheels of the leading wheelset attached to the front bogie, using VIA and SIMPACK simulation tools*

In figure (5.63), the longitudinal contact forces on the left and right wheelset of the leading wheelset are presented. The results are in close agreement with obtained results for the simulation carried out by SIMPACK package. The longitudinal forces affecting the right wheel has the highest value as the outer wheel is always subjected to higher creep values during the curve negotiation

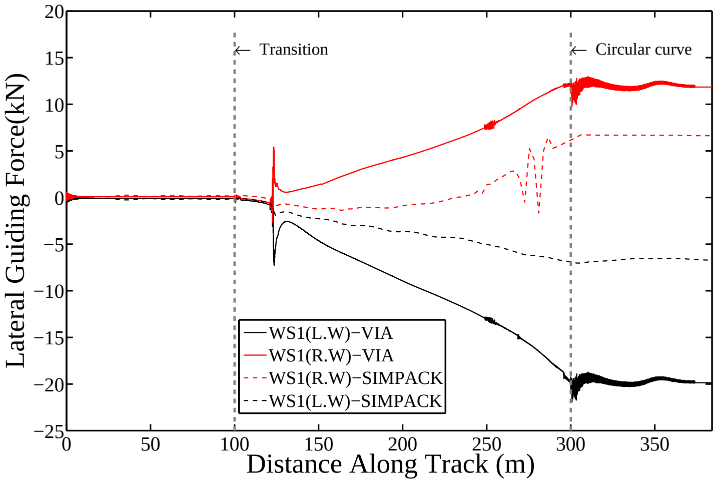

Figure 5.64. *Lateral guiding foces on the left wheel(L.W) and right wheel(R.W) of the leading wheelset for a forward velocity of 25.6m/s, using VIA and SIMPACK simualtion tools*

Figure (5.64) depicts the comparison between the lateral creep forces obtained by VIA and SIMPACK simulation tools. The leading wheelset always is focused as it is subjected to high lateral guiding forces negotiating the track, and these results are in agreement with the literatures[4, 24].

## 5.6 Application of Polach contact model

In the work presented, FASTSIM model is used for the calculation of the tangential forces. In the following section, Polach contact model is introduced in the Multibody simulation tool (VIA) proposed in the current work to replace the FASTSIM model. The objective for the application of different model for the calculation of the tangential forces is proposed to demonstrate the flexibility of the simulation tool to replace the contact model and use others without the need for any modifications in the main structure of the Multibody program used in the dynamic analysis of railway vehicles.

The comparisons between the results obtained using FASTSIM and Polach model are presented in the following figures, starting by the displacements and ending by the variation in the contact force calculation.

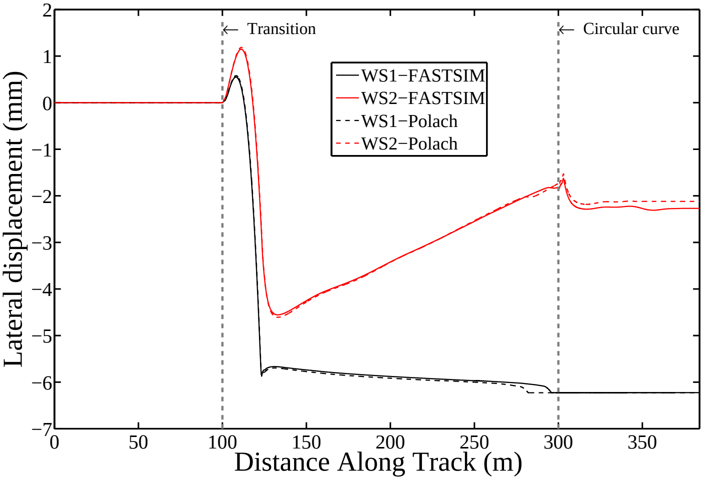

Figure 5.65. *Lateral shift of the leading and trailing wheelset of the fornt bogie for a forward velocity of 25.6m/s, using FASTSIM and Polach models*

In figure (5.65) the lateral shifts of the leading and trailing wheelset attached to the front bogie frame of the TGV 001 vehicle are presnented. The results correspond to a vehicle moving with a velocity of 25.6m/s, being the contact forces calculated by FASTSIM and Polach creep force models. In the results, there is a good agreement between both models for used in the determination of the tangential contact forces.

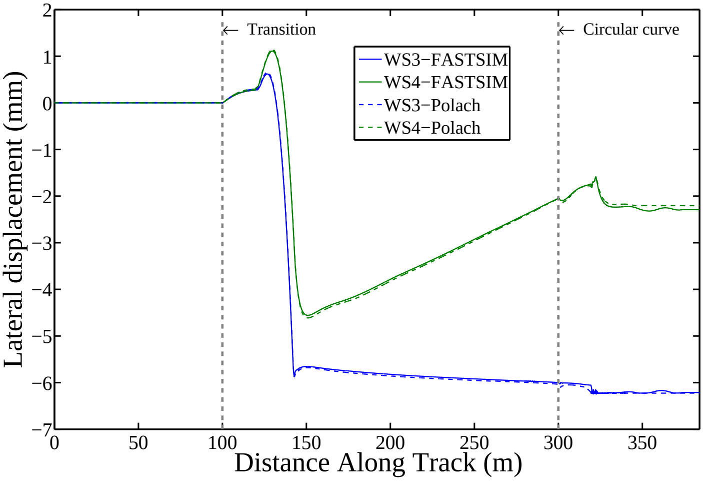

Figure 5.66. *Lateral shift of the leading and trailing wheelset of the rear bogie for a forward velocity of 25.6m/s, using FASTSIM and Polach models*

Figure (5.66) depicts the variation in the lateral shift of the third and fourth wheelset of the vehicle negotiating the designed track. The results obtained by both models applied for the calculation of the tangential forces show a good agreement with each otheres as well as a good agreement with the obtained results by the simulation carried out using SIMPACK at the same operation conditions.

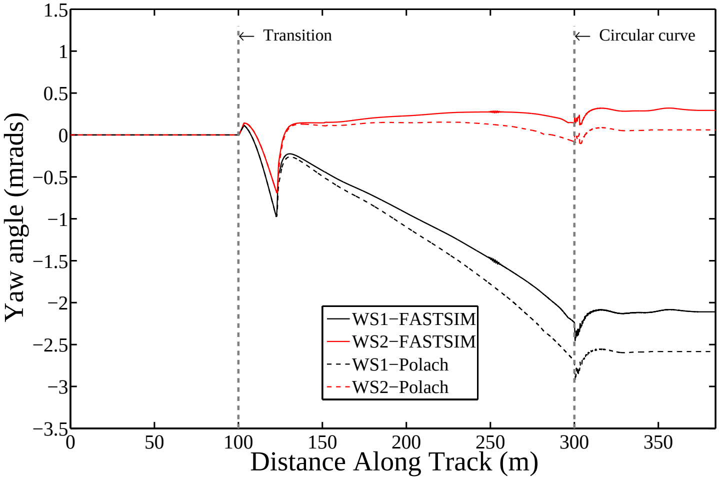

Figure 5.67. *Yaw angle variation for the leading and trailing wheelset of the fornt bogie for a forward velocity of 25.6m/s, using FASTSIM and Polach models*

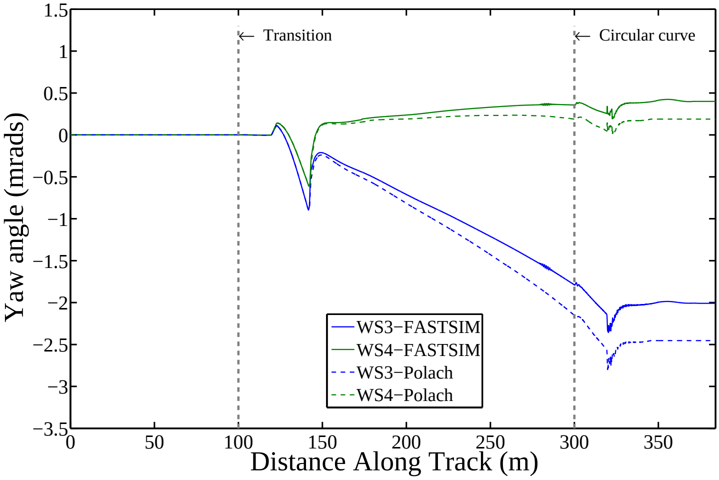

Figure 5.68. *Yaw angle variation for the leading and trailing wheelset of the rear bogie for a forward velocity of 25.6m/s, using FASTSIM and Polach models*

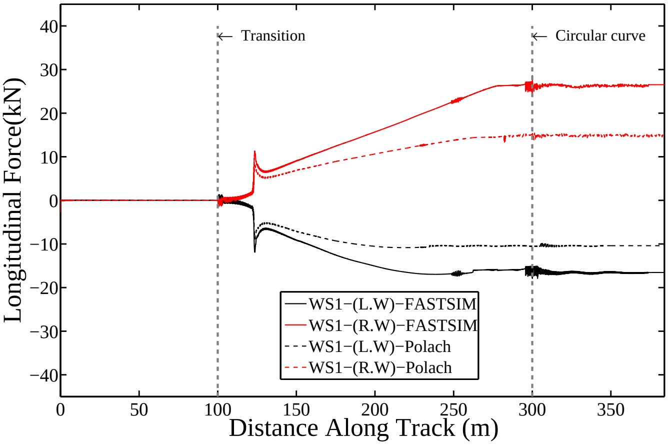

FIGURE 5.69. *Longitudinal creep forces on the left and right wheels of the leading wheelset attached to the front bogie, using FASTSIM and Polach models*

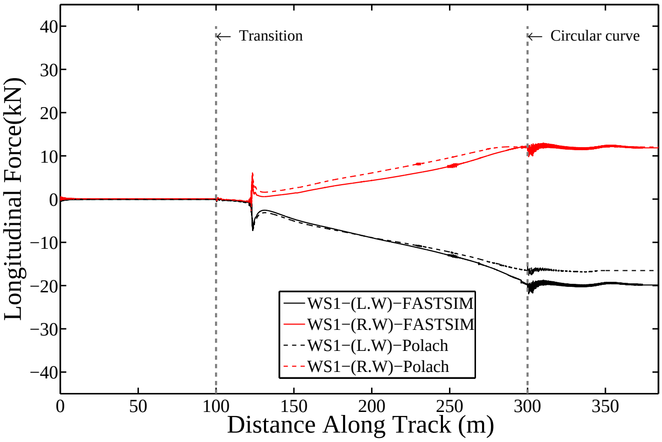

FIGURE 5.70. *Lateral creep forces on the left and right wheels of the leading wheelset attached to the front bogie, using FASTSIM and Polach models*

Figures (5.70) and (5.69) correspond to the dynamic analysis carried out for the TGV 001 vehicle model presented in section (5.3.2). The normal contact forces are calculated through Hertz model. The creep forces are calculated by two creep force law applied in the anlysis FASTSIM as well as Polach.

The obtained results show a close agreement with the obtained results by the FASTSIM creep model and Polach model as the spin creepage is not taken into account in the calculation of the creep forces.

# Chapter 6

# Conclusions and Future works

## 6.1 Conclusions

In the presented work, a computational tool used for the dynamic analysis of railway vehicle systems is developed using multibody system formulation. These techniques of multibodies permit the precise analysis large displacements between the solids that compose the railway vehicle systems without the need of linearization such as in vibration methods. The simulation tool used in the dynamic analysis railway systems is developed in MATLAB environment.

In order to integrate all the relevant characteristics inherent to railway systems, some special capabilities are implemented in the multibody code. The presented developments include a methodology used in the parameterization of the track without taking the effect of track irregularities into account. An efficient wheel-rail contact model developed by the investigation group is proposed and implemented in order to detect the location of the contact points online during the dynamic simulation with high precision. The contact model not only capable of the detection of multiple contact points, but also it has a high computational efficiency.

The mathematical model of the proposed code is created using multibody formulation. Independent coordinates are used to define the general motion of a three dimensional rigid body forming a component of the multibody system. Cartesian coordinates are implemented in order to be easily used in the formulation of the developed multibody code.

The equations of motion of the multibody system are obtained for non constrained systems by means of Lagrange's principles which is used to determine the equation of motion of a rigid body. The solution of the algebraic set of equations are avoided as there is no kinematic constrained applied for the multibody system.

In the dynamic analysis of the railway vehicles, the description of the track model is required. In the presented work, the track centreline is parameterized using analytical segment approach which depends on the formation of the track using different segments interconnected by transition curves. The designed track in this thesis- without loss of generality- is composed of straight line segment connected to circular curve with constant radius, by means of a transition curve of Clothoid type.

An efficient methodology is implemented in the multibody code to accurately detect the coordinates of the contact points. the wheel-rail contact model used in the presented work, is based on the virtual interpenetration between the wheel and rail surfaces. The intersection between the wheel and rail profiles is reduced into the solution of the intersection problem between a straight line and conical segment, where the wheel profile is presented as a conical segment produces from the revolution of the wheel profile points about the axis parallel to the contact plane, and the rail profile is obtained as an extrusion of the rail profile points along the direction of motion.

By knowing the relative motion of the wheel with respect to the rail, a set of nonlinear equations areas are solved to find the points of intersection of the rail straight line with the wheel conical segments. By this way the contact area is defined by set of longitudinal strips produces by the solution of the geometrical contact problem at the wheel-rail interface

The wheel-rail contact forces play a crucial rule in the vehicle dynamic behaviour. In the presented work, the normal contact force is calculated using Hertz normal contact model. On the other hand, the tangential contact problem is solved by means of three creep force laws implemented in the multibody code ,namely: Kalker linear theory; FASTSIM algorithm and Polach nonlinear creep force law. The use of different creep force models depicts the flexibility of the simulation tool in realizing important changes on the contact model without the need of making changes on the main structure of the developed code.

The developed simulation tool VIA is applied to different case tests in order to validate the obtained results as well as the determination of the suitability of the proposed methodology to achieve different type of analysis on railway systems. For this issue, the VIA simulation tool is used to analyze the dynamic behaviour of the Manchester Benchmark vehicle number one, negotiating track case number one. The obtained results show a good agreement with the results obtained by the commercial packages used in the analysis of the Benchmark.

A comparison has been made between the obtained dynamic results produce from the simulation tool VIA for TGV001 locomotive vehicle in different operating scenarios, and the results obtained during my exchange period realized in the Politecnico di Milano, obtained by SIMPACK program. The results demonstrate good agreement between both simulation tools at the same operating conditions.

The developed simulation tool presented in this thesis is designed in a flexible form that permits the possibility to change and realize modifications taking into account the following aspects:

- The adaptation of the multibody formulation to railway systems in such form that linearizations which correspond to the rotation of the systems forming the vehicle is not included in the methodology proposed.
- Modelling the wheel-rail contact problem based on the virtual interpenetration between the wheel and rail surfaces.

By this way it is possible to present an adopted model used in the dynamic analysis of low frequency range. The proposed assumptions are the same assumptions adopted by other commercial simulation packages like: SIMPACK, VAMPIRE, GENSYS. The implementation of such assumptions in the developed simulation tool in this thesis permits the application of new models and realization of important modifications like:

- The possibility of modelling and implementation of real wheel-rail contact models such as non Hertezian models.
- The possibility of modelling and implementation of flexible tracks as well as the implementation of bridge structures as the coupling between the vehicle equation of motion and structure equation of motion is achieved by the transmitted forces between both systems.

The simulation tools developed for low frequency range present an important utility in the development of railway systems. The developed work in the thesis presents the beginning of transferring process of the new technologies in the railway sector from Spain to Egypt, and this was a principle motivation in the development of the presented work and at the same time the ability of implementation of new developed models developed by the research group in Valencia Technical University such as

- The implementation of flexible track models that consider the track dynamic structure [6, 7] at the required frequency range.
- The implementation of the flexibility of the wheelset [9, 62]. As it is considered as a fundamental tool in the study of the wheel flat problem as well as rail corrugation.
- The implementation of advanced wheel rail contact models. For the calculation of the normal force non Hertzian contact models are of interest, and on the other hand the use of instationary contact models [8] for the tangential contact force calculation.

## 6.2 Future developments

The development of advanced railway vehicles is a complex research field that requires new ideas and novel design solutions. So the future work in the field of railway dynamics will not finish comparing with the large challenges can be faced by the research efforts in the enhancement of passenger comfort and rapid transportation using railway transportation methods. But the future work proposed by the end of this work for the improvement of the vehicle models and enhancement methodologies, can be summarized in the following points

- The use of a flexible multibody approach, in which the vehicle components can be modelled as flexible bodies, can be an alternative technique to be used in the future.
- The inclusion of nonlinear spring elements, with defined stiffness characteristics and clearance, could lead to important improvements when modelling the primary and secondary suspension elements.
- The use of advanced techniques for the calculations of the wheel-rail interaction problem, including the non Hertzian contact models.
- The inclusion of track flexibility, and the coupling between the vehicle model and track structure model.

# Appendix A

# Kinematic and Dynamic Background

## A.1 Introduction

In this appendix, all the matrices used in the mathematical formulations of the models used in the kinematic presentation of the wheelset and general solid body, are presented with accurate description for all the identities and variables used in each. The calculation of each transformation matrix used in the formulation is explained in this part, its time derivative is also derived, detailed description for the and inertia matrices of the solids are also included.

## A.2 Rotation matrix

### A.2.1 Rotation matrix definition

In multibody systems, the components may undergo large relative translational and rotational displacements. To define the configuration of a body in the multibody system in space, one must be able to determine the location of every point on the body with respect to a selected inertial frame of reference. To this end, it is more convenient to assign for every body in the multibody system a body reference in which the position vectors of the material points can be easily described. The position vectors of these points can then be found in other coordinate systems by defining the relative position and orientation of the body coordinate system with respect to the other coordinate systems. Six variables are sufficient for definition of the position and orientation of one coordinate system $X_i$ $Y_i$ $Z_i$ with respect to another coordinate system X Y Z. As shown in figure (A.1), three variables define the relative translational motion between the two coordinate systems. This relative translational motion can be measured by the position vector of the origin $O_i$ of the coordinate system $\mathrm{X_i}$ $\mathrm{Y_i}$ $\mathrm{Z_i}$ with respect to the coordinate system X Y Z. The orientation of one coordinate system with respect to another can be defined in terms of three independent variables[57].

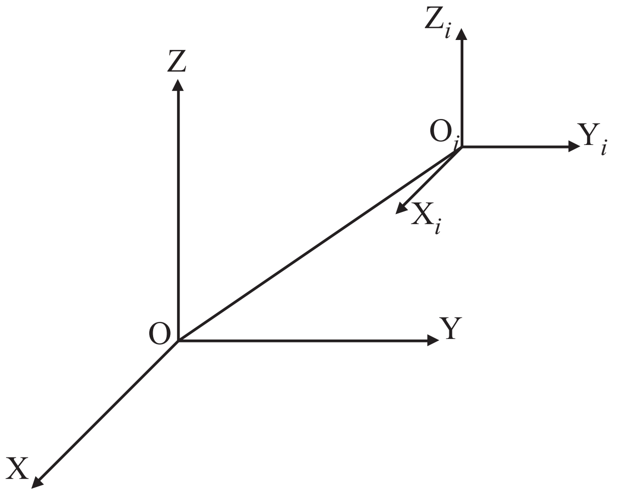

Figure A.1. *Two different coordinate systems* X Y Z *and* $\mathrm{X_i}$ $\mathrm{Y_i}$ $\mathrm{Z_i}$

### A.2.2 Derivation of the rotation matrix

There are several formulations used to represent the rotation matrix such as *Rodriguez formula* ,*Euler parameters* and finally *Euler angles formulations*. These forms are used to determine the rotation matrix and here we use the last method depending on the definition of Euler angles representing the required transformation

### A.2.3 Euler angles

The third formulation that can be used for the representation of the rotation matrix is using *Euler angles*. These angles are used to carry out the transformation from one coordinate system to another using successive rotations performed in a known sequence. Furthermore these angles used to determine the successive rotations about three axes which are not orthogonal in general, so we consider the coordinate system Z,Y and X, which represent our global frame of reference and we will show the rotation matrices produced from rotation about X-axis with an angle $\theta_x$, which can be defined in the railway application field by the an angle $\phi$ which represent the cant angle, rotation about Y-axis with angle $\theta_y$ that can be defined in the railway application by the pitch angle $\theta$, and finally rotation about Z-axis with an angle $\theta_z$ that can be defined in the railway application by the angle of attack $\psi$.

### A.2.4 Basic rotations

As it was introduced the orientation of a body in the space may be defined by knowing the rotations made by the body with respect to the spatial coordinates. In the following part the rotation matrices about the main spatial coordinates are represented.

#### A.2.4.1 Rotation about X-axis

In notations used in the following context we will define the rotation matrix with the symbol $\mathbf{A}_i$, where $i$ represents the corresponding axis of rotation (i.e $i = x$, $y$, and $z$). The rotation matrix produced from the rotation about X-axis with an angle $\theta_x$, figure (A.2), can be defined as

$$\mathbf{A}_x = \begin{bmatrix} 1 & 0 & 0 \\ 0 & \cos\theta_x & -\sin\theta_x \\ 0 & \sin\theta_x & \cos\theta_x \end{bmatrix} \tag{A.1}$$

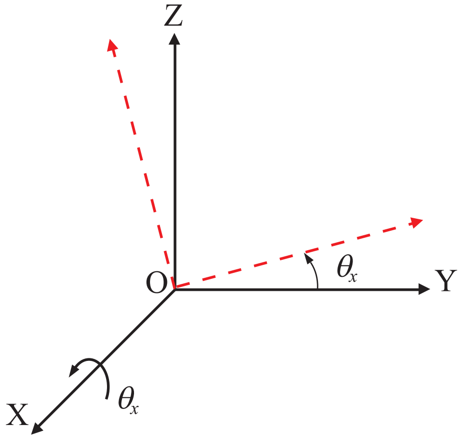

FIGURE A.2. *Rotation about X-axis with angle $\theta_x$*

#### A.2.4.2 Rotation about Y-axis

The rotation matrix produced from the rotation about Y-axis with an angle $\theta_y$ figure (A.3), can be defined as

$$\mathbf{A}_y = \begin{bmatrix} \cos\theta_y & 0 & \sin\theta_y \\ 0 & 1 & 0 \\ -\sin\theta_y & 0 & \cos\theta_y \end{bmatrix} \tag{A.2}$$

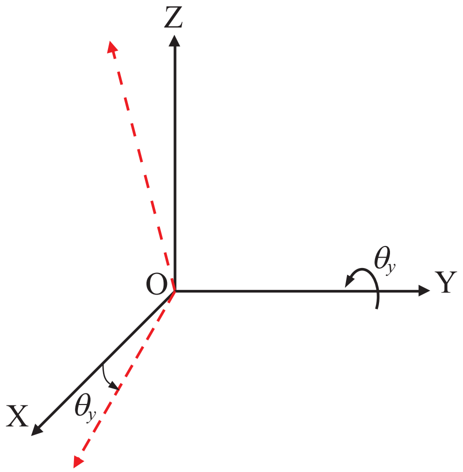

Figure A.3. *Rotation about* Y*-axis with angle* $\theta_y$

#### A.2.4.3 Rotation about Z-axis

The rotation matrix produced from the rotation about Z-axis with an angle $\theta_z$ figure (A.4), can be defined as

$$\mathbf{A}_z = \begin{bmatrix} \cos\theta_z & -\sin\theta_z & 0 \\ \sin\theta_z & \cos\theta_z & 0 \\ 0 & 0 & 1 \end{bmatrix} \tag{A.3}$$

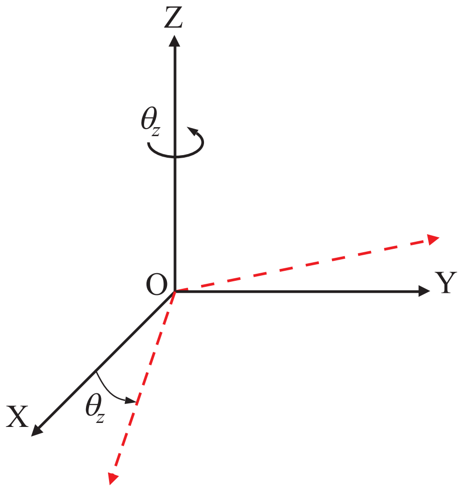

FIGURE A.4. *Rotation about* Z*-axis with angle* $\theta_z$

## A.3 Successive rotations

In this part we will represent the final rotation matrix produced from a known sequence of successive rotations, here in this part we should have to know that there are two procedures for the representation of the successive rotations, the first called *single-frame* method and the other is called *multiframe* method.

### A.3.1 Single-frame method

In this method fixed frame of reference is defined and after each rotation we define the rotational axes and the unite vectors with respect to the fixed coordinate system. Now if we consider a set of consecutive rotations using the following rotation angles $\theta_1$, $\theta_2$... $\theta_n$ about the unite vectors $v_1$, $v_2$... $v_n$ respectively, the rotation matrices produced after each rotation can be calculated using any formulation from the mentioned methods used to derive the rotation matrix and denoted as $\mathbf{A}_1$, $\mathbf{A}_2$... $\mathbf{A}_n$ . After $n$ successive rotations we can calculate the final transformation matrix as

$$\mathbf{A} = \mathbf{A}_n\, \mathbf{A}_{n-1} ... \mathbf{A}_2\, \mathbf{A}_1 \tag{A.4}$$

Where $\mathbf{A}_1$ is equal to the identity matrix.

### A.3.2 Multiframe method

This method can be discussed by this simple example. Consider that the body shown in figure(A.5) is subjected to two successive rotations, the first rotation is with an angle $\theta_1$ about Y-axis producing the configuration of coordinates shown in position(2), and the second rotation with an angle $\theta_2$ about Z-axis producing the configuration of the coordinate system shown in position(3).The orientation of coordinate system of position(2) with respect to coordinate system shown in position(1) can be described by defining the matrix $\mathbf{A}_{21}$, also the orientation of the coordinate system shown in position(3) with respect to the coordinate system shown in position(2) by defining the matrix $\mathbf{A}_{32}$. Where $n$ is the number of position

## A.4 Transformation matrices

It is the matrix required to present the different identities such as the kinematics identities and the dynamic identities of a specified reference system with respect to another frame of reference .

### A.4.1 Track transformation matrix

This matrix is the matrix required to transform from the track reference frame to the global reference frame and it is calculated here by making three consecutive rotation, first rotation about Z-axis and then about Y-axis and finally about X-axis

$$\mathbf{A} = \mathbf{A}_z\,\mathbf{A}_y\,\mathbf{A}_x \tag{A.5}$$

$$\mathbf{A} = \begin{bmatrix} \cos\theta_z\,\cos\theta_y & -\sin\theta_z\,\cos\theta_x + \cos\theta_z\,\sin\theta_y\,\sin\theta_x & \sin\theta_z\,\sin\theta_x + \cos\theta_z\,\sin\theta_y\,\cos\theta_x \\ \sin\theta_z\,\cos\theta_y & \cos\theta_z\,\cos\theta_x + \sin\theta_z\,\sin\theta_y\,\sin\theta_x & -\cos\theta_z\,\sin\theta_x + \sin\theta_z\,\sin\theta_y\,\cos\theta_x \\ -\sin\theta_y & \cos\theta_y\,\sin\theta_x & \cos\theta_y\,\cos\theta_x \end{bmatrix} \tag{A.6}$$

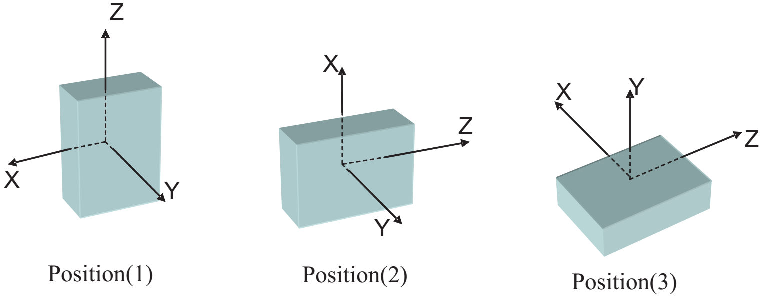

Figure A.5. *Successive rotation of a solid body about its reference coordinates*

### A.4.2 Solid transformation matrix

This matrix is the matrix required to transform from the track reference frame to the solid reference frame and it is calculated here by making three consecutive rotation, first rotation about Z-axis and then about X-axis and finally about Y- axis.

$$\mathbf{B} = \mathbf{B}_z \, \mathbf{B}_x \, \mathbf{B}_y \tag{A.7}$$

$$\mathbf{B} = \begin{bmatrix} \cos\theta_z \, \cos\theta_y \, - \, \sin\theta_z \, \sin\theta_x \, \sin\theta_y & -\sin\theta_z \, \cos\theta_x & \cos\theta_z \, \sin\theta_y + \sin\theta_z \, \sin\theta_x \, \cos\theta_y \\ \sin\theta_z \, \cos\theta_y + \cos\theta_z \, \sin\theta_x \, \sin\theta_y & \cos\theta_z \cos\theta_x & \sin\theta_z \, \sin\theta_y \, - \, \cos\theta_z \, \sin\theta_x \, \cos\theta_y \\ -\cos\theta_x \, \sin\theta_y & \sin\theta_x & \cos\theta_x \cos\theta_y \end{bmatrix} \tag{A.8}$$

### A.4.3 Intermediate transformation matrix

This matrix is the matrix required to transform from the track reference frame to the intermediate reference frame and it is calculated here by making three consecutive rotation, first rotation about Z-axis and then about X-axis.

$$\mathbf{B} = \mathbf{B}_z \, \mathbf{B}_x \tag{A.9}$$

$$\mathbf{B}_{zx} = \begin{bmatrix} \cos\theta_z & -\sin\theta_z \, \cos\theta_x & \sin\theta_z \, \sin\theta_x \\ \sin\theta_z & \cos\theta_z \cos\theta_x & -\cos\theta_z \, \sin\theta_x \\ 0 & \sin\theta_x & \cos\theta_x \end{bmatrix} \tag{A.10}$$

## A.5 Angular velocity matrices

### A.5.1 Absolute angular velocity matrix

$$\boldsymbol{\omega} = \boldsymbol{\tau} + \boldsymbol{L}\dot{\boldsymbol{\theta}} \tag{A.11}$$

where $\boldsymbol{\tau}$ is the absolute angular velocity of the track and it can be calculated knowing the value of the angular velocity $\bar{\boldsymbol{\tau}}$ represented in the track reference frame. The value of $\bar{\boldsymbol{\tau}}$ can be calculated by defining the skew symmetric matrix of the track angular velocity vector represented in the track reference frame $\bar{\bar{\boldsymbol{\tau}}}$.

### A.5.2 Skew symmetric matrix of the track angular velocity vector

$$\tilde{\bar{\boldsymbol{\tau}}} = \mathbf{A}^{\mathrm{T}}\,\dot{\mathbf{A}} \tag{A.12}$$

$$\tilde{\bar{\boldsymbol{\tau}}} = \begin{bmatrix} 0 & -\cos\theta_y\,\dot{\theta}_z\,\cos\theta_x + \sin\theta_x\,\dot{\theta}_y & \cos\theta_y\,\dot{\theta}_z\,\sin\theta_x + \cos\theta_x\,\dot{\theta}_y \\ \cos\theta_y\,\dot{\theta}_z\,\cos\theta_x - \sin\theta_x\,\dot{\theta}_y & 0 & -\dot{\theta}_x + \sin\theta_y\,\dot{\theta}_z \\ -\cos\theta_y\,\dot{\theta}_z\,\sin\theta_x - \cos\theta_x\,\dot{\theta}_y & \dot{\theta}_x - \sin\theta_y\,\dot{\theta}_z & 0 \end{bmatrix} \tag{A.13}$$

### A.5.3 Track angular velocity vector represented in track frame

$$\bar{\boldsymbol{\tau}} = \begin{bmatrix} \dot{\theta}_x - \sin\,\theta_y\,\dot{\theta}_z \\ \cos\,\theta_y\,\dot{\theta}_z\,\sin\,\theta_x + \cos\,\theta_x\,\dot{\theta}_y \\ \cos\,\theta_y\,\dot{\theta}_z\,\cos\,\theta_x - \sin\,\theta_x\,\dot{\theta}_y \end{bmatrix} \tag{A.14}$$

### A.5.4 Absolute relative angular velocity of the solid

The value of the matrix **L** depends on the rotation sequence. It represents the matrix that relates the absolute angular velocity vector of the rigid body defined in the global reference frame to the time derivative of the orientation parameters[shabana, chamarro- shabana railroad]. Then by definition of the unite vectors $v_1$, $v_2$, and $v_3$ acting along the three axes of rotations $Z$, $X$, and $Y$ respectively with respect to the global reference frame figure. (A.6), we can define the matrix $\bar{\mathbf{L}}$ as it is represented in the track reference frame.

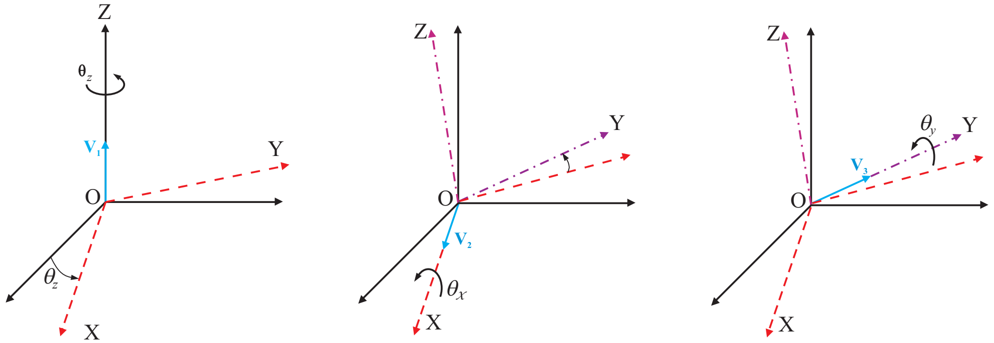

FIGURE A.6. *Consecutive rotations of the solid*

$$\mathbf{v}_1 = \begin{bmatrix} 0 & 0 & 1 \end{bmatrix}^{\mathrm{T}} \tag{A.15}$$

$$\mathbf{v}_2 = \begin{bmatrix} \cos\theta_z & \sin\theta_z & 0 \end{bmatrix}^{\mathrm{T}} \tag{A.16}$$

$$\mathbf{v}_3 = \begin{bmatrix} -\sin\theta_z\,\cos\theta_x & \cos\theta_z\,\cos\theta_x & \sin\theta_x \end{bmatrix}^{\mathrm{T}} \tag{A.17}$$

then the relative angular velocity matrix can be defined corresponding to figure (A.6) as follow

$$\bar{\boldsymbol{L}}\dot{\boldsymbol{\theta}} = \begin{bmatrix} \mathbf{v}_2 & \mathbf{v}_3 & \mathbf{v}_1 \end{bmatrix} \dot{\boldsymbol{\theta}} \tag{A.18}$$

the matrix $\bar{\boldsymbol{L}}$ defined in the track reference frame can be found by

$$\bar{\boldsymbol{L}} = \begin{bmatrix} \cos\theta_z & -\sin\theta_z\,\cos\theta_x & 0 \\ \sin\theta_z & \cos\theta_z\,\cos\theta_x & 0 \\ 0 & \sin\theta_x & 1 \end{bmatrix} \tag{A.19}$$

By knowing the transformation matrix $\mathbf{B}$ we can express the matrix $\boldsymbol{L}$ in the solid frame of reference as follow

$$\bar{\bar{\boldsymbol{L}}} = \mathbf{B}^{\mathrm{T}}\,\bar{\boldsymbol{L}} \tag{A.20}$$

$$\bar{\bar{\boldsymbol{L}}} = \begin{bmatrix} \cos\theta_y & 0 & -\cos\theta_x\sin\theta_y \\ 0 & 1 & \sin\theta_x \\ \sin\theta_y & 0 & \cos\theta_x\cos\theta_y \end{bmatrix} \tag{A.21}$$

## A.6 Inertia properties of the solid body

### A.6.1 Mass matrix of solid

$$\mathbf{M}_s = m_s \, \mathbf{I}_{3\times3} \tag{A.22}$$

where $m_s$ is the mass of the solid and $\mathbf{I}$ is $3 \times 3$ identity matrix.

### A.6.2 Inertia matrix of solid

$$\boldsymbol{J}_{\theta\theta} = \begin{bmatrix} J_{xx} & 0 & 0 \\ 0 & J_{yy} & 0 \\ 0 & 0 & J_{zz} \end{bmatrix} \tag{A.23}$$

The elements $J_{ij}$ represent the mass moment of inertia of the solid body and for rigid bodies these terms are constants, also when $i \neq j$ then it called the product of inertia, but for deformable bodies these terms are time independent.

## A.7 Time derivative of transformation matrices

### A.7.1 Time derivative of the track transformation matrix

Recalling the expression of the transformation matrix in the track frame of reference

$$\mathbf{A} = \mathbf{A}_z \, \mathbf{A}_y \, \mathbf{A}_x \tag{A.24}$$

the time derivative of the matrix $\mathbf{A}$ can be written as

$$\dot{\mathbf{A}} = \frac{\partial \mathbf{A}}{\partial t} \tag{A.25}$$

but the matrix $\mathbf{A}$ is not a function of the time, then by using the chain rule, the time derivative of the matrix $\mathbf{A}$ can be written as

$$\dot{\mathbf{A}} = \frac{\partial \mathbf{A}}{\partial \theta} \, \frac{\partial \theta}{\partial t} \tag{A.26}$$

$$\dot{\mathbf{A}} = \frac{\partial \mathbf{A}}{\partial \theta_z} \, \dot{\theta}_z + \frac{\partial \mathbf{A}}{\partial \theta_y} \, \dot{\theta}_y + \frac{\partial \mathbf{A}}{\partial \theta_x} \, \dot{\theta}_x \tag{A.27}$$

the partial derivative of the matrix $\mathbf{A}$ with respect to the three rotation angles as follow

$$\frac{\partial \mathbf{A}_x}{\partial\,\theta_x} = \begin{bmatrix} 0 & 0 & 0 \\ 0 & -\sin\theta_x & -\cos\theta_x \\ 0 & \cos\theta_x & -\sin\theta_x \end{bmatrix} \tag{A.28}$$

$$\frac{\partial \mathbf{A}_y}{\partial\,\theta_y} = \begin{bmatrix} -\sin\theta_y & 0 & \cos\theta_y \\ 0 & 0 & 0 \\ -\cos\theta_y & 0 & -\sin\theta_y \end{bmatrix} \tag{A.29}$$

$$\frac{\partial \mathbf{A}_z}{\partial\,\theta_z} = \begin{bmatrix} -\sin\theta_z & -\cos\theta_z & 0 \\ \cos\theta_z & -\sin\theta_z & 0 \\ 0 & 0 & 0 \end{bmatrix} \tag{A.30}$$

### A.7.2 Time derivative of body transformation matrix

The same can be done for the transformation matrix **B** between the solid frame of reference and the track frame of reference

$$\mathbf{B} = \mathbf{B}_z\,\mathbf{B}_x\,\mathbf{B}_y \tag{A.31}$$

$$\dot{\mathbf{B}} = \frac{\partial \mathbf{B}}{\partial\,t} \tag{A.32}$$

$$\dot{\mathbf{B}}_{zx} = \frac{\partial \mathbf{B}_{zx}}{\partial\,\theta_z}\,\dot{\theta}_z + \frac{\partial \mathbf{B}_{zx}}{\partial\,\theta_x}\,\dot{\theta}_x \tag{A.33}$$

### A.7.3 Time derivative of intermediate transformation matrix

The same for the transformation matrix $\mathbf{B_{zx}}$

$$\mathbf{B}_{zx} = \mathbf{B}_z\,\mathbf{B}_x \tag{A.34}$$

$$\dot{\mathbf{B}}_{zx} = \frac{\partial \mathbf{B}_{zx}}{\partial\,t} \tag{A.35}$$

$$\dot{\mathbf{B}}_{zx} = \frac{\partial \mathbf{B}_{zx}}{\partial\,\theta_z}\,\dot{\theta}_z + \frac{\partial \mathbf{B}_{zx}}{\partial\,\theta_x}\,\dot{\theta}_x \tag{A.36}$$

# Appendix B

# Tables Used

| | $\mathbf{c_{11}}$ | | | $\mathbf{c_{12}}$ | | | $\mathbf{c_{23}}$ | | | $\mathbf{c_{33}}$ | | |
|---|---|---|---|---|---|---|---|---|---|---|---|---|
| g | $\boldsymbol{\nu = 0}$ | **0.25** | **0.5** | $\boldsymbol{\nu = 0}$ | **0.25** | **0.5** | $\boldsymbol{\nu = 0}$ | **0.25** | **0.5** | $\boldsymbol{\nu = 0}$ | **0.25** | **0.5** |
| (a/b) | | | | | | | | | | | | |
| 0.1 | 2.51 | 3.31 | 4.85 | 2.51 | 2.52 | 2.53 | 0.334 | 0.473 | 0.731 | 6.42 | 8.28 | 11.7 |
| 0.2 | 2.59 | 3.37 | 4.81 | 2.59 | 2.63 | 2.66 | 0.483 | 0.603 | 0.809 | 3.46 | 4.27 | 5.66 |
| 0.3 | 2.68 | 3.44 | 4.80 | 2.68 | 2.75 | 2.81 | 0.607 | 0.715 | 0.889 | 2.49 | 2.96 | 3.72 |
| 0.4 | 2.78 | 3.53 | 4.82 | 2.78 | 2.88 | 2.98 | 0.720 | 0.823 | 0.977 | 2.02 | 2.32 | 2.77 |
| 0.5 | 2.88 | 3.62 | 4.83 | 2.88 | 3.01 | 3.14 | 0.827 | 0.929 | 1.07 | 1.74 | 1.93 | 2.22 |
| 0.6 | 2.98 | 3.72 | 4.91 | 2.98 | 3.14 | 3.31 | 0.930 | 1.03 | 1.18 | 1.56 | 1.68 | 1.86 |
| 0.7 | 3.09 | 3.81 | 4.97 | 3.09 | 3.28 | 3.48 | 1.03 | 1.14 | 1.29 | 1.43 | 1.50 | 1.60 |
| 0.8 | 3.19 | 3.91 | 5.05 | 3.19 | 3.41 | 3.65 | 1.13 | 1.25 | 1.40 | 1.34 | 1.37 | 1.42 |
| 0.9 | 3.29 | 4.01 | 5.12 | 3.29 | 3.54 | 3.82 | 1.23 | 1.36 | 1.51 | 1.27 | 1.27 | 1.27 |
| (b/a) | | | | | | | | | | | | |
| 1.0 | 3.40 | 4.12 | 5.20 | 3.40 | 3.67 | 3.98 | 1.33 | 1.47 | 1.63 | 1.21 | 1.19 | 1.16 |
| 0.9 | 3.51 | 4.22 | 5.30 | 3.51 | 3.81 | 4.16 | 1.44 | 1.59 | 1.77 | 1.16 | 1.11 | 1.06 |
| 0.8 | 3.65 | 4.36 | 5.42 | 3.65 | 3.99 | 4.39 | 1.58 | 1.75 | 1.94 | 1.10 | 1.04 | 0.954 |
| 0.7 | 3.82 | 4.54 | 5.58 | 3.82 | 4.21 | 4.67 | 1.76 | 1.95 | 2.18 | 1.05 | 0.965 | 0.852 |
| 0.6 | 4.06 | 4.78 | 5.80 | 4.06 | 4.50 | 5.04 | 2.01 | 2.23 | 2.50 | 1.01 | 0.892 | 0.751 |
| 0.5 | 4.37 | 5.10 | 6.11 | 4.37 | 4.90 | 5.56 | 2.35 | 2.62 | 2.96 | 0.958 | 0.819 | 0.650 |
| 0.4 | 4.84 | 5.57 | 6.57 | 4.84 | 5.48 | 6.31 | 2.88 | 3.24 | 3.70 | 0.912 | 0.747 | 0.549 |
| 0.3 | 5.57 | 6.34 | 7.34 | 5.57 | 6.40 | 7.51 | 3.79 | 4.32 | 5.01 | 0.868 | 0.674 | 0.446 |
| 0.2 | 6.96 | 7.78 | 8.82 | 6.96 | 8.14 | 9.79 | 5.72 | 6.63 | 7.89 | 0.828 | 0.601 | 0.341 |
| 0.1 | 10.7 | 11.7 | 12.9 | 10.7 | 12.8 | 16.0 | 12.2 | 14.6 | 18.0 | 0.795 | 0.526 | 0.228 |

Table B.1. *Kalker's creepage and spin coefficients*

# Bibliography

[1] J. Ambrósio. *Advances in Computational Multibody Systems.* Springer, Dordrecht, Netherland, 2005.

[2] F. M. L. Amirouche. *Fundamentals of Multibody Dynamics: Theory and Applications.* Birkhäuser, Boston, 2006.

[3] C. Andersson and T. Abrahamsson. Simulation of interaction between a train in general motion and track. *Vehicle System Dynamics*, 38(6), 2002.

[4] E. Andresson, M. Berg, and S. Stichel. *Rail Vehicle Dynamics, Fundamentals and Guidlines.* Royal Institute of Technology (KTH), Stockholm, Sweden, 1998.

[5] JB. Ayasse and H. Chollet. Determination of the wheel rail contact patch in semi-hertzian conditions. *Vehicle System Dynamics*, 43(3), 2005.

[6] L. Baeza and H. Ouyang. A railway track dynamics model based on modal substructuring and a cyclic boundary condition. *Journal of Sound and Vibration*, 330, 2011.

[7] L. Baeza, A. Roda, and J.C.O. Nielsen. Railway vehicle/track interaction analysis using a modal substructuring approach. *Journal of Sound and Vibration*, 293, 2006.

[8] L. Baeza, F. J. Fuenmayor, J. Carballeira, and A. Roda. Influence of the wheel-rail contact instationary process on contact parameters. *Journal of Strain Analysis*, 42, 2007.

[9] L. Baeza, J. Fayos, A. Roda, and R. Insa. High frequency railway vehicle-track dynamics through flexible rotating wheelsets. *Vehicle System Dynamics*, 46, 2008.

[10] J. Baumgarte. Stabilization of constraint and integrals of motion in dynamical systems. *Computer Methods in Appllied Mechanics and Engineering*, 1, 1972.

[11] F. Braghin, S. Bruni, and G. Diana. Experimental and numerical investigation on the derailment of a railway wheelset with solid axle. *Vehicle System Dynamics*, 44(4), 2006.

[12] R V . Dukkipati. *Vehicle Dynamics.* CRC Press, New York, 2000.

[13] B. M. Eickhoff, J. R. Evans, and A. J. Minnis. A review of modelling methods for railway vehicle suspension components. *Vehicle System Dynamics*, 24(6-7), 1995.

[14] J. A. Elkins and H. Wu. Newcriteria for flange climb derailment. *ASME/IEEE Joint Railroad Conference*, 2000.

[15] Coenrad Esveld. *Modern Railway Track.* MRT- Production, Netherlands, 2001.

[16] C. W. Gear. Numerical solution of differential-algebric equations. *IEEE Translations on Circuit theory*, 18, 1981.

[17] V K. Grag and R V . Dukkipati. *Dynamics of Railway Vehicle Systems.* Academic Press, New York, 1984.

[18] H.Hertz. *Collected Works.* Leipzig, Germany, 1895.

[19] R. Huston. *Multibody Dynamics.* Butterworth-Heinemann, Stonehan, Massachussets, 1990.

[20] M. Ishida, T. Moto, and M. Takikawa. The effect of lateral creepage force on rail corrugation on low rail at sharp curves. *Wear*, 253, 2002.

[21] S. Iwnicki. Manchester benchmarks for rail vehicle simulation. *Vehicle System Dynamics*, 30(3-4), 1998.

[22] S. Iwnicki. Manchester benchmarks for rail vehicle simulation. *Vehicle System Dynamics*, 31, 1999.

[23] S. Iwnicki. Simulation of wheel-rail contact forces. *Fatigue Fracture Engineering Material and Structures*, 26, 2003.

[24] S. Iwnicki. *Handbook of Railway Vehicle Dynamics.* CRC Press, New York, 2006.

[25] S. Iwnicki and A. H Wickens. Validation of a matlab railway vehicle simulation using a scale roller rig. *Vehicle System Dynamics*, 30, 1998.

[26] J. Jalon and E. Bayo. *Kinematic and Dynamic Simulation of Multibody Systems: The Real-Time Challenge.* Springer-Verlage, New York, 1994.

[27] T. Jendel and M. Berg. Prediction of wheel profile wear. *Vehicle System Dynamics*, 37, 2002.

[28] K. L. Johnson. *Contact Mechanics.* Cambridge University Press, Cambridge, 1987.

[29] J. J . Kalker. *On the Rolling Contact of Two Elastic Bodies in the Presence of Dry Friction.* PhD thesis, Delfet University of Technology, Delfet, The Netherlands, 1979.

[30] J. J. Kalker. Survey of wheel-rail rolling contact theory. *Vehicle System Dynamics*, 8(4), 1979.

[31] J. J. Kalker. Wheel-rail rolling contact. *Wear*, 144, 1979.

[32] J. J. Kalker. A fast algorithm for the simplified theory of rolling-contact. *Vehicle System Dynamics*, 11(1), 1982.

[33] J. J. Kalker. Three dimensional elastic bodies in rolling contact. *Kluwer Academic publishers, Dordrecht*, 1990.

[34] E. Kassa, C. Andersson, and J. C. O. Nielsen. Simulation of dynamic interaction between trainand railway turnout. *Vehicle System Dynamics*, 44(3), 2006.

[35] W. Kik and J. Piotrowski. A fast approximate method to calculate normal load at contact between wheel and rail and creep forces during rolling. In *Processing of the second Mini Conference on CONATC Mechanics and Wear of Wheel/Rail Systems*. Budapest, Julay-1996.

[36] W. Kik and H. Steinborn. Wheel/rail connexion element for use in a multibody algorithm. In *8th IAVSD Symposium - Dynamics of Vehicles on Road and Tracks*. Cambridge, Massachusetts, 1984.

[37] W. Kik, D. Moelle, C. Bogo, and G. Ferrarotti. The manchester benchmarks adams/rail - medyna statement of methods. *Supplement of to the Vehicle System Dynamics. The Mancherster Benchmarks for Rail Vehicle Simulation*, 31, 1999.

[38] W. Kortum and R. S. Sharp. Multibody computer codes in vehicel system dynamics. *Vehicle System Dynamics*, Supplement 22, 1993.

[39] E. Meli, M. Malvezzi, S. Papini, L. Pugi, and A. Rindi. A railway vehicle multibody model for real-time application. *Vehicle System Dynamics*, 46(2), 2008.

[40] A. D. Monk-Steel, D. J. Thompson, F. G. de Beer, and M. H. A. Janssens. An investigation into the influence of longitudinal creepage on railway squeal noise due to lateral creepage. *Journal of Sound and Vibration*, 293, 2006.

[41] M. E. Mortenson. *Geometric Modeling*. Wiley, New York, New York, 1985.

[42] M. J. Nadal. Theorie de la stabilite des locomotives - part ii. movement de lacet. *Annales des Mines*, 10, 1896.

[43] Parviz E. Nikravesh. *Computer-Aided Analysis of Mechanical Systems*. Parentice Hall, Engelwood cliffs, New York, 1988.

[44] A. A. Pazos. *Nuevos Desarrollos para la Resolución del Problema de Contacto Rueda-Carril y su Aplicación a Simulaciones Dinámicas*. PhD thesis, Escuela superior de Ingenieros industriales, Universidad De Navarra, 2005.

[45] J. Piotrowski and H. Chollet. Wheel-rail contact models for vehicle system dynamics including multi-point contact. *Vehicle System Dynamics*, 43(6-7), 2005.

[46] J. Piotrowski and W. Kik. A simplified model of wheel/rail contact mechanics for non-hertzian problems and its application in rail vehicle dynamic simulations. *Vehicle System Dynamics*, 46(1), 2008.

[47] O. Polach. A fast wheel-rail forces calculation computer code. *Vehicle System Dynamics*, Supplement 33, 1999.

[48] J. Pombo. *A multibody methodology for railway dynamics applications.* PhD thesis, Instituto Superior Técnico, Universidad Técnica de Lisboa, 2004.

[49] J. Pombo and J. Ambrósio. Development of roller coaster model. In *Proceeding of the Métodos Numéricos en Ingeniería V,(J. Goicolea et al Eds.).* SEMNI, Madrid, Spain, 2002.

[50] J. Pombo and J. Ambrósio. General spatial curve joint for rail guided vehicles: kinematics and dynamics. *Multibody System Dynamics*, 9, 2003.

[51] J. Pombo and J. Ambrósio. A computational efficient general wheel-rail contact detection method. *Journal of Mechanical Science and Technology*, 19(1), 2005.

[52] J. Pombo and J. Ambrósio. A new wheel-rail contact model for railway dynamics. *Vehicle System Dynamics*, 45(10), 2007.

[53] R. E. Roberson and R. Schwertassek. *Dynamics of Multibody Systems.* Springer-Verlag, Berlin, Germany, 1988.

[54] W. Rulka and A. Eichberger. Simpack- an analysis and design tool for mechanical systems. *Vehicle System Dynamics*, Supplement 22, 1993.

[55] J-C. Samin and P. Fisette. *Symbolic modeling of multibody systems.* Kluwer Academic Publishers, Dordrecht, the Netherlands, 2004.

[56] W. Schiehlen. *Multibody Systems Handbook.* Springer-Verlag, Berlin, Germany, 1990.

[57] A. A. Shabana. *Dynamics of Multibody Systems, Second Edition.* Cambridge University Press, Cambridge, United Kingdom, 1998.

[58] A. A. Shabana and J. R. Sany. A survey of rail vehicle track simulation and flexible multibody dynamics. *Nonlinear Dynamics*, 26, 2001.

[59] A. A. Shabana, K. E. Zaazaa, J. L. Escalona, and J. R. Sany. Development of elastic force model for wheel/rail contact problems. *Journal of Sound and Vibration*, 269, 2004.

[60] A. A. Shabana, R. Chamorro, and C. Rathod. A multi-body system approach for finite-element modelling of rail flexibility in railroad vehicle applications. *Proc. IMechE, Part K: Journal of Multi-body*, 222(1), 2008.

[61] A. A. Shabana, K. E. Zaazaa, and H. Sugiyam. *Rail Road Vehicle Dynamics : A Computational Approach.* CRC Press, Taylor and Francis group, 2008.

[62] P.T. Torstensson, J.C.O. Nielsen, and L. Baeza. High-frequency vertical wheel-rail contact forces at high vehicle speeds -the influence of wheel rotation. *Notes on Numerical Fluid Mechanics and Multidisciplinary Design*, 118, 2012.

[63] H. Weinstock. Wheel climb derailment criteria for evaluation of rail vehicle safety. *Proceedings of the ASME Winter Annual Meeting*, 84-WA/RT-1, 1984.

[64] P. Wriggers. *Computational Contact Mechanics.* JohnWiley and Sons, Hoboken, NJ, 2002.

[65] W. Zhai, K. Wang, and C. Cai. Fundamentals of vehicle-track coupled dynamics. *Vehicle System Dynamics*, 47(11), 2009.